The TRF1 telomere protein is essential for the generation and maintenance of iPS cells and marks both pluripotent and adult stem cells

Inauguraldissertation

Zur Erlangung der Würde eines Doktors der Philosophie. Vorgelegt der Philosophisch-Naturwissenschaftlichen Fakultät der Universität Basel

von

Ralph Philipp Schneider

aus

Würenlingen, AG

Madrid, 2013

Genehmigt von der Philosophisch-Naturwissenschaftlichen Fakultät auf Antrag von:

Prof. Dr. María Blasco

Prof. Dr. Markus Affolter

Prof. Dr. Gerhard Christofori

Basel, den 18. September 2012

Prof. Dr. Jörg Schibler

Dekan

CONTENT

1. ABSTRACT

1.1. ENGLISH

Telomeres are nucleoprotein structures that protect the chromosomal ends from being recognized by DNA repair mechanisms as DNA double strand breaks. The Telomeric DNA is bound by various proteins that force the whole structure to fold in the so-called telomeric loop, hiding the DNA ends in the double stranded DNA. One of those sheltering proteins is the telomere repeat binding factor 1 (TRF1) which binds to the double-stranded telomeric DNA and is implicated in telomere length regulation. TRF1-deficient mice are embryonic lethal at the blastocyst stage and the conditional deletion of TRF1 in stratified epithelia leads to hair follicle stem cell defects, suggesting thus a role for TRF1 in stemness.

To address this and also the possibility of using TRF1 as an *in vivo* telomere length marker, here we generated a reporter mouse carrying a *knock-in* (KI) allele in which TRF1 is fused to the reporter protein eGFP. We find that eGFP-TRF1 expression is maximal at the adult stem cell compartments in the mouse, including the hair follicle stem cell niche and Lgr5-positive ($Lgr5^{+}$) and Lgr5-low/negative stem cells at the intestinal crypts, and that eGFP-TRF1 expression is uncoupled from telomere length. Conditional deletion of TRF1 in the small intestine leads to a rapid collapse of the villi/crypt structures coincidental with increased DNA damage and apoptosis, indicating that TRF1 is essential to maintain small intestine homeostasis. Thus, TRF1 both marks adult stem cell compartments and is essential for their functionality. In line with this, we found very high levels of eGFP-TRF1 in induced pluripotent stem (iPS) cells, levels that are uncoupled from telomere elongation associated to reprogramming. TRF1 in iPS cells is expressed heterogeneous and coincident with the in-built heterogeneity of Nanog expression in iPS cell colonies. Selection of high eGFP-TRF1 iPS cells correlated with a higher pluripotency as indicated by their ability to form teratomas and chimeras. By using various loss-of-function approaches, we show that TRF1 is necessary for both the induction and the maintenance of pluripotency, by preventing the induction of DNA damage response and apoptosis. Finally, supporting the notion that TRF1 is a key factor for pluripotency we make the unprecedented finding that TRF1 is a direct target of the transcription factor Oct3/4, which binds to the TRF1 promoter and increases the transcription of TRF1, thus providing a mechanistic link between TRF1 and pluripotency.

These findings render TRF1 a novel marker for stem cells, those cells having the highest abundance of TRF1 in a given tissue. Also they deploy the eGFP-TRF1 mouse model as a useful tool for following up such stem cells *in vivo* and *in vitro*.

1.2. DEUTSCH

Werden lose Chromosomenenden von DNS-Reparaturmechanismen erkannt führt dies zu Chromosomenfusionen, Zellseneszenz und Apoptose. Telomere, die Endstücke chromosomaler DNS sind Nukleoprotein-Strukturen mit der Aufgabe die Chromosomenenden davor zu schützen. Die telomerische DNS wird dabei von verschiedenen Proteinen erkannt, gebunden und zu einer Schleife geformt, deren Ende in der telomer-duplex DNA versteckt wird. Eines dieser Schutzproteine ist der „Telomere repeat binding factor 1“ (TRF1), welches die doppelsträngige Telomer-DNS bindet und bei der Regulation der Telomerlänge beteiligt ist. Wird TRF1 depletiert, sterben Embryonen bereits als Blastozysten, zeigen aber keine Telomeranomalitäten. Das konditionelle Ausschalten von TRF1 im mehrschichtigen Epithel (Keratin 5 exprimierendes Epithel) führt jedoch zu hoher Telomerfragilität und zum Verlust von Haarfollikeln was auf einen Stammzelldefekt hindeutet.

Um mögliche Stammzelleigenschaften sowie die Möglichkeit von TRF1 als *in vivo* Telomerlängenindikator zu eruieren, wurde hier eine knock-in Maus generiert, bei der eine eGFP-Kassette in das Aminoende des TRF1-Lokus fusioniert wurde. Mit diesem Model konnte ich zeigen, dass die eGFP-TRF1-Expression in den adulten Stammzellnischen der Haarfollikel und der Dünndarm-Krypten erhöht ist. Konditionelles ausknocken von TRF1 im Dünndarm führte zu einem schnellen Kollaps der Villi/Krypt-Struktur sobald TRF1 in allen Stammzellen eliminiert war. Übereinstimmend mit den erhöhten TRF1-Levels in adulten Stammzellen, zeigten auch induzierte, pluripotente Stammzellen (iPSz) eine deutlich erhöhte Expression von eGFP-TRF1, was aufgrund aktiver Telomerase und sich verlängernder Telomere erwartet werden konnte. Überraschenderweise ist die Menge an TRF1 während des Reprogramierungsprozesses überproportional zur Telomerlänge angestiegen; auch in Zellen die keine Fähigkeit hatten die Telomere zu verlängern. Die Expression von eGFP-TRF1 in iPS-Zellkolonien ist heterogen und korreliert mit Nanog, einem Stammzellmarker der in iPS-Zellen ebenfalls variiert und die Pluripotenz der Zellen positiv beeinflusst. IPS-Zellen mit hoher eGFP-TRF1 Expression waren potenter, subkutane Teratome zu bilden und beteiligten sich an der Formation von Chimären. Mit verschiedenen TRF1 knock-out und knock-down Studien konnte ich belegen, dass TRF1 für die Induktion, wie auch für die Aufrechterhaltung der Pluripotenz essentiell ist. Ebenfalls bewiesen wir, dass OCT3/4, ein Transkriptionsfaktor für Pluripotenzgene, an die TRF1 Promoter-Region bindet und die TRF1 Transkription positiv beeinflusst.

Diese Resultate zeigen TRF1 als einen wesentlichen Faktor der für Pluripotenz und einem neuen Marker für Stammzellen *in vitro* und *in vivo.* EGFP-TRF1 konnte aber nicht als *in vivo* Telomerlängenindikator etabliert werden.

1.3. ESPAÑOL

Los telómeros son estructuras nucleoproteicas que evitan que los extremos de los cromosomas sean reconocidos por los mecanismos de reparación del ADN como roturas en la doble hebra de ADN. El ADN telomérico está unido a varias proteínas que facilitan la formación del denominado bucle telomérico, y que protege los extremos del ADN bicatenario. La proteína TRF1 (telomere repeat binding factor 1) es un miembro del complejo proteíco especializado de protección telomérica que se une al ADN cadena doble y está implicada en la regulación de la longitud telomérica. Los ratones deficientes en TRF1 adolecen de letalidad embrionaria en la etapa de blastocito y la deleción condicional de esta proteína en el epitelio estratificado conduce a defectos en las células madre del folículo piloso, lo que sugiere por tanto una implicación funcional de TRF1 en pluripotencia.

Con el fin de elucidar esta conexión entre TRF1 y pluripotencia y también el posible empleo de TRF1 como un marcador de longitud telomérica in vivo, generamos un ratón "reporter" que contiene un alelo knock-in (KI) en el que TRF1 está fusionada a la proteína eGFP. La expresión de eGFP-TRF1 alcanza, de manera independiente de la longitud telomérica, valores máximos en los compartimentos de células madre adultas, entre los que se incluyen el nicho de células madre del folículo piloso y las células madre Lgr5-positivas (Lgr5+) y Lgr5-negativas (Lgr5-) de las criptas intestinales. La deleción condicional de TRF1 en el intestino delgado desencadena un rápido colapso de las vellosidades y criptas intestinales, coincidente con un aumento en el daño en el ADN y en la apoptosis, lo cual indica que TRF1 es esencial en el mantenimiento de la homeostasis del intestino delgado. Por consiguiente, TRF1 demarca los compartimentos de células madre adultas y es indispensable para su funcionalidad. En consonancia con lo anterior, describimos la presencia de niveles muy elevados de eGFP-TRF1 en las células madre pluripotentes inducidas (células iPS), valores que son independientes del alargamiento telomérico asociado a la reprogramación nuclear. Además, los niveles de TRF1 entre las diferentes células de las colonias de Ips son heterogéneos y coincidentes con la también intrínsecamente heterogénea expresión de Nanog. En las células iPS los altos niveles de eGFP-TRF1 correlacionan con una mayor pluripotencia, asociada a una mayor capacidad para formar teratomas y quimeras. Por medio de diferentes ensayos de pérdida de función, demostramos que TRF1 es necesaria para la inducción y mantenimiento de la pluripotencia, evitando que se desencadene la respuesta de daño en el ADN y la apoptosis. Por último, la idea de que TRF1 sea un factor clave se ve respaldada por el hallazgo sin precedentes de que TRF1 es una diana directa del factor de transcripción Oct3/4, cuya unión al promotor de *TRF1* activa la transcripción de *TRF1*, lo que proporciona un mecanismo que conecta la proteína telomérica TRF1 con la pluripotencia.

Estos resultados convierten a TRF1 en un nuevo marcador de células madre, debido a que su expresión es máxima en las células madre de un tejido dado y al modelo de ratón eGFP-TRF1 en una útil herramienta para el seguimiento de estas células madre in vivo e in vitro.

2. ABREVIATIONS

4-OHT	4-hydroxytamoxifen
53bp1	p53 Binding Protein 1
a.u.f./a.u.	Arbitrary units (of Fluorescence)
ALT	Alternative Lengthening of Telomeres
APB	ALT associated PML Body
ATM	Ataxia Telangiectasia Mutated
ATR	Ataxia Telangiectasia Related
BER	Base Excision Repair
BubR1	uninhibited Benzimidazole Receptor 1
ChIP	Chromatin Imunoprecipitation assay
Chk1	Checkpoint kinase 1
Chk2	Checkpoint kinase 2
CY3	Cyanine3 dye (a dye emitting light at 570nm)
DC	Dyskeratosis Congenita
DDR	DNA-Damage Repair
DNA-PK	DNA-activated Protein Kinase
DKC1	Dyskerin1
DSB	Double Strand Break
eGFP	Enhanced Green Fluorescent Protein
ES	Embryonic Stem (cells)
Fig.	Figure
FISH	Fluorescence *In Situ* Hybridisation
H3K9	Histone 3 Lysine 9

H4K20	Histone 4 Lysine 20
HR	Homologous Recombination
iPS cells	Induced Pluripotent Stem cells
K5	Keratin 5 (promoter)
KI	Knock-In
KSR	Knockout Serum Replacement
LIF	Leukaemia Inhibitory Factor
Mad1	Mitotic arrest deficient 1
MEF	Mouse Embryonic Fibroblast
MHC	Major Histocompatibility Complex
MTS	Multitelomeric Signals
Neo	Neomycin selection cassette
NER	Nucleotide Excision Repair
NHEJ	Non-Homologous End Joining
NLS	Nuclear Localisation Signal
O/N	Over Night
P#	Passage number
PINX1	PIN2-Interacting protein1
PML	Promyelocytic Leukemia
PNA	Peptide Nucleic Acid
Q-FISH	Quantitative Fluorescence *in situ* Hybridisation
RAP1	Repressor Activator Protein 1
pRB	Retinoblastoma-Protein
ROS	Reactive Oxygen Species

SCF	Sister Chromatid Fusion
TANK1	Tankyrase 1
TANK2	Tankyrase 2
TERC	Telomerase RNA Component
TERT	Telomerase Reverse Transcriptase
TIF	Telomere dysfunction Induced Foci
TIN2	TRF1 Interacting Protein 2
T-loop	Telomere loop
TRF1/TERF1	Telomere Repeat binding Factor 1
TRF2/TERF2	Telomere Repeat binding Factor 2
TRFH	Telomere Repeat binding Factor Homology domain
WB	Western Blot
WRN	Werner
XPF	Xeroderma Pigmentosum group F
γH2AX	Gamma phosphorylated histone H2AX

3. INTRODUCTION

3.1. THE HISTORY OF TELOMERES

Telomeres where first mentioned by Hermann Müller and Barbara McClintock. They noticed that chromatic fusions were not present at the very end of chromosomes. Therefore, they postulated a protecting structure that defends the chromosomal extremities from fusion events (McClintock, 1941; Müller, 1938). This structure, as vague as its existence remained, was denominated telomere, a term deriving from the Greek words *telos* (end) and *meros* (part).

In 1971 after the deoxyribonucleic acid (DNA) structure was revealed by Watson and Crick (Watson & Crick, 1953), Alexey Olovnikov (Olovnikov, 1971) and later James Watson (Watson, 1972) postulated on theoretical grounds the “end replication problem” of the semi conservative DNA replication. They predicted that DNA, if its replication is RNA primed, could not be completely duplicated and that this must gradually shorten the DNA from its ends with every replication cycle. Olovnikov further suggested that this could be the underlying effect for the findings in the work of Hayflick and Moorhead (Olovnikov, 1971) that showed that human fibroblasts have a limit of 50 to 70 cell cycles before they abrogate replication and enter senescence. This limit is referred to as the Hayflick limit (Hayflick & Moorhead, 1961; Ohki et al, 2001; Olovnikov, 1971). It was Elisabeth Blackburn and Joe Gall that unravelled the structure of the chromosome ends and showed that eukaryotic telomeres consist of tandem repeated oligonucleotid sequences (Blackburn & Gall, 1978). As the telomeres shorten during lifetime, the discovery of the telomerase - a reverse transcriptase that can re-elongate telomeres, was a next important milestone in telomere biology. This finding gave the basis for tools to demonstrate the dependency on telomere sustaining mechanisms of tumors and the tumor suppressive function of shortened telomeres (Blasco et al, 1997; Greider & Blackburn, 1985; Hanahan & Weinberg, 2000).

35 years after the discovery of the first telomeric sequence, we now have a broad knowledge of telomeres and telomere-linked fields. Telomeres are now known to be nucleoprotein structures protecting the ends of chromosomes from being detected as double strand breaks by DNA repair mechanisms preventing fusions, recombination and degradation (Chan & Blackburn, 2002; de Lange, 2005). In vertebrates, telomeres are composed of the tandem repeated TTAGGG sequence that are bound by telomere specific proteins which force this nucleoprotein complex into a characteristic telomere structure (de Lange, 2005).

3.2. STRUCTURE OF TELOMERES

Telomeric DNA in vertebrates are gene-poor regions at the ends of the linear chromosomes. They are constituted of tandem repeated 5'-TTAGGG-3' sequences. In a healthy human these repeats span in average 5 to 15kB (de Lange et al, 1990) whereas the average murine telomere spans between 15 and 40kB depending on the genetic background (Hemann & Greider, 2000; Zijlmans et al, 1997). Within different organisms of the same species, telomere length is not homogeneous, varies from tissues to cell types, cells (Canela et al, 2007a; Flores et al, 2008) and even within different DNA ends of the same chromosome (Lansdorp et al, 1996; Zijlmans et al, 1997). These variations do not alter the function of the telomeres as long as their size does not underrun a critical length, required for a proper maintenance of genomic stability (Blasco et al, 1997; Lee et al, 1998). At the end of the repetitive telomere sequence, there is a guanine-rich, single stranded 3' overhang of approximately 150 to 200 bp (also known as G-strand overhang; Fig 1). The presence of this structure is a direct consequence of the end replication problem that occurs in RNA primed DNA duplication (further explanation in point 3.5) (de Lange, 2002; Klobutcher et al, 1981; Ohki et al, 2001; Wright et al, 1997).

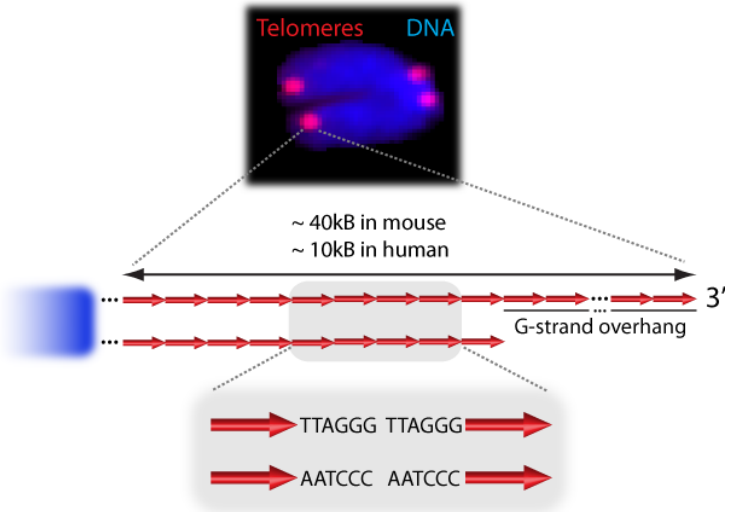

Figure 1: Telomere structure

Top: Visible is a condensed mouse metaphase chromosome. Its telomeres are labelled in red with a Cy3 fused PNA probe. It is observable that different arms of the same chromosome have a different telomere length.

Middle and bottom: Schematic depiction of a vertebrate Telomere with the characteristic TTAGGG repeats and the single stranded 3'-G-rich overhang. Within the different species the repeat number can change severely.

3.3. THE SHELTERIN COMPLEX PROTEINS

For scaffold and protection purposes a six-protein complex known as the shelterin is bound to mammalian telomeres (de Lange, 2002; de Lange, 2005). Out of these proteins, two are bound to the repeats of double stranded telomeric DNA and one binds the single

DNA strand of the G-rich overhang. The double strand binding proteins are the Telomere Repeat binding Factor 1 (TRF1) and the Telomere Repeat binding Factor 2 (TRF2), two proteins that show a high primary structure homology (Bianchi et al, 1997; Bilaud et al, 1997; Broccoli et al, 1997; Chong et al, 1995). TRF1 and TRF2 interact with each other through TRF1 Interacting Nuclear factor2 (TIN2) that itself also binds to TPP1 **(Fig. 2)** (Houghtaling et al, 2004; Ye et al, 2004a). Protection Of Telomeres (POT1) binds to the single stranded G-rich overhang (de Lange, 2005) and it is connected to the shelterin complex through direct binding to TPP1, the mouse homolog of ACD **(Fig. 2A)** (Houghtaling et al, 2004; Ye et al, 2004b). RAP1 binds TRF2 and is implicated in Telomere length alteration but it is not required for correct telomere capping. In addition, it has several extratelomeric roles such as a transcriptional modulator of NF-κB or the silencing of subtelomeric proteins (Martinez & Blasco, 2011; Martinez et al, 2010). Table 1 summarizes the telomeric roles of the shelterin proteins.

In mammals, complementary proteins bind to the telomere repeat binding factors. TRF1 for example is associated with Tankyrase1, Tankyrase2 and PINX1 (Chen et al, 2008) which will be discussed in more detail in chapter 3.9. TRF2 is associated with several proteins that have a role in DNA repair. Amongst them are the helicases WRN and BLM, the DNA-PKs complex (associated with non-homologous end joining (NHEJ)), the MRE11/NBS1/RAD50 complex (associated with homologous recombination (HR)), the ADP-ribosilases PARP1 and PARP2 (associated with base excision repair (BER)), the complex of the endonucleases ERCC1/XPF (associated with the nucleotide excision repair (NER)) (Dantzer et al, 2004; Opresko et al, 2002; Zhu et al, 2000; Zhu et al, 2003) and Apollo/SNM1B nuclease implicated in the telomere end modulation (Wu et al, 2012). Even though the role of these proteins at the telomere is not exclusive, they are important for maintaining the protective function of telomeres.

Proteins	Role at the telomere
TRF2, TRF1, TIN2, TPP1 and RAP1	Protection from recombination
POT1	G-strand overhang protection
TRF2, TRF1, TIN2, TPP1 and RAP1	Length regulation
TRF1, TRF2, POT1, (RAP1)	Inhibition of DNA damage response
TRF1	Telomere replication facilitation
TPP1	Telomerase recruitment

Table 1: Roles of the different shelterin proteins at the telomeres as known up to date. Many of them also have extra-telomeric roles that are not indicated here. RAP1 null induces DDR but does not increase telomere fusions. Reviewed by (Martinez & Blasco, 2011)

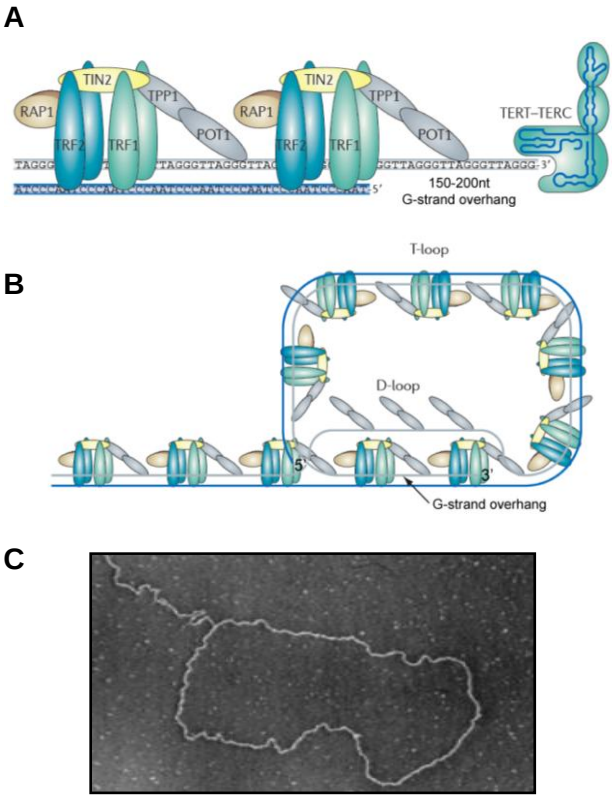

Figure 2: Shelterin and T-loop structure.

A: Schematic depiction of the nucleoprotein structure of a telomere and the binding pattern and partners of the shelterin proteins. Of note is that only TRF1, TRF2 and POT1 are directly binding to telomeric DNA. RAP1, TIN2 and TPP1 are localized at the telomere via a linker protein. Visible on the right is the enzyme Telomerase composed by the subunits TERT and TERC.
B: Telomere nucleoprotein structure forming the T-loop by the invasion of the G-strand overhang into the telomeric DNA, leaving a displacement D-loop that is bound by POT1. Adapted from (Martinez & Blasco, 2011).
C: Transmission electron-microscope picture of telomeric chromatin forming up the T-loop in HELA cells (Griffith et al, 1999).

3.4. The T-loop model and DNA Damage Response

According to a widely accepted hypothesis, mammalian telomeres can to have two known conformations. They can either be linear, or they can be closed, forming a structure known as the telomere loop (T-loop), as shown in Figure 2 B&C. The linear telomere conformation **(Fig. 2A)** has the advantage that the telomerase can access the telomere easily but this suffers from a major drawback: In this state, the chromosomal end remains unprotected in the nucleoplasma (de Lange, 2002; Loayza & De Lange, 2003; Ye & de Lange, 2004). This is the advantage and probably the evolutionary reason why a telomeric loop conformation was established. In the T-loop the telomeric DNA-Protein complex forms a characteristic structure where the single stranded G-rich overhang is invading the double stranded telomeric DNA. At the double strand DNA entry-site this invasion creates a displacement D-loop (in which the G-rich strand presents additional binding sites to POT1) **(Fig. 2B)** (Goytisolo & Blasco, 2002; Greider, 1999; Griffith et al, 1999). This protecting structure is important in eukaryotic cells as the DNA-damage repair (DDR) mechanisms can recognize and “repair” broken DNA strands. These mechanisms re-join two free ends of DNA regardless whether they result from a DNA break or from unprotected chromosome ends. Thus one of the main functions of telomeres is to hide the chromosome ends from being detected and processed as DNA double strand breaks (Chan & Blackburn, 2004).

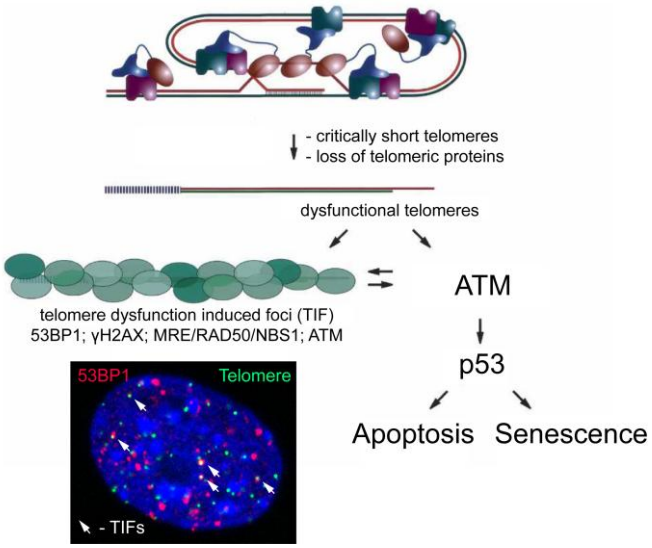

Figure 3: DNA damage response of by dysfunctional telomeres.

Dysfunctional telomeres that can be induced either by critically short telomere of insufficient telomere capping by other reasons, force the cell into senescence and apoptosis in a p53/pRB mediated manner. Dysfunctional telomeres are made visible with a double labelling of telomeres and a DNA damage marker like 53BP1. Depiction is adapted from (de Lange, 2005).

Nevertheless, telomeres may remain in the open conformation either due to telomere shortening to a critical length that is not sufficient to initiate a T-loop, or by the lack of telomeric proteins destabilizing this sheltering complex. At sites of free chromosome ends, it is proposed that proteins responsible for the DDR transduction (53BP1, γH2AX, NBS1, ATM, ATR, DNA-PK) accumulate and induce a signalling cascade that results in transcriptional activation of tumor suppressor genes such as p53, p21, p16, Chk1 and Chk2. They force cells with DDR signalling into p53/pRB-dependent senescence or apoptosis **(Fig.3)** (Artandi & Attardi, 2005; Goytisolo & Blasco, 2002; Martinez et al, 2009; Sfeir et al, 2009; Smogorzewska & de Lange, 2002; van Steensel & de Lange, 1997). Telomeres that are recognized by DDR mechanisms and show corresponding marks are referred to as telomere dysfunction induced foci (TIF). The activated DNA-PK leads to the initiation of NHEJ, resulting in cells that show end-to-end telomere fusions from both, different chromosomes and sister chromatids. This evades the immediate initiation of senescence and is another marker for telomere dysfunction (Donate & Blasco, 2011; Martinez et al, 2009; Sfeir et al, 2009).

3.5. TELOMERE SHORTENING

As mentioned earlier, the 5' end of telomeres cannot be duplicated completely what causes a shortening of 50 to 200bp in every cell cycle. The reason for this decrease lies in the antiparallel characteristics of the double DNA and the nature of semiconservative DNA replication.

DNA-polymerases can only add bases to the 3' end of a newly synthesised DNA strand. Therefore, in replication forks, the daughter DNA strands are distinguished in a leading and a lagging strand (Fig.4). In the leading strand the DNA polymerase can continuously operate

along with the progression of the replication fork machinery in a 5'-3' direction. On the lagging strand however, the polymerase moves in the opposite direction to the replication fork and DNA synthesis must be accomplished in a discontinuous manner. Therefore, in the opened DNA of the replication fork, DNA-primases introduce short pieces of complementary RNA to the lagging strand. They function as primers and give a 3'-OH substrate to the DNA-polymerase for the synthesis of the lagging strand. Discontinuous DNA fragments, the Okazaki fragments, appear interspersed by RNA primers **(Fig. 4)** (Okazaki et al, 1967). In turn, these RNA-primers are further degraded and a DNA-polymerase fills the gap with corresponding DNA-bases. At the end of the chromosome, when the most distal RNA priming sequence is degraded the polymerase is not able to replicate the full DNA in this lagging manner due to its necessity of a 3'-hydroxy end. For this reason the newly synthesised 5'-DNA strand remains shorter than its complement, parental DNA strand. This is the phenomenon of the end replication problem in semiconservative DNA replication and leads to a replication or age related telomere shortening (Ohki et al, 2001). On the other hand, the leading strand is synthesising the entire DNA, finishing blunt ended. Here the EXO1 and Apollo/SNM1B nucleases digest DNA from the 5' end to form a G-strand overhang, required for the formation of the protective T-loop. This DNA degradation results in a shortened 5' DNA strand and a further shortened telomere **(Fig. 4)** (Wu et al, 2012).

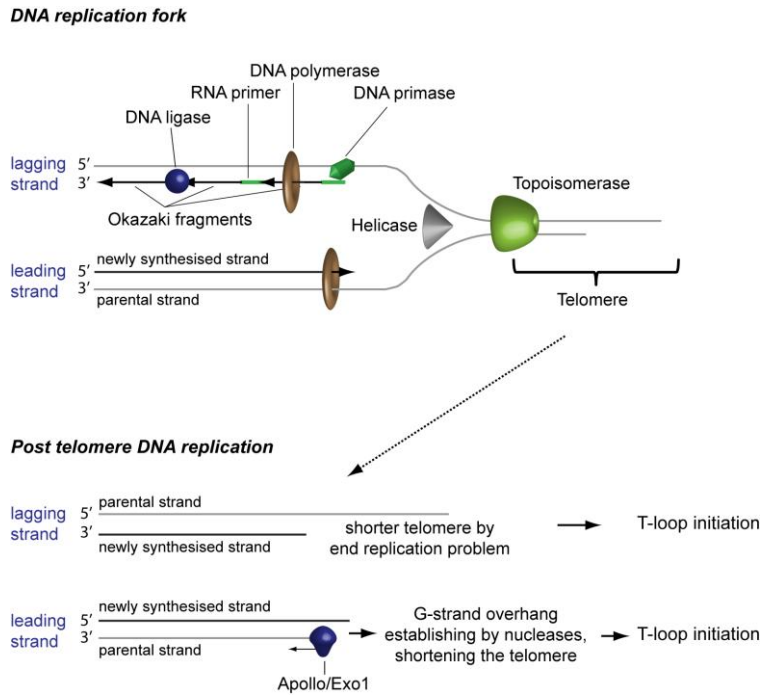

Figure 4: The end replication problem

Top: Depicted is a replication fork progressing towards the telomere. The DNA replication of the lagging strand cannot be completed as the DNA polymerase needs a 3' end that is not available at the distal end of the telomere. As a result, the DNA shortens with every cell cycle.
Bottom: Post replication nucleases (Apollo and Exo1) degrade parts of the 5' telomere end of the leading strand. This allows the blunt ended DNA to form a G-strand overhang and the initiation of a protecting T-loop, leaving a shortened telomere.

Another pathway for telomere shortening departs from the fact that telomeres are more prone to single strand damage due to oxidative stress when compared to the rest of the genome. This causes single strand breaks by Reactive oxygen species (ROS) that lead to an increased S1-nuclease sensitivity and concomitant telomere erosion (von Zglinicki et al, 2000). Other reasons for telomere shortening are known. They are however of minor importance.

3.6. TELOMERASE DEPENDENT TELOMERE ELONGATION

To compensate for the loss in telomere length, cells can *de-novo* re-elongate telomeres with the enzymatic complex telomerase (Blackburn, 2001; Collins & Mitchell, 2002; Greider & Blackburn, 1985). This complex consists of a constitutive protein subunit, the telomerase reverse transcriptase (TERT) and an inducible telomere RNA subunit (TERC) (Fig. 2A). In addition, a single molecule of dyskerin1 (DKC1) is stabilizing the telomerase composite (Cohen et al, 2007). This complex forms up a reverse transcriptase that recognizes the 3'-hydroxy group of the G-strand overhang where it acts as a reverse transcriptase, adding telomeric repeats. During this step, the RNA subunit TERC is used as a template which explains the repetitive TTAGGG sequence of telomeres (Greider & Blackburn, 1985). As mentioned earlier, the accessibility for the telomerase complex to the telomere depends on the telomere conformation. A short telomere or a telomere with low amounts of shelterins is more accessible for the telomerase due to its loose or open conformation. Consequently, in the closed form (T-loop) the 3' end is less approachable impeding the access of the telomerase to the telomeres resulting in a more rapid shortening. This can be seen as a mechanism by which, the telomeres autoregulate their own length (Marcand et al, 1997). In the absence of the T-loop, it has been proposed that telomerase can protect short telomere by simply binding to them, hiding the DNA ends from DNA repair mechanisms (Masutomi et al, 2003).

Telomerase is predominantly expressed in cells of the inner cell mass (ICM), embryonic stem (ES) cells and in several tissue specific adult stem cell compartments (Allsopp et al, 2003; de Lange & DePinho, 1999; Greenberg et al, 1998; Hoffmeyer et al, 2012; Montgomery et al, 2011; Schepers et al, 2011; Varela et al, 2011). In adult stem cells however the telomerase activity is not sufficient to maintain telomere length over successive cell divisions and differentiation. The ensuing telomere shortening is suggested to be one of the molecular mechanisms underlying organism aging (Flores et al, 2008; Harley et al, 1990). One possible exception is the testis, where TERT is expressed to high levels and elongates telomeres during lifespan so that older fathers have offspring with longer telomeres (Eisenberg et al, 2012; Montgomery et al, 2011).

3.7. Alternative mechanism of telomere length maintaining

In the absence of a functional telomerase complex telomere length homeostasis can be achieved by a different mechanism. This alternative lengthening of telomeres (ALT) pathway is able to maintain or elongate the telomeric (and subtelomeric) DNA via homologous recombination. This pathway was found in various tumors and several immortalized cell lines. Cells that use the ALT pathway are characterized by the presence of highly heterogeneous telomere lengths and telomere association with promyelocytic leukaemia (PML) protein, forming the ALT-associated-PML bodies or APBs (Bryan et al, 1997; Bryan et al, 1995; Dunham et al, 2000; Muntoni & Reddel, 2005). This pathway however is not capable of maintaining the telomeres of protozoan organisms for a long period of time and is therefore of minor importance for counteracting the age related telomere loss.

3.8. Telomeres, senescence and aging

As seen above, telomeres get shorter with every DNA replication, until they have shortened to a critical length that does not allow the initiation of the T-loop conformation anymore. This leads to the appearance and the initiation of the DDR resulting in stalled proliferation (Vaziri, 1997). *In vitro*, human cells stop dividing after 50-70 cell cycles before they enter a state called replicative senescence which *in vivo* reduces the self renewing potential of corresponding tissues. It is thought that telomere shortening is one of the main causes of this limited duplication capacity (Harley et al, 1990). Telomeric association to replicative senescence is underlined by the fact that ectopic (re-) expression of telomerase is able to prevent many cell types from entering senescence (Bodnar et al, 1998; Vaziri & Benchimol, 1998; Yang et al, 1999). Conversely, telomerase inhibition in immortalised cells leads to the induction of replicative senescence (Ohmura et al, 1995).

In mice, the effect of short telomeres on the ageing process was demonstrated in the *TERC*$^{-/-}$ mouse, a model deficient for active telomerase (Blasco et al, 1997). These mice lose regenerative capabilities of tissues and organs such as the hematopoietic system, reproductive organs, epithelia, liver, heart and blood vessels (Blasco et al, 1997; Franco et al, 2002; Herrera et al, 2000; Herrera et al, 1999a; Herrera et al, 1999b; Lee et al, 1998; Leri et al, 2003; Samper et al, 2002). This ultimately leads to premature ageing symptoms such as growth retardation, hair loss, skin ulceration and reduced wound healing resulting in a reduced mean and absolute lifespan (Garcia-Cao et al, 2006; Herrera et al, 1999b; Rudolph

et al, 1999). Interestingly, in further generations of *TERC*$^{-/-}$ mice the longevity decreases continuously and the onset of the age related symptoms appear even earlier leading to infertility in the 3rd generation (in C57Bl6 genetic background) (Garcia-Cao et al, 2006; Herrera et al, 1999b). Further investigations revealed that *TERC*$^{-/-}$ mice are characterized by highly increased numbers of short telomeres that lack the possibility to form the protecting T-loop. Subsequently, the critically short telomeres are recognised as DNA damage and DNA repair mechanisms are initiated causing chromosome fusions as seen in chapter 2.4. Strikingly, the re-expression of functional telomerase rescues premature telomere shortening, protecting from chromosomal fusions and the mentioned phenotypes (Samper et al, 2001). Even though it was thought that adult stem cells cycle with a low frequency, they also suffer from telomere shortening in *TERC*$^{-/-}$ mice. Stem cells with shortened telomeres reveal lower tissue renewal capacities. Similarly to the differentiated cells, the premature ageing effects can be rescued by the reintroduction of telomerase (Donate & Blasco, 2011; Flores et al, 2005; Siegl-Cachedenier et al, 2007).

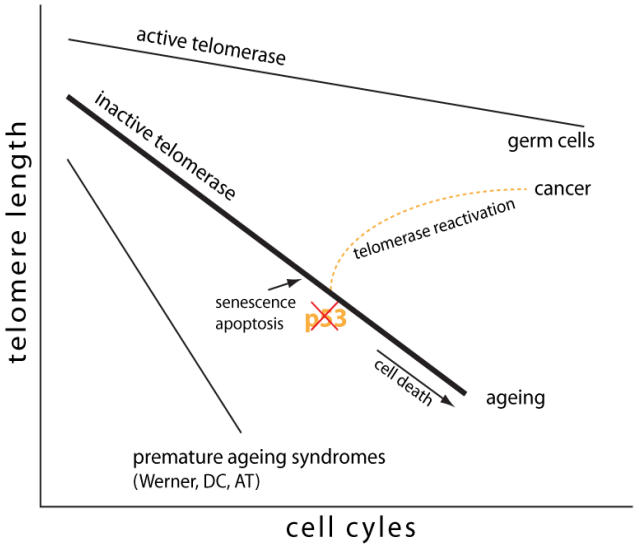

Figure 5: Schematic depiction of the relation between telomere length aging and cancer.

3.8.1. TELOMERE ASSOCIATED DISEASES

Patients with defective telomerase and telomeres show premature aging that is often accompanied by diseases associated with telomere dysfunction.

3.8.1.1. Dyskeratosis Congenita (DC)

DC is a rare disease with a prevalence of 1 in 1'000'000. It is characterized by dystrophic nails, skin hyperpigmentation and oral leukoplakia, an epithelial dysplasia of oral mucosa (Carroll & Ly, 2009; Drachtman & Alter, 1995). During infancy, mucocutaneous disorders appear followed by bone marrow failure and aplastic anaemia that are usually fatal. Gradually, various premature aging symptoms such as pulmonary diseases, dental abnormalities, oesophagostenosis and alopecia can appear. On average, patients die before the age of 16 (Carroll & Ly, 2009; Drachtman & Alter, 1995). DC is linked to a telomerase

dysfunction as many patients have been found to carry a mutation in one of the three main components of the telomerase complex (DKC1, TERT or TERC) (Carroll & Ly, 2009; Martinez & Blasco, 2011). Also telomere interacting proteins such as TIN2 have been shown to contribute to the disease (Savage et al, 2008). Mutations in these genes can lead to shortened telomeres, genomic instability and a higher incidence of sporadic cancer, all symptoms that are found in DC patients (Carroll & Ly, 2009).

3.8.1.2.Acquired aplastic anaemia

Acquired aplastic anaemia is a disorder characterized by a hypocellular bone marrow. The leukocytes in such patients show severely shorter telomeres if compared to age matched healthy individuals. This disease could be linked to mutations in TERT, TERC and the shelterin complex proteins TRF1, TRF2 and TIN2 (Carroll & Ly, 2009; Martinez & Blasco, 2011; Savage et al, 2006).

3.8.1.3.Idiopathic Pulmonary Fibrosis (IPF)

IPF is a degenerative and rare lung disease where patients suffer from dyspnea, cough and an impaired gas exchange. IPF has a prevalence of 4 in 100'000 individuals and is likely to occur in DC patients. In 12% of the patients a mutation in the telomerase components TERT and TERC could be found (Armanios et al, 2007; Tsakiri et al, 2007).

3.8.1.4.Telomeres and Cancer

Telomere shortening, as seen in the $TERC^{-/-}$ mouse, has a tumor suppressing effect (Blasco et al, 1997; Gonzalez-Suarez et al, 2003; Gonzalez-Suarez et al, 2000). Critically short telomeres and/or loss of telomere binding proteins causes telomere uncapping and loss of telomere protection. Under p53/pRB competent conditions, this results in genomic instability activating the DDR cascade that forces the cell into cell cycle arrest or apoptosis **(Fig. 5).** In cells with p53 depletion, short telomeres contribute to chromosomal instability, a prerequisite for prone cells to transform (Deng et al, 2008). Interestingly, in 80 to 90% of all the human cancer, transformed cells acquire telomerase activity during tumorigenesis **(Fig 5)**. This counteracts telomere shortening in fast cycling cells and consequently increases cancer cell viability allowing a tumor to maintain telomeres stable; a hallmark of cancer (Bodnar et al, 1998; Hanahan & Weinberg, 2000; Shay & Wright, 2006; Shay & Wright, 2011).

The ambiguous role of telomeres in cancer and tumor suppression is further underlined by the fact that models with facilitated telomere elongation (mainly by TERT overexpression) are more prone to spontaneous transformation, accentuating that telomere erosion over age is a relevant tumor suppressing property, limiting the proliferation potential of a transformed cell (Artandi et al, 2002; Canela et al, 2004; Cayuela et al, 2005; Gonzalez-Suarez et al, 2001). Elevated susceptibility of spontaneous cancer in *K5-TERT* overexpressing mice (constitutively expressing TERT in stratified epithelial tissues) could be rescued by crossing with mice carrying an enhanced expression of p53, p16 and p19ARF tumor suppressors. Those mice not only had lower tumor susceptibility, but also showed a 40% increase of median lifespan and resistance for ageing-associated pathologies (Tomas-Loba et al, 2008). These findings show that for an organism it is a constant balancing act keeping the correct relation to telomere length; not favouring cancer prone cells with long telomeres but also counteracting early ageing phenotypes emerging from short telomeres.

3.9. THE TELOMERE REPEAT BINDING FACTOR 1

The murine TRF1 is a 56kD protein encoded on chromosome 1 in the band qA3. According to the consensus coding sequence project (CCDS), it consists of 10 exons and spans a distance of 37812 bases that are further transcribed, spliced and translated into a 421 amino acid protein. The fully transcribed TRF1 protein is mainly recruited to the end of chromosomes where it binds as a dimer to the double stranded DNA of the telomeres. The full length protein contains four functional domains **(Fig. 6)**. The amino end domain does not show an evolutionary conserved primary sequence, but in vertebrates it is characterized by a high density of acidic amino-acids giving the domain a low pH (pH~3). This domain shows the most marked difference to the homologue protein TRF2. The TRF2 protein has predominantly basic amino-acids in this position that force the telomeric DNA into a more condensed state, stabilizing the T-loop conformation. The acidic domain of TRF1 is followed by the TRF homology (TRFH) domain that is responsible for homodimerisation and interaction with the shelterin complex protein TIN2. Towards the C-terminus the protein contains the nuclear localisation motif as well as the highly conserved Myb-domain that allows the TRF1 protein sequence specific DNA binding to telomeres **(Fig. 6)** (Bianchi et al, 1997; Broccoli et al, 1997; Fairall et al, 2001; Poulet et al, 2009; Poulet et al, 2011; Smith & de Lange, 1997).

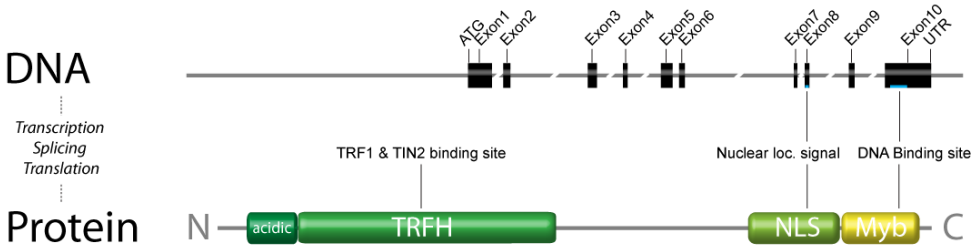

Figure 6: Murine TRF1 locus on top and protein structure on the bottom. N- to C-terminus: The acidic domain with a pH around 3; the *TRF homology domain* (TRFH) for protein-protein interaction; the nuclear localisation signal (NLS) and the Myb-domain, responsible for the telomeric localisation.

The TRF1-DNA telomere binding efficiency can be regulated post-translationally by tankyrase 1 and 2 that poly-ADP-ribosylate TRF1 (Cook et al, 2002; Donigian & de Lange, 2007; Smith et al, 1998). ADP-ribosylation releases TRF1 from the telomere making it accessible for polyubiquitination and degradation through the proteasomic pathway. This implies that the displacement of TRF1 allows a faster attachment of telomerase to the telomere (Chang et al, 2003; Lee et al, 2006). This suggestion is further strengthened by various over-expression assays demonstrating that TRF1 acts as a negative telomere length regulator (Ancelin et al, 2002; Munoz et al, 2009; Smogorzewska et al, 2000; van Steensel & de Lange, 1997). Another telomere length regulation mechanism emerges from the TRF1 binding protein PIN2-interacting protein1 (PINX1). PINX1 is reported to be a telomerase inhibitor that binds to the TRFH domain of TRF1 and to the TERT subunit inhibiting its activity thereby counteracting telomere lengthening (Zhou & Lu, 2001). Apart from the telomerase hindering effects of TRF1 another telomere shortening mechanism was suggested as the TRF1 overexpression-dependent telomere shortening was rescued by the ablation of the XPF-nuclease. This indicates increased XPF nucleolytic activity at chromosal ends in TRF1 overexpressing cells and is similar to what has been reported for the TRF2 over-expression (Munoz et al, 2009; Munoz et al, 2005; Smogorzewska et al, 2000). Overexpressed TRF1 in addition co-localizes with BubR1 and Mad2, two spindle assembly checkpoint proteins preventing cells from undergoing aberrant mitosis (Munoz et al, 2009).

On the other hand, complete TRF1 deletion in mouse leads to early embryonic lethality at the blastocyst stage between embryonic days E5-6. Rather interesting is the fact, that those telomeres do not show any telomere capping abnormalities or telomere length defects (Karlseder et al, 2003). If TRF1 ablation is induced later in development, TRF1 underlines its important role in the maintaining of telomere capping (Martinez et al, 2009; Sfeir et al, 2009). The conditional knock-out, *in vitro* as well as *in vivo*, leads to a severe induction of telomere fragility as determined by increased occurrence of multitelomeric signals (MTS), sister chromatid fusions at the telomeres and chromosome concatenation

(Martinez et al, 2009). This causes an increase of telomere dysfunction induced foci (TIFs), indicating the induction DNA damage response (DDR). The damage signalling at such aberrant telomeres is mediated via phosphorylated ATM and the ATM/ATR downstream checkpoint kinases CHK1 & CHK2 leading to the rapid induction of p53 and pRB mediated senescence that can, to a great extent, be rescued in a p53 null background (Martinez et al, 2009).

Such TRF1 deletion in stratified epithelia ($TRF1^{lox/lox}$; K5-Cre) has been well characterized. These mice die perinatally and show severe skin degeneration effects such as hyperpigmentation, lack of mature hair follicles and missing sebaceous glands. Until postnatal day 6, these mice show compensatory preneoplastic lesions in all stratified epithelia. However, $TRF1^{\Delta/\Delta}$; K5-Cre; $p53^{-/-}$ mice show a rescue of hair follicle stem cells, skin hyperpigmentation as well as increased survival, underlining that the observed phenotype is p53 mediated. In later stages, double deficient mice develop different telomere-associated, hyperproliferative epithelial abnormalities like oral leukoplakia and nail dystrophy (Martinez et al, 2009). These are characteristics also found in the telomere associated human diseases dyskeratosis congenita, aplastic anaemia and idiopathic pulmonary fibrosis (Armanios et al, 2007; Mitchell et al, 1999; Tsakiri et al, 2007; Yamaguchi et al, 2005). As the uncapped telomeres induce genomic instability, it is not surprising, that long lived K5-Cre; $TRF1^{\Delta/\Delta}$; $p53^{-/-}$ mice develop spontaneous, invasive and genomically unstable squamous cell carcinomas (Martinez et al, 2009).

The regulation of TRF1 is widely unclear although various binding sites for pluripotency transcription factors were reported (Loh et al, 2006). This goes along with the hypothesis that long telomeres in pluripotent cells would consequently require more TRF1 to cover the increased number of telomere repeats.

The above mentioned findings show that TRF1 is preventing telomere-induced genetic instability in proliferating cells. In addition, they make TRF1 knock-out models valuable tools to study the molecular mechanisms underlying telomere-associated diseases that are caused by unprotected telomeres due to critical shortage or by telomere uncapping.

3.10. TELOMERES AND IPS CELLS

3.10.1. WHAT ARE IPS CELLS

Embryonic Stem (ES) cells are capable of differentiating into all somatic cell types and have an unlimited self-renewal capacity. Therefore, among all cells, they are thought to have the greatest potential for medicinal and research purposes. Nevertheless, ES cells have to be isolated from the inner cell mass of an embryo which, for humans is tightly regulated and limited in most countries. Additionally, at the time ES cells differentiate they face the problem of augmented immunological incompatibility with a host organism due to an increase of the major histocompatibility complexes (MHC) (Fairchild et al, 2005). Therefore clinical use of ES cells is limited to tissues with a low immune response. Similar problems are faced with other methods generating undifferentiated cells such as somatic cell nuclear transfer into a fertilized oocyte or the cell fusion approach where a somatic cell and an embryonic stem cell are fused (reviewed in (Hochedlinger & Jaenisch, 2006)).

Knowing the wide potential of undifferentiated cells in medicine and research, a huge effort was made to find a way to reprogram somatic cells to avoid the use of ES cells. In 2006 Takahashi and Yamanaka reported a method of reprogramming murine fibroblasts through the expression of four known transcription factors. They demonstrated for the first time that lentiviral based expression of OCT4 (Octamer3/4), SOX2 (SRY box-containing gene 2), Krüppel-like factor 4 (KLF4) and c-MYC reprograms cells, as seen by their ES cell like morphology and properties (see next chapter). These reprogrammed cells were named induced pluripotent stem (iPS) cells (Takahashi & Yamanaka, 2006). A few months later, the same group was able to reprogram human fibroblasts using the same protein expressing cocktail, indicating that the signalling underlying pluripotency is an evolutionary conserved network (Takahashi et al, 2007). Many researchers were following these findings and additionally came up with different protein cocktails for reprogramming; including the finding that c-Myc is not required for reprogramming (Nakagawa et al, 2008; Wernig et al, 2008).

As lentiviral integration sites are a potential oncological risk in the usage of iPS cells in therapies, current research is following on reprogramming techniques with non integrating methods such as the use of adenoviral vectors (Stadtfeld et al, 2008b) or microRNA (Subramanyam et al, 2011) bringing iPS cells closer to clinical use. Initial remarkable studies in mice could already show the wide potential iPS cells have in cell replacement treatments. Examples include the rescue of sickle cell anaemia (Hanna et al, 2007; Wang et al, 2009) or the Fanconi anaemia (Raya et al, 2009).

3.10.2. PROPERTIES OF IPS CELLS

Similar to ES cells, IPS cells grow in colonies on fibroblast feeder cells or gelatin coated dishes. They require a special culturing environment including the leukaemia inhibitory factor (LIF) and knockout serum replacement (KSR) (Bryja et al, 2006; Cheng et al, 2004; Nichols et al, 1990; Takahashi & Yamanaka, 2006). Under these conditions, iPS cells maintain a normal karyotype and pluripotency over numerous cell cycles and tissue culture passages. This was demonstrated by teratoma formation assays by subcutaneous injection of reprogrammed iPS cells in severe combined immunodeficient (SCID) mice. Like ES cell teratomas, well reprogrammed iPS cells initiate teratomas that contain differentiated tissues from all three germ layers (endoderm, mesoderm and ectoderm) (Takahashi & Yamanaka, 2006). Another assay showing the ES properties of iPS cells is the aggregation of fertilized morulae with iPS cells in which competent iPS cells participate in chimerism and germline transmission (Okita et al, 2007; Stadtfeld et al, 2008a).

IPS cells also show a similar gene expression pattern to ES cells initiated by the removing of tissue specific epigenetic patterns, leading to an ES cell like expression of the proteome (Maherali et al, 2007; Mikkelsen et al, 2008; Takahashi & Yamanaka, 2006; Wernig et al, 2008). In both cell types the transcription factor Nanog is upregulated by KLF4 and the PI3K, MAPK and JAK/STAT pathways. These pathways are activated by Interleukin-6 (IL-6) family cytokines including Leukaemia Inhibitory Factor (LIF), a factor that is essential in the iPS/ES culture medium for mice **(Fig. 7)**. Nanog, OCT3/4 and SOX2 form a signalling loop for the mutual maintenance of expression. These three transcription factors are required to activate downstream pluripotency-associated genes. The feedback-loop can be interrupted by retinoic acid that inhibits OCT3/4 and leads to differentiation of the iPS cells; a protocol that is widely used to follow differentiation induced changes (reviewed in (Hanley et al, 2010)).

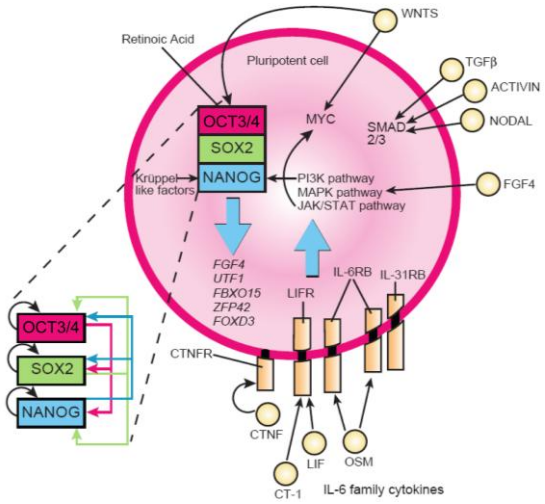

Figure 7: Cell signalling associated with the maintenance of pluripotency.
The binding of IL-6 family cytokines to their respective cell surface receptors activates PI3K, MAPK and JAK/STAT pathways. The MAPK pathway is also stimulated by FGF4. Smad 2/3 signalling is activated in the presence of TGFβ family ligands. WNT signalling is enhancing OCT3/4 expression and shares MYC as a common target with the JAK/STAT pathway. Krüppel-like factors and signals from the PI3K pathway stimulate the expression of Nanog. OCT3/4, SOX2 and NANOG form a signalling loop for the mutual maintenance and autregulate its expression. These three transcription factors also activate downstream pluripotency-associated genes including FGF4, UTF1, FBXO15, ZFP42 and FOXD3. Retinoic acid induces differentiation by inhibition of OCT3/4. Adapted from (Hanley et al, 2010).

3.11. TELOMERES IN iPS CELLS

After the introduction of iPS cells it became of great interest whether telomeres also acquire ES cell like characteristics such as elongated telomeres and a more open telomere chromatin structure. Indeed, similar to ES, iPS cells express high levels of telomerase. Active telomerase in post reprogrammed iPS cells drastically elongates telomeres to a length that is comparable to ES cells (Marion et al, 2009b). Moreover, telomeric chromatin structure of reprogrammed MEFs is altered during reprogramming. H3K9m3 and H4K20m3 heterochromatic marks are decreased in iPS cells compared to their parental cells, leading to a more open and plastic structure of telomeres (Marion et al, 2009b; Meshorer et al, 2006). Of note, and in agreement with the longer telomeres, TERRA (telomeric RNA) levels are increased in iPS cells when compared to the parental cells. TERRAs are thought to be a negative regulator of telomere length possibly counteracting telomere elongation in iPS cells once telomeres have become hyperlong (Marion et al, 2009b; Schoeftner & Blasco, 2008).

Cells with critically short telomeres have a decreased reprogramming efficiency indicating that there is a minimum telomere length necessary for efficient reprogramming (Marion et al, 2009b). Cells with critically short telomeres or missing shelterin components present high numbers of uncapped telomeres that give substrate to the DDR cascade that further initiates a p53 dependent cell cycle arrest, explaining the low reprogramming efficacy by genomic instability (Marion et al, 2009a). Abrogation of p53 bypasses the decrease in reprogramming in genomically unstable cells (Belmonte et al, 2009; Hong et al, 2009; Li et al, 2009; Marion et al, 2009a; Tejera et al, 2010).

3.12. TISSUE STEM CELLS

3.12.1. WHAT ARE TISSUE STEM CELLS?

Embryonic stem cells are cells with pluripotent capacity; i.e. they are able to differentiate to all cell types following the differentiation of the blastocyst inner cell mass. Once these cells initiate this process, they are dedicated to only one cell lineage and lose the ability to differentiate into cells of different tissues. Further, in the adult organisms, only a low fraction of cells remain in a fairly undifferentiated state keeping their potential to differentiate into the various cell types of a tissue. These adult tissue stem cells are located in dedicated regions, called the stem cell niches. The niche creates a microenvironment that is able to control stem cell behaviour and maintaining the undifferentiated state as postulated already in 1978 by

Schofield, much before the first tissue stem cell could be isolated (Hsu & Fuchs, 2012; Schofield, 1978). *In vivo* and in comparison to other cells of the tissue, stem cells are mainly slow cycling, have the capacity to replenish themselves and give rise to more committed, uni- or multipotent cells downstream in the cell-lineage. Thereby, different adult tissues have different requirements. In fast renewing tissues such as the intestine, the epidermis and blood, stem cells are constantly in use as they need to replace the lost cells continuously (Fuchs, 2009; Li & Clevers, 2011). Other tissues such as muscles and the brain are dormant and their stem cells are only activated upon stimuli such as learning or injury. This diverging stem cell behaviour is also found in cancer stem cells where they have been found to cycle in a fast and/or slower, dormant manner. New evidence also suggests slow and faster cycling stem cell in high turnover tissues (Hsu & Fuchs, 2012).

3.12.2. TELOMERASE IN TISSUE STEM CELLS

A basic level of active telomerase is found in tissue stem cells but its activity is not sufficient to maintain the telomere length over the organism lifespan (Collins & Mitchell, 2002). The erosion of telomere length is thought to be one of the underlying mechanisms of aging. The rationale is that “old” stem cells that have accumulated DNA damage have lowered proliferation potential. The subsequent loss of production of sufficient progenitors leads to the aged appearance of tissues. This, on the other hand reduces the risk of cancer induced by cells with genomic instability, explaining the advantage of a non-constitutively active telomerase (reviewed in (Collins & Mitchell, 2002; Shay & Wright, 2011)). The expression of active telomerase was found to be regulated to a certain extent by the WNT/β-catenin signalling that directly and indirectly (via KLF4) initiate TERT expression (Hoffmeyer et al, 2012). However, the precise regulation of the telomerase in tissue stem cells remains widely elusive to date.

Signalling pathways of tissue stem cells are widely understood. However, their location and valuable tissue stem cell markers are still not well defined. Therefore this field is under constant development. Below, I describe current knowledge concerning the skin and the small intestine stem cells.

3.12.3. SKIN STEM CELLS AND THE HAIR FOLLICLE

Hair follicles, the epithelial structure that gives rise to hair, develop within the early ectoderm when inductive and repressive signals allow the budding of hair follicle cells into the subcutis. Once established, the interfollicular epidermis and the sebaceous gland (SG) are subjected to constant self renewal, whereas the cells of the hair follicle (HF) lineage cycle

between growth (anagen), involution (catagen) and resting (telogen) phases **(Fig. 8A)**. The latter (HF cells) require therefore an extensive tissue expansion in anaphase whereas in catagen and telogen the cell turnover is minimal.

For a long time, using BrdU label retaining experiments as a trait to localize stem cells, it was believed that skin stem cells were located exclusively in the (telogen-) bulge region of the hair follicle. For above described reasons, the HF lineage stem cells retained BrdU for over two hair cycles and were believed to be the only cells in the hair follicle and skin with stemness potential (Cotsarelis et al, 1990). Recent findings however, have led to the development of a different view. Lineage tracing experiments, where whole tissues are rebuilt from one cell type widened the number of niches and initiated a new concept of adult skin stem cells. It is now believed, that the hair follicle contains a variety of stem cells **(Fig 8B)**. These stem cells, are divided into 3 pools (epidermal, sebaceous (SG), and hair follicle (HF)) and contribute to their distinct cell lineages in the hair follicle, replenishing cells that are lost by daily use. (Alonso & Fuchs, 2006; Cotsarelis et al, 1990; Fuchs & Horsley, 2008; Woo & Oro, 2011). We now know that all stem cells of the three different compartments, as seen in figure 8B (depicted is a telogen state hair follicle), can give rise to fully functional hair follicles, generating all the structures, including the corresponding niches with their stem cells. This is important in case of homeostasis disruption such as injury where whole stem cell pools might be lost. The different stem cells can be distinguished either by morphology or with help of different markers as seen in figure 8B (Barker et al, 2007; Fuchs & Horsley, 2008; Jensen et al, 2009; Levy et al, 2007; Snippert et al, 2010).

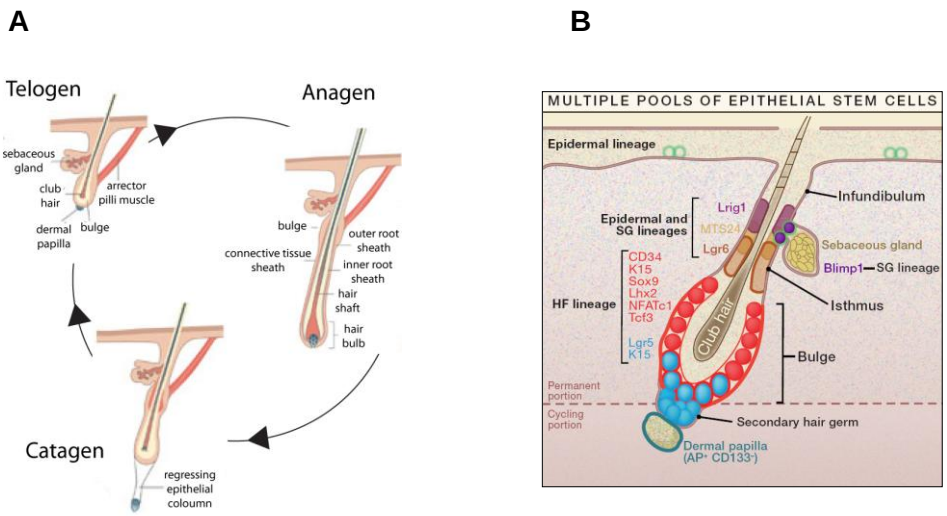

Figure 8: Hair follicle cycle and stem cell niches in the hair follicle

A: Simplified hair cycle depiction. Hair follicles grow synchronously; they cycle from the telogen state into anagen and then with apoptosis in the lower 3rd of the hair follicle they regress in catagen ending up in the resting telogen phase (Fuchs, 2007). **B:** Schematic depiction of a telogen hair follicle. Visible is its anatomy and the various stem cell lineages, niches and locations (Woo & Oro, 2011).

3.12.4. TELOMERES IN SKIN STEM CELLS

In 2008 Flores et al. established a new method to map the number of telomere repeats in a nucleus. The technique named “telomapping”, allows the comparison of telomeres within a tissue and therefore, to distinguish between nuclei with variable telomere lengths. In this method, telomeres are labelled by a CY3 fused telomeric-PNA probe as used in the established Quantitative-Fluorsecent *In Situ* Hybridisation (Q-FISH) telomere measurement techniques (see materials and methods). The average CY3 intensity measured for each nucleus is used to generate a heat map, representing the telomere length with a colourcode. The colder colours (green) depict nuclei with short telomeres and the warmer colours (red) correspond to long telomeres **(FIG. 9)**.

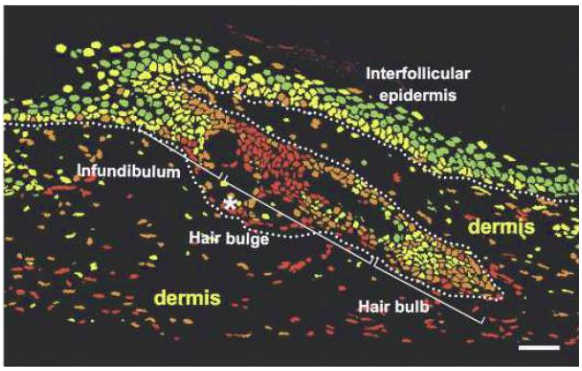

Figure 9: Hair follicle with a heat map according to the telomere length of each cell. The warmer the colour, the longer the telomeres per nuclei. The longest telomeres are found in the epidermal, sebaceous and hair follicle stem cell niches, here named as “Hair bulge”. (Flores et al, 2008)

Due to a lower cycling frequency and residual telomerase activity, cells in the adult stem cell niche are commonly those with the longest telomeres in a tissue. This effect allows the telomapping technique to localize adult stem cell niches, independent of *bona-fide* stem cell markers (Flores et al, 2008). In the skin, the longest telomeres were found in the bulge region, whereas the bulge region in the original publication was including the stem cells from the HF-, the SG- as well as some stem cells of the epidermal lineage (Fig 8 & 9). Telomere length decreased from these cells towards the bulb and the infundibulum with the shortest telomeres in the outer layers of the interfollicular epidermis **(Fig. 9)** (Flores et al, 2008). As visible in the above images the warm colours go along with stem cell markers (Lrig1, Lgr6, Blimp1, MTS24,...) that were recently established as seen in Fig. 8B (reviewed in (Woo & Oro, 2011).

3.12.5. SMALL INTESTINE

To maintain a constant nutrient uptake the small intestine in mammals completely renews itself every 3 to 5 days, putting the intestinal epithelium under high replicative pressure (Hsu & Fuchs, 2012). This high turnover is sustained by intestinal stem cells. It has been shown that different types of stem cells are responsible for the tissue homeostasis. On the one hand, there are cycling stem cells that express the G-protein-coupled receptor LGR5 **(Fig. 10)**. Lineage tracing experiments have shown that these cells have the potential to give rise to complete crypts and villi (Barker et al, 2007). On the other hand, there are the slow cycling, BrdU retaining stem cells localized above the strong LGR5 positive cells still expressing low amounts of LGR5 (position +4 to +7 from the crypt bottom). Not all the cells of this region are stem cells but lineage tracing experiments with various stem cell markers demonstrated that many of those cells are capable of establishing whole villi and crypt structures. (Montgomery et al, 2011; Sangiorgi & Capecchi, 2008; Takeda et al, 2011). This makes the LGR5 positive stem cells dispensable (Tian et al, 2011).

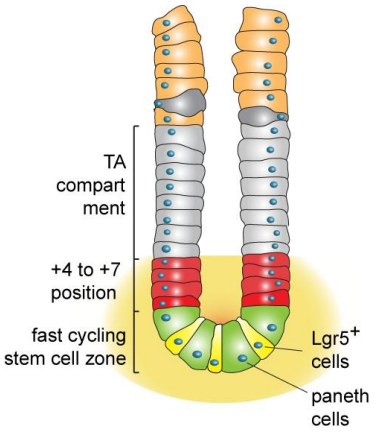

Figure 10: Intestinal crypt/villi

Organisation of an intestinal crypt where the Lgr5+ stem cells are depicted in yellow, interspersed with paneth cells (green). Further up are the +4 to +7 positioned stem cells that still express low amounts of Lgr5 followed by the transient amplifying (TA) compartment. Depicted in orange are the cells of the villi.

The lack of stem cell hierarchy and the functional equivalency led to the hypothesis that the slower cycling cells are mainly a reserve pool in case of tissue injury, whereas the faster-cycling Lgr5+ cells are of main importance for small intestine homeostasis (Hsu & Fuchs, 2012). Strengthening this theory is the fact that LRIG1, a *bona-fide* stem cell marker that was described in skin stem cells, is also present in the small intestine (Jensen et al, 2009; Wong et al, 2012). LRIG1 is a negative feedback regulator of ErbB which itself is driving cells towards differentiation. LRIG1 is therefore essential for maintaining stem cells multipotent (Gur et al, 2004; Jensen et al, 2009; Laederich et al, 2004; Wong et al, 2012). In the small intestine, as one of the first markers, it resembles both the cycling compartment and the slow cycling compartment of stem cells showing that both cell types have stem cells properties (Wong et al, 2012).

3.12.6. TELOMERES IN INTESTINE STEM CELLS

In the small intestinal epidermis, telomeres were compared using the telomapping technique (described in point 3.12.4). Also in this tissue the cells that were the most differentiated i.e. paneth and villi cells had the shortest average telomere length. They are followed by the transient amplifying cells and the stem cells with the longest telomeres (around position +4; **Fig 11A**) (Flores et al, 2008). This is in agreement with the general understanding of intestinal tissue homeostasis at the time this paper was published. The findings from Flores et al. are also in agreement with the findings that telomerase expressing cells are situated above the strong LGR5 expressing cells **(Fig. 11B)** (Montgomery et al, 2011). New insights into the intestinal tissue stem cell biology, especially the detection of the cycling LGR5 positive stem cells, interspersing the differentiated paneth cells, were not taken into account in the publication of Flores et al.. A telomere comparison was made in this thesis and is visible in the result part **(result Fig. 24B&D)**.

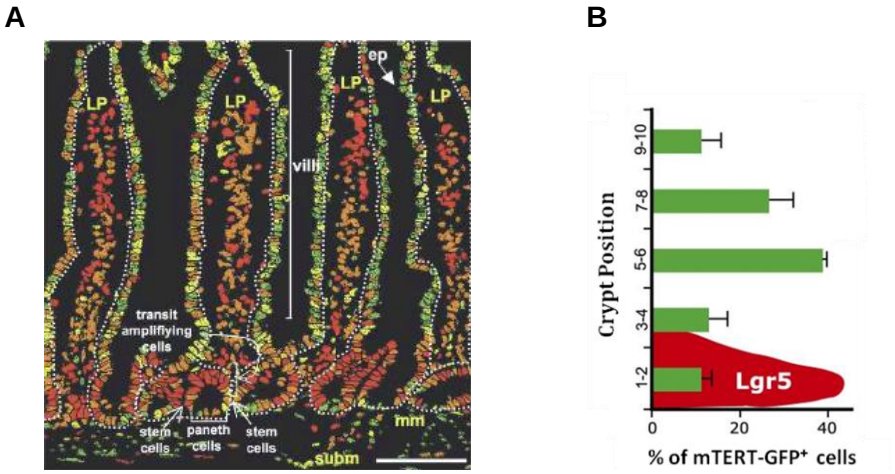

Figure 11: Telomap and telomerase expression of intestinal crypts

(A) Shown in this telomap are the nuclei with the least telomeric repeats (colder colours) in the villi epithelium as well as in nuclei at the crypt bottom. The crypt that is divided into transient amplifying- and stem cells shows longer telomere with the highest amounts of telomeric repeats in the stem cells (warm colours) (Flores et al, 2008). **(B)** Percentages mTERT-GFP expressing cells in the small intestine by their position in the crypt and percentage of the total number of GFP positive cells (Montgomery et al, 2011). This corresponds with the general understanding of the slow cycling stem cells above the strong LGR5 positive, cycling stem cells.

4. AIMS OF THE STUDY

1. Generate and characterize the phenotype of an eGFP-tagged TRF1 mouse model.
2. Study the abundance and distribution of eGFP-TRF1 in different tissues of the murine organism and its localisation within different tissues with respect to the telomere length.
3. Study the potential of TRF1 as a stemness indicator and its role in reprogramming.
4. Study possible mechanisms by which TRF1 can be regulated.

5. RESULTS

5.1. TRF1 DECREASES DISPROPORTIONALLY OVER AGE

Upon analysis of human and murine TRF1 in the interfollicular epidermis a 40% decrease of its expression from young to old individuals was observed (Figure 1A-D). As TRF1 binds the double stranded DNA portion of the telomere one would expect that the erosion of telomeres and the decrease of TRF1 seen at telomeres would occur approximately at the same rate. Interestingly, if compared to the telomere length decrease previously seen in mice (Flores et al, 2008), the decrease of mTRF1 is disproportional (mTRF1 decrease: 40% vs. telomere decrease: 2-3% (Flores et al, 2008)). Also in human, within the same tissue sections used for measuring the TRF1 expression, the telomere intensity measured by a tissue Q-FISH only decreased 16% (Figure 1E). This indicates that the amount of TRF1 bound to telomeres does not solely depend on telomere length and that its regulation might have further, yet unknown biological functions.

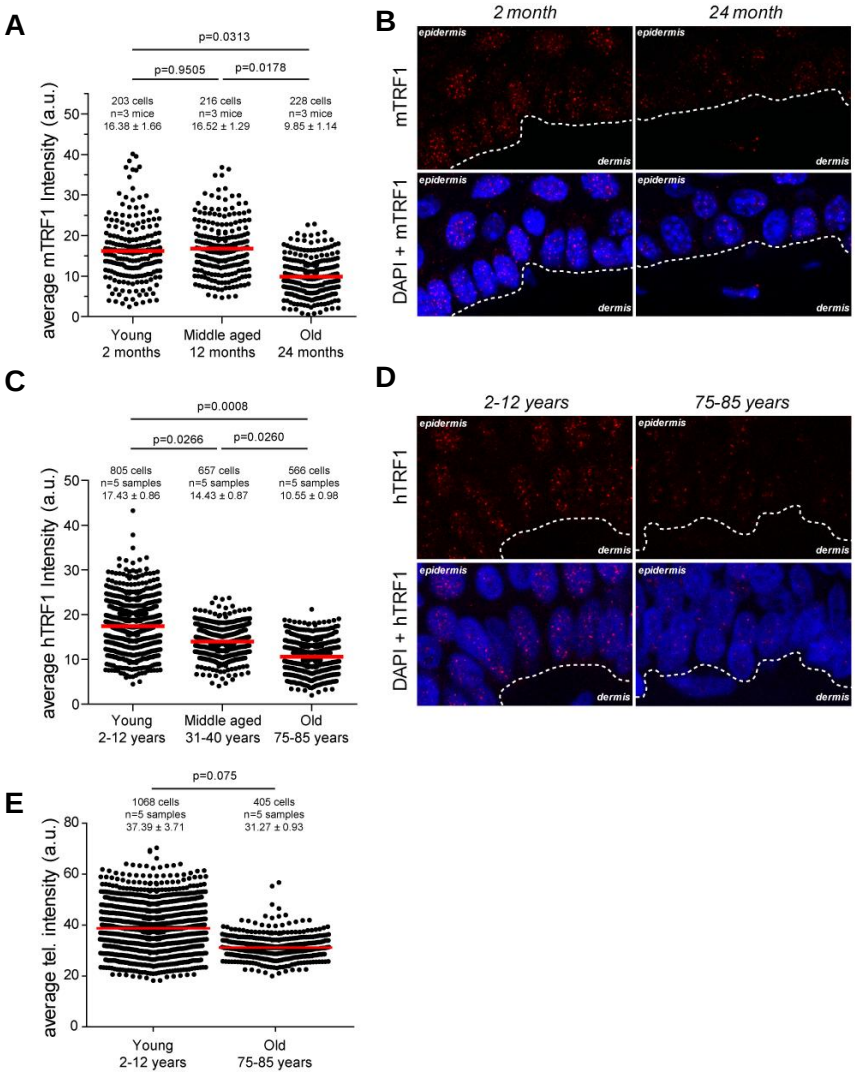

Figure 1: TRF1 decreases disproportionally and more than telomere length throughout human and mouse aging.

TRF1 quantification and representative pictures of murine (A&B) and human (C&D) tissue samples of back skin interfollicular epidermis of young, middle aged and old individuals. Ages are indicated. In both mouse and human, the decrease of TRF1 intensities is around 40%. Indicated is the average nuclear TRF1 intensity. Measurements of the telomere intensity per nucleus (of the same human tissue samples) showed under-proportional telomere erosion (16%) over age if compared to TRF1 expression (E). Statistical comparisons were done using one tailed student *t*-test.

5.2. GENERATION OF MICE WITH A *KNOCK-IN EGFP-TRF1* ALLELE

To further study the relation of TRF1 to telomere length and other possible roles of TRF1, we designed an eGFP-TRF1 *knock-in* construct from which a mouse was generated (materials and methods). The construct consists of an eGFP-tag inserted directly behind the ATG start-codon in the first exon of the TRF1 locus (Fig. 1A). The neomycin selection cassette was flanked by loxP sites and an additional crossing step with CMV-CRE mice was used to generate the eGFP-TRF1 allele **(Fig. 2A)**.

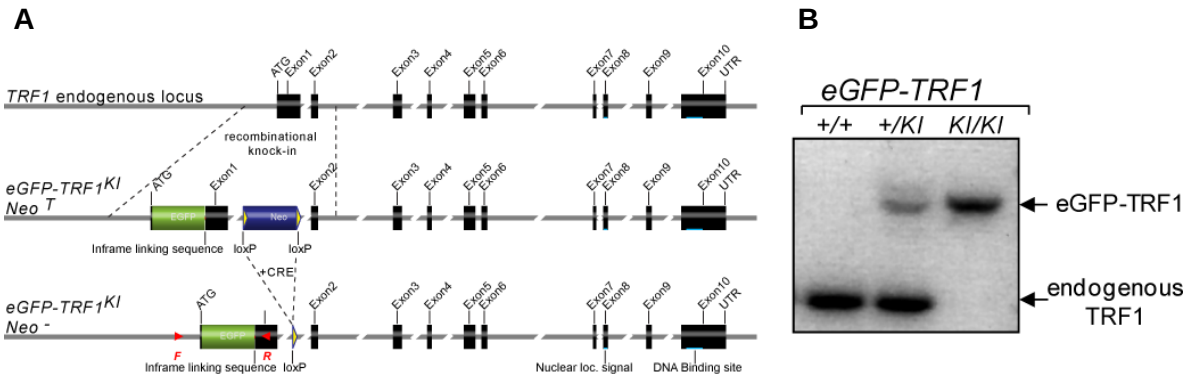

Figure 2: The *eGFP-TRF1* locus

(A) Schematic representation of the *TRF1* and the *eGFP-TRF1* allele. (B) Confirmation of the different alleles by PCR analysis. F/R: forward/reverse primer for PCR analysis, Neo: neomycin cassette.

Crosses between heterozygous *knock-in* allele carrying mice revealed that wild-type and heterozygous *eGFP-TRF1*$^{+/KI}$ mice were born following Mendelian ratios **(Fig 3A)**. They are viable and fertile and show no overt phenotypes previously related to TRF1 loss of function such as, loss of skin hair follicles, growth retardation and hyperpigmentation **(Fig. 3B-C)**; (Martinez et al, 2009). Nevertheless, we failed to obtain viable mice of the *eGFP-TRF1*$^{KI/KI}$ genotype, indicating embryonic lethality associated to this allele. Embryonic lethality occurred around day E13.5, as only 6% of the viable embryos were of the *eGFP-TRF1*$^{KI/KI}$ genotype versus the 25% expected ratio from *eGFP-TRF1*$^{+/KI}$ crosses **(Fig. 3A)**. As complete loss of function of TRF1 in mice leads to early embryonic lethality at the blastocyst stage (Karlseder et al, 2003), the observed late embryonic lethality of homozygous *eGFP-TRF1*$^{KI/KI}$ embryos suggests that the *eGFP-TRF1* allele is hypomorphic and the resulting fusion protein is partially functional.

Complete, conditional loss of function in of TRF1 was shown to lead to end-to-end fusions and presence of telomeres with multitelomeric signals (MTS) related to increased telomere fragility, as well as to drastic activation of a persistent DNA damage response

(DDR) at chromosome ends, which fully impairs cell division (Martinez et al, 2009; Sfeir et al, 2009). In line with this, although *eGFP-TRF1*$^{KI/KI}$ MEFs are able to divide *in vitro* (**Fig. 3D**), they show decreased proliferation rates and slightly increased senescence-associated β-gal staining if compared with wild-type and heterozygous cells **(Fig 3E)**, underlining the expected hypomorphic phenotype (Martinez et al, 2009; Sfeir et al, 2009).

A

birth ratios	+/+	+/KI	KI/KI
mendelian ratio	25%	50%	25%
obtained (abs. numbers)	30.6% (30)	69.4% (68)	0(0)

MEF ratios (E13.5)			
mendelian ratio	25%	50%	25%
obtained	28.6%(10)	65.7%(23)	5.7%(2)

Mice gender ratio	Female	Male
obtained	48%(47)	52%(51)

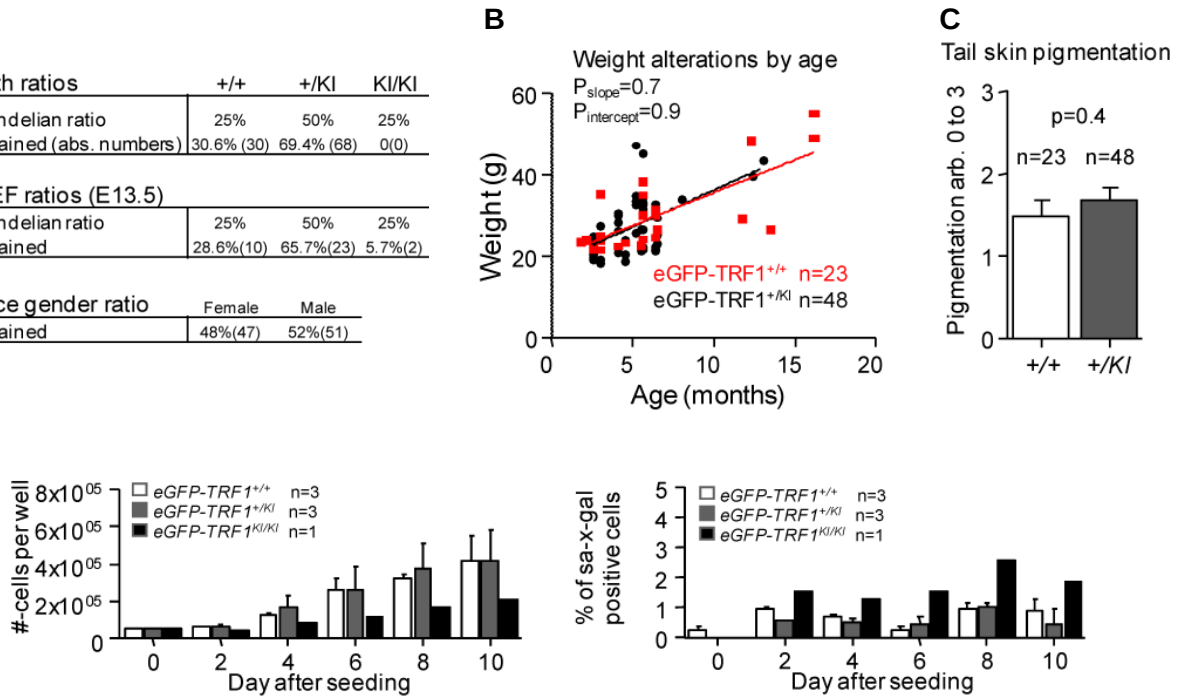

Figure 3: Phenotypes of the *eGFP-TRF1* allele.

(A) Birth-, MEFs- and gender-ratios (absolute numbers in brackets). Note the disproportional percentage of *eGFP-TRF1*$^{KI/KI}$ MEFs and the fact that no *eGFP-TRF1*$^{KI/KI}$ mouse is born. Wild-type and *eGFP-TRF1*$^{+/KI}$ MEFs and mice correspond to the expected Mendelian ratio. **(B)** Weight alterations over age are not detected in *eGFP-TRF1*$^{+/+}$ and *eGFP-TRF1*$^{+/KI}$ mice (male and female). Statistical calculations are done by linear regression *F*-Function for intercept and elevation. **(C)** Tail-pigmentation alterations could not be detected between wild-type and *eGFP-TRF1*$^{+/KI}$ mice. Error bars, SEM. Statistical comparisons were done using two tailed student *t*-test. **(D & E)** Growth- and senescence-curves (senescence activated β–gal) of *eGFP-TRF1*$^{+/+}$, *eGFP-TRF1*$^{+/KI}$ and *eGFP-TRF1*$^{KI/KI}$ MEFs (E11.5). No significant differences between *eGFP-TRF1*$^{+/+}$ and *eGFP-TRF1*$^{+/KI}$ MEFs are seen. Statistic comparisons with *eGFP-TRF1*$^{KI/KI}$ was not possible due to insufficient MEF harvest. MEF passage number=2; error bars, SEM. Statistical comparisons were done using two sided student *t*-test.

The lower proliferation rates in *eGFP-TRF1*$^{KI/KI}$ MEFs are concomitant with increased telomere fragility in these cells. This includes slightly augmented frequencies of sister telomere fusions (1-2 sister chromatid fusions per metaphase, a frequency that is 10-fold lower than that for a complete TRF1 abrogation) and increased frequencies of multitelomeric signals, to a level that is similar to TRF1-null MEFs **(Fig. 4 A-C)** (Martinez et al, 2009). However, this degree of telomere dysfunction in *eGFP-TRF1*$^{KI/KI}$ MEFs did not lead to a persistent DDR activation as indicated by similar frequencies of 53BP1-positive cells and by 53BP1 foci co-localizing with telomeres (telomere dysfunction induced foci, or TIFs) in all three genotypes **(Fig. 4 D&E)**. The fact that expression of the eGFP-TRF1 fusion protein does not lead to a persistent DDR activation is likely to reflect the largely normal telomere capping function of the fusion protein as indicated by very low frequencies of sister-chromatid end-to-end fusions in *eGFP-TRF1*$^{KI/KI}$ MEFs.

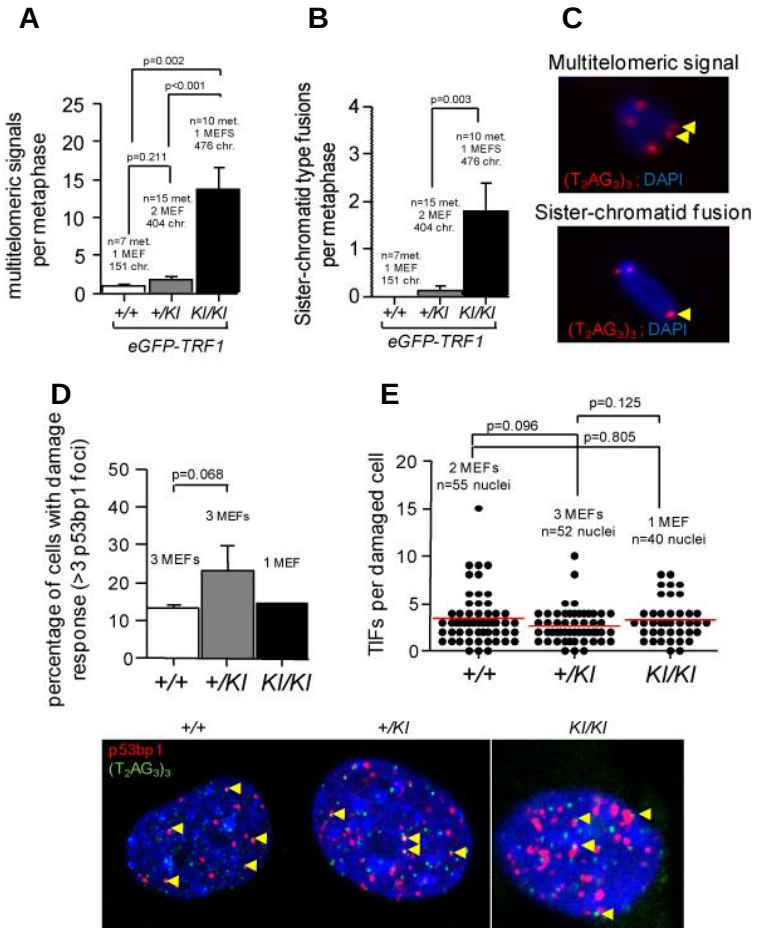

Figure 4: Elevated telomeric fragility in the absence of an increased DDR activation at *eGFP-TRF1*$^{KI/KI}$ telomeres.

(A) Detection of telomere fragility in MEFs by telomeres stained with a telomeric FISH-probe. Increased numbers of multitelomeric signals (MTS) and sister chromatid type fusions (SCF) **(B)** are found in the *eGFP-TRF1*$^{KI/KI}$ MEFs. **(C)** Yellow arrows in the representative images highlight MTS (top) and sister chromatid type fusions (bottom). Blue: dapi; red: telomers. **(D)** DNA-Damage Response (DDR) analysis by 53BP1 atibody in MEFs. Neither the percentage of 53BP1 positive/damaged cells nor the number of telomere dysfunction induced foci (TIF) **(E)** are significantly altered through the genotypes. Yellow arrows in representative pictures highlight TIFs, corresponding to the indicated genotype. Blue, dapi; red, 53BP1; green, telomeres. MEF passage number=2; error bars, SEM; Statistical comparisons were done using two sided student *t*-test.

5.3. THE EGFP-TRF1 FUSION PROTEIN IS NUCLEAR AND TRACKS TELOMERES *IN-VIVO*

The largely normal telomere capping in *eGFP-TRF1*$^{KI/KI}$ MEFs suggests that the fusion protein is able to bind and protect telomeres. To address this, we determined whether the expression of the eGFP-TRF1 fusion-protein was nuclear and co-localized with telomeres. As expected, we detected eGFP expression within the nuclei of living MEFs by confocal microscopy in both heterozygous- and homozygous-KI cells but not in wild-type cells **(Fig. 5A)**. Furthermore, eGFP expression co-localized with TRF1 and the shelterin proteins RAP1 and TPP1, as indicated by double immunofluorescence with antibodies against these proteins in *eGFP-TRF1*$^{+/KI}$ MEFs **(Fig. 5B)**. Together, these results indicate that the eGFP-TRF1 fusion protein is expressed in the nucleus and localizes to telomeres. This can be used as a new tool to track TRF1 expression as well as telomeres *in vivo* by using direct fluorescence. See below (chapter 5.4) for additional data with induced pluripotent stem (iPS) cells showing that eGFP-TRF1 is able to accomplish the known interactions with the members of the shelterin complex and that it is able to bind to telomeric DNA-repeats.

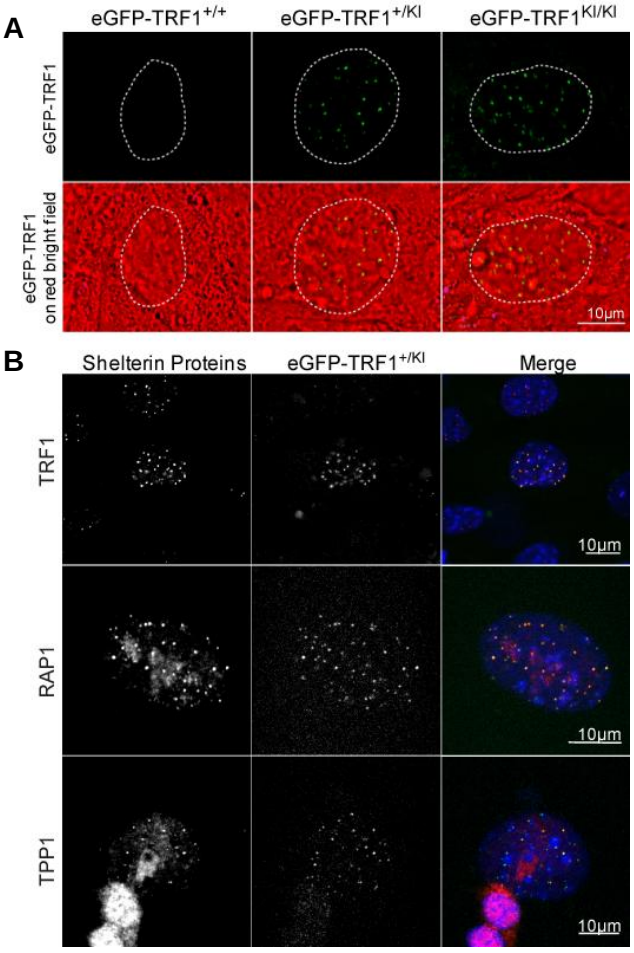

Figure 5. eGFP-TRF1 protein is nuclear and localizes to telomeres.

(A) Expression of eGFP-TRF1 fusion protein in living *eGFP-TRF1*$^{+/KI}$ and *eGFP-TRF1*$^{KI/KI}$ MEFs (passage 2). Top panels: eGFP-TRF1 fluorescence including red, contrasted bright field picture on the bottom to determine nuclear localization (nuclei are indicated by the dotted line). **(B)** Co-localization studies between the indicated shelterin proteins TRF1, RAP1 and TPP1 with eGFP-TRF1 in *eGFP-TRF1*$^{+/KI}$ MEFs (passage 2). Green, eGFP-TRF1; red, immunostained shelterins with 2nd antibodies labelled with Cy3 (TRF1 & Rap1) or A555 (TPP1).

5.4. HIGH TRF1 EXPRESSION IS ASSOCIATED TO INDUCTION OF PLURIPOTENCY IN INDUCED PLURIPOTENT STEM (iPS) CELLS

To address the regulation of TRF1 expression during nuclear reprogramming and pluripotency with active telomerase, we generated iPS cells from MEFs of the different genotypes. The efficacy of reprogramming was lowered in the homozygous *knock-in* whereas WT and heterozygous MEFs had similar efficiency **(Fig. 6A)**. Even though the KI/KI genotype led to a lower reprogramming efficacy, iPS cells from the three genotypes gave rise to chimeric mice upon morulae aggregation. However, the amount of chimerism in the *eGFP-TRF1*$^{KI/KI}$ aggregates was much lower compared to wild-type and heterozygous **(Fig. 6 B&C)**. On the other hand, KI/KI cells were capable of forming differentiating teratomas (see chapter 5.7). These results indicate that the *eGFP-TRF1*$^{KI/KI}$ iPS cells are pluripotent even though the parental MEFs show mild telomere fragility phenotypes and a lower percentage of chimerism.

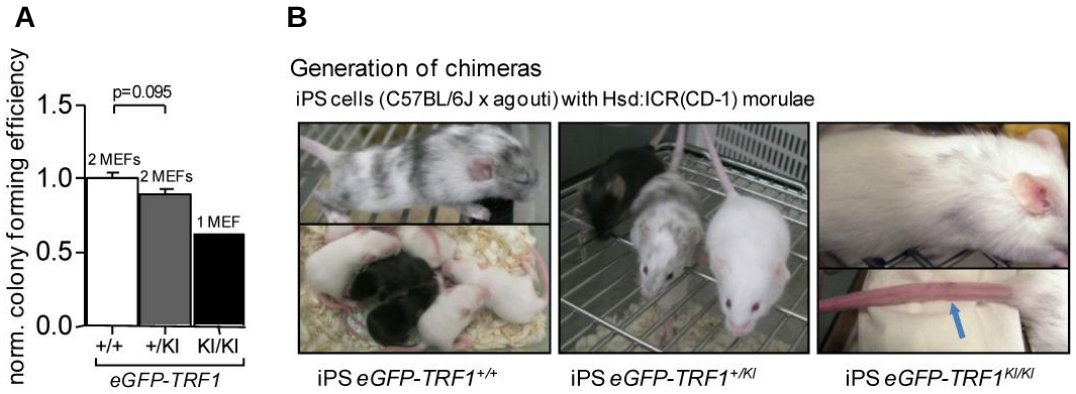

C

Chimera generation of eGFP-TRF1 iPS-clones; aggregation with HSD:ICR(CD-1) morulae.

iPS clone	Morulae aggregated	Cells injected	Pubs born	Chimeras Sex (% Pigmentation)
iPS 2-12 **eGFP-TRF1**$^{+/+}$(p4)	185	5-15	20	4M(100%); 1M (60%); 3BEP
iPS 2-8 **eGFP-TRF1**$^{+/+}$ (p4)	25	5-15		0
iPS 1-6 **eGFP-TRF1**$^{+/KI}$ (p4)	150	5-15	10	1M (50%)
iPS 2-1 **eGFP-TRF1**$^{+/KI}$ (p5)	195	5-15	19	1M (70%); 1M (60%); 1F (100%); 1BEP
iPS 1-7 **eGFP-TRF1**$^{KI/KI}$ (p4)	135	5-15	9	0
iPS 1-10 **eGFP-TRF1**$^{KI/KI}$ (p5)	67	5-15	7	1F(10%)

Abreviations: **M**: male, **F**: female, **BEP(s)**: black eyed pup (pups that died before fur characterization)

Figure 6. Generation of *eGFP-TRF1* iPS cells and chimeras

(A) Colony forming efficiency of reprogrammed MEFs normalized to WT. Alkaline phosphatase positive iPS colonies per optical field were counted. The efficiency is lowered in the eGFP-TRF1$^{KI/KI}$ MEFs by around 45% whereas the WT and heterozygous MEFs do not show a significant alteration. Error bars, SEM; statistical comparisons, using two sided student *t*-test. **(B&C)** Numbers and representative images of chimeric mice obtained from morulae aggregation (HSD:ICR (CD-1)) with iPS cells of the indicated genotype. In the case of *eGFP-TRF1*$^{KI/KI}$ iPS cells, only one chimeric mouse was obtained showing low chimerism. For the other genotypes we obtained chimeric mice with high chimerism.

We next performed a Chromatin Immunoprecipitation (ChIP) analysis in iPS cells to confirm that the eGFP-TRF1 fusion protein could bind telomeric repeats. We found, using eGFP specific antibodies, that eGFP-TRF1 was located at telomeric chromatin in both heterozygous *eGFP-TRF1*$^{+/KI}$ and homozygous *eGFP-TRF1*$^{KI/KI}$ iPS cells but absent from wild-type iPS telomeres **(Fig. 7A)**. As expected, in the heterozygous *eGFP-TRF1*$^{+/KI}$ cells around half the amount of telomeric repeats were detected by ChIP when compared to *eGFP-TRF1*$^{KI/KI}$ iPS cells **(Fig. 7B)**. To address whether expression of eGFP-TRF1 could interfere with the expression of the untagged TRF1 allele, we analyzed the levels of wild-type TRF1 in the heterozygous *eGFP-TRF1*$^{+/KI}$ iPS cells by western blot. As shown in **Fig. 7C,** expression of the eGFP tagged protein does not affect endogenous TRF1 expression (for quantitative western blot analysis, refer to Fig 8A&B). In order to further test the *in vivo* functionality of the eGFP-TRF1 protein when compared with the untagged TRF1 protein, we performed an immunoprecipitation using anti-GFP antibody in *eGFP-TRF1*$^{KI/KI}$*, eGFP-TRF1*$^{+/KI}$*, and eGFP- TRF1*$^{+/+}$ iPS cells and analyzed the isolated protein complexes by mass spectroscopy. This proteomic analysis showed that the telomere constitutive proteins TPP1, RAP1, TRF1, TIN2, and POT1 (de Lange, 2005) were specifically coimmunoprecipitated in both, the knock-in homozygous and heterozygous iPS cells **(Fig. 7C)**. These results clearly indicate that the eGFP-TRF1 protein interacts with the telomeric repeats (shown by the ChIP analysis: **Fig. 7D**) and with other members of the shelterin complex that are known to be pulled down together with TRF1.

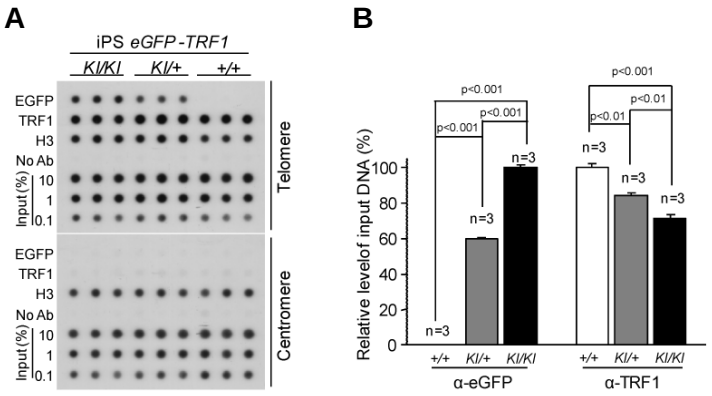

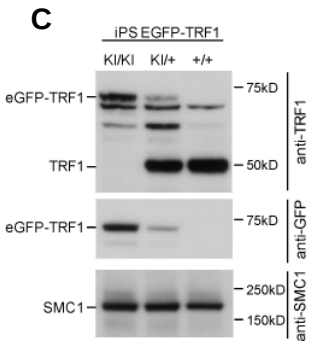

D

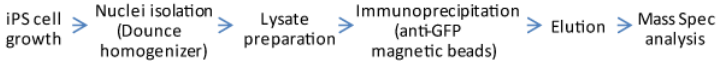

	TOTAL			EGFP-TRF1KI/KI				EGFP-TRF1KI/+			
Shelterin detected	ΣCoverage	Σ# PSMs	Σ# Peptides	Score	Coverage (%)	# PSM	# Peptides	Score	Coverage (%)	# PSM	# Peptides
TPP1	49.04	30	15	558.88	41.83	18	13	270.54	31.73	12	9
RAP1	46.31	18	13	398.64	43.26	13	12	166.65	16.54	5	5
TERF1	33.97	20	12	339.97	27.79	13	10	162.22	17.81	7	6
TIN2	21.98	10	8	78.62	19.32	7	7	68.76	10.63	3	3
POT1	13.44	7	7	122.85	9.53	5	5	34.04	3.91	2	2

Figure 7. Chromatin immunoprecipitation (ChIP) with iPS cells.

(A) Chromatin immunoprecipitation (ChIP) was performed with iPS cells of the indicated genotypes using antibodies against eGFP, TRF1 and H3 (control). Immunoprecipitated material was transferred to a nitrocellulose membrane and probed with a 1.6 kb telomeric probe (upper panel) and with a mouse major satellite probe (lower panel). **(B)** Quantification of ChIP values for telomere and centromere repeats, as indicated. The amount of immunoprecipitated DNA was normalized to the pre-immune serum (input). n= number of independent iPS clones used. Error bars, SEM; statistical comparisons, using two sided student *t*-test. **(C)** Western-blot analysis of *KI/KI*, *KI/+*, and +/+ *eGFP-TRF1* iPS cells. Note that the anti-TRF1 panel shows both eGFP-tagged and non-tagged TRF1 protein. The anti-GFP panel indicates that eGFP-TRF1 band is specific. Cohesin SMC1 was used as a loading control and molecular weights are indicated in the right part of the panels. **(D)** Schematic representation of the coimmunoprecipitation and mass spectroscopy proteins identification experiment and selected results of shelterin proteins. All identified peptides corresponding to shelterin proteins are indicated together with their coverage percentage, peptide spectrum matching (PSM) and the number of identified peptides (Peptides) in the *eGFP-TRF1*$^{KI/KI}$ iPS, *the eGFP-TRF1*$^{+/KI}$ iPS and in both iPS indicated as “total”.

We also addressed whether TRF1 expression itself and that of the eGFP-TRF1 fusion protein was regulated during reprogramming. To this end, we performed western blotting analysis where we found that endogenous TRF1 protein expression is highly increased, in wild-type iPS cell clones compared to their parental MEFs **(Fig. 8A&B)**. The increase of the TRF1 expression associated to reprogramming was in the same range as that of the pluripotency genes *Oct3/4* and Nanog, suggesting that TRF1 may be related to induction of pluripotency **(Fig. 8A&B)**. Western blotting analysis also showed induction of endogenous TRF1 in heterozygous *eGFP-TRF1*$^{+/KI}$ iPS, although to lower levels than *eGFP-TRF1*$^{+/+}$ iPS cells owed to the presence of a single copy of the endogenous *TRF1* gene, and was undetectable in homozygous *eGFP-TRF1*$^{KI/KI}$ iPS cells **(Fig. 8A&B)**. Inversely, the eGFP-TRF1 protein was highly expressed in *eGFP-TRF1*$^{KI/KI}$ iPS cells, to around half the levels in heterozygous *eGFP-TRF1*$^{+/KI}$ iPS cells, and was undetectable in wild-type iPS cells **(Fig. 8A&B)**. These results were also confirmed by FACS analysis, which showed that the eGFP-intensity in *eGFP-TRF1*$^{KI/KI}$ is approximately two fold higher compared to that seen in *eGFP-TRF1*$^{+/KI}$ **(Fig. 8C left)**. FACS analysis also confirmed similarly high Nanog expression in iPS cells of the three genotypes **(Fig. 8C right)**, supporting their pluripotency.

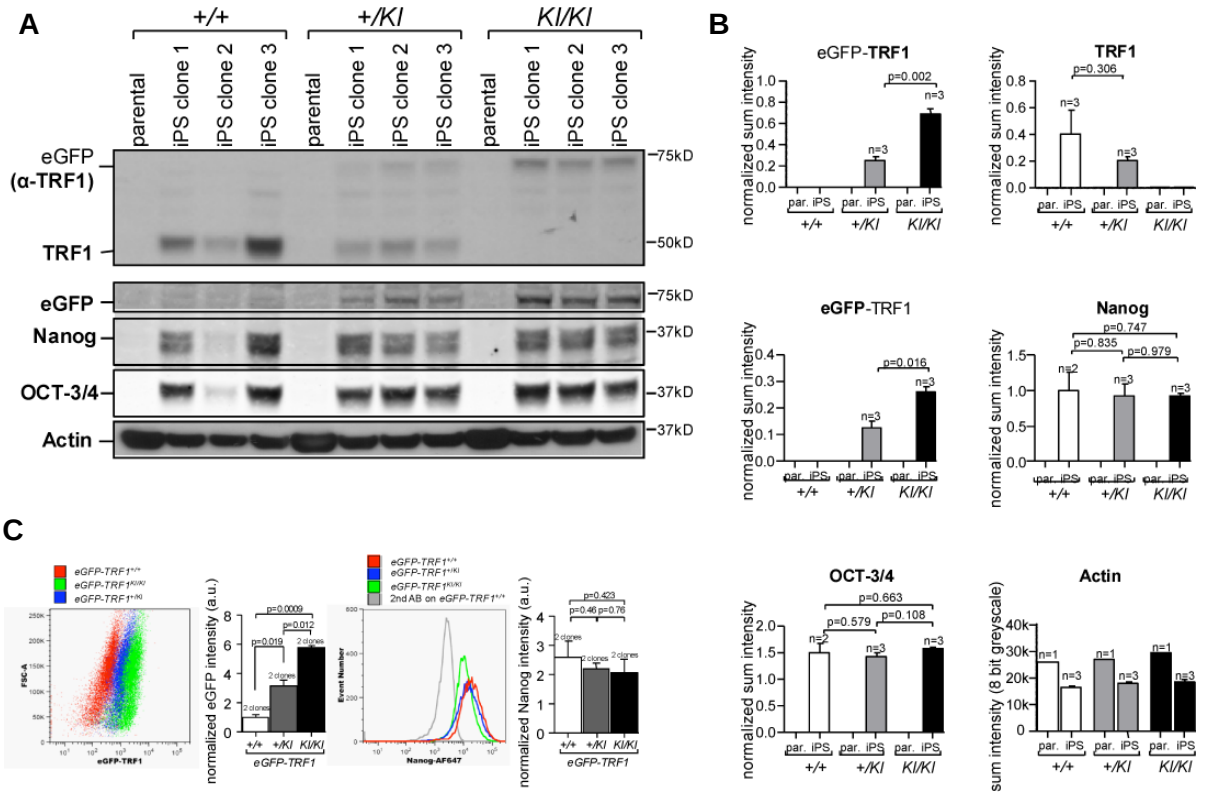

Figure 8. TRF1 gets highly upregulated during reprogramming

(A&B) Western blotting against eGFP, TRF1, Nanog, OCT3/4 and Actin (loading control) of nuclear fractions of passage 3 parental MEFs (par.) and three independent iPS clones (passage 5) derived from them. Note that not all the iPS clones are perfectly reprogrammed and therefore show a different proteome, visible in wild-type iPS clone 2 were TRF1, Nanog and OCT3/4 show lower expression. Normalization was performed by division of the intensity integral of specific bands by the intensity integral of the loading control (Actin). Error bars, SEM; statistical comparison: two sided student *t*-test. **(C)** FACS analysis of iPS cells (passage 7) of the indicated genotype shows similar results as obtained by western blotting (left). Nanog quantification of fixed iPS cells shows that the Nanog expression is not altered in the different genotypes. Red, *eGFP-TRF1*$^{+/+}$; Blue, *eGFP-TRF1*$^{+/KI}$; Green, *eGFP-TRF1*$^{KI/KI}$; Grey, *eGFP-TRF1*$^{+/KI}$ without 1st AB. Error bars, SEM; statistical analysis by two sided student *t*-test.

In summary, both endogenous TRF1 and the knock-in eGFP-TRF1 expression are dramatically activated upon induction of pluripotency, in a fashion that resembles that of the Oct3/4 and Nanog pluripotency genes. The high expression of Nanog and OCT3/4 in *eGFP-TRF1*$^{KI/KI}$ iPS clones is in agreement with successful generation of chimeric mice from these cells **(Fig. 6 B&C)**, and further supports generation of pluripotent iPS cells expressing fluorescent eGFP-TRF1.

5.5. eGFP-TRF1 LEVELS DO NOT CORRELATE WITH TELOMERE LENGTH DURING INDUCTION OF PLURIPOTENCY

Previous work showed that during the generation of iPS cells telomerase is activated and telomeres undergo a net telomere elongation, which continues post-reprogramming until reaching the hyper-long telomeres of ES cells (Marion et al, 2009b). To address whether eGFP-TRF1 fluorescence correlated with telomere length *in vivo*, we determined telomere length at different passages of iPS cells by using the telomeric Q-FISH technique directly on fixed iPS colonies. IPS cells (P7) from all the three genotypes were able to elongate telomeres to a similar extent compared to the telomeres of corresponding parental MEFs **(Fig. 9A-C)**. Strikingly, however, while wild-type and *eGFP-TRF1*$^{+/KI}$ telomeres continued growing with increasing passages until reaching hyper-long ES cell telomeres at passage 36, the telomeres of *eGFP-TRF1* homozygous iPS cells ceased to further elongate between passage 7 and 16 **(Fig. 9C)**. The inability of *eGFP-TRF1*$^{KI/KI}$ iPS cell telomeres to show further elongation might be related to increased telomeric aberrations in this genotype, mostly consisting of MTS, or may suggest a role of TRF1 in telomerase recruitment which is partially impaired by the eGFP-TRF1 fusion protein. In this regard, TPP1, a TRF1-interacting protein, was previously described to be required for telomerase-mediated telomere elongation during reprogramming (Tejera et al, 2010). These results highlight the importance of TRF1 for telomere length maintenance *in vivo*, and could provide a mechanistic explanation for the short telomere phenotype associated to some human diseases linked to putative defects in shelterin function (Savage et al, 2008; Savage et al, 2011).

Next, we measured the eGFP-TRF1 intensity per telomere and per nucleus to address whether it was directly correlated with telomere length changes during reprogramming. No linear correlation between telomere length and eGFP intensity was observed. In particular, while telomere length increased by about 1.7-fold when comparing MEFs with iPS cells at passage 7 **(Fig. 9B)**, the eGFP intensity increased by >20-fold at this point (underestimating the eGFP intensity by saturated detection due to weak signal in the parental clones and 2D analysis) **(Fig. 9E)**. Furthermore, while eGFP-TRF1 levels were maintained stable from passage 7 onwards, telomeres kept elongating until passage 36 **(Fig. 9B,C,E,F)**. This suggests that increased TRF1 level at the induction of pluripotency precedes telomere elongation, again in line the notion that elevated TRF1 levels are characteristic of the pluripotent state. These results are in accordance with the findings in figure 1, where TRF1 levels were shown to decrease independent of telomere shortening over age.

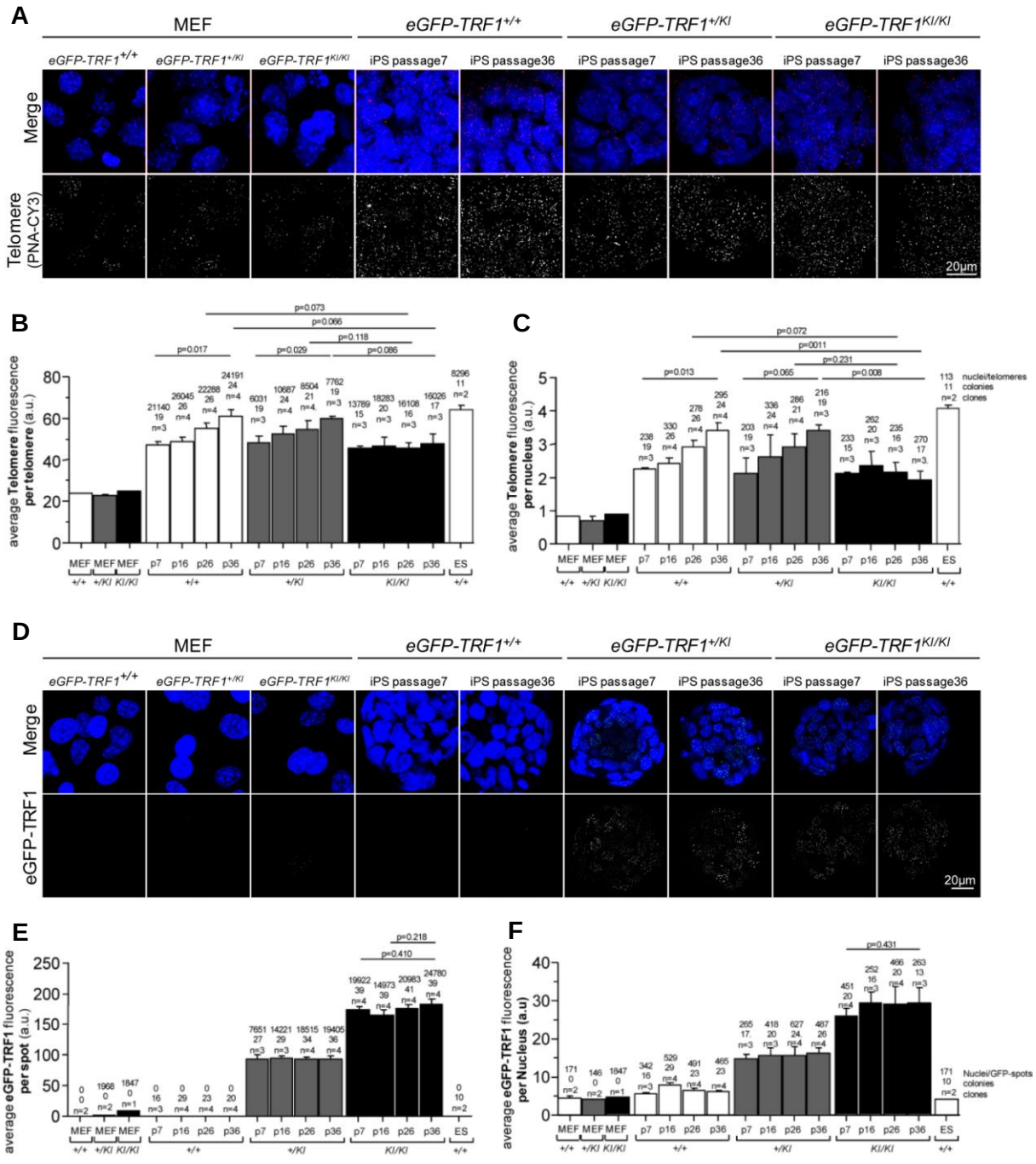

Figure 9. Defective telomere length maintenance in eGFP-TRF1 homozygous iPS cell clones.

(A) Representative images of parental MEFs (passage 3) and iPS cells of indicated genotype and passages, labelled with a telomeric Q-FISH probe. Pictures were enhanced equally for better visibility. Blue, Dapi; red/grey, tel-PNA-Cy3 probe. **(B)** Analysis of average telomere fluorescence per telomere of the indicated MEFs (passage 3) and increasing passages of corresponding iPS cell clones. ES cells at passage 9 were included as controls. Statistical comparisons were done using two sided student *t*-test. Error bars, SEM. **(C)** Analysis of average telomere fluorescence per nucleus of the indicated MEFs (passage 3) and increasing passages of corresponding iPS cell clones. Wild-type ES cells at passage 9 were included as controls. Statistical comparisons were done using two sided student *t*-test. Error bars, SEM. **(D)** Representative image of parental MEF (passage 3) and iPS cells of indicated genotype and passages analyzed for eGFP-TRF1. Pictures were enhanced equally for better visibility. Blue, Dapi; green/grey, eGFP-TRF1 fluorescence. **(E, F)** Analysis of the relative eGFP-TRF1 expression in parental MEFs (passage 3) and iPS cells of the corresponding genotype and passage number. Intensity of eGFP-TRF1 per telomere spot (E) and per nucleus (F) was measured. Statistical comparisons were done using two sided student *t*-test. Error bars, SEM. ES at passage 9 are included as controls.

To confirm our results and to exclude analysis artefacts, we studied TRF1 protein levels during reprogramming of MEFs deficient for TPP1 previously shown by our lab to fail to elongate telomeres in the process of generation of iPS cells (Tejera et al, 2010). To this end we used *Tpp1*$^{lox/lox}$ MEFs transduced with a lentiviral vector expressing Cre-shp53. Strikingly TRF1 levels were highly upregulated in *Tpp1*$^{\Delta/\Delta}$ *Cre-shp53* iPS cells when compared to the parental MEFs reaching similarly high levels to those of wild-type controls **(Fig. 10A,B)**. These results clearly demonstrate that TRF1 upregulation at the induction of pluripotency is uncoupled from telomere elongation by telomerase.

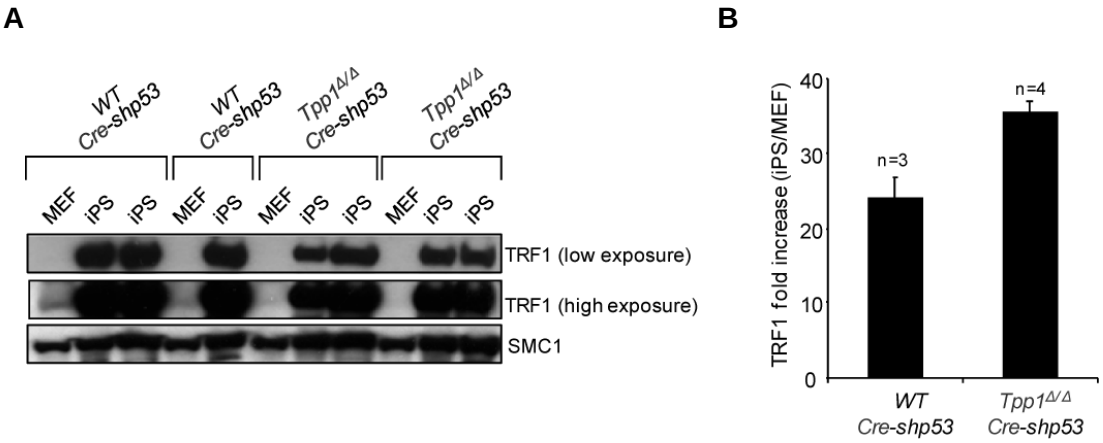

Figure 10. TRF1 is uncoupled from telomere elongation.

(A&B) TRF1 is highly over expressed in iPS cells, even in the absence of telomere elongation. **(A)** Expression of TRF1 in *wild-type* and *Tpp1*$^{\Delta/\Delta}$ MEF- and iPS cells as detected by western-blot. Note that TRF1 expression is highly increased in iPS cells if compared to parental MEF, even in *Tpp1*$^{\Delta/\Delta}$ iPS cells that do not elongate telomeres during reprogramming. SMC1 was used as a loading control for nuclear extract. **(B)** Quantification of TRF1 from A, relative to SMC1. Error bars, SEM. n= independent iPS clones.

5.6. TRF1 EXPRESSION POSITIVELY CORRELATES WITH NANOG PROTEIN EXPRESSION IN IPS CELLS

To confirm the effects seen above, the experiment was repeated in a less automated manner. We studied the distribution of eGFP fluorescence in iPS cell clones of the different genotypes compared to the parental MEFs. In agreement with increased TRF1 expression associated with reprogramming, average eGFP-TRF1 fluorescence per nucleus was increased in *eGFP-TRF1*$^{+/KI}$ and *eGFP-TRF1*$^{KI/KI}$ iPS colonies compared to the parental MEFs **(Fig. 11A&B)**. We also observed a significant increase in telomere length in all genotypes (on metaphase spreads), in agreement with telomere elongation during reprogramming **(Fig. 11C&D)** (Marion et al, 2009b). After normalization with wild-type eGFP-

background values, *eGFP-TRF1*$^{KI/KI}$ iPS colonies showed approximately double the amount of eGFP compared with the *eGFP-TRF1*$^{+/KI}$ iPS colonies **(Fig. 11A&B)**. Intriguingly, we observed that eGFP-TRF1 fluorescence was not homogenously distributed and varied greatly from nucleus to nucleus within the same iPS cell colony **(Fig. 11B)**, suggesting that not all cells within an iPS cell colony are identical with respect to TRF1 expression .

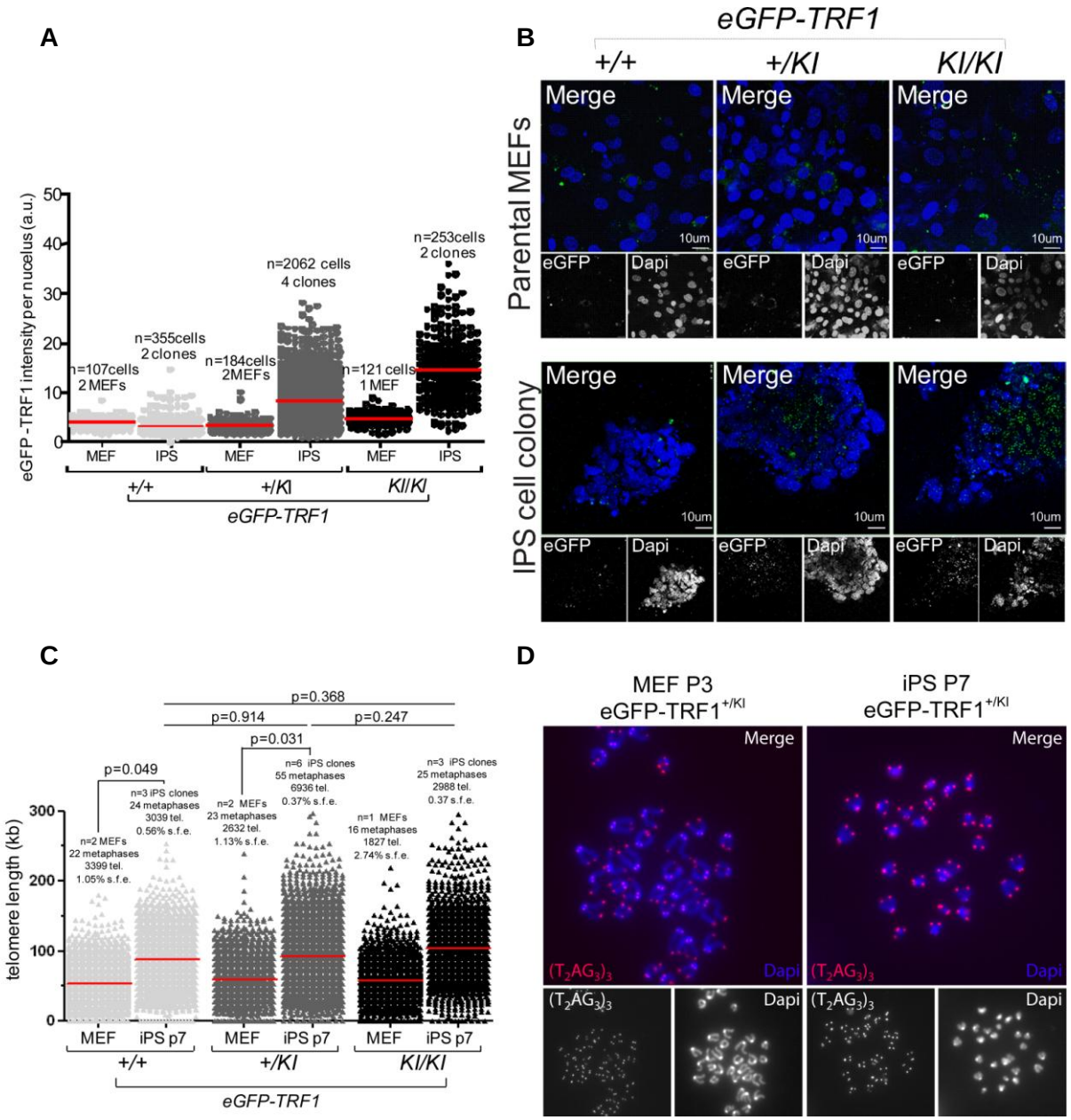

Figure 11. Increased eGFP-TRF1 expression after nuclear reprogramming.

(A) Quantification of eGFP-TRF1 expression in indicated genotypes and cell types. Values indicate the average eGFP-TRF1 intensities per nucleus. **(B)**. Blue, dapi; red, telomeres. MEF passage number =3, iPS passage number =6. **(C)** Analysis of a telomeric metaphase Q-FISH, measuring the telomere lengths of iPS cells and their corresponding MEFs. Differences in the telomeric length from MEF to iPS are similar in all three genotypes. Note, the increase in telomere length of *eGFP-TRF1*$^{+/KI}$ and *eGFP-TRF1*$^{KI/KI}$ iPS cells is underproportional to the average increase of eGFP-TRF1 expression in A&B. MEF passage number =3, iPS passage number =7. Statistical comparisons were done using two sided student *t*-test. (D) Representative pictures of the Q-FISH stained telomeres (red) in parental MEFs (left) and their corresponding iPS cell (right).

To understand the nature of the cell-to-cell eGFP-TRF1 heterogeneity in iPS colonies, we performed double immunofluorescence with OCT3/4 and Nanog antibodies. It has been previously reported that Nanog levels fluctuate and are not homogenous within ES and iPS cell cultures (Chambers et al, 2007; Villasante et al, 2011). Interestingly, we observed a positive correlation between Nanog and eGFP-TRF1 protein levels in *eGFP-TRF1*$^{+/KI}$ and *eGFP-TRF1*$^{KI/KI}$ nuclei **(Fig.12A)**. So that 50% of the iPS cells showing higher eGFP-TRF1 expression were also found to have higher Nanog expression than 50% of iPS cells with lower eGFP fluorescence **(Fig. 12B&C)**. Of note, a similar correlation was not observed in the case of OCT3/4 protein levels, which are also greatly upregulated in iPS colonies **(Fig. 12A top right picture),** further supporting a specific correlation between eGFP-TRF1 and Nanog protein levels. We confirmed this positive correlation between Nanog and eGFP-TRF1 by using flow cytometry analysis **(Fig. 12D&E)**. In particular, we separated the cells into G1 (2n) and G2 (4n) populations and each cohort of the eGFP-TRF1 expressing cells were further split into high and low Nanog expressing cells (ratio 1:1 see materials and methods). Concomitant with results obtained by immunofluorescence, we found increased eGFP-TRF1 expression in the Nanog^{high} compared to Nanog^{low} cells both in heterozygous-KI and homozygous-KI iPS cells. The results obtained in heterozygous iPS cells were not significant, most likely due the low eGFP intensity which is difficult to detect by our instruments **(Fig. 12D)**.

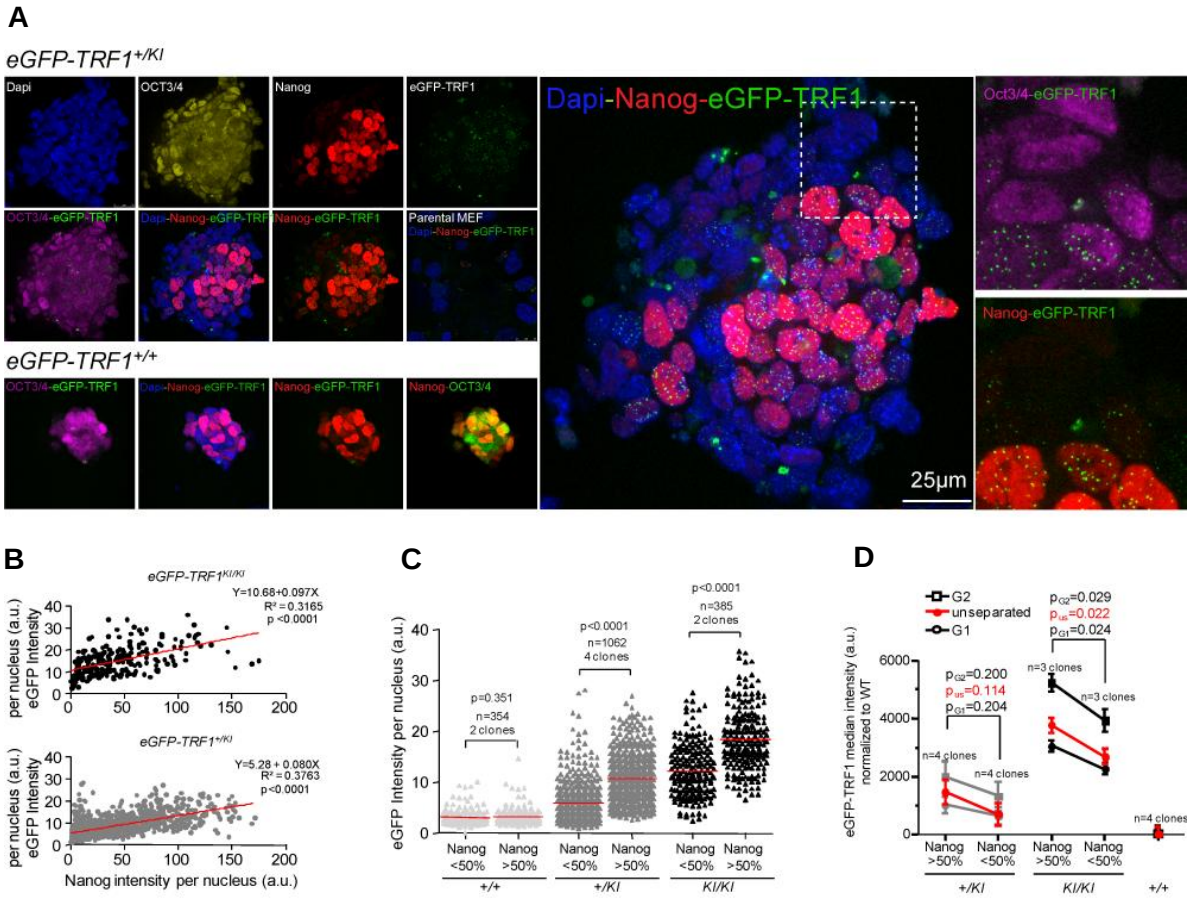

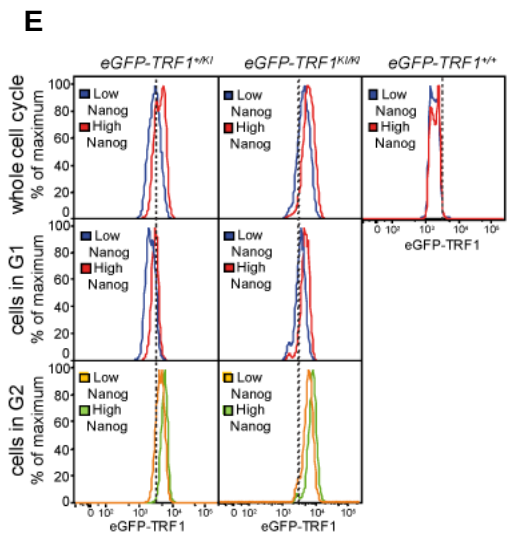

Figure 12. Expression of eGFP-TRF1 in iPS cells is correlated with high levels of Nanog

(A) Staining of iPS colonies (passage 6) with antibodies against Nanog and OCT3/4. Note that the eGFP-TRF1 expression pattern is similar to that of Nanog. IPS passage number 6. **(B+C)** Analysis, showing the positive correlation between eGFP-TRF1 fluorescence intensity and Nanog expression levels in *eGFP-TRF1*$^{+/KI}$ and *eGFP-TRF1*$^{KI/KI}$ iPS cells (passage 6). Analysis depicts mean fluorescence intensities of eGFP-TRF1 and Nanog per nucleus. Statistical comparison in B was done using two sided student *t*-test and in C by linear regression analysis. **(D&E)** FACS analysis of wild-type, *eGFP-TRF1*$^{+/KI}$ and *eGFP-TRF1*$^{KI/KI}$ iPS cells (passage 7) grouped into Nanog^{low}- and Nanog^{high} expressing cells (1:1). A positive correlation between *eGFP-TRF1* expression and Nanog-expression is found, similar to findings in parts B&C. Cell cycle states where separated by Hoechst staining. Statistical comparison was done using paired student *t*-test; us: unseparated

Next, we addressed whether the positive correlation between eGFP-TRF1 and Nanog protein expression also occurred at the transcriptional level. To this end, we sorted live iPS cells (in G1 cell cycle state) into eGFP-TRF1 high and low expressing cells (40%:40%) and analyzed Nanog mRNA levels by RT-qPCR. First, we confirmed increased *egfp-trf1* mRNA levels in heterozygous-KI and homozygous-KI iPS cells compared to wild-type iPS cells. *EGFP-TRF1*$^{+/KI}$ iPS cells showed approximately half the expression of *egfp-trf1* if compared to *eGFP-TRF1*$^{KI/KI}$ iPS cells **(Fig. 13A)**. According to expectations from immunostainings, eGFP^{high} iPS cells showed more Nanog mRNA expression than eGFP^{low} cells in both heterozygous-KI and homozygous-KI clones **(Fig. 13A)**. As control, Nanog mRNA was undetectable in wild-type MEFs and greatly elevated in the corresponding wild-type iPS cells **(Fig. 13A)**. Of note, *oct3/4* mRNA levels were similar in eGFP^{high} and eGFP^{low} iPS cells in both heterozygous-KI and homozygous-KI clones. Interestingly, eGFP-TRF1^{low} iPS cells that were grown for 3 days in gelatin coated dishes, were capable of re-establishing new iPS cell colonies with high expression of Nanog and eGFP-TRF1 **(Fig. 13B)**, suggesting that high TRF1 levels can be re-established.

Also in agreement with eGFP-TRF1^{high} pluripotent cells within iPS populations, we found elevated *mtert* mRNA levels in eGFP^{high} iPS cells compared to eGFP^{low} iPS cells (Agarwal et al, 2010). Elevated *mtert* expression in the eGFP^{high} iPS cells also correlated with longer telomeres in these cells compared to the eGFP^{low} iPS cells **(Fig. 13C**). In summary, both, the pluripotency markers, Nanog and *mtert* as well as telomere length are increased in the eGFP^{high} iPS cells compared to eGFP^{low} iPS cells, suggesting that elevated *egfp-trf1* mRNA levels correlate with increased pluripotency.

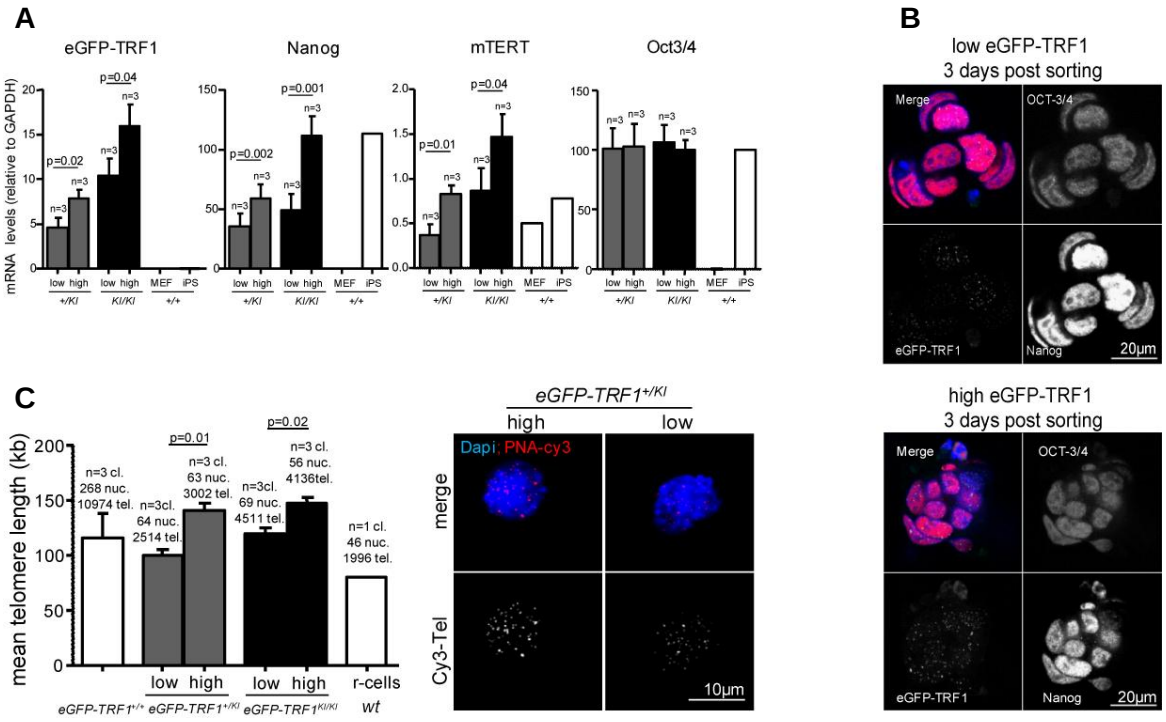

Figure 13. eGFP-TRF1 levels correspond with Nanog, mTERT and telomere length

(A) mRNA levels of *Nanog, Oct3/4, mTert*, and *eGFP-TRF1* in *eGFP-TRF1*$^{+/KI}$ and *eGFP-TRF1*$^{KI/KI}$ iPS clones (passage 7) after sorting for eGFP-TRF1 high and low levels (40%:40%) in the G1 cell cycle state. A positive correlation between eGFP-TRF1 fluorescence and mRNA levels of *egfp-trf1,* Nanog and *mtert* but not for *oct3/4 was observed*. Statistical analysis is done with paired *t*-tests. Error bars, SEM. **(B)** IPS cells sorted for high and low levels *eGFP-TRF1*$^{+/KI}$ are both able to re-establish the pattern of known pluripotency markers such as Nanog (merge (red); bottom right hand picture, grey) and OCT3/4 (top right hand picture). Also depicted are eGFP-TRF1 (merge (green); bottom left hand picture) and Dapi (merge (blue)). **(C)** Telomere length analysis by telomeric Q-FISH of *eGFP-TRF1*$^{+/KI}$ and *eGFP-TRF1*$^{KI/KI}$ iPS-cells sorted according their eGFP-TRF1 content. Analyses of telomere-lengths show an increased telomere length in cells with high eGFP-TRF1 levels. Telomere length was calculated from the known telomere length of the "r" cell line (Experimantal Procedures). IPS passage number: 6-7. Statistical analysis is done with single sided paired *t*-tests. Error bars, SEM.

Finally, we addressed whether the higher amounts of eGFP-TRF1 in pluripotent iPS cells were associated with the pluripotent state *per se* or could be related to increased division rates in these cells. To this end, we grew iPS cells on gelatine coated dishes in a medium containing fetal bovine serum (FBS), which is known to induce increased proliferation and loss of pluripotency (Bryja et al, 2006; Cheng et al, 2004). As expected, iPS cells grown under these conditions showed increased proliferation rates (**Fig. 14A).** On the other hand, eGFP-TRF1 expression was decreased in *eGFP-TRF1*$^{KI/KI}$ iPS cells after 4 days in FBS. The same trend was seen in the faster cycling *eGFP-TRF1*$^{+/KI}$ cells. The non significant decrease can be explained with the low eGFP-intensity in heterozygous cells that is close to the detection limit of the cytometer **(Fig. 14B)**. The eGFP-TRF1 decrease was concomitant with a change in cell morphology towards a more differentiated state, known to

resemble the properties of the primary endoderm and the trophoectoblast **(Fig. 14C)** (Bryja et al, 2006; Cheng et al, 2004). These findings indicate that high eGFP-TRF1 expression in iPS cells is associated to pluripotency and lost upon differentiation of these cells, independent of the cell cycle frequency.

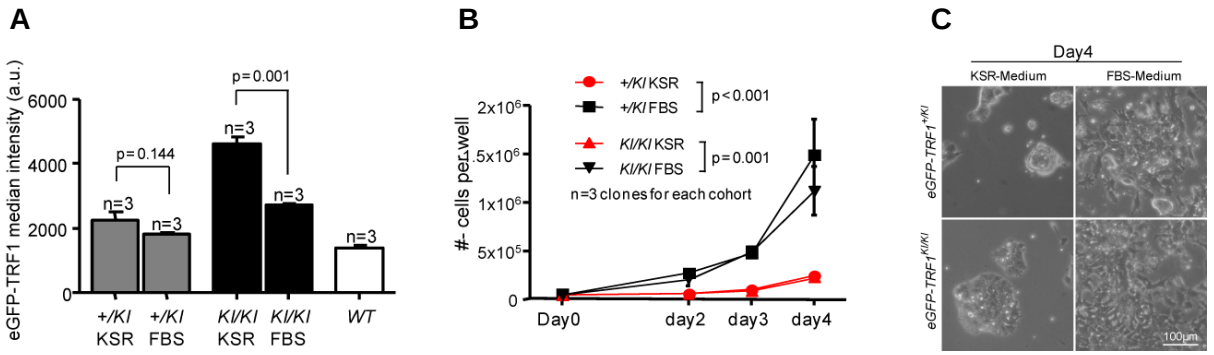

Figure 14. Expression level of eGFP-TRF1 does not correlate with the replication frequency.

(A) *eGFP-TRF1*$^{+/KI}$ (*+/KI*) and *eGFP-TRF1*$^{KI/KI}$ (*KI/KI*) iPS clones grown on gelatine for four days in medium with knockout serum replacement (KSR) or in medium with fetal bovine serum (FBS). Cells cultured in FBS medium show lower eGFP intensities as measured on trypsinised and alive cells by flow cytometry. Statistical analysis is done on median values with single sided paired *t*-tests. Error bars, SEM. **(B)** IPS cells grown in FBS medium show significantly increased proliferation rates compared to the same clones grown in KSR medium. Cell count was done with standard Neubauer cytometry. Statistical analysis is done with the two way ANOVA test. Error bars, SEM. **(C)** Representative images of *eGFP-TRF1*$^{+/KI}$- and *eGFP-TRF1*$^{KI/KI}$-clones at day 4 of FBS addition. In the left column we see the clones grown in KSR and on the right, the same clones grown in medium containing FBS. The cells on the right hand side show a clear pattern of differentiation.

5.7. eGFP-TRF1^{HIGH} CELLS REPRESENT A SUBPOPULATION OF iPS CELLS WITH HIGHER PLURIPOTENCY POTENTIAL

To further determine the properties of eGFP^{high} iPS cells compared to eGFP^{low} iPS cells, we tested their respective abilities to form chimeras and teratomas, an indication of their pluripotency potential. To this end, we sorted eGFP^{high} and eGFP^{low} iPS (eGFP-TRF1$^{+/KI}$) cells in the G1 cell cycle state (avoiding possible differences in telomere numbers and therefore eGFP-TRF1 levels; see in experimental procedures). For teratoma formation, we injected the sorted iPS cells with the highest and lowest (40%:40%) eGFP-TRF1 fluorescence into the flanks of nude mice. Strikingly, only the eGFP-TRF1^{high} sorted iPS cells were capable of forming teratomas and no teratomas were obtained with the eGFP-TRF1^{low} sorted iPS **(Fig. 15A&B)**. Furthermore, teratomas obtained from eGFP-TRF1^{high} sorted iPS cells showed all three germ layers indicating that they are pluripotent **(Fig. 15C)**. Similar to the iPS colonies in vitro, expression of eGFP-TRF1 highly correlated with the expression of Nanog in teratoma sections, indicating that the undifferentiated regions expressed higher amounts of eGFP-TRF1 compared to more differentiated areas **(Fig. 15D&E)**. This confirms

that TRF1 expression is an indicator of the degree of differentiation within the tumor. Wild-type iPS cells were not able to form teratomas when injected into nude mice. This, might be due to the limited amount of cells (1.5x10^6 cells per injection) that can be sorted and used for this experiment as well as the harsh sorting environment. Further, it points to a positive selection for pluripotent iPS cells of the *eGFP-TRF1$^{+/KI}$* genotype. Cells that are administered without sorting (2x10^6 cells per injection) are able to form teratomas and differentiate into all the 3 germ layers. However, they have a later onset and show growth retardation.

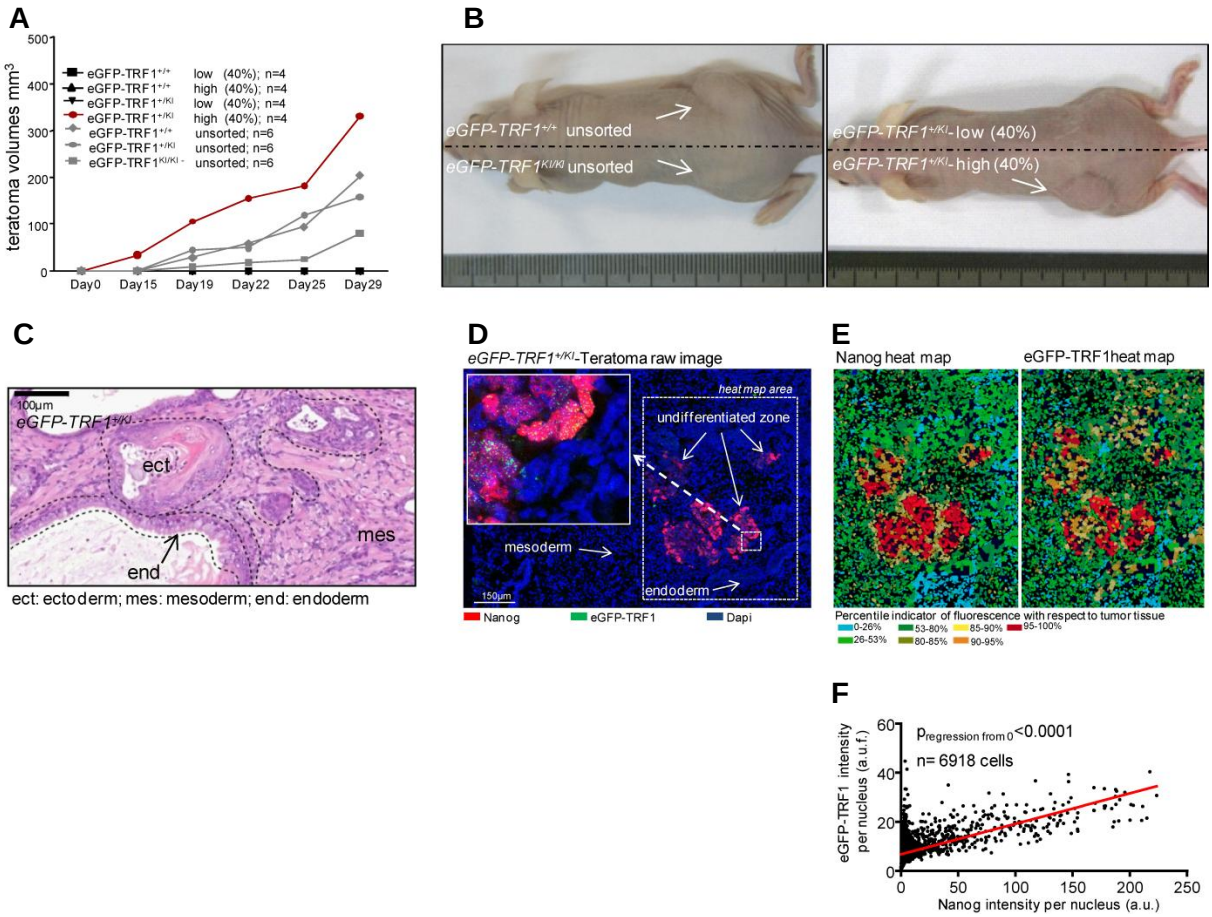

Figure 15. High expression of eGFP-TRF1 marks pluripotent iPS cells

(A) Teratoma formation by iPS cells (passage 4) sorted for high and low eGFP-TRF1 expression in the G1 phase of the cell cycle (red) and by non-sorted iPS cells (grey). From the sorted cells, only *eGFP-TRF1$^{+/KI}$* high iPS cells formed teratomas. Of the unsorted cells all the different genotypes formed teratomas with a later onset. The earlier teratoma onset of the sorted eGFP-TRF1^{high} iPS cells compared to the unsorted cells indicates that high eGFP-TRF1 expression marks a subpopulation of more pluripotent stem cells within the bulk iPS cells. Depicted are the means of tumor volume per genotype and day after injection. **(B)** Representative images of nude mice injected with unsorted *wild-type* and *eGFP-TRF1$^{KI/KI}$* iPS cells (left picture) and sorted for high and low eGFP-TRF1 in *eGFP-TRF$^{+/KI}$* iPS cells (right). **(C)** Representative image of an *eGFP-TRF1$^{+/KI}$* teratoma stained for H&E showing all the three germ layers (endoderm: end; mesoderm: mes; ectoderm: ect). **(D)** Representative picture of a teratoma induced by *eGFP-TRF1$^{+/KI}$* iPS cells. The OCT section was stained for Nanog (red). In the depiction we can see, that there are regions that did not differentiate or dedifferentiated again (Nanog positive cells). In those regions, in opposite to the more differentiated sites, we can detect a highly increased amount of eGFP-TRF1 at the telomeres. **(E)** Heat maps of the indicated region in D. The left heat map shows a colorcoded picture in which the cells with high Nanog expression have warmer colors and vice versa. A very similar pattern is seen in the eGFP-TRF1-heat map done in the same way. **(F)** Statistical correlation analysis of the teratoma cells for the expression eGFP-TRF1 and Nanog. We see a significant correlation for eGFP-TRF1 expression and Nanog. Statistical analysis is done for the linear regression.

Similar results were obtained using iPSc's, sorted as described above, for morulae aggregation in a chimera forming assay. EGFP^{low} iPS cells sorted from *eGFP-TRF1*$^{+/KI}$ clones did not contribute to chimera formation whereas the high eGFP-TRF1 containing iPS cells contributed to chimeric mice represented in the high percentages of chimerism **(Fig. 16 A&B).**

A

iPS clone	Embryos Injected	Cells injected	Embryos Transfered	Pups born	Chimeras
iPS *eGFP-TRF1*$^{+/+}$ pool cl. 2-8/1-5 LOW	57	5 to 6	57	2	1M (50%)
iPS *eGFP-TRF1*$^{+/+}$ pool cl. 2-8/1-5 HIGH	57	5 to 6	57	4+ 1 dead	1M (40%) 1F (30%)
iPS *eGFP-TRF1*$^{+/KI}$ pool cl. 2-1/1-6 LOW	61	5 to 6	61	2+ 1dead	0
iPS *eGFP-TRF1*$^{+/KI}$ pool cl. 2-1/1-6 HIGH	66	5 to 6	66	17+ 3 dead	1M (80%) 1F (70%) 1M (50%) 1M (40%) 1F (30%)

B

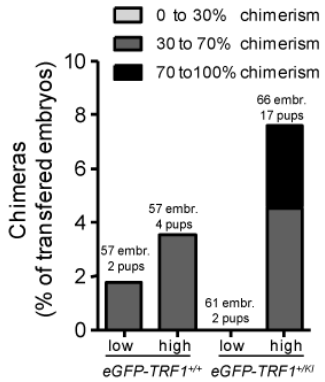

Figure 16. High expression of eGFP-TRF1 marks pluripotent iPS cells

(A&B) Numbers and graphical depiction of the chimera formation assay with iPS cells sorted for low and high eGFP-TRF1 expression. Note that only the sorted eGFP-TRF1^{high} iPS cells from the *eGFP-TRF1*$^{+/KI}$ genotype contributed to chimeras. Sorting of the wild-type iPS cells was based on the background levels treat them the same as the eGFP-TRF1 cells.

Together, these results support the notion that TRF1 expression levels are indicative of the level of pluripotency of iPS cells. Thus, the higher the expression levels of TRF1, the higher the pluripotency potential.

5.8. TRF1 IS ESSENTIAL FOR REPROGRAMMING

Having seen higher expression levels of TRF1 in undifferentiated cells, we set out to determine whether TRF1 itself behaved like other pluripotency genes and was essential for the reprogramming of MEFs into iPS cells. To this end, we reprogrammed MEFs deficient for TRF1 and simultaneously abrogated p53. The deletion of p53 in *TRF1*$^{\Delta/\Delta}$*; p53*$^{-/-}$*-Cre* MEFs, was able to rescue proliferative defects associated with TRF1 deficiency and facilitated reprogramming of cells with severe telomeric damage (Marion et al, 2009a; Martinez et al, 2009). Strikingly, we repeatedly failed to obtain any iPS cell colonies in the *TRF1*$^{\Delta/\Delta}$*; p53*$^{-/-}$*-Cre* cultures **(Fig. 17A)**. All colonies formed showed no *TRF1* excision and contained the *TRF1*$^{lox/lox}$*; p53*$^{-/-}$*-Cre* **(Fig. 17B)**. This indicates that TRF1 deficiency completely blocks reprogramming, even in the absence of p53. In agreement with an essential role for TRF1 in reprogramming, TRF1 deficiency prevented some of the key events associated with the process of reprogramming. One of them is the appearance of *ssea-1* mRNA expressing clones in the first week post reprogramming **(Fig. 17C)** (Stadtfeld et al, 2008a). Another key event that was impaired in TRF1-deficient cultures is the induction of high transcription levels of the pluripotency genes Nanog and o*ct3/4* at the time of appearance of the first iPS clones at day 14 post-infection **(Fig. 17D)**.

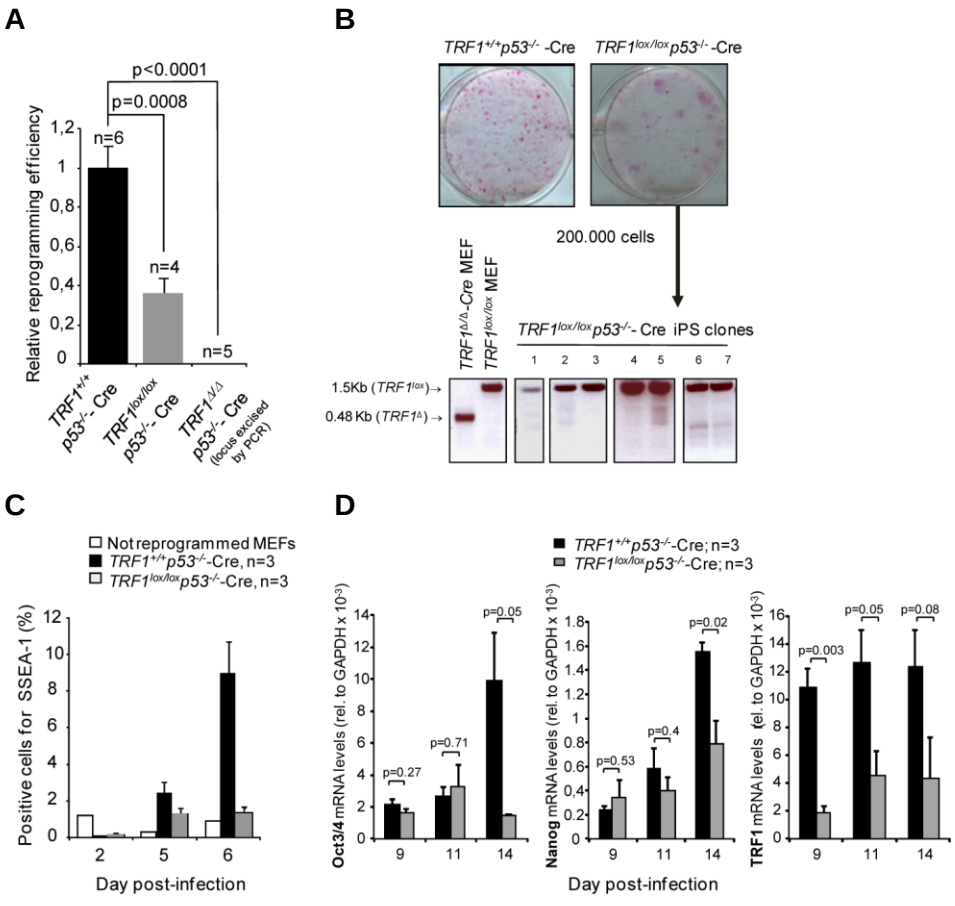

Figure 17. Very high TRF1 levels during reprogramming are essential for the generation of iPS cell clones.

(A) Relative reprogramming efficiencies of the indicated cells. Note that the only iPSs colonies obtained from the *TRF1*$^{lox/lox}$-Cre MEFs came from cells without TRF1 excision. Statistical comparisons were done using two sided student *t*-test. Error bars, SEM. n= independent experiments. **(B)** Reprogramming plates stained with alkaline phosphatase. The number of parental MEFs used is indicated. Analysis of TRF1 excision in iPS colonies obtained from *TRF1*$^{lox/lox}$ *p53*$^{-/-}$ -Cre MEFs by PCR. Note that all the clones keep the TRF1$^{lox/lox}$ locus. **(C)** Kinetics of mRNA expression of *ssea-1* pluripotency marker during reprogramming, as measured by flow cytometry. Non-reprogrammed MEFs are shown as negative control. Error bars, SEM. n= experiments from independent MEFs. **(D)** mRNA levels of *oct3/4, Nanog* and *trf1* at days 9, 11 and 14 of reprogramming, before appearance of iPS colonies. The mRNA levels are measured by qRT-PCR relative to *GAPDH* mRNA levels. Statistical comparisons were done using two sided student *t*-test. Error bars, SEM. n= independent MEFs.

5.9. INDUCTION OF APOPTOSIS, CHROMOSOMAL ABERRATIONS AND DDR ACTIVATION IN TRF1-DEFICIENT IPS CELLS

Next, we wondered whether TRF1 is just a marker of pluripotency or if it is important for the maintenance of pluripotency in iPS cells. To this end, we generated *TRF1*-null iPS cells using primary MEFs carrying a conditional loxP-flanked *TRF1* and an inducible *Cre-ERT2* recombinase (*RERTn)* allele. After reprogramming of *TRF1*$^{lox/lox}$*; RERTn*$^{+/ERT}$ and *TRF1*$^{+/+}$*; RERTn*$^{+/ERT}$ MEFs, the resultant iPS cells were cultured in the presence of 4-hydroxytamoxifen (4-OHT) to obtain *TRF1*$^{\Delta/\Delta}$ and *TRF1*$^{+/+}$ iPS cells. It has been previously described that TRF1 deficiency in MEFs induces telomere uncapping, telomere fragility and a rapid induction of cell-cycle arrest and senescence, mediated by the p53 and pRb pathway activation (Martinez et al, 2009). As iPS cells are very sensitive to DNA damage, we checked whether *TRF1*$^{\Delta/\Delta}$ iPS cells undergo apoptosis. At day 6 of 4-OHT treatment we observed an increase in apoptosis in *TRF1*$^{\Delta/\Delta}$*; RERTn*$^{+/ERTOHT}$ iPS cells compared to the *TRF1*$^{+/+}$*; RERTn*$^{+/ERTOHT}$ iPS cells, while there were no significant differences in control-treated iPS cells **(Fig. 18A&B)**. To address whether TRF1 deficiency causes telomeric aberrations in iPS cells, we performed a telomeric Q-FISH on metaphases (Experimental Procedures). As expected, *TRF1*$^{\Delta/\Delta}$*; RERTn*$^{+/ERTOHT}$ iPS cells showed higher levels of MTS, sister-chromatid and chromosome fusions at day 3 and day 6 after 4-OHT treatment **(Fig. 18C)**, suggesting increased telomere fragility and telomere uncapping, due to TRF1 abrogation. The DDR activation was analyzed by co-staining of γH2AX and TRF1 in iPS cells at day 3 of 4-OHT treatment. We observed a significant increase in the percentage of γH2AX positive cells **(Fig. 18D&E)** in *TRF1*$^{\Delta/\Delta}$*; RERTn*$^{+/ERTOHT}$ cells with low levels of TRF1 compared to *TRF1*$^{+/+}$*; RERTn*$^{+/ERTOHT}$ and *TRF1*$^{\Delta/\Delta}$*; RERTn*$^{+/ERTOHT}$ cells with incomplete *TRF1* excision was detected. These findings are in agreement with the results from TRF1-null MEFs. Finally, we confirmed *TRF1* abrogation in *TRF1*$^{\Delta/\Delta}$*; RERTn*$^{+/ERTOHT}$ iPS cells by qRT-PCR **(Fig. 18F)** at

day 3 and 6 of 4-OHT treatment. These results confirm an important role of TRF1 in IPS cell maintenance.

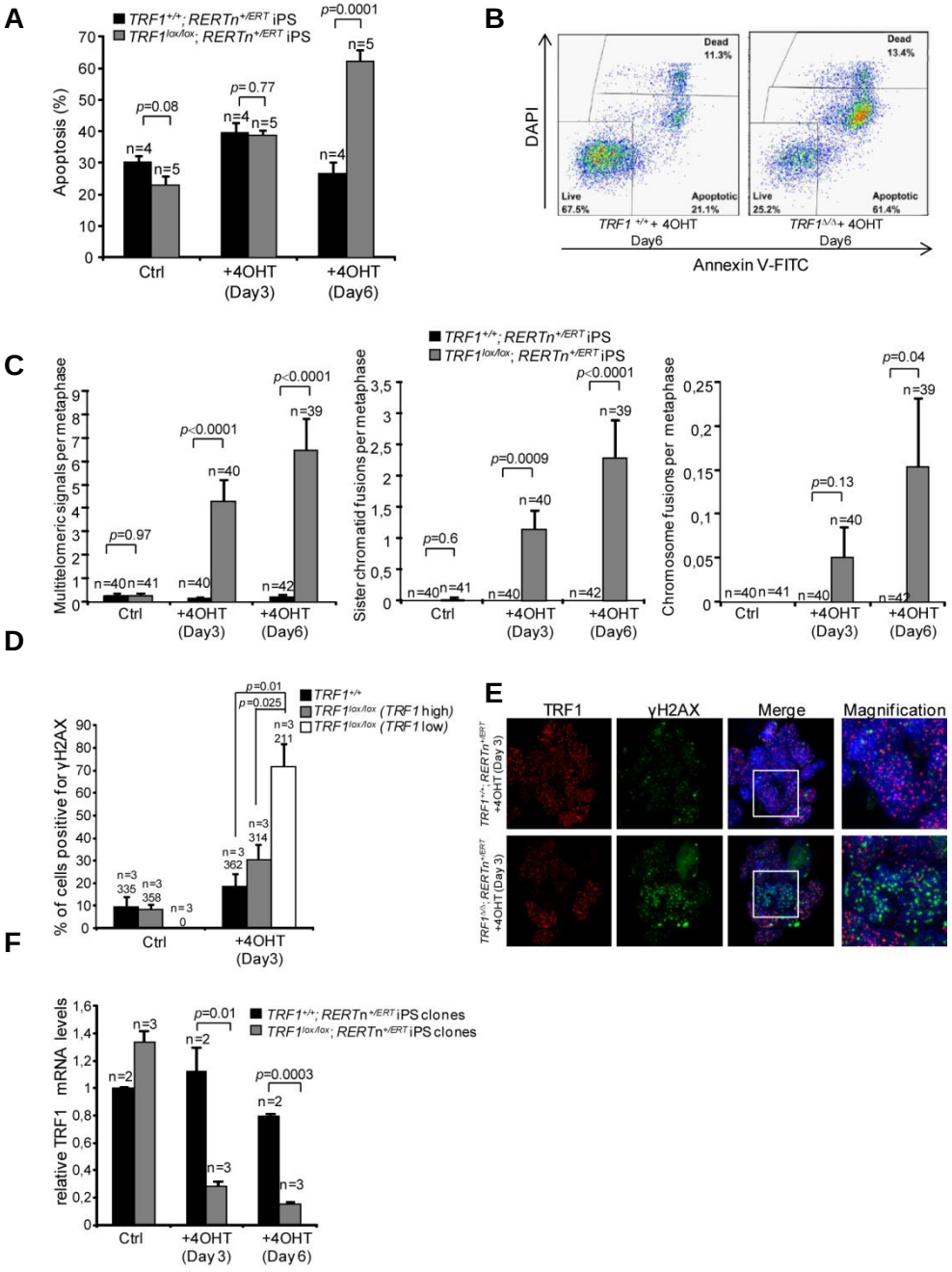

Figure 18. Conditional TRF1 ablation in iPS cells leads to apoptosis, chromosomal aberrations and DDR activation

(A) Apoptosis was determined by Annexin staining on control treated iPS cells and iPS cells at day 3 and 6 of 4-hydroxytamoxifen treatment. n= number of iPS clones analyzed. Statistical comparisons were done using two sided student *t*-test. Error bars, SEM. **(B)** Representative FACS profiles at day 6 of 4-hydroxytamoxifen treatment. **(C)** Frequency of aberrations in metaphase spreads of the indicated genotypes and conditions. n= number of metaphases from a total of two iPS clones per genotype. Statistical comparisons were done using two sided student *t*-test. Error bars, SEM. **(D)** Percentage of γH2AX positive cells in non-treated (Ctrl) and treated with 4-hydroxytamoxifen (Day 3) iPS cells. n= number of iPS clones used for the analysis. The total number of cells analyzed per genotype is shown. Statistical comparisons were done using two sided student *t*-test. Error bars, SEM. **(E)** Representative images of TRF1 and γH2AX immunofluorescence co-staining. **(F)** mRNA levels of TRF1 decrease with time of 4-OHT treatment as it is depicted for day 3 and day 6. In the left panel we see control treated cell at day 3 where no difference in the TRF1 mRNA levels was detected.

Knowing that TRF1 deficiency completely blocks reprogramming in a p53-null background and, that TRF1 is essential for iPS cell maintenance **(Fig. 17A)**, we set to confirm this essential role for TRF1 in reprogramming by knocking-down TRF1 expression during the reprogramming process. To this end, $p53^{-/-}$ MEFs were reprogrammed using a cocktail of the three reprogramming factors (lentiviral Oct4, Klf4 and Sox2) and a lentiviral vector expressing either TRF1 shRNA or a scramble shRNA as a control. Reprogramming efficiency was calculated as the number of iPS cell colonies obtained relative to the total number of cells initially infected (infection efficiency was measured in quintuple infections with the three factors, GFP plus the lentiviral vector, and analyzed by flow cytometry to detect the proportion of GFP-positive cells). We observed that a reduced expression of TRF1 during reprogramming strongly decreases the reprogramming capacity of the cells **(Fig. 19A)** in agreement with an essential role for TRF1 in reprogramming. As the abrogation of TRF1 induces a strong DDR and increases the presence of chromosome termini with MTS, telomere uncapping (presence of DSB signalling) and SCF (Martinez et al, 2009) we next studied whether knocking-down TRF1 expression during the reprogramming process induces the appearance of the above mentioned pheotypes. First, we measured the expression of γH2AX that has been shown to mark the presence of DNA double-strand breaks, including those associated with critically short or dysfunctional telomeres. Eight days after the reprogramming initiation with the reprogramming cocktail and the scramble or TRF1 shRNAs, colonies were not yet detectable. The readout on the other hand already showed a significant increase of the nuclear intensity of γH2AX in cells with reduced levels of TRF1 **(Fig. 19B)**. This suggests that this damage could, at least in part, be responsible for the deficient reprogramming capacity of these cells. Next, we determined the frequency of MTS at day 10 post infection, when iPS colonies were not yet present, and at day 17, when iPS colonies were clearly detectable. We observed that infection with the reprogramming factors did not increase the frequency of MTS at day 10 p.i. , neither in cells deficient for TRF1 nor in cells with normal levels of TRF1 **(Fig. 19C, left)**. However, at day 17 p.i. a significant increase in MTS was detected in cells deficient for TRF1 when compared with cells with normal levels of TRF1 **(Fig. 19C, right)**, suggesting that accumulation of MTS may be a consequence of the multiple cell divisions required to generate an iPS colony.

Together, these findings indicate that TRF1 is essential both for the induction and maintenance of pluripotency in iPS cells.

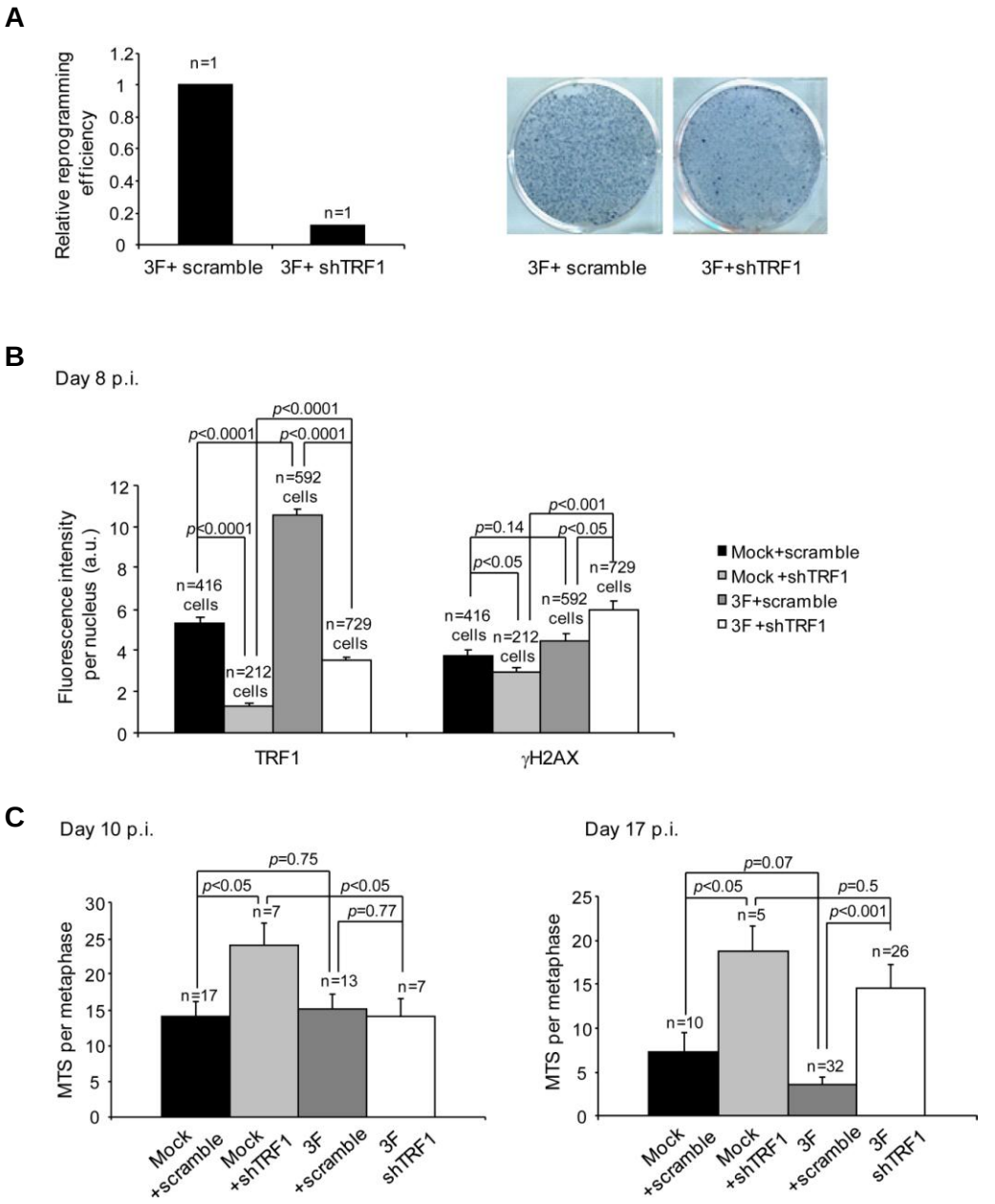

Figure 19. Down-regulation of TRF1 during reprogramming significantly impairs reprogramming and induces DNA damage and telomere aberrations

(A) Left, quantification of relative reprogramming efficiency of primary p53$^{-/-}$ MEF infected with three reprogramming factors (retroviral) plus scramble shRNA or TRF1 shRNA (lentiviral). Efficiency of iPS generation was calculated as the number of alkaline phosphatase- positive colonies and normalized to retroviral infection efficiency as determined by GFP fluorescence. Note that down-regulation of TRF1 expression strongly reduces reprogramming efficiency. Right, representative images of the reprogramming plates. **(B)** Quantification of TRF1 and γH2AX immunofluorescence after infection with the indicated viral cocktails (day 8 p.i). Note that down-regulation of TRF1 expression significantly increases the presence of γH2AX in cells infected with the reprogramming factors. Indicated statistics was performed using a Student's t-test. Error bars, SEM. n= number of cells analyzed. **(C)** Frequency of multitelomeric signals in cells 10 days (no presence of iPS colonies) or 17 days (presence of iPS cells) after infection with the indicated viral cocktails. Note that down-regulation of TRF1 expression increases the presence of multitelomeric signals in the resulting iPS cells at day 17 p.i. The number of metaphases analyzed in each case is indicated. Statistical comparisons were done using two sided student t-test. Error bars, SEM.

5.10. TRF1 EXPRESSION LEVELS ARE MODULATED BY THE OCT3/4 TRANSCRIPTION FACTOR BY DIRECTLY BINDING TO TRF1 PROMOTER IN PLURIPOTENT CELLS

The results described above indicate an unprecedented role for TRF1 linked to induction and maintenance of pluripotency in iPS cells, which is independent of telomere elongation by telomerase. Interestingly, this is not restricted to the *in vitro* generated iPS cells, as TRF1 levels are also upregulated during the *in vitro* establishment of mouse embryonic stem (ES) cells coincidental with upregulation of known pluripotency genes, such as *Sox2* or *Oct3/4* (Varela et al, 2011). Thus, we next set out to address the mechanism by which TRF1 is upregulated associated to the induction of pluripotency. Recent ChIP-sequencing experiments showed that the pluripotency factor OCT3/4 can bind to TRF1 promoter regions (Loh et al, 2006), suggesting that OCT3/4 could be responsible for TRF1 upregulation during reprogramming. To directly test this, we transduced wild-type MEFs with each of the "Yamanaka factors" (namely *Oct3/4*, *Sox2* and *Klf4*) using retroviral vectors (Experimental Procedures). Three days after infection a significant increase in TRF1 levels was detected only in *Oct3/4*-transduced MEFs, even in the absence of reprogramming. *Sox2*- or *Klf4*-transduced MEFs did not show such increased TRF1 levels when compared to wild-type MEFs **(Fig. 20)**. Of note, even though OCT3/4 was sufficient to induce TRF1 in MEFs, TRF1 levels in established iPS were still significantly higher **(Fig. 20)**. These results suggest that OCT3/4 is sufficient to induce TRF1 upregulation during the reprogramming process, but additional factors are required for full TRF1 induction in iPS cells.

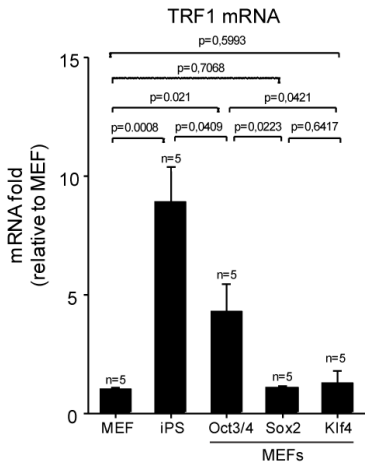

Figure 20. The transcription factor OCT3/4 modulates TRF1 expression in pluripotent cells .

TRF1 expression levels in MEFs transduced with either Oct3/4, Sox2 or Klf4, as estimated by qRT-PCR. Depicted is mRNA fold increase relative to TRF1 levels in wild-type MEFs three days after transduction with the indicated retroviral vectors. Note that Oct3/4/4 is the only factor that is able to increase TRF1 levels in the absence of cellular reprogramming. Non-transduced MEFs and wild-type iPS cells are included for reference. n=number of independent MEF clones used per condition. Bars represent the average of all the independent experiments performed. Statistical comparisons were done using two sided student *t*-test. Error bars, SEM.

OCT3/4 is one of the core components of the “Yamanaka’s Reprograming Coctail” (Niwa, 2007; Takahashi et al, 2007), and very few reports have shown feasible alternatives for substituting OCT3/4 in the reprogramming of somatic cells (Heng et al, 2010; Redmer et al, 2011). We have already demonstrated that eGFP-TRF1 strongly co-localizes with Nanog by immunofluorescence in eGFP-TRF1$^{+/KI}$ iPS cells **(Fig. 12A-E)**. Moreover, we have shown that forced OCT3/4 expression is sufficient to induce TRF1 upregulation in differentiated cells **(Fig. 20)**. Given its importance together with Nanog in the maintenance of stem cell identity and self-renewal, together with the essential nature of TRF1 in pluripotent cells, we wanted to test whether OCT3/4 or Nanog are able to directly bind the TRF1 promoter in mouse pluripotent cells. This was addressed with ChIP-qRT-PCR experiments in ES- and iPS cells **(Fig. 21A-C)**. We immunoprecipitated chromatin bound OCT3/4 and Nanog and analyzed either OCT3/4 promoter (OCT3/4-Pr), Nanog promoter (Nanog-Pr), TRF1 promoter (TRF1-Pr) or an unrelated control region upstream of TRF1 promoter (Ctrl Region) **(Fig. 21C)**. In ES cells, we were able to detect significant binding of OCT3/4 protein to both, OCT3/4-Pr, Nanog-Pr and TRF1-Pr. We also detected Nanog binding to its own promoter and that of OCT3/4; however, TRF1-Pr was not detected upon Nanog ChIP-qRT-PCR **(Fig. 21A)**. To demonstrate that OCT3/4 binding to TRF1 promoter was not an exclusive feature of mouse ES cells, we performed the same ChIP-qRT-PCR experiments in iPS cells, confirming our previous observations **(Fig. 21B)**. These results demonstrate that OCT3/4 that itself is depending on bona-fide pluripotency markers such as Nanog or SOX2, can directly regulate TRF1 levels which supports the hypothesis that TRF1 is an essential protein during the acquisition of pluripotency. Nanog has been shown to bind to the TRF1 locus, but functional assays implicating its role in TRF1 regulation remain to be verified (Loh et al, 2006).

A

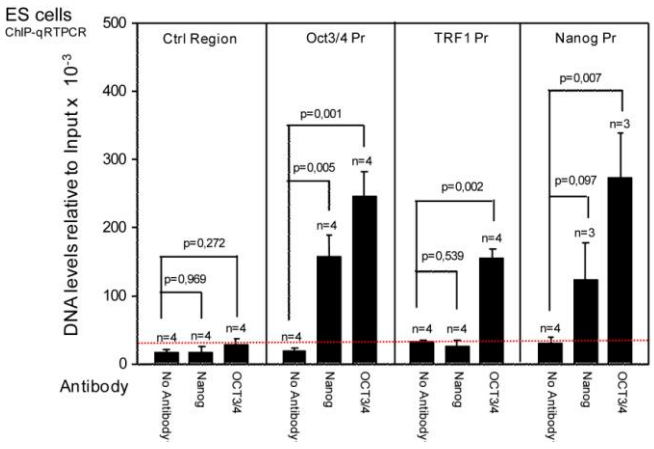

B

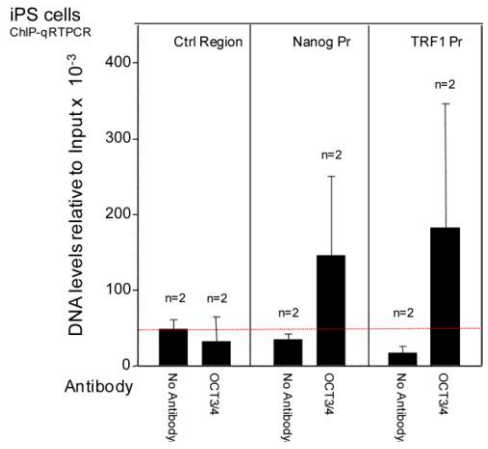

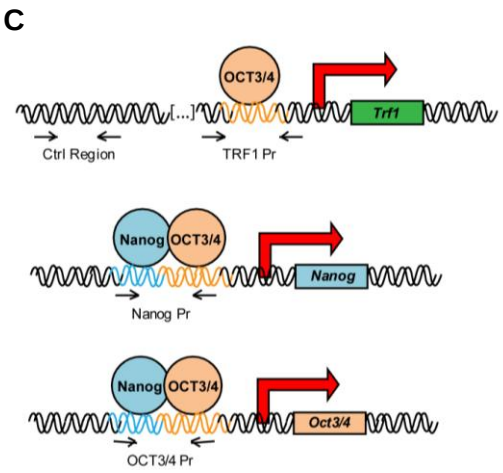

Figure 21. The transcription factor Oct3/4 modulates TRF1 expression in pluripotent cells by directly binding to TRF1 promoter.

DNA levels, as measured by qRT-PCR after Chromatin Immunoprecipitation (ChIP) in ES cells **(A)** or iPS cells **(B)**. The amount of DNA in each ChIP was normalized to its corresponding input DNA levels (total genomic DNA not subjected to immunoprecipitation). The antibodies used are indicated under each bar of the graph, the regions amplified by qRT-PCR are indicated on top of the panels (Ctrl Region, control region; Oct3/4 Pr, Oct3/4 promoter; TRF1 Pr, Terf1 promoter; and Nanog Pr, Nanog promoter). Note that OCT3/4 binds to *Trf1*, Nanog and *Oct3*/4 promoters, while Nanog does only bind to Nanog and *Oct3/4* promoters but not that of TRF1. n=number of independent immunoprecipitations performed. Bars represent the mean of at least three experiments. Statistical comparisons were done using two sided student *t*-test. Error bars, SEM. **(C)** Schematic representation of the genomic regions and primer pairs used for the ChIP-qRT-PCR analysis described in **(A)** and **(C)**.

5.11. eGFP-TRF1 EXPRESSION AS A MARKER FOR ADULT STEM CELL COMPARTMENTS

5.11.1. TAIL SKIN HAIR FOLLICLE

Having established new roles of TRF1 in pluripotent iPS- and ES cells; the TRF1 expression pattern in tissues and in their corresponding stem cells became of great interest. Previous work in our lab described that cells harbouring the longest telomeres within a tissue are enriched in the known stem cell compartments, while cells showing shorter telomeres are normally located in the differentiated compartments (Flores et al, 2008). In the case of the small intestine stem cell niche, cells with the longest telomeres were enriched at the +4 to +7 positions within the crypt as well as in the TA area, while cells with the shortest telomeres where more abundant in the 0 to +3 and villi regions (Flores et al, 2008). In the case of the skin, cells with the longest telomeres where enriched at a broad defined hair bulge region and telomere length progressively decreased via TA compartments with the shortest telomeres at the interfollicular epidermis (Flores et al., 2008). Here, we set to address whether TRF1 expression showed a similar distribution to that of telomere length in both small intestine and skin adult stem cell compartments. To this end, we followed eGFP expression in both tail skin and small intestine from *eGFP-TRF1*$^{+/KI}$ mice.

In tail skin, we found maximum eGFP-TRF1 fluorescence at the known stem cell compartments of the epidermis (EP), sebaceous gland (SG) and hair follicle (FOL) (Ito et al, 2005; Jensen et al, 2009; Snippert et al; Woo & Oro, 2011), and eGFP fluorescence was minimal in the interfollicular epidermis where differentiated cells are present **(Fig. 22A-C)**.

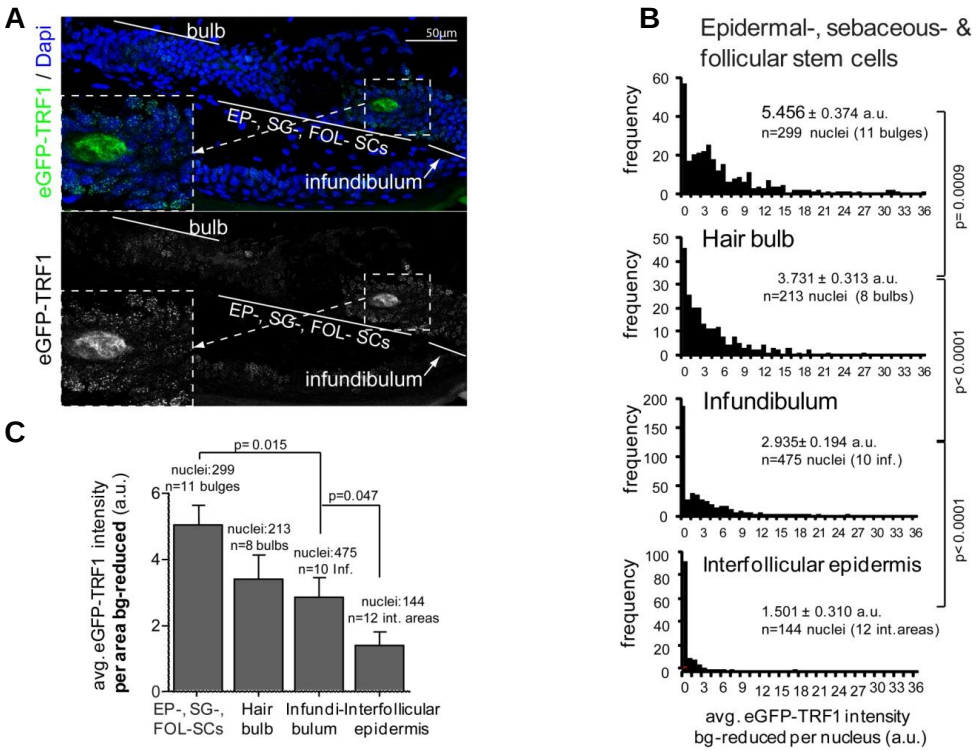

Figure 22. eGFP-TRF1 expression is maximal in adult stem cell compartments of the skin

(A) Representative image of eGFP-TRF1 fluorescence in the indicated compartments of tail-skin follicles in the telogen state. EGFP-TRF1 intensity decreases from the putative stem cell niches towards all the more differentiated compartments (interfollicular skin). **(B&C)** Quantification of eGFP-TRF1 fluorescence in the Epidermal- (ED), sebaceous gland (SG)-, follicular (FOL) stem cells, bulb, infundibulum (inf.) and interfollicular areas (int. area) of the tail-skin follicles. There is a significant decrease of the average (avg.) background (bg) corrected eGFP-TRF1 fluorescence when going from the putative stem cell niches towards the more differentiated compartments. Statistical analysis is done by two sided *t*-tests. Error bars, SEM.

To confirm an enrichment of eGFP-TRF1 in the stem cell compartment, we next studied eGFP-TRF1 fluorescence in CK15-positive cells, a bona fide marker of hair follicle stem cells (Liu et al, 2003). As shown in **Fig. 23A&B**, CK15-positive cells in the tail skin were enriched at the hair bulge, epidermal- and sebaceous gland stem cells and showed higher eGFP fluorescence compared to CK15-negative cells. This result is in line with previous findings from our group showing that the longest telomeres are enriched at the CK15-positive cells (Flores et al, 2008). Interestingly, we noticed that changes in the expression of eGFP-TRF1 between the different skin compartments were much more pronounced than changes in telomere length. In particular, while telomere length decreased from the hair stem cells to interfollicular epidermis by 30% (Flores et al, 2008), we observed a drop in eGFP-TRF1 fluorescence of around 70% for the same compartments **(Fig. 22A-C)**. This finding suggest that TRF1 levels, also in the adult stem cell compartments, are uncoupled from the telomere length, similar to the findings in *in-vitro* conditions, where iPS cells show a massive, disproportional increase in TRF1 levels compared to their parental embryonic fibroblasts.

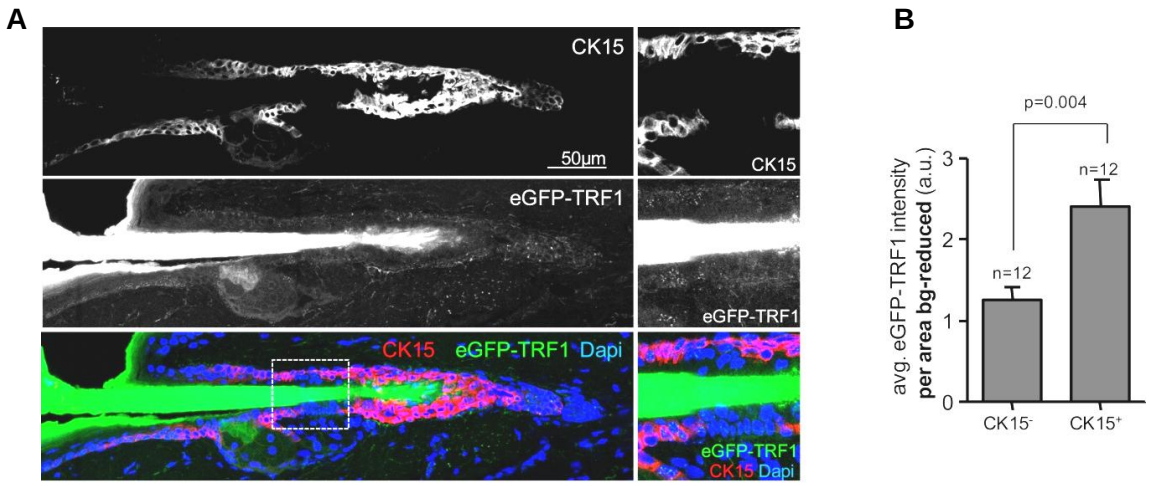

Figure 23. High expression of eGFP-TRF1 marks pluripotent iPS cells

(A) Representative Image of a telogen tail-skin hair follicle stained for Cytokeratin15 (CK15) (top picture). In the middle picture eGFP-TRF1 fluorescence is visible. The close-up, as marked in the third row merge picture, is depicted on the right of each picture showing CK15 positive and negative cells. **(B)** Quantification of the average background (bg) corrected eGFP-TRF1 fluorescence in CK15 positive and negative tail-skin follicle cells. We can see a significant increase from CK15 negative to positive cells Statistical analysis is done using two sided *t*-tests ; Error: SEM.

5.11.2. INTESTINAL STEM CELLS

Next, the small intestine stem cell compartments were addressed. In this case, the highest eGFP fluorescence was found in the area above the region containing paneth cells (position 0 to +3), namely from cellular position +4 to +7 and the lowest expression at the villi **(Fig. 24A-E)**, also in agreement with previous findings for long telomeres (Flores et al, 2008). Similar to our observations *in vitro* and tail skin tissue samples, we detected a much more abrupt drop in eGFP fluorescence than in telomere length when comparing the less differentiated to the more differentiated compartments. In particular, eGFP-TRF1 expression was lowered from positions +4 to +7 to villi cells by 94% **(Fig. 24D)**, while telomeres in the same compartments shortened by only 14% (Flores et al, 2008). We confirmed these findings also for endogenous TRF1 expression by performing immunofluorescence with anti-TRF1 antibody **(Fig. 24C&E)**. In this case, we observed a decrease of TRF1 expression of 80% from positions +4 to +7 to villi cells**.**

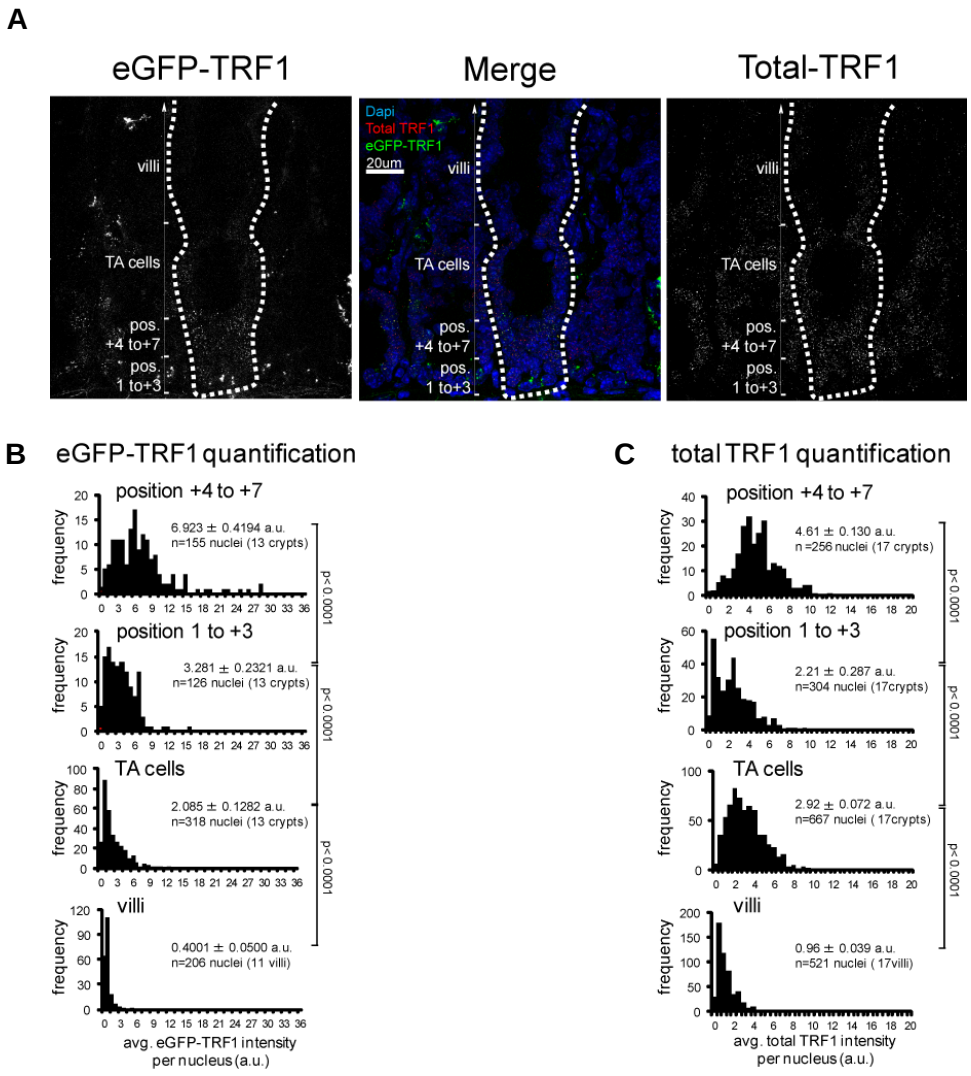

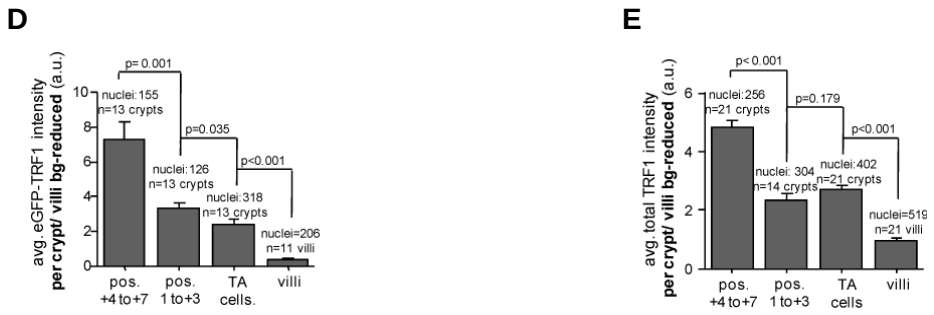

Figure 24. eGFP-TRF1 expression is maximal in adult stem cell compartments of the small intestine

(A) Representative image of eGFP-TRF1 fluorescence (left), Merge image (middle) and a total TRF1 staining (right) in small intestine-crypt/villi. The highest eGFP-TRF1 and TRF1 fluorescence is located in the positions +4-+7 of the intestinal crypt and decreases towards the more differentiated cell types in the crypt/villi. **(B)** Quantification of the average background (bg) corrected eGFP-TRF1 fluorescence in the indicated compartments of the intestinal crypt/villi. We see the highest eGFP-TRF1 expression in cells located at positions +4 to +7. It decreases towards the more differentiated regions. Indicated is the background corrected mean green value per nucleus. Statistical analysis is done using two sided *t*-tests. **(C)** Quantification of the eGFP-TRF1 and the total TRF1 in the different compartments of the intestinal crypt/villi. We see a significant decrease of eGFP-TRF1 expression in nuclei from the putative stem cell niche (position +4 to +5) towards the more differentiated regions. Indicated is the background corrected mean TRF1 value per nucleus. Error, SEM; statistical comparisons were done using two sided student *t*-test. **(D&E)** Quantification of the eGFP-TRF1 and total TRF1 expression, analyzed per intestinal crypt of the different areas. Error bars, SEM; statistical comparisons were done using two sided student *t*-test.

There is recent evidence to suggest that small intestine stem cells are located at the bottom of the crypts at position 0 to +3 and that they can be identified by high Lgr5 expression, whereas neighbouring paneth cells are more differentiated and do not express Lgr5 (Schepers et al, 2011). In order to address whether $Lgr5^+$ cells also show high TRF1 expression compared to the Lgr5-negative paneth cells, we determined TRF1 fluorescence in Lgr5-eGFP reporter mice (Barker et al, 2007).

We readily noticed that TRF1 expression was not homogeneous at the bottom of the crypt, with the eGFP-positive cells ($Lgr5^+$) showing the highest TRF1 expression, comparable to that of +4 to +7 cells **(Fig. 25A&B)**. Interestingly, this marked difference in TRF1 expression between the $Lgr5^+$ cells and the rest of the 0 to+3 positioned cells was not observed in the case of telomere length. This further supports the hypothesis that TRF1 expression is uncoupled from telomere length, also in the adult stem cell compartments **(Fig. 25A-D)**. The fact that we did not see significant changes in telomere length between the $Lgr5^+$ and Lgr5-negative cells, both having significantly shorter telomeres than cells at the +4 to +7 position, is in agreement with our previous findings (Flores et al, 2008) but in contrast with recent findings by other authors (Sato et al, 2010). Our results would suggest that, in terms of telomere length, the paneth-cell interspersing Lgr5-positive cells are not those with the longest telomeres and, presumably, the cell population with longer telomeres may

contain additional stem cells, in line with recent findings that Lgr5^{+} cells are dispensable for maintenance of intestine homeostasis (Tian et al, 2011) and the idea of fast and slow cycling stem cells in the small intestine.

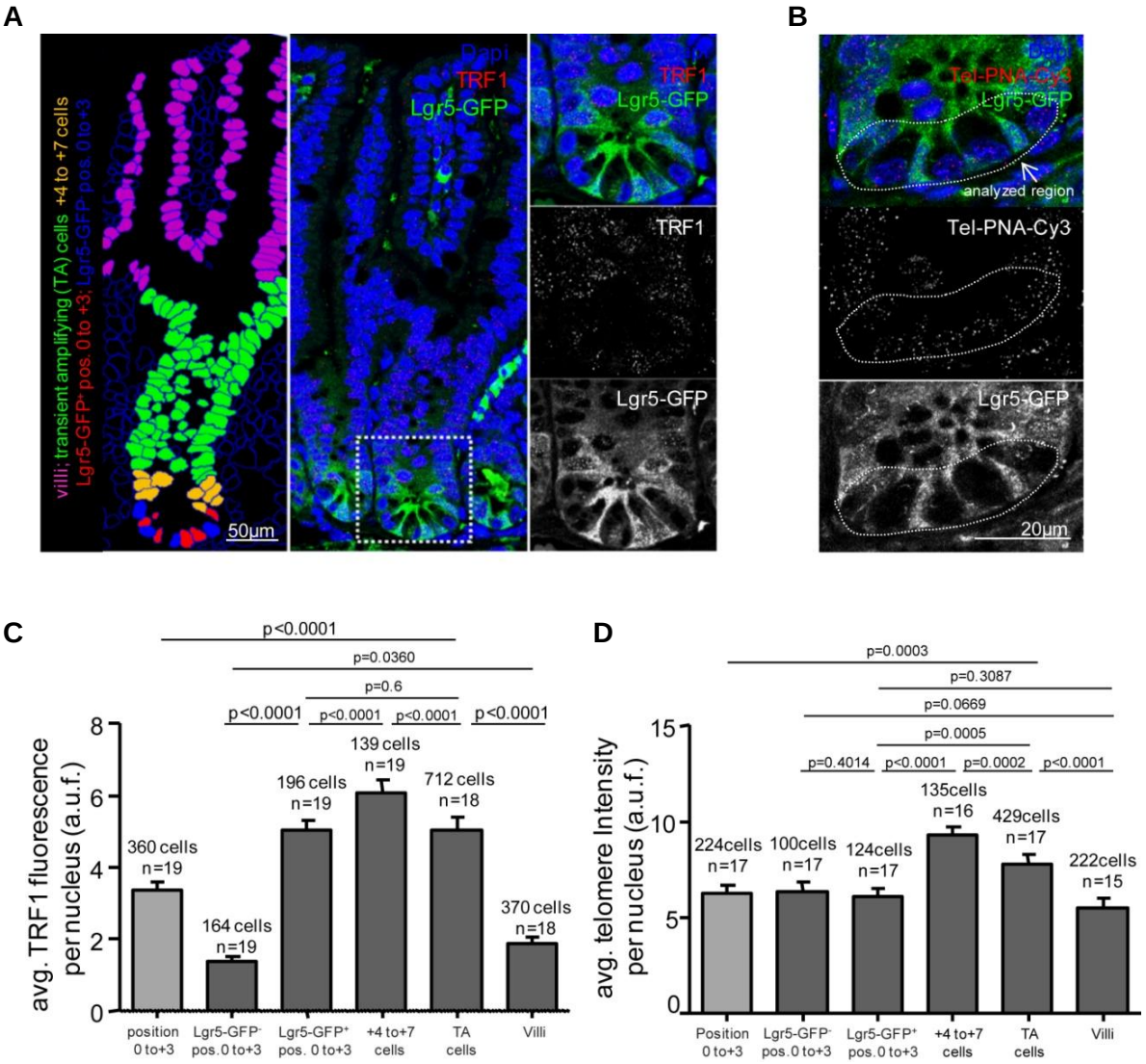

Figure 24. High expression of eGFP-TRF1 marks pluripotent iPS cells

(A) Left panel: different cell types of the intestinal crypt/villi using the indicated color-code. Right panels: Lgr5-eGFP fluorescence (green; close-up at the bottom), TRF1 fluorescence (red; middle close-up), and merged TRF1 and Lgr5-eGFP fluorescence (close-up at the top) in small intestine crypt/villi of a heterozygous Lgr5-eGFP mouse. **(B)** Quantification of average TRF1 fluorescence per nucleus in arbitrary units (a.u) in the indicated compartments. The highest expression of TRF1 is seen at the +4 to +7-cells followed by the Lgr5-GFP^{+} and TA cells. Note that Lgr5-GFP^{+}-cells in the crypt express much higher levels of TRF1 than the neighboring Paneth cells. From +8 position to the villi, cells express less TRF1 coincidental with increased differentiation of those cells. Calculations made by two tailed, paired (within crypts) *t*-test. Error: SEM. **(C)** Representative picture of an anti Lgr5-GFP GFP-telomere immuno-FISH. Bottom panel: Lgr5-GFP fluorescence marks the Lgr5+-cells. Middle panel: Tel-PNA-Cy3 probe shows telomeres fluorescence. Top panel: merged picture shows similar telomere intensity in the Lg5+ and Lgr5- cells in the 0 to +3 compartment. **(D)** Remarkably, in the 0 to +3 region the telomeres of Lgr5-GFP^{+} cells compared to the +4 to +7 position are severely shortened. We do not see any statistical difference in telomere length between paneth (Lgr5-GFP^{-}) cells and Lgr5-GFP^{+} cells in the 0 to +3 region (J). Calculations made by two tailed paired (within crypts) *t*-test. Error: SEM.

Together, these findings underline a previously unnoticed enrichment of TRF1 expression in the adult stem cell compartments of mouse tissues. Furthermore, the fact that TRF1 expression drops more acutely than telomere length when going from stem cell compartments to the most differentiated compartments within tissues, underlines a role for TRF1 that is independent of telomere length regulation.

5.12. CONDITIONAL ABLATION OF TRF1 IN INTESTINE LEADS TO SEVERE INTESTINAL ATROPHY

To address whether TRF1 is essential for tissue homeostasis, we conditionally knocked out TRF1 in the small intestine by crossing the *TRF1*$^{lox/lox}$ mouse model previously generated in our laboratory (Martinez et al, 2009) with a Villin-CreERT2 expressing mouse (el Marjou et al, 2004), thus targeting TRF1 deletion to villin expressing tissues. In this mouse model, the Cre-ERT2 is homogeneously expressed along the crypt-villus axis in both differentiated and undifferentiated cells (Janssen et al, 2002; Pinto et al, 1999; Robine et al, 1997). By PCR, we detected specific excision of TRF1 in the Villin-expressing tissues such as the small intestine and colon but not the spleen (negative control) **(Fig. 26A)**. This resulted in a marked decrease in TRF1 protein expression as shown in the heatmaps of figure 26B**.** In particular, while control *TRF1*$^{+/+}$*;Villin-CreERT2*$^{+/T}$ mice show a normal small intestine morphology and normal TRF1 expression enriched at the crypts (particularly at the +4 to +7 position) (**Fig. 26B,** top panel; **Fig. 28A**), *TRF1*$^{lox/lox}$*;Villin-CreERT2*$^{+/T}$ mice show a dramatic decrease of TRF1 expression in most intestinal cells (**Fig. 26B,** bottom panel; **Fig. 28A**). This was concomitant with severe weight loss in some individuals (**Fig. 26C)** and aberrant intestinal morphology going from moderate lesions to severe lesions where the normal structure of the cript/villi was lost (**Fig. 27A,** left panel). In the moderate lesions, we observed a shortening of the villis and a diffuse inflammatory infiltration with lymphoid cells. Interestingly, almost all crypts that were moderately lesioned contained at least one cell at position +4 to +7 with residual TRF1 expression. (**Fig. 27A,** left-middle panels). Moderate lesions additionally led to a lower density of crypts/villi (**Fig. 27B**). In the severe lesions the morphology of the intestine was lost, showing severely atrophic microvillis, a higher amount of lymphoid infiltrates and a lamina propia in the duodenum without Brunners glands concomitant with a complete loss of TRF1 expression (**Fig. 27A,** left-bottom panels). This was coincidental with an increased abundance of apoptotic cells and cells with big-, endoreduplicated nuclei (**Fig. 27A,** right panel; quantification in **Fig. 27C&D**). The highest amount of apoptotic and endoreduplicated cells was found at the stem cell region from +4 to + 7 positions **(Fig. 27C&D).** Increased apoptosis was also confirmed by caspase3-positive staining (**data not shown).**

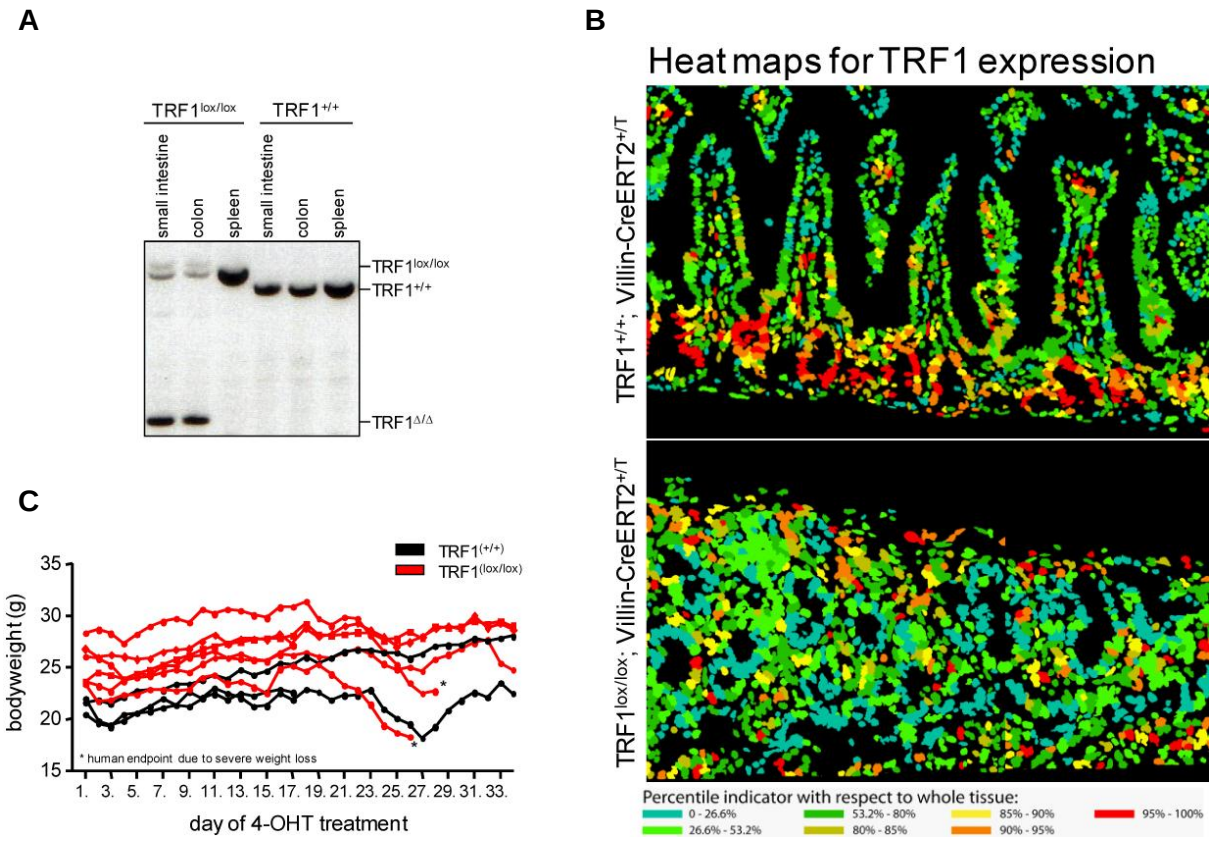

Figure 26. Conditional TRF1 deletion in the small intestine leads to severe degeneration of villi and crypts coincidental with increased DNA damage, apoptosis and replication problems at the stem cell areas.

(A) PCR confirmation of TRF1 excision in the villin-expressing tissues of the colon and the small intestine but not in the spleen. The upper TRF1$^{lox/lox}$ band might correspond to lymphocytes present in the intestine. **(B)** Heat maps indicating the amount of TRF1 per nucleus in the intestine (warmer colors stand for higher amounts of TRF1). The small intestine areas showing chronic lesions are completely ablated for TRF1 expression (bottom). **(C)** Bodyweight of *TRF1$^{+/+}$; Villin-CreERT2$^{+/T}$* (black) and *TRF1$^{lox/lox}$; Villin-CreERT2$^{+/T}$* (red) mice during the treatment with 4-OHT. Two *TRF1$^{lox/lox}$; Villin-CreERT2$^{+/T}$* mice lost weight rapidly (indicated by *) and had to be sacrificed.

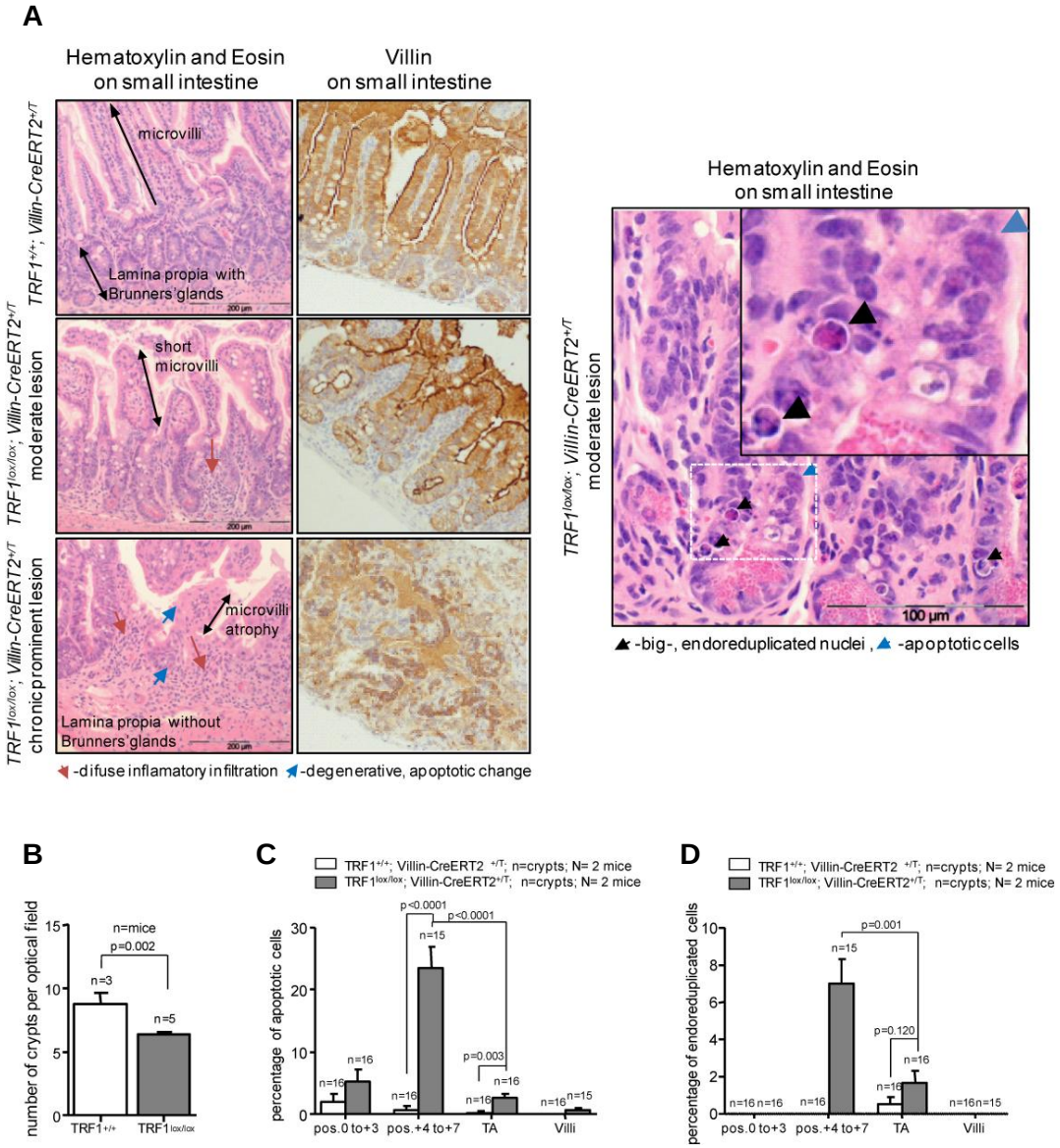

Figure 27. Conditional TRF1 deletion in the small intestine leads to severe degeneration of villi and crypts coincicental with increased DNA damage, apoptosis and replication problems at the stem cell areas.

(A) Left panel: Hematoxylin & Eosin staining (H&E) and Villin immunostaining of *TRF1*$^{+/+}$*; Villin-CreERT2*$^{+/T}$ and *TRF1*$^{lox/lox}$*; Villin-CreERT2*$^{+/T}$ intestines treated with 4-OHT showing moderate and severe permanent chronic lesions. In the treated intestines epithelial columnar absorptive cells disappear leading to a shortening of the villi (middle and lower pictures). In the severe cases, the epithelial lining is lost and a chronic inflammatory response is seen in mucosa and lamina propria (bottom pictures). Right panel picture: a representative H&E image showing apoptotic and endoreduplicated nuclei in *TRF1*$^{lox/lox}$*; Villin-CreERT2*$^{+/T}$ intestines upon treatment with 4-OHT (black arrows for apoptosis; blue arrow for endoreduplication). A close up picture of the designated area is also shown. **(B)** The number of crypts per optical field is significantly decreased in *TRF1*$^{lox/lox}$*; Villin-CreERT2*$^{+/T}$ intestines compared to the *TRF1*$^{+/+}$ mice. Indicated is the average number of crypts that are visible on a 200x magnification of an intestine, lined parallel to the picture border. Error bars, SEM; statistical comparisons were done using two sided student *t*-test. **(C&D)** Percentage of apoptotic and endoreduplicated cells in the indicated crypt compartments and genotypes. The highest numbers of apoptotic and endoreduplicated nuclei are found at positions +4 to +7, which contain a putative stem cell population. Error bars, SEM; statistical comparisons were done using two sided student *t*-test.

Next, we addressed whether increased apoptosis was associated with increased DNA damage upon TRF1 deletion (Martinez et al, 2009). We observed increased levels of γH2AX positive cells in all intestinal compartments with the highest amounts in epithelial cells from intestines with a chronic prominent lesion caused by *Trf1* deletion **(Fig. 27A&B)**. In addition, we observed increased abundance of telomere induced foci, which represent telomeres co-localizing with DNA damage foci (**Fig. 27B&C**), indicating that the DNA damage response induced by TRF1 ablation is most likely due to telomere dysfunction (Martinez et al, 2009). Intestines with moderate lesions shown in Fig 27B showed remaining TRF1 expression in their crypts (arrow), predominantly at the +4 to +7 positions.

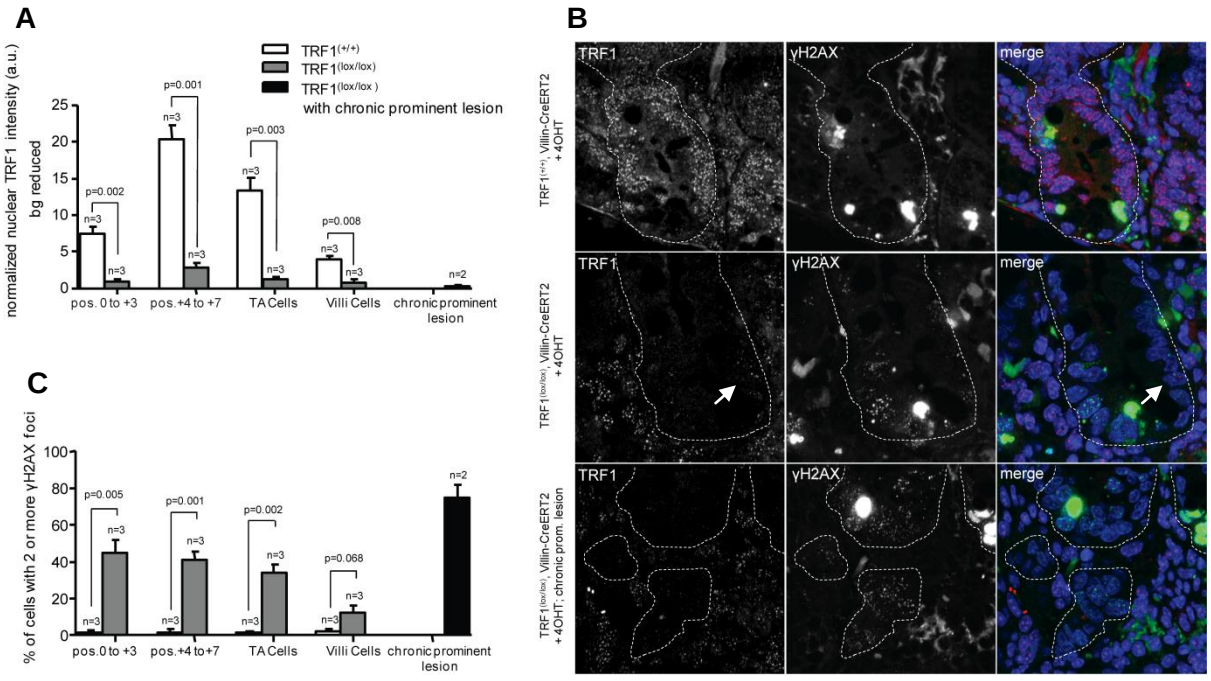

Figure 28. TRF1 ablation induces DNA damage response

(A) Graph of background (bg) reduced TRF1 intensities (in arbitrary units (a.u.)) per nucleus in *TRF1$^{lox/lox}$; Villin-CreERT2$^{+/T}$* and *TRF1$^{+/+}$; Villin-CreERT2$^{+/T}$* mice treated with 4-hydroxitamoxifen (4OHT) after immunofluorescence staining. There is a significant TRF1 intensity decrease upon ablation of TRF1 expression. Almost no TRF1 could be detected in intestines from mice that showed atrophic intestinal structures with a chronic permanent lesions of the intestine, where no compartments could be identified. Error bars, SEM; statistical comparisons were done using two sided student *t*-test. **(B)** Representative γH2AX and TRF1 immunofluorescence pictures of *TRF1$^{lox/lox}$; Villin-CreERT2$^{+/T}$*, and *TRF1$^{+/+}$; Villin-CreERT2$^{+/T}$* intestines. Arrows point to residual TRF1 in cells predominantly located at the +4 to +7 position. **(C)** Percentage of cells with 2 or more γH2AX foci is significantly increased in all compartments of the *TRF1$^{lox/lox}$; Villin-CreERT2$^{+/T}$* intestines. Error bars, SEM; statistical comparisons were done using two sided student *t*-test.

Interestingly, we observed that TRF1 deletion also lead to a significant shortening of telomeres in all the intestinal compartments, with the most prominent shortening in the cells located at the +4 to +7 position of the crypts, containing a potential stem cell population (**Fig. 29A&B**), suggesting increased duplication rates at the stem cell pools to compensate severe intestinal atrophy and severe cell loss owed to TRF1 ablation.

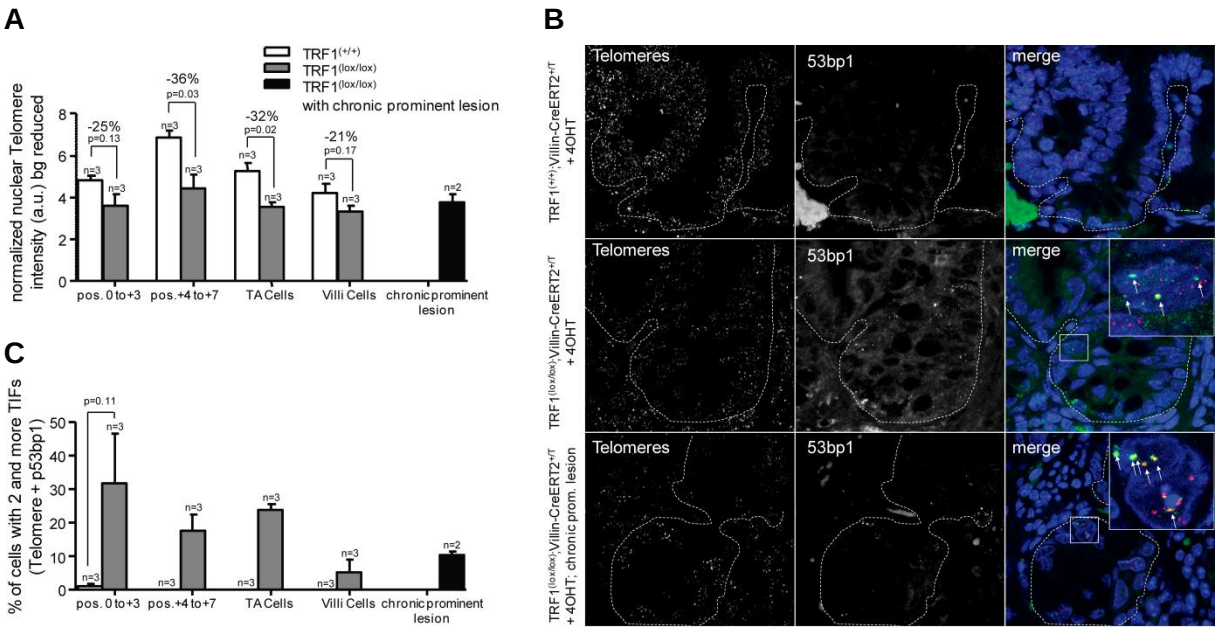

Figure 29. Telomere ablation leads to a hyperproliferative compensation of cells accompanied with telomere shortening and TIFs

(A) Graph of background corrected intensities per nucleus of Q-FISH labelled telomeres. We see in all 4 intestinal compartments a decrease of telomere length. The most pronounced decrease is seen at the position +4 to +7 in the intestinal crypt. This finding points to a hyperproliferation of the cells in this region, possibly to compensate for severe intestinal atrophy as the consequence of TRF1 deletion. **(B)** Representative pictures of immuno-telomere Q-FISH on intestines of either genotype treated with 4OHT. An intestine with a chronic atrophic intestinal structure, where no compartments could be identified, is also included in the analysis (bottom). **(C)** Cells with 2 or more telomere induced foci (TIF, telomeres positive for 53bp1 foci). Statistical analysis was not always possible as in the *wild-type* condition as no TIFs were detected. Error bars, SEM; statistical comparisons were done using two sided student *t*-test. Error bars, SEM; statistical comparisons were done using two sided student *t*-test.

5.13. CONTRIBUTING AUTHORS

José Alejandro Palacios

Helping with the CHIP and co-IP experiments

Miguel Foronda

qRT-PCR analysis of lentiviral infected MEFs and ChIP-qRT-PCR

Ianire Garrobo & Rosa Maria Marion

Various reprogramming assays and knock-down experiments in the part about TRF1 being essential for nuclear reprogramming.

Sagrario Ortega

General help with teratoma and chimera formation assays.

6. DISCUSSION

6.1. THE RATIONALE BEHIND THE GENERATION OF THE EGFP-TRF1 MOUSE

Telomeric DNA is bound by a protein complex called shelterin. It protects chromosome ends from being recognized as a DSB by DNA repair mechanisms which would initiate cell cycle arrest and senescence or apoptosis. A key component of this shelterin protein complex is the telomere repeat binding factor 1. TRF1 binds the double stranded telomeric sequence acting as a scaffold for other shelterin proteins building up a protective, loop forming nucleoprotein structure at the chromosome ends. As TRF1 binds to the double stranded telomeric DNA, which makes up the majority of the telomere, it was expected that the amount of TRF1 would correlate with the telomere length (Chong et al, 1995; Zhong et al, 1992). Based on this hypothesis we generated a mouse model that expresses a knocked-in eGFP tag in the TRF1 locus. This model would give us a tool to measure the telomere length indirectly, but *in vivo*.

The analysis of TRF1 levels in murine and human skin samples of different ages clearly showed that TRF1 expression does decrease with age, which is in agreement with age dependent telomere shortening. However, analyzing the telomeres we could see that the telomere length decrease is much less pronounced when compared to the TRF1 expression drop (i.e. the amount of detected TRF1 per nucleus decreased by 40% whereas the amount of detected telomere repeats decreased around 10-fold less). These results suggested that different molecular mechanisms than telomere length underlie the regulation of TRF1 levels throughout life. The eGFP-TRF1 reporter mouse, even if it can only partially be used to follow telomere length, would give us a valuable tool to study the expression of TRF1 in normal and pathological conditions (i.e. ageing and cancer), the identification of new TRF1 partners and to track telomeres in living cells upon exposure to different agents and stimuli (i.e. FRAP assays under different conditions, telomere localization within the nucleus,...).

6.2. THE EGFP-TRF1 FUSION PROTEIN LOCALIZES TO TELOMERES

As in our mouse model the relatively big eGFP-Tag is fused to the TRF1 protein the proper localisation of the eGFP-TRF1 knock-in protein was not certain. The tag could stericaly shroud the DNA binding site or interfere with other important properties of the protein. Importantly, we could show in MEFs that the eGFP emission co-localizes with other factors of the shelterin complex, known to concentrate at the telomeres. This gave us the certainty that we can trace telomeres *in vivo* by the localization of the eGFP emission. This is useful for processes from which we know that the telomere localisation is of crucial

importance such as the telomere aggregation and localisation at the nuclear lamina (Raz et al, 2008) or the inner nuclear envelope localisation in meiotic spermatocytes during the nuclear membrane polarisation (Scherthan et al, 2000; Siderakis & Tarsounas, 2007).

6.3. eGFP-TRF1 FUSION PROTEIN BINDS TO TELOMERIC REPEATS AND INTERACTS WITH THE KNOWN SHELTERIN PROTEINS

As seen by ChIP assay, the eGFP-TRF1 fusion protein is able to bind to the telomeric DNA. This excludes that the telomeric localisation of the fusion protein is conducted by other shelterin proteins that bind TRF1 (i.e. TIN2 (Kim et al, 1999)) and direct TRF1 to the shelterin complex without the necessity of eGFP-TRF1 to bind the telomeric DNA. Moreover, in a coimmunoprecipitation experiment followed by a mass spectrometry analysis we found that the eGFP-TRF1 fusion protein binds to the known binding partners and pulls down, with good scores, all the shelterin complex proteins that were also found in a wild-type TRF1 pull down. This clearly indicates that the fusion protein is able to interact with its binding partners and that it can form dimers with endogenous TRF1 and with itself. This also indicates that the TRF1 binding site of the TRF-homology domain is not affected by the eGFP-tag (Fairall et al, 2001).

6.4. HYPOMORPHIC BEHAVIOUR IN THE *eGFP-TRF1*-HOMOZYGOUS MICE

The WT and the *eGFP-TRF1/TRF1* heterozygous cells and mice do not show any phenotypical differences neither *In-vitro* nor *in-vivo*. However, the homozygous-KI genotype shows several phenotypes that are caused by the eGFP knock-in tag insertion. The most overt is the late embryonic lethality. This, if compared to the classical TRF1 knockout mouse that die at the blastocyst stage (Karlseder et al, 2003), indicates that the eGFP-TRF1 fusion protein is partially functional as embryos are viable until around day E13.5. The causes underlying embryonic lethality in the homozygous-KI mice are not known. *In-vitro* the homozygous-KI MEFs show an increased amount of multitelomeric signals (that represent stalled replication forks as described in (Martinez et al, 2009; Sfeir et al, 2009)), growth retardation and a lower efficiency of nuclear reprogramming. On the other hand, and in contrast to conditional TRF1-null cells, KI/KI cells are able to cycle, induce iPS cells that give raise to differentiated teratomas and contribute to chimerism and the tagged protein interacts with all the known shelterin complex proteins. In addition in eGFP-TRF1$^{KI/KI}$ cells, there was no indication of an activated DDR that would initiate senescence due to uncapped telomeres. The eGFP-TRF1 protein functionality could also be seen when eGFP-TRF1$^{+/KI}$ mice were

crossed with TRF1$^{lox/lox}$; K5-Cre mice. The resulting TRF1$^{eGFP\text{-}KI/\Delta}$; K5-Cre mice did not have the macroscopic phenotypes seen in TRF1$^{lox/lox}$; K5-Cre mice. In contrast to TRF1$^{\Delta/\Delta}$; K5-Cre mice that die perinatally, they showed normal hair growth, no hyperpigmentation and long time survival and normal weight (data not shown). This demonstrates that the eGFP-TRF1 protein has at most a mild hypomorphic behaviour in stratified epithelia. However, the fact that the eGFP-TRF1 allele in homozygosis is embryonic lethal underscores the important role for TRF1 during embryogenesis where TRF1 not only has telomere capping functions (Karlseder et al, 2003). It is possible that the eGFP-tag at the amino terminal of the TRF1 protein sterically interferes with the proper function of the TRF1 protein. As discussed above, eGFP-TRF1 localizes at the correct position indicating that the NLS as well as the DNA binding domain function properly. Given the fact that they are the most distant domains (in the primary protein structure) to the eGFP knock-in tag, the closer located TRFH and the acidic domain have a higher possibility to be affected by the eGFP-Tag (see Introduction Fig. 5 and results Fig. 2). Of those, the TRFH domain seems to be fully functional as the shelterin complexing partner binding as well as the homodimerisation can be initiated with eGFP-TRF1 protein. The only functional domain that is left to be possibly affected is the acidic domain at the N-terminus of TRF1 and the closest domain to the eGFP-tag.

It has recently been shown that TRF2 is able to condense the telomeric DNA. The basic domain plays an important role for the execution of this function, and is located at the N-terminus of TRF2, neutralizing the negative surface charge of the telomere DNA allowing its compaction into nucleosomes (Baker et al, 2011). The TRF1 acidic domain is found in the same position and exerts the opposite function. If this domain is absent or impaired, TRF1 is also able to condense DNA, pointing to the role of the TRF1 acidic domain in preserving the chromatin in a more open, plastic structure (Marion et al, 2009b; Poulet et al, 2011). Additionally, TRF2 is an inhibitor of the resolvase enzyme, an enzyme that is important in resolving of Holiday junctions, stalled replication forks and the opening of the T-loop that is recognized as a Holiday junction (Lewin et al, 2008; Poulet et al, 2009). If the eGFP-Tag indeed interferes with the acidic domain it might potentiate the resolvase inhibition, counteracting the cleavage of stalled replication forks and leave an increased number of stalled replication forks. These suggestions are in accordance with our findings of increased multitelomeric signals in the eGFP-TRF1$^{KI/KI}$ MEF and iPS cells that are detected by Q-FISH as multitelomeric signals (Sfeir et al, 2009). The fact that the eGFP-TRF1$^{KI/KI}$ MEFs are able to be reprogrammed and the lack of a phenotype, similar to that seen in TRF1-null mice, argues that the eGFP-TRF1 tag does not interfere with other TRF1 properties.

In some experiments (i.e. western blots) we could see, that in the eGFP-TRF1$^{+/KI}$ samples the amount of eGFP-TRF1 is slightly lower if compared to the endogenous TRF1.

This might indicate that there is a slight favouring for endogenous TRF1. On the other hand this might also be caused by the antibodies used that are unable to bind to their TRF1 epitope by the eGFP-tag.

In summary we can conclude, that eGFP-TRF1mice can be used *in vitro* and *in vivo* as a tool to follow telomeres, allowing a closer insight into TRF1 biology. However, it should be kept in mind that both homozygous-KI cells and mice (embryos) are influenced by eGFP-tag and show hypomorphic behaviour.

6.5. TRF1 EXPRESSION DURING NUCLEAR REPROGRAMMING

We have shown that the amount of TRF1 bound to the telomeres is not directly correlated to the telomere length. Over age, the amount of TRF1 decreases to a higher extent than the amount of telomeric DNA repeats, suggesting that TRF1 expression as well as its binding to telomeres is not directly regulated by telomere length. To get a closer insight into the properties of TRF1 we decided to reprogram MEFs obtaining eGFP-TRF1 iPS cells. IPS cells express active telomerase and consequently elongate their telomeres (Marion et al, 2009b). This gives us the possibility to study the behaviour of TRF1 during reprogramming and in pluripotency. Even though the reprogramming efficiency in eGFP-TRF1$^{KI/KI}$ is lower when compared to WT and heterozygous-KI, these cells were able to undergo nuclear reprogramming forming ES cell like colonies. From MEFs with the same telomere length in all the genotypes and only faint eGFP-TRF1 detection in heterozygous- and homozygous-KI, reprogramming initiated the telomerase dependent telomere elongation that lead to iPS cells with telomeres twice as long after seven passages. Interestingly, at around 16 passages the KI/KI iPS cells abruptly abrogated their telomere elongation. The underlying mechanism of this observation remains to be elucidated and we can only speculate that the accumulation of multitelomeric signals inhibits a further elongation or that the interference of the eGFP-tag that in iPS cells is abundant in a higher density, sterically impairs the telomerase function.

Comparing telomere lengths in iPS cells of all three genotypes with their corresponding eGFP emission, an unexpected but very interesting behaviour of the telomere bound TRF1 could be observed. While the telomere lengths increased by approximately two fold at passages ≥7, the amount of telomere bound eGFP-TRF1 had increased to much higher extents at early passages after reprogramming. Further, the levels of eGFP-TRF1 remain high while telomeres keep elongating pointing to a yet unknown role of TRF1 in pluripotent cells. This hypothesis is supported by the observation that in aging skin, older skin loses its reproductive potential and simultaneously decreases the detectable TRF1 in a disproportional manner to the telomere length, suggesting a role of TRF1 in tissue

regeneration capacity. We could further show that the TRF1 upregulation is similar to the increase in Nanog and OCT3/4 levels during nuclear reprogramming. This is in agreement with a previous report showing that TRF1 is among the most upregulated genes associated with pluripotency and at that state going along with telomerase dependent telomere elongation (Boue et al, 2010). A final but important proof that the TRF1 expression is uncoupled from telomere length is the fact that during reprogramming of TPP1-null MEFs, TRF1 levels are also highly increased. This is striking as TPP1 is the shelterin complex protein responsible for bringing active telomerase to telomeres. TPP1-deficient cells are not able to elongate the telomeres after nuclear reprogramming (Tejera et al, 2010). These results clearly demonstrated for the first time that the levels of TRF1 are independent of telomere length. Nevertheless, this interesting new finding means that the eGFP-TRF1 mouse model can no longer be used as an *in vivo* telomere measurement tool

6.6. TRF1 INDICATES THE PLURIPOTENCY POTENTIAL OF A CELL

The fact that iPS cells from all the three genotypes are able to contribute to chimerism and induce teratomas that differentiate into the three germ layers, indicates a complete reprogramming of the parental MEF cells. In addition, the iPS-exome showed an increased expression of pluripotency markers such as OCT3/4 as well as Nanog. The latter is expressed at different levels in iPS cells of the same colony and marks proportionally the vigour of pluripotency (Chambers et al, 2007; Villasante et al, 2011). Following Nanog expression pattern of iPS cells, a similar pattern of the eGFP signal in the iPS colonies was encountered. Plotting the intensities of Nanog and eGFP-TRF1 against each another a significant positive correlation was revealed. In contrast, the expression of OCT3/4 was expressed homogeneously in iPS cell colonies. To investigate a possible correlation of TRF1 with high pluripotency, iPS cells were sorted for their eGFP-TRF1 content. Cells that expressed a high level of TRF1, in contrast to iPS cell expressing low TRF1 levels, were successfully able to induce teratomas and to form chimeras. These results suggest that TRF1 expression correlates with pluripotency potential.

EGFP-TRF1 expression in iPS cells sorted for high and low eGFP-TRF1 content was conserved from RNA transcription levels. The transcription *of eGFP-TRF1* and *Nanog* mRNA showed the same high/low pattern on messenger RNA, whereas *oct3/4* was transcribed to same extents in eGFP-TRF1^{high} and eGFP-TRF1^{low} iPS cells. Together with *Nanog* and *eGFP-TRF1*, *mTert* another stem cell indicator, was also found to be transcribed to higher levels in eGFP-TRF1^{high} cells. These findings suggest that expression levels of TRF1 are correlated with increased pluripotency in iPS cells.

6.7. TRF1 IS REQUIRED DURING REPROGRAMMING

Importantly, we show here that high TRF1 levels are not only a marker for pluripotency as demonstrated by a higher ability to form teratomas and chimeric mice, but also that TRF1 is essential both for reprogramming as well as for the maintenance of the pluripotent state. In particular, TRF1-deficient MEFs completely fail to be reprogrammed, even in the absence of p53 that has been shown to rescue cell growth (Marion et al, 2009a; Martinez et al, 2009). Furthermore, conditional deletion of TRF1 in already established iPS cells leads to rapid elimination of iPS cells coincidental with increased DNA damage and apoptosis. Whether this phenomenon occurs in a p53 dependant manner is not known as p53 might not be completely functional in ES or iPS cells (Hong & Stambrook, 2004; Tichy, 2011). However it demonstrates that the protection from telomere damage by TRF1 is essential for the maintenance of pluripotency. These results are in marked contrast with efficient reprogramming of cells with severe telomere shortening and uncapping due to telomerase- or TPP1-deficiency (Marion et al, 2009a; Tejera et al, 2010). Together, these results suggest that TRF1 is an important factor for reprogramming of differentiated cells into induced pluripotent stem cells as well as for the maintenance of pluripotency.

6.8. HIGH LEVELS OF TRF1 MARK TISSUE STEM CELLS COMPARTMENTS

Knowing that TRF1 plays an essential role in nuclear reprogramming and is highly expressed in pluripotent stem cells, we set to address the levels of eGFP-TRF1 in tissue. As expected, high levels of eGFP-TRF1 were detected in the known stem cell compartments of the skin and in the intestine. Moreover, if compared to telomere length, the decrease in TRF1 levels in stem cells to differentiated cells was disproportional when compared to the telomere length decrease as seen by Flores et al. (2008) using very similar detection and analysis methods. In particular, in the small intestine where new stem cell pools are discovered frequently, we found differences in the various stem cell compartments in accordance to their stemness potential as determined by LGR5 and the position of the cells in the intestinal crypts (Barker et al, 2007; Montgomery et al, 2011; Schepers et al, 2011; Tian et al, 2011). Moreover, we could show with our fluorescence detection technique, that the $LGR5^+$ cells, interspersing the LGR5-negative paneth cells do not have longer telomeres compared to the cells at the crypt positions +4 to +7. This is a marked contrast to the published results of (Sato et al, 2010) that suggest that the $LGR5^+$ cells in the bottom of the crypt have the longest telomeres. Also in tail skin hair follicles we were able to demonstrate that the stem

cell pools for the sebaceous gland, the hair follicle and the epidermis express higher amounts of TRF1 if compared to the more differentiated cells in the same tissue. In conclusion we can say that in tissue, similar to iPS cells, TRF1 expression levels are a good marker for stemness within the same tissue. This change in levels is even more pronounced than telomere length differences and gives us a new marker to detect tissue stem cells.

6.9. Regulation of TRF1 expression in iPS and ES cells

We showed that TRF1 in ES and iPS cells is upregulated in a telomere length independent manner. Therefore we set to address the reason for this upregulation. From previous research we know that the promoter region of TRF1 has a potential binding site for OCT3/4 (Loh et al, 2006). A functional assay, expressing OCT3/4 in MEFS as well as a CHIP followed by a q-RT-PCR gave us proof that OCT3/4 is indeed able to initiate *TRF1* transcription by binding to its promoter region. However, the *trf1* levels did not reach the levels of *trf1*-mRNA in iPS cells. This suggests that the OCT3/4 dependent increase of TRF1 expression is not the only mechanism for increased TRF1 transcription. In our q-RT-PCR Nanog did not bind the analyzed promoter region, but in a ChIP-PET assay done by Loh et al. (2006) Nanog binds to TRF1 with four overlapping PETs suggesting a very high interaction probability. It is therefore fair to speculate that Nanog itself or Nanog dependent downstream factors are responsible for a further increase in TRF1 expression. This would explain the heterogeneous expression pattern of TRF1 in iPS colonies and the similar characteristics of eGFP-TRF1^{high} and Nanog^{high} iPS cells.

6.10. Conditional ablation of TRF1 in the small intestine

To demonstrate that TRF1 expression is essential for the maintenance of tissue homeostasis we generated a new mouse model where we conditionally deleted TRF1 in the villin expressing tissues. This led to the disruption of the tissue homeostasis similar as observed in skin (Martinez et al, 2009). As long as TRF1 in the stem cell population in crypts was maintained above a critical threshold, the crypt/villi morphology was not disrupted, even though shorter villis and an increased uncapping of telomeres were detected. Interestingly however, as soon as all the cells in a crypt lost the functional TRF1 alleles, the intestine completely collapsed and lost its structure and functions. This was accompanied by intestinal atrophy, diffuse inflammatory infiltration and weight loss of mice in which the main parts of their intestines showed TRF1 deficiencies. Interestingly, crypts with a moderate phenotype

showed severe telomere shortening. The highest amount of telomere shortening was observed in position +4 to +7, the sites where we observed the highest amounts of TRF1 under normal conditions and where the slow cycling stem cells are present. This points to the immense importance of the intestinal stem cells and their requirement to replenish lost cells that either undergo apoptosis or get lost in the intestinal epithelium due to senescence and mechanical loss. It also shows that the constant proliferating pressure on stem cells leads to a compensatory telomere shortening in stem cells and together with the mentioned finding that all remaining crypts have stem cells with TRF1 underlines the importance of TRF1 in intestinal tissue homeostasis and stem cells.

In summary, we describe here new roles for the telomere protective protein, TRF1, in adult stem cells as well as pluripotent stem cells, that are independent of telomere length and which highlight an essential role for telomere protection mediated by TRF1 in stem cell biology. On the one hand, high TRF1 levels mark adult stem cell compartments as well as pluripotent stem cells. Moreover, TRF1 is essential for both, maintenance of adult stem cell compartments of intestine and skin, as well as for the induction and maintenance of pluripotency in iPS cells. Supporting the notion that TRF1 is a key factor for pluripotency we make the unprecedented finding that TRF1 is a direct target of OCT3/4, which binds to the TRF1 promoter and is sufficient to upregulate TRF1, thus providing a mechanistic link between TRF1 and pluripotency.

7. CONCLUSIONS

1. An eGFP-TRF1 knock in mouse model was generated where the eGFP-tag is located in exon 1 just behind the ATG start-codon.

2. The expressed eGFP-TRF1 fusion protein binds to telomeric DNA and allows us to follow the telomeres and TRF1 protein *in vivo* and *in vitro* by the eGFP emitted signal but shows a hypomorphic phenotype in the homozygous knock in.

3. TRF1 levels are highly upregulated in induced pluripotent stem cells in a telomere independent manner. This is partially due to the activation by the pluripotency transcription factor OCT3/4 by binding the TRF1 promoter region.

4. In iPS cell colonies, TRF1 expression correlates with the Nanog expression and indicates a higher level of pluripotency within iPS colonies. Therefore, the sorting of eGFP-TRF1^{high} cells allows us to distinguish between more pluripotent iPS cells when compared to eGFP-TRF1^{low} iPS cells.

5. Tissue stem cells of skin and intestine have elevated levels of TRF1 abundant at their telomeres. The high increase of TRF1 in those cells is independent from telomere length.

6. TRF1 is essential for the induction and maintenance of pluripotency as its deletion inhibits pluripotency by established reprogramming factors and conditional ablation of TRF1 leads to loss of viability in iPS cells.

7. TRF1 is essential for small intestine homeostasis. Its deletion induces inflammation and apoptosis induced by DNA damage response pathways, leading to complete destruction of the crypt/villi morphology.

8. TRF1 loss in the small intestine induces telomere shortening, most prominent in the stem cell position, most likely due to compensatory hyperproliferation replenishing the lost cells.

8. EXPERIMENTAL PROCEDURES

8.1. GENERATION OF THE EGFP-TRF1 KNOCK-IN MOUSE MODEL

The targeting construct and mice with the targeted TRF1 allele were generated by genOway (France; as seen in result part **Fig. 2A**) using standard procedures. The neomycin-resistance (NEO) cassette was excised by crossing with mice carrying the Cre-recombinase. Wild-type, *eGFP-TRF1*$^{+/KI}$ and *eGFP-TRF1*$^{KI/KI}$ mice were generated and maintained at the CNIO mouse facility.

Genotyping of the eGFP-TRF1 allele was performed by PCR as depicted with primers flanking the possible eGFP-cassette.

Forward Primer: 5'-CAGGGTTAAATGCTCATGTTTATGGCG-3'

Reverse Primer: 5'-TGCTCTGGAGAATCCGAATCTGTCC-3'

8.2. GENERATION OF MEFS

Primary MEFs were isolated from E13.5 or E11.5 embryos. Briefly: Uterus was removed and put into PBS with antibiotic at 37°C. Uterus wall was cut to take out the embryos. Liver was removed as well as a part of the head (for genotyping). Embryo was chopped in a 6cm dish with a razorblade in 2x trypsin (Invitrogen 25300-054) in PBS, incubated at 37°C for 20min, dispersed with a Pasteur pipette and incubated for another 20min. Cells were further transferred to a 10cm dish and grown with 15ml DMEM (Invitrogen 31966021) with 10%FCS (Dundee cell products LTD DS1003) and standard tissue culture antibiotics (Gibco 15240).

8.3. GENERATION OF IPS CELLS

Reprogramming of eGFP-TRF1 iPS cells from the indicated genotypes was performed as described by (Blelloch et al, 2007). The cells (like all the iPS cells described in this thesis) were grown in full iPS medium (DMEM; Invitrogen 31966021) supplemented with 15% KSR (Knockout Serum Replacement; Invitrogen 10828028) + LIF (1000U/ml; ESGROTM, Millipore ESG1107) + non-essential amino acids (MEM Non-Essential Aminoacids Solution; 1X; Invitrogen 11140035) + 2-mercaptoethanol (0.5 mM; Invitrogen 31350) + Pen/Strep (1X) on gelatin coated plates. Medium was changed daily and at 70-80% of confluence cells were trypsinized and passed onto a new dish with a 1:7 dilution.

The generation *Tpp1*$^{\Delta/\Delta}$ iPS cells have been described before by (Tejera et al, 2010). ***TRF1*$^{lox/lox}$*; p53*$^{-/-}$ and *TRF1*$^{+/+}$*; p53*$^{-/-}$** MEFs were infected once with retroviral Cre-

recombinase as previously described (Martinez et al, 2009). Puromycin (2µg/mL; Sigma-Aldrich P8833) selection was added 48 hours after the infection. Selected cells were reprogrammed as previously described (Marion et al, 2009a). Obtained iPS colonies were picked 2-3 weeks after infection and expanded on feeder fibroblasts. Feeder fibroblasts were generated by exposition $2x10^7$ to $6x10^7$ cells/ml in a 50ml Falcon tube to a gamma ray emitting source at a total dose of 3000 rads.

Reprogramming and generation of TRF1-null iPS cells. We reprogrammed **TRF1$^{lox/lox}$ and *TRF1$^{+/+}$; RERTn$^{+/ERT}$*** MEFs (Guerra et al, 2003) as described above. The resulting iPS clones were picked and treated with 4-hydroxytamoxifen (Sigma-Aldrich 10013) to obtain *TRF1$^{\Delta/\Delta}$* and *TRF1$^{+/+}$* iPS cells, respectively. IPS from both genotypes were seeded at low density (50,000 cells per well in 6well-plates) on feeders or gelatin coated (for qRT-PCR analysis) dishes and treated with 4-hydroxytamoxifen at a final concentration of 0.2µM in complete iPS medium, which was replaced daily.

TRF1 deletion in iPS cells was obtained from *TRF1$^{lox/lox}$; p53$^{-/-}$* Cre MEFs. The Genotype was checked by PCR with:
Forward primer: E1-popout 5′-ATAGTGATCAAAATGTGGTCCTGGG-3′
Reverse primer: SA1 5′-GCTTGCCAAATTGGGTTGG-3′.

Efficiency of reprogramming was determined by alkaline phosphatase activity (AP detection kit, Chemicon International), following the manufacturer's instruction.

8.4. CHIMERA FORMATION

The ability of the iPS clones to generate chimeras *in vivo* was tested by aggregation with CD1 (albino) morulae following standard procedures as described in (Marion et al, 2009b). At least two independent iPS clones from each genotype (sorted and unsorted) were tested.

8.5. WESTERN BLOTTING

Whole cell and nuclear protein extracts as described by (Martinez et al, 2009), were used for western blot analysis. Protein concentration was determined using the Bio-Rad DC Protein Assay (Bio-Rad). Up to 25µg of protein per extract were separated in SDS–polyacrylamide gels by electrophoresis. After protein transfer onto nitrocellulose membrane (Whatman), the membranes were incubated with the indicated antibodies (see below).

Antibody binding was detected after incubation with a secondary antibody coupled to horseradish peroxidase using chemiluminescence with the ECL detection KIT (GE Healthcare) or by antibodies coupled to Alexa680 (Invitrogen) emitting light at 700nm upon excitation. Detection was performed on an Odyssey Clx (Li-COR) infrared detector.

Antigen	Dilution	Providor	Product number
Nanog	1:5000	Millipore	AB5731
Actin	1:7500	Sigma	a2228
eGFP	1:1800	Invitrogen	a11122
eGFP	1:3000	Clontech	JL8 632380
Oct3/4	1:500	Santa Cruz	sc-9081
SMC1	1:1000	Bethyl	A300-055A
TRF1	1:5000	Abcam	ab-10579
Villin	1:5000	Dako	M3637

8.6. Immunostainings on MEFs, iPS cells, and tissue sections

Cells were grown on gelatin covered glass bottom dishes (24 well plates; MatTek). **Cells and OCT** sections were fixed with 4% formaldehyde in PBS for 8min at 37°C, permeabilized in 0.5%Triton-X100 in PBS and blocked with 100% Australian FBS (GENYCELL) for 40min at room temperature (RT).

Paraffin Tissue sections were deparaffinised and a citrate antigen retrieval was performed at pH 6.5 (TRF1) or with CC1M-Buffer (Ventana). For direct eGFP-TRF1 detection combined with an immunostaining fresh frozen tissue sections (14µm) from tissue embedded in tissue freezing medium (Jung) were used. Sections were further blocked with 100% Australian FBS (GENYCELL) for 40min at RT.

The antibodies for all tissues and cells were applied overnight at 4ºC in antibody diluents with background reducing agents (Invitrogen). Primary antibodies used see table. Secondary antibody incubation was performed after three 5min washing steps with PBS for 40min at RT. The nuclei were counterstained in a 4µg/ml DAPI/PBS solution before mounting with Vectashield (Vector).

8.6.1. PRIMARY ANTIBODIES

Antigen	Dilution	Providor	Product number
GFP	1:500	Roche	11814460001
Nanog	1:180	Novus	NB100-58842
Oct3/4	1:180	Santa Cruz	sc-9081
TRF1	1:250	Homemade by Munoz et al., 2005	
TPP1	1:200	Gift Dr. Else, University of Michigan	
Rap1	1:100	Bethyl	A300-306A
γH2AX	1:500	Millipore	05-636
53BP1	1:200	Novus	NB100-304

8.7. STANDARD Q-FISH PROTOCOL

Slides were washed in PBS and further fixed in 4% formaldehyde (Sigma)/PBS for 2min followed by a 3x5min washing step with PBS. Slides were further incubated in 0.1% porcine pepsine (Sigma), 0.01M HCL (Merck) for 10min at 37°C, washed with PBS and another fixing and washing step was performed. Slides were then dehydrated in 70%, 90% and 100% Ethanol dilutions. Slides were further air dried and the Q-FISH labelling probe mix was applied. The probe mix consists of 10mM Tris, 25mM MgCl, 9mM citric acid, 82mM Na_2HPO_4 (adjusted to pH 7), 70% deionised formamide (Sigma), 0.25% blocking reagent (Roche) and 0.5µg/ml Telomeric PNA-probe (Panagene). Slides were further covered with a cover slip and the DNA was denatured on a pre-warmed heating plate at 85°C for 3min. Slides were then incubated for 3 hours in a wet chamber at RT , followed by a 2x15min washing step in 70% formamide, 10mM Tris and 0.1% BSA (Sigma). After another 2 x 15min of washing with 0.08% Tween20 (Sigma)/TBS slides were incubated in a 4µg/ml dapi (Sigma) solution and mounted with Vectashield (VectorTM)

Telomeric PNA-probe was generated at Panagene directed against telomeric repeats. The PNA sequence is: Cy3-00-CCCTAACCCTAACCCTAA-Lys

8.8. TELOMERE LENGTH AND CYTOGENETIC ANALYSIS USING TELOMERE Q-FISH ON METAPHASES AND INTERPHASES

For **metaphase Q-FISH analysis**, cells were incubated with 0.1 mg/ml colcemide (Gibco) for 4 h at 37°C, swollen in hypotonic buffer (10mMTris-HCL at pH 7.5, 10mM NaCl, 5mM $MgCl_2$) for 10 min at 37°C, and fixed with methanol/acetic acid as described in (Samper et al, 2001). Metaphases were dropped onto slides and the Q-FISH protocol was performed as described above. For the determination of the telomere length we used the TFL-Telo software (Zijlmans et al, 1997). The metaphases were additionally scored by eye for the presence of multitelomeric signals and sister type chromatid fusions by superimposing the telomere image on the DAPI chromosome image. Where telomere lengths are indicated, the values were calculated by a linear correlation to L5278-R cells (r-cell). Their telomere length remains stable and was determined before at 79.4kb of length (Canela et al, 2007b).

For **interphase Q-FISH analysis**, MEFs and iPS cells were plated on gelatin covered glass bottom dishes (24well plates; MatTek) and fixed with methanol/acetic acid (3:1). A standard Q-FISH protocol was performed as described above but in the case of iPS cell colonies the denaturation step was carried out in a water bath at 80°C and the PNA probe incubation step was repeated after two hours of incubation. The total PNA probe incubation was increased to a total of 6 hours in the case of iPS cell colonies to get a good diffusion of PNA probe through the colonies. Where telomere lengths are indicated, the values were calculated by a linear correlation to L5278-R cells (r-cell). Their telomere length remains stable and was determined before at 79.4kb of length (Canela et al, 2007b).

8.9. IMMUNOFISH

In cells, immunostainings were performed as described above. After washing the excess of secondary antibodies with PBS, cells were fixed in 4% formaldehyde/PBS for 2min, dehydrated with ethanol, and incubated with the PNA probe against telomeric repeats labelled with CY3 (Panagene). The probe was thereby diluted in only 50% of formamide instead of 70% as described in the standard Q-FISH protocol. The technique is also described in (Gonzalo et al, 2006; Samper et al, 2001).

In tissues, as a first step the telomeric Q-FISH was performed using citrate antigen retrieval (10 mM sodium citrate (pH 6.5) cooked under pressure for 2 min) instead of pepsin antigen retrieval avoiding complete digestion of antigens. Further the slides, without formaldehyde fixation, were dehydrated by decreasing ethanol dilutions as seen in the

standard protocol, air dried and the PNA incubation step followed as described above. After the first washing steps with formamide a normal immunostaining was performed as described in the paragraph for immunostainings for tissues. No additional antigen retrieval was applied.

8.10. MICROSCOPY

Image acquisition: Fluorescence staining as well as the endogenous *eGFP-TRF1* emission and the Q-FISH were acquired in a confocal high-resolution Leica TCS-SP5 (AOBS) microscope. 8-bit image layer stacks were taken with a step size of 0.8 µm and maximum projected by the LAS AF (Leica) software for analysis.
The metaphase Q-FISH was acquired with a Fluorescence microscope (Leica DM RA2) at 1000x for telomere measurement with TFL Telo software as described above.

Segmentation and quantification of objects for the analysis of fluorescence intensities of all stainings that were analyzed was performed with Definiens Developer XD1.2, XD 1.5 or XD 2.0 software (Definiens). Nuclei and spots were segmented with cellenger and developer algorithms or by hand. Algorithms were written by hand and are available upon request. Intensities were exported with an own made developer ruleset into excel readable files (rulesets are not published in this thesis but information about them can be asked at www.lifelength.com). Where indicated the intensities, were converted into heat-maps of the different tissues with the Definiens Developer using an own made algorithm calculating the indicated fluorescence intensity percentiles and assigning the colour code fully automated. Lgr5-GFP positive nuclei in the intestine and tail skin were selected by hand for further analysis of their nuclei.

The quantification of eGFP-TRF1 in mouse tissue was done on fresh frozen tissue. The tissue cuts as well as cells were fixed in 4% PFA/PBS for 4min at 37ºC washed in PBS and embedded with Vectashield (Vector). Pictures were acquired on the same day to avoid signal intensity losses by eGFP degradation. The analysis was done with an own made Definiens Developer algorithm including a background reduction taking into account the mean, non-spot green-channel intensity per nucleus due to the high autofluorescence in the eGFP emitting spectrum.

Quantification of TIFs in TRF$^{\Delta/\Delta}$ intestines has been analyzed by an automated costaining-analysis with an own made Definiens algorithm after a Cellenger spot-segmentation for Telomeres (red) and 53bp1 foci (green). Telomeres that overlapped with 53bp1 Foci were considered as TIFs.

8.11. PREPARATION OF NUCLEAR EXTRACT FOR IMMUNOPRECIPITATION AND MASS SPECTROSCOPY ANALSYSIS

eGFP-TRF1 KI/KI, KI/+ and +/+ iPS cells (1.50 x 107) were resuspended in 15mL of osmotic buffer (10mM Hepes pH 7.5, 210mM manitol, 70mM sucrose, 1mM EDTA, 1X protease inhibitor cocktail (Sigma), 1mM NaVO4, 5mM beta-glycerophosphate, 0.1 M PMSF, 5mM NaF) and cytoplasmic membrane was broken using a Dounce homogenizer. Nuclei were pelleted by centrifugation at 800g for 10min at 4°C, resuspended in 1mL of RIPA buffer (150mM NaCl, 10mM Tris pH 7.5, 0.1% SDS, 1% Triton, 1% deoxycholate, 5mM EDTA) and lyzed for 30min in a rotating wheel for 30min at 4°C. Nuclear lysate was sheared by sonication during for 15min (30s ON and 30s OFF) and then cleared by centrifugation at 13000rpm for 15min. Total nuclear lysates were immnunoprecipitad using µMACS™ GFP Tagged Protein Isolation Kit (Miltenyibiotec; 130-091-125). Immunoprecipitated complexes were digested following the FASP protocol (Wisniewski et al, 2009) using sequentially LysC (Wako) and Trypsin (Trypsin Gold, Promega). Peptides were loaded in a Reprosil AQ Pur C18 (250mm x 0.075mm) capillary column (Dr. Maisch GmBH) with 0.1% formic acid and separated at a flow of 300ml/min in a 175min linear gradient generated by an Eksigent nanoLCultra 1D+ (Eksigent). The column was directly coupled to a LTQ-Orbitrap-Velos mass spectrometer through a 20µm I.D., 10µm tip, silica PicoTip nanospray emitter (New Objective) operated at 1.8kV. The mass spectrometer was programmed to acquire spectra in a data dependent mode. The survey scans were acquired in the Orbitrap mass analyzer with resolution 60,000 at m/z 400 with lock mass option enabled for the 445.120024 ion. For each MS scan, up to the 15 most intense peaks with charge state ≥2 and above an intensity threshold of 1000 were selected for sequencing and fragmented in the ion trap by collision induced dissociation with normalized collision energy of 40%, activation q=0.25, activation time of 10ms, and one microscan. To minimize redundant sequence of peptides, masses sequenced more than once were dynamically excluded for 60 sec.

The raw data generated was processed with the Protein discoverer program 1.2 (Thermo). Database search was performed by MASCOT 2.2 search engine (www.matrixscience.com) interrogating the IPI_mouse database V3.81 (Mar2011) 59,593 entries with a precursor tolerance of 10ppm and fragment tolerance of 0.3Da. The search considered cysteine carbamidomethylation as fixed modification, oxidation of methionine as variable modification and allowed up to two missed cleavages for protease. Only peptides and proteins with a FDR lower than 1% were considered for identification.

8.12. FLOW CYTOMETRY ANALYSIS

Trypsinized iPS cells grown in KSR-ES-medium were washed in PBS supplemented with 1% FBS, fixed in 3% PFA (Sigma) at RT for 15min and permeabilised with PBS +0.1% Triton-X100 (Sigma) followed by a PBS + 1% FBS blocking step. Nanog expression was determined using an α-Nanog antibody at 1:200 dilution (Novus; NB100-58842) at RT for 45min, followed by a secondary antibody labelled with AlexaF647.

SSEA-1 expression during reprogramming was assessed by flow cytometry, as previously described (Li *et al*., 2009).

Samples were acquired on a FACS Canto-II or a LSRII Fortessa (for SSEA-1) (BD, San Jose, CA) using pulse processing to exclude cell aggregates and debris. At least 20'000 events were collected per sample. Data was analyzed using FlowJo Software v.9.1 (Treestar, Eugene, OR).

8.13. FLUORESCENCE ACTIVATED CELL SORTING

IPS cells were trypsinized and washed in PBS supplemented with 1% FBS and re-suspended in DMEM 1unit/ml LIF, 3% KSR and 3mM EDTA. Wild-type, *eGFP-TRF1*$^{+/KI}$ and *eGFP-TRF1*$^{KI/KI}$ cells were FACS sorted on an Aria II (BD, San Jose, CA) according to their eGFP-TRF1 levels of expression into high and low fraction (1/1). Cell aggregates and dead cells were excluded by using pulse processing and DAPI. 1x10^{6} cells for each fraction were collected, centrifuged, washed with PBS and prepared for following experiments.

For eGFP-TRF1-level dependent **teratoma and chimera formation**: iPS cells were grown on feeders. For all the experiments, the cells were trypsinized and incubated with 10µg/ml Hoechst (Invitrogen H1399) in iPS medium at a concentration of 1x10^{6} cells/ml for 30min at 37°C. Tubes were sporadically shaken to increase the Hoechst uptake. Cells were further filtered to evade aggregates and sorted for the G1 phase and eGFP-TRF1 amount. In **Fig. 1**, the sorting strategy is depicted. Only cells in from the G1 phase were analyzed due to the increased amount of DNA and telomere ends giving additional binding sites for the eGFP-TRF1 increasing the eGFP-intensity in S and G2 cell cycle phases.

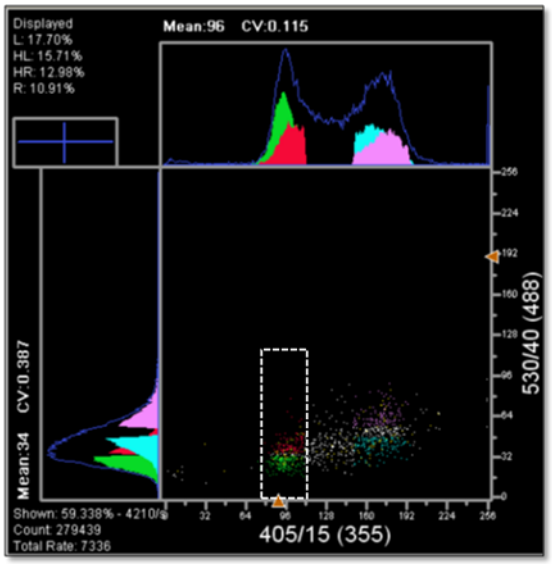

Fig. 1: eGFP-TRF1 cell sorting strategy.

Visible on top are cells incubated with Hoechst for depicting the cell cyle. Cells from the G1 peak were further separated into cells with high and low eGFP-TRF1 intensity; depicted in red and green in the left panel. In the bottom right panel, cells that were used for Teratoma and chimera formation are lined in the dotted rectangle.

8.14. TERATOMA FORMATION

IPS-cells were sorted as described above. $1.5x10^6$ cells were directly after the sorting concentrated to 100µl of PBS and subcutaneously injected into the flanks of nude mice, according to their amount of eGFP-TRF1. For the unsorted teratoma assay, $2x10^6$ untreated and unsorted iPS cells in PBS suspension were injected into the flanks of nude mice. The variation of the cells is explained by the fact that not more than $1.5x10^6$ could be sorted without drawback on the cell viability.

8.15. QUANTITATIVE REAL-TIME PCR

Total RNA from cells was extracted with Trizol (Life Technologies). Samples were treated with DNase I before reverse transcription. Reverse Transcription was done using random priming and iScript™ (BioRad) according to the manufacturer's protocol (*eGFP-TRF1*-iPS cells) or using Ready-To-Go You-Prime First-Strand Beads kit (GE Healthcare) according to the manucafturer's protocl.

Quantitative real-time PCR was performed with an ABI PRISM 7700 (Applied Biosystems), using DNA Master SYBR Green I mix (Applied Biosystems) according to the manufacturers protocol. All values were obtained in triplicates.

Primers used:

mNanog-F, 5’-AGGGTCTGCTACTGAGATGCTCTG-3’;

mNanog-R, 5’-CAACCACTGGTTTTTCTGCCACCG-3’;

mEndoOct3/4-R, 5’-TGCGGGCGGACATGGGGAGATCC-3’;

mEndoOCT3/4-F, 5’-TCTTTCCACCAGGCCCCCGGCTC-3’;

mTERT-F, 5’-GGATTGCCACTGGCTCCG-3’;

mTERT-R, 5’-TGCCTGACCTCCTCTTGTGAC-3’;

eGFP-TRF1-F, 5’-CCTGAGCAAAGACCCCAAC-3’;

eGFP-TRF1-R, 5’-TCCTCCTGCTCTGGAGAATC-3’.

m*TRF1*-F: 5’-GTCTCTGTGCCGAGCCTTC-3’;

m*TRF1*-R: 5’-TCAATTGGTAAGCTGTAAGTCTGTG-3’;

Gapdh-F, 5’-TTCACCACCATGGAGAAGGC-3’;

Gapdh-R, 5’-CCCTTTTGGCTCCACCCT-3’;

TRF1-Pr-F: GAAGGGGAAGAGGGAGTGAG

TRF1-Pr-R: TTGTCAGGCACCTGTCTCAG

TRF1-PrCtrlRegion-F: TCAGGAATGTCCCCTGAGAT

TRF1-PrCtrlRegion-R: GCATTCCCTTCGGGTATTTT

Nanog-Pr-F: GAAGGGGAAGAGGGAGTGAG

Nanog-Pr-R: TTGTCAGGCACCTGTCTCAG

OCT3/4-Pr-F: CTCTCGTCCTAGCCCTTCCT

OCT3/4-Pr-R: CCTCCACTCTGTCATGCTCA

Calculations were made using the ΔCt method as described (Yuan et al, 2006).

8.16. INFECTION OF MEFS FOR TRF1 MRNA AMOUNT MEASUREMENT

Two days before infection, $4x10^5$ 293T cells were transfected with Fugene6 (Roche) following manufacturer's instructions and using 4 mg of pCL-Eco and 4 mg of each plasmid of interest (pMX-Sox2, pMX-KLF4 or pMX-OCT3/4). The day after, MEF were seeded at a density of $2x10^5$ cells in a p35 well and fresh media wash added to the 293T cells. The following day medium was collected, filtered through a 0,45mm filter and 8mg/ml polybrene was added; 1ml of filtered medium was added to each well containing the MEF seeded the day before; infection was repeated every twelve hours, to a total of four times and cells were harvested three days after the last infection for RNA isolation and subsequent qRT-PCR analysis.

8.17. *EGFP-TRF1* CHIP ASSAY

ChIP assays were performed as previously described (Garcia-Cao et al, 2004). In brief, after cross-linking and sonication, chromatin from $4x10^6$ cells were used per each immunoprecipitation with protein anti-GFP agarose beads (MBL International, D-153-8) and the following antibodies: 6 µg of anti-histone H3 (# ab1791, Abcam), 8 µl of polyclonal rabbit anti-TRF1 serum at (homemade and described in (Munoz et al, 2005)). The immunoprecipitated DNA was transferred to a Hybond N+ membrane using a dot blot apparatus. The membrane was then hybridized with either a telomeric probe containing TTAGGG repeats or a probe recognizing major satellite sequences, which is characteristic of pericentric heterochromatin. Quantification of the signal was performed with ImageJ software (NIH). The amount of telomeric and pericentric DNA after ChIP was normalized for the total telomeric DNA.

8.18. CHROMATIN IMMUNOPRECIPITATION FOLLOWED BY QUANTITATIVE REAL-TIME PCR (CHIP QRT-PCR).

ChIP-qPCR was performed as previously described by (Martinez et al, 2010). A total of 20 ng of total DNA were used in each qPCR reaction. SYBR-green reagent was used for qPCR following manufacturer's instructions. Ct for every amplified region was normalized to its corresponding INPUT Ct, taking into account sample dilution for data representation. Antibodies used: Nanog 4µg (Novus; NB100-58842); Oct3/4 µg (Santa Cruz sc-9081).

8.19. FBS-MEDIUM CULTURING OF iPS CELLS

iPS cells at passage 4 and 5 were grown in Medium (DMEM; Invitrogen 31966021) supplemented with 15% KSR (Knockout Serum Replacement; Invitrogen 10828028) + LIF (1000U/ml; ESGROTM, Millipore ESG1107) + non-essential amino acids MEM Non-Essential Aminoacids Solution (1X; Invitrogen 11140035) + 2-mercaptoethanol (0.5 mM; Invitrogen 31350) + Pen/Strep (1X) on gelatin coated plates. Cells were trypsinised and 50'000 cells of each clone were seeded in gelatin coated 6-well plate wells. The control cells were cultured under KSR-medium conditions as explained in the reprogramming section. The other cells were grown in medium containing LIF and 15% of FBS (ES cell tested) instead of KSR. The medium was changed daily. For flow cytometry analysis and cell count by Neubauer cytometer, samples were collected by trypsinisation. For flow cytometry analysis the cells were washed twice in PBS and incubated with DAPI to exclude dead cells. Cell for analysis were resuspended in PBS containing 1% of BSA and 1mM EDTA. Pictures were captured on a bright field microscope with 100x magnification.

8.20. LENTIVIRAL TRANSDUCTIONS OF THE SHRNAS

Experiments were performed on MEFs from *p53*$^{-/-}$ embryos (MEFs, of C57BL6 genetic background) reprogramming was performed as described above. Lentiviral transduction: Retroviral supernatants were produced in HEK-293T cells (ATCC® Number CRL-11268™) (5x106 cells per 100-mm-diameter dish) transfected with the ecotropic packaging plasmid pCL-Eco (4 µg) together with either one of the following retroviral constructs (4 µg), pMXs-Klf4, pMXs-Sox2 or pMXs-Oct3/4 (obtained from Addgene) or pBabe Hygro (kindly donated by Francisco Real). Similarly, lentiviral supernatants were produced in HEK-293T cells (5x106 cells per 100-mm-diameter dish) transfected with the packaging plasmids pMDLg/pRRE (3.25 µg), pRSV.Rev (1.25 µg), pMD2.G VSVG (1.75 µg) (obtained from Addgene), and either one of the following shRNA lentiviral constructs (5 µg), pLKO.1-puro-scramble shRNA (obtained from Addgene) or pLKO.1-puro-TRF1 shRNA (bacterial glicerol stock (TRCM0000071298, obtained from Sigma-Aldrich). Transfections were performed using Fugene-6 transfection reagent (Roche) according to the manufacturer's protocol. Two days later, viral supernatants (10 ml) were collected serially during the subsequent 48 hours, at 12 hour intervals, each time adding fresh medium to the cells (10 ml). The recipient MEFs had been seeded the previous day (2x105 cells per 60-mm-diameter dish) and received 1 ml

of each of the corresponding viral supernatants. The following viral cocktails were used: pBabe Hygro and pLKO.1-puro-scramble shRNA (mock-scrambled), pBabe Hygro and pLKO.1-puro-TRF1 shRNA (mock-shTRF1), pMXs-Klf4, pMXs-Sox2, pMXs-Oct3/4 and pLKO.1-puro-scramble shRNA (3F-scramble), pMXs-Klf4, pMXs-Sox2, pMXs-Oct3/4 and pLKO.1-puro-TRF1 shRNA (3F-shTRF1). The procedure was repeated every 12 hours for 2 days (a total of 4 additions). After infection was completed, media was replaced with standard ES media supplemented with knockout serum replacement (KSR, Invitrogen) and with puromycin to select for the shRNAs vectors. Cultures were maintained in the presence of drug selection with daily medium changes. Reprogramming was assessed 2 weeks post-infection by counting alkaline phosphatase-positive colonies. Alkaline phosphatase staining was performed according to manufacturer´s instructions (BCIP/NBT Color Development Substrate, Promega). The results were normalized to the respective efficiencies of retroviral transduction as assessed by transducing with the three pMXsOct3/4, pMXsKlf4, pMXsSox2 retroviruses plus a retrovirus expressing GFP.

8.21. GENERATION OF MICE WITH CONDITIONAL TRF1 ABLATION IN THE SMALL INTESTINE

Seven to nine-week old *TRF1*$^{lox/lox}$*; Villin-CreERT2*$^{+/T}$ mice and control *TRF1*$^{lox/lox}$*; Villin-CreERT2*$^{+/T}$ mice were injected intraperitonealy with 1mg 4-hydroxytamoxifen (Sigma) dissolved (by sonication) in 100µl corn oil (Sigma). Injections were performed on a daily base (for 34 days). Mouse weight was measured every day. Two *TRF1*$^{lox/lox}$*; Villin-CreERT2*$^{+/T}$ mice had to be sacrificed before day 34 due to severe weight loss. Of all the mice the intestines were extracted washed out with PBS and prepared for western blot analysis, DNA-extraction and paraffin embedding after fixation over night with formalin. Two small intestines were extracted on an early time point to check if excision is taking place from them, the TRF+/+ intestine was used in further experiments as control.

8.22. IHC STAININGS AND QUANTIFICATION

Immunohistochemistry was performed on deparaffinised sections processed with 10 mM sodium citrate (pH 6.5) cooked under pressure for 2 min. Slides were washed in water, then in TBS-Tween20 0.5%, blocked with peroxidase, washed with TBS-Tween20 0.5 % again and blocked with fetal bovine serum followed by another washing step. Further, the slides were incubated with the primary antibodies: Villin at 1:2000 dillution (Dako; M3637) or

caspase 3 activated at 1:200 (R&D SYSTEMS; AF835).Slides were then incubated with secondary antibodies conjugated with peroxidase (Dako). For signal development DAB (Dako) was used as a substrate. Sections were slightly counterstained with haematoxylin and analyzed by light microscopy.

Apoptotic cells from H&E staining were histologically characterized by shrunk cytoplasm, condensed chromatin and the breakdown of the nucleus into fragments. Additionally we observed epithelial cells with irregular nucleus sizes (more than two times larger than normal) those cells were considered as endoreduplicated cells.

In caspase 3 activated stained slides, cells that were positive for the peroxidise reaction where counted in a light microscope by eye.

8.23. TAIL SKIN PIGMENTATION

Tail skin hyperpigmentation was macroscopically analyzed according to (Stout & Blasco, 2009).

9. REFERENCES

Agarwal S, Loh YH, McLoughlin EM, Huang J, Park IH, Miller JD, Huo H, Okuka M, Dos Reis RM, Loewer S, Ng HH, Keefe DL, Goldman FD, Klingelhutz AJ, Liu L, Daley GQ (2010) Telomere elongation in induced pluripotent stem cells from dyskeratosis congenita patients. *Nature* **464**(7286)**:** 292-296

Allsopp RC, Morin GB, DePinho R, Harley CB, Weissman IL (2003) Telomerase is required to slow telomere shortening and extend replicative lifespan of HSCs during serial transplantation. *Blood* **102**(2)**:** 517-520

Alonso L, Fuchs E (2006) The hair cycle. *J Cell Sci* **119**(Pt 3)**:** 391-393

Ancelin K, Brunori M, Bauwens S, Koering CE, Brun C, Ricoul M, Pommier JP, Sabatier L, Gilson E (2002) Targeting assay to study the cis functions of human telomeric proteins: evidence for inhibition of telomerase by TRF1 and for activation of telomere degradation by TRF2. *Mol Cell Biol* **22**(10)**:** 3474-3487

Armanios MY, Chen JJ, Cogan JD, Alder JK, Ingersoll RG, Markin C, Lawson WE, Xie M, Vulto I, Phillips JA, 3rd, Lansdorp PM, Greider CW, Loyd JE (2007) Telomerase mutations in families with idiopathic pulmonary fibrosis. *N Engl J Med* **356**(13)**:** 1317-1326

Artandi SE, Alson S, Tietze MK, Sharpless NE, Ye S, Greenberg RA, Castrillon DH, Horner JW, Weiler SR, Carrasco RD, DePinho RA (2002) Constitutive telomerase expression promotes mammary carcinomas in aging mice. *Proc Natl Acad Sci U S A* **99**(12)**:** 8191-8196

Artandi SE, Attardi LD (2005) Pathways connecting telomeres and p53 in senescence, apoptosis, and cancer. *Biochem Biophys Res Commun* **331**(3)**:** 881-890

Baker AM, Fu Q, Hayward W, Victoria S, Pedroso IM, Lindsay SM, Fletcher TM (2011) The telomere binding protein TRF2 induces chromatin compaction. *PLoS One* **6**(4)**:** e19124

Barker N, van Es JH, Kuipers J, Kujala P, van den Born M, Cozijnsen M, Haegebarth A, Korving J, Begthel H, Peters PJ, Clevers H (2007) Identification of stem cells in small intestine and colon by marker gene Lgr5. *Nature* **449**(7165)**:** 1003-1007

Belmonte C, Brock JA, Viana F (2009) Converting cold into pain. *Exp Brain Res* **196**(1)**:** 13-30

Bianchi A, Smith S, Chong L, Elias P, de Lange T (1997) TRF1 is a dimer and bends telomeric DNA. *EMBO J* **16**(7)**:** 1785-1794

Bilaud T, Brun C, Ancelin K, Koering CE, Laroche T, Gilson E (1997) Telomeric localization of TRF2, a novel human telobox protein. *Nat Genet* **17**(2)**:** 236-239

Blackburn EH (2001) Switching and signaling at the telomere. *Cell* **106**(6)**:** 661-673

Blackburn EH, Gall JG (1978) A tandemly repeated sequence at the termini of the extrachromosomal ribosomal RNA genes in Tetrahymena. *J Mol Biol* **120**(1)**:** 33-53

Blasco MA, Lee HW, Hande MP, Samper E, Lansdorp PM, DePinho RA, Greider CW (1997) Telomere shortening and tumor formation by mouse cells lacking telomerase RNA. *Cell* **91**(1)**:** 25-34

Blelloch R, Venere M, Yen J, Ramalho-Santos M (2007) Generation of induced pluripotent stem cells in the absence of drug selection. *Cell Stem Cell* **1**(3)**:** 245-247

Bodnar AG, Ouellette M, Frolkis M, Holt SE, Chiu CP, Morin GB, Harley CB, Shay JW, Lichtsteiner S, Wright WE (1998) Extension of life-span by introduction of telomerase into normal human cells. *Science* **279**(5349)**:** 349-352

Boue S, Paramonov I, Barrero MJ, Izpisua Belmonte JC (2010) Analysis of human and mouse reprogramming of somatic cells to induced pluripotent stem cells. What is in the plate? *PLoS One* **5**(9)**:** e12664

Broccoli D, Smogorzewska A, Chong L, de Lange T (1997) Human telomeres contain two distinct Myb-related proteins, TRF1 and TRF2. *Nat Genet* **17**(2)**:** 231-235

Bryan TM, Englezou A, Dalla-Pozza L, Dunham MA, Reddel RR (1997) Evidence for an alternative mechanism for maintaining telomere length in human tumors and tumor-derived cell lines. *Nat Med* **3**(11)**:** 1271-1274

Bryan TM, Englezou A, Gupta J, Bacchetti S, Reddel RR (1995) Telomere elongation in immortal human cells without detectable telomerase activity. *EMBO J* **14**(17)**:** 4240-4248

Bryja V, Bonilla S, Cajanek L, Parish CL, Schwartz CM, Luo Y, Rao MS, Arenas E (2006) An efficient method for the derivation of mouse embryonic stem cells. *Stem Cells* **24**(4)**:** 844-849

Canela A, Klatt P, Blasco MA (2007a) Telomere length analysis. *Methods Mol Biol* **371:** 45-72

Canela A, Martin-Caballero J, Flores JM, Blasco MA (2004) Constitutive expression of tert in thymocytes leads to increased incidence and dissemination of T-cell lymphoma in Lck-Tert mice. *Mol Cell Biol* **24**(10)**:** 4275-4293

Canela A, Vera E, Klatt P, Blasco MA (2007b) High-throughput telomere length quantification by FISH and its application to human population studies. *Proc Natl Acad Sci U S A* **104**(13)**:** 5300-5305

Carroll KA, Ly H (2009) Telomere dysfunction in human diseases: the long and short of it! *Int J Clin Exp Pathol* **2**(6)**:** 528-543

Cayuela ML, Flores JM, Blasco MA (2005) The telomerase RNA component Terc is required for the tumour-promoting effects of Tert overexpression. *EMBO Rep* **6**(3)**:** 268-274

Chambers I, Silva J, Colby D, Nichols J, Nijmeijer B, Robertson M, Vrana J, Jones K, Grotewold L, Smith A (2007) Nanog safeguards pluripotency and mediates germline development. *Nature* **450**(7173)**:** 1230-1234

Chan SR, Blackburn EH (2004) Telomeres and telomerase. *Philos Trans R Soc Lond B Biol Sci* **359**(1441)**:** 109-121

Chan SW, Blackburn EH (2002) New ways not to make ends meet: telomerase, DNA damage proteins and heterochromatin. *Oncogene* **21**(4)**:** 553-563

Chang W, Dynek JN, Smith S (2003) TRF1 is degraded by ubiquitin-mediated proteolysis after release from telomeres. *Genes Dev* **17**(11)**:** 1328-1333

Chen Y, Yang Y, van Overbeek M, Donigian JR, Baciu P, de Lange T, Lei M (2008) A shared docking motif in TRF1 and TRF2 used for differential recruitment of telomeric proteins. *Science* **319**(5866)**:** 1092-1096

Cheng J, Dutra A, Takesono A, Garrett-Beal L, Schwartzberg PL (2004) Improved generation of C57BL/6J mouse embryonic stem cells in a defined serum-free media. *Genesis* **39**(2)**:** 100-104

Chong L, van Steensel B, Broccoli D, Erdjument-Bromage H, Hanish J, Tempst P, de Lange T (1995) A human telomeric protein. *Science* **270**(5242)**:** 1663-1667

Cohen SB, Graham ME, Lovrecz GO, Bache N, Robinson PJ, Reddel RR (2007) Protein composition of catalytically active human telomerase from immortal cells. *Science* **315**(5820)**:** 1850-1853

Collins K, Mitchell JR (2002) Telomerase in the human organism. *Oncogene* **21**(4)**:** 564-579

Cook BD, Dynek JN, Chang W, Shostak G, Smith S (2002) Role for the related poly(ADP-Ribose) polymerases tankyrase 1 and 2 at human telomeres. *Mol Cell Biol* **22**(1)**:** 332-342

Cotsarelis G, Sun TT, Lavker RM (1990) Label-retaining cells reside in the bulge area of pilosebaceous unit: implications for follicular stem cells, hair cycle, and skin carcinogenesis. *Cell* **61**(7)**:** 1329-1337

Dantzer F, Giraud-Panis MJ, Jaco I, Ame JC, Schultz I, Blasco M, Koering CE, Gilson E, Menissier-de Murcia J, de Murcia G, Schreiber V (2004) Functional interaction between poly(ADP-Ribose) polymerase 2 (PARP-2) and TRF2: PARP activity negatively regulates TRF2. *Mol Cell Biol* **24**(4)**:** 1595-1607

de Lange T (2002) Protection of mammalian telomeres. *Oncogene* **21**(4)**:** 532-540

de Lange T (2005) Shelterin: the protein complex that shapes and safeguards human telomeres. *Genes Dev* **19**(18)**:** 2100-2110

de Lange T, DePinho RA (1999) Unlimited mileage from telomerase? *Science* **283**(5404)**:** 947-949

de Lange T, Shiue L, Myers RM, Cox DR, Naylor SL, Killery AM, Varmus HE (1990) Structure and variability of human chromosome ends. *Mol Cell Biol* **10**(2)**:** 518-527

Deng Y, Chan SS, Chang S (2008) Telomere dysfunction and tumour suppression: the senescence connection. *Nat Rev Cancer* **8**(6)**:** 450-458

Donate LE, Blasco MA (2011) Telomeres in cancer and ageing. *Philos Trans R Soc Lond B Biol Sci* **366**(1561)**:** 76-84

Donigian JR, de Lange T (2007) The role of the poly(ADP-ribose) polymerase tankyrase1 in telomere length control by the TRF1 component of the shelterin complex. *J Biol Chem* **282**(31)**:** 22662-22667

Drachtman RA, Alter BP (1995) Dyskeratosis congenita. *Dermatol Clin* **13**(1)**:** 33-39

Dunham MA, Neumann AA, Fasching CL, Reddel RR (2000) Telomere maintenance by recombination in human cells. *Nat Genet* **26**(4)**:** 447-450

Eisenberg DT, Hayes MG, Kuzawa CW (2012) Delayed paternal age of reproduction in humans is associated with longer telomeres across two generations of descendants. *Proc Natl Acad Sci U S A* **109**(26)**:** 10251-10256

el Marjou F, Janssen KP, Chang BH, Li M, Hindie V, Chan L, Louvard D, Chambon P, Metzger D, Robine S (2004) Tissue-specific and inducible Cre-mediated recombination in the gut epithelium. *Genesis* **39**(3)**:** 186-193

Fairall L, Chapman L, Moss H, de Lange T, Rhodes D (2001) Structure of the TRFH dimerization domain of the human telomeric proteins TRF1 and TRF2. *Mol Cell* **8**(2)**:** 351-361

Fairchild PJ, Robertson NJ, Cartland S, Nolan KF, Waldmann H (2005) Cell replacement therapy and the evasion of destructive immunity. *Stem Cell Rev* **1**(2)**:** 159-167

Flores I, Canela A, Vera E, Tejera A, Cotsarelis G, Blasco MA (2008) The longest telomeres: a general signature of adult stem cell compartments. *Genes Dev* **22**(5)**:** 654-667

Flores I, Cayuela ML, Blasco MA (2005) Effects of telomerase and telomere length on epidermal stem cell behavior. *Science* **309**(5738)**:** 1253-1256

Franco S, Alsheimer M, Herrera E, Benavente R, Blasco MA (2002) Mammalian meiotic telomeres: composition and ultrastructure in telomerase-deficient mice. *Eur J Cell Biol* **81**(6)**:** 335-340

Fuchs E (2007) Scratching the surface of skin development. *Nature* **445**(7130)**:** 834-842

Fuchs E (2009) The tortoise and the hair: slow-cycling cells in the stem cell race. *Cell* **137**(5)**:** 811-819

Fuchs E, Horsley V (2008) More than one way to skin. *Genes Dev* **22**(8)**:** 976-985

Garcia-Cao I, Garcia-Cao M, Tomas-Loba A, Martin-Caballero J, Flores JM, Klatt P, Blasco MA, Serrano M (2006) Increased p53 activity does not accelerate telomere-driven ageing. *EMBO Rep* **7**(5)**:** 546-552

Garcia-Cao M, O'Sullivan R, Peters AH, Jenuwein T, Blasco MA (2004) Epigenetic regulation of telomere length in mammalian cells by the Suv39h1 and Suv39h2 histone methyltransferases. *Nat Genet* **36**(1)**:** 94-99

Gonzalez-Suarez E, Goytisolo FA, Flores JM, Blasco MA (2003) Telomere dysfunction results in enhanced organismal sensitivity to the alkylating agent N-methyl-N-nitrosourea. *Cancer Res* **63**(21)**:** 7047-7050

Gonzalez-Suarez E, Samper E, Flores JM, Blasco MA (2000) Telomerase-deficient mice with short telomeres are resistant to skin tumorigenesis. *Nat Genet* **26**(1)**:** 114-117

Gonzalez-Suarez E, Samper E, Ramirez A, Flores JM, Martin-Caballero J, Jorcano JL, Blasco MA (2001) Increased epidermal tumors and increased skin wound healing in transgenic mice overexpressing the catalytic subunit of telomerase, mTERT, in basal keratinocytes. *EMBO J* **20**(11)**:** 2619-2630

Gonzalo S, Jaco I, Fraga MF, Chen T, Li E, Esteller M, Blasco MA (2006) DNA methyltransferases control telomere length and telomere recombination in mammalian cells. *Nat Cell Biol* **8**(4)**:** 416-424

Goytisolo FA, Blasco MA (2002) Many ways to telomere dysfunction: in vivo studies using mouse models. *Oncogene* **21**(4)**:** 584-591

Greenberg RA, Allsopp RC, Chin L, Morin GB, DePinho RA (1998) Expression of mouse telomerase reverse transcriptase during development, differentiation and proliferation. *Oncogene* **16**(13)**:** 1723-1730

Greider CW (1999) Telomeres do D-loop-T-loop. *Cell* **97**(4)**:** 419-422

Greider CW, Blackburn EH (1985) Identification of a specific telomere terminal transferase activity in Tetrahymena extracts. *Cell* **43**(2 Pt 1)**:** 405-413

Griffith JD, Comeau L, Rosenfield S, Stansel RM, Bianchi A, Moss H, de Lange T (1999) Mammalian telomeres end in a large duplex loop. *Cell* **97**(4)**:** 503-514

Guerra C, Mijimolle N, Dhawahir A, Dubus P, Barradas M, Serrano M, Campuzano V, Barbacid M (2003) Tumor induction by an endogenous K-ras oncogene is highly dependent on cellular context. *Cancer Cell* **4**(2)**:** 111-120

Gur G, Rubin C, Katz M, Amit I, Citri A, Nilsson J, Amariglio N, Henriksson R, Rechavi G, Hedman H, Wides R, Yarden Y (2004) LRIG1 restricts growth factor signaling by enhancing receptor ubiquitylation and degradation. *EMBO J* **23**(16)**:** 3270-3281

Hanahan D, Weinberg RA (2000) The hallmarks of cancer. *Cell* **100**(1)**:** 57-70

Hanley J, Rastegarlari G, Nathwani AC (2010) An introduction to induced pluripotent stem cells. *Br J Haematol* **151**(1)**:** 16-24

Hanna J, Wernig M, Markoulaki S, Sun CW, Meissner A, Cassady JP, Beard C, Brambrink T, Wu LC, Townes TM, Jaenisch R (2007) Treatment of sickle cell anemia mouse model with iPS cells generated from autologous skin. *Science* **318**(5858)**:** 1920-1923

Harley CB, Futcher AB, Greider CW (1990) Telomeres shorten during ageing of human fibroblasts. *Nature* **345**(6274)**:** 458-460

Hayflick L, Moorhead PS (1961) The serial cultivation of human diploid cell strains. *Exp Cell Res* **25:** 585-621

Hemann MT, Greider CW (2000) Wild-derived inbred mouse strains have short telomeres. *Nucleic Acids Res* **28**(22)**:** 4474-4478

Heng JC, Feng B, Han J, Jiang J, Kraus P, Ng JH, Orlov YL, Huss M, Yang L, Lufkin T, Lim B, Ng HH (2010) The nuclear receptor Nr5a2 can replace Oct4 in the reprogramming of murine somatic cells to pluripotent cells. *Cell Stem Cell* **6**(2)**:** 167-174

Herrera E, Martinez AC, Blasco MA (2000) Impaired germinal center reaction in mice with short telomeres. *EMBO J* **19**(3)**:** 472-481

Herrera E, Samper E, Blasco MA (1999a) Telomere shortening in mTR-/- embryos is associated with failure to close the neural tube. *EMBO J* **18**(5)**:** 1172-1181

Herrera E, Samper E, Martin-Caballero J, Flores JM, Lee HW, Blasco MA (1999b) Disease states associated with telomerase deficiency appear earlier in mice with short telomeres. *EMBO J* **18**(11)**:** 2950-2960

Hochedlinger K, Jaenisch R (2006) Nuclear reprogramming and pluripotency. *Nature* **441**(7097)**:** 1061-1067

Hoffmeyer K, Raggioli A, Rudloff S, Anton R, Hierholzer A, Del Valle I, Hein K, Vogt R, Kemler R (2012) Wnt/beta-catenin signaling regulates telomerase in stem cells and cancer cells. *Science* **336**(6088)**:** 1549-1554

Hong H, Takahashi K, Ichisaka T, Aoi T, Kanagawa O, Nakagawa M, Okita K, Yamanaka S (2009) Suppression of induced pluripotent stem cell generation by the p53-p21 pathway. *Nature* **460**(7259)**:** 1132-1135

Hong Y, Stambrook PJ (2004) Restoration of an absent G1 arrest and protection from apoptosis in embryonic stem cells after ionizing radiation. *Proc Natl Acad Sci U S A* **101**(40)**:** 14443-14448

Houghtaling BR, Cuttonaro L, Chang W, Smith S (2004) A dynamic molecular link between the telomere length regulator TRF1 and the chromosome end protector TRF2. *Curr Biol* **14**(18)**:** 1621-1631

Hsu YC, Fuchs E (2012) A family business: stem cell progeny join the niche to regulate homeostasis. *Nat Rev Mol Cell Biol* **13**(2)**:** 103-114

Ito M, Liu Y, Yang Z, Nguyen J, Liang F, Morris RJ, Cotsarelis G (2005) Stem cells in the hair follicle bulge contribute to wound repair but not to homeostasis of the epidermis. *Nat Med* **11**(12)**:** 1351-1354

Janssen KP, el-Marjou F, Pinto D, Sastre X, Rouillard D, Fouquet C, Soussi T, Louvard D, Robine S (2002) Targeted expression of oncogenic K-ras in intestinal epithelium causes spontaneous tumorigenesis in mice. *Gastroenterology* **123**(2)**:** 492-504

Jensen KB, Collins CA, Nascimento E, Tan DW, Frye M, Itami S, Watt FM (2009) Lrig1 expression defines a distinct multipotent stem cell population in mammalian epidermis. *Cell Stem Cell* **4**(5)**:** 427-439

Karlseder J, Kachatrian L, Takai H, Mercer K, Hingorani S, Jacks T, de Lange T (2003) Targeted deletion reveals an essential function for the telomere length regulator Trf1. *Mol Cell Biol* **23**(18)**:** 6533-6541

Kim SH, Kaminker P, Campisi J (1999) TIN2, a new regulator of telomere length in human cells. *Nat Genet* **23**(4)**:** 405-412

Klobutcher LA, Swanton MT, Donini P, Prescott DM (1981) All gene-sized DNA molecules in four species of hypotrichs have the same terminal sequence and an unusual 3' terminus. *Proc Natl Acad Sci U S A* **78**(5)**:** 3015-3019

Laederich MB, Funes-Duran M, Yen L, Ingalla E, Wu X, Carraway KL, 3rd, Sweeney C (2004) The leucine-rich repeat protein LRIG1 is a negative regulator of ErbB family receptor tyrosine kinases. *J Biol Chem* **279**(45)**:** 47050-47056

Lansdorp PM, Verwoerd NP, van de Rijke FM, Dragowska V, Little MT, Dirks RW, Raap AK, Tanke HJ (1996) Heterogeneity in telomere length of human chromosomes. *Hum Mol Genet* **5**(5)**:** 685-691

Lee HW, Blasco MA, Gottlieb GJ, Horner JW, 2nd, Greider CW, DePinho RA (1998) Essential role of mouse telomerase in highly proliferative organs. *Nature* **392**(6676)**:** 569-574

Lee TH, Perrem K, Harper JW, Lu KP, Zhou XZ (2006) The F-box protein FBX4 targets PIN2/TRF1 for ubiquitin-mediated degradation and regulates telomere maintenance. *J Biol Chem* **281**(2)**:** 759-768

Leri A, Franco S, Zacheo A, Barlucchi L, Chimenti S, Limana F, Nadal-Ginard B, Kajstura J, Anversa P, Blasco MA (2003) Ablation of telomerase and telomere loss leads to cardiac dilatation and heart failure associated with p53 upregulation. *EMBO J* **22**(1)**:** 131-139

Levy V, Lindon C, Zheng Y, Harfe BD, Morgan BA (2007) Epidermal stem cells arise from the hair follicle after wounding. *FASEB J* **21**(7)**:** 1358-1366

Lewin B, Krebs JE, Goldstein ES, Kilpatrick ST (2008) Lewin's Genes X. **Chapter 16.9:** 406-409

Li H, Collado M, Villasante A, Strati K, Ortega S, Canamero M, Blasco MA, Serrano M (2009) The Ink4/Arf locus is a barrier for iPS cell reprogramming. *Nature* **460**(7259)**:** 1136-1139

Li L, Clevers H (2011) Coexistence of quiescent and active adult stem cells in mammals. *Science* **327**(5965)**:** 542-545

Liu Y, Lyle S, Yang Z, Cotsarelis G (2003) Keratin 15 promoter targets putative epithelial stem cells in the hair follicle bulge. *J Invest Dermatol* **121**(5)**:** 963-968

Loayza D, De Lange T (2003) POT1 as a terminal transducer of TRF1 telomere length control. *Nature* **423**(6943)**:** 1013-1018

Loh YH, Wu Q, Chew JL, Vega VB, Zhang W, Chen X, Bourque G, George J, Leong B, Liu J, Wong KY, Sung KW, Lee CW, Zhao XD, Chiu KP, Lipovich L, Kuznetsov VA, Robson P, Stanton LW, Wei CL, Ruan Y, Lim B, Ng HH (2006) The Oct4 and Nanog transcription network regulates pluripotency in mouse embryonic stem cells. *Nat Genet* **38**(4)**:** 431-440

Maherali N, Sridharan R, Xie W, Utikal J, Eminli S, Arnold K, Stadtfeld M, Yachechko R, Tchieu J, Jaenisch R, Plath K, Hochedlinger K (2007) Directly reprogrammed fibroblasts show global epigenetic remodeling and widespread tissue contribution. *Cell Stem Cell* **1**(1)**:** 55-70

Marcand S, Gilson E, Shore D (1997) A protein-counting mechanism for telomere length regulation in yeast. *Science* **275**(5302)**:** 986-990

Marion RM, Strati K, Li H, Murga M, Blanco R, Ortega S, Fernandez-Capetillo O, Serrano M, Blasco MA (2009a) A p53-mediated DNA damage response limits reprogramming to ensure iPS cell genomic integrity. *Nature* **460**(7259)**:** 1149-1153

Marion RM, Strati K, Li H, Tejera A, Schoeftner S, Ortega S, Serrano M, Blasco MA (2009b) Telomeres acquire embryonic stem cell characteristics in induced pluripotent stem cells. *Cell Stem Cell* **4**(2)**:** 141-154

Martinez P, Blasco MA (2011) Telomeric and extra-telomeric roles for telomerase and the telomere-binding proteins. *Nat Rev Cancer* **11**(3)**:** 161-176

Martinez P, Thanasoula M, Carlos AR, Gomez-Lopez G, Tejera AM, Schoeftner S, Dominguez O, Pisano DG, Tarsounas M, Blasco MA (2010) Mammalian Rap1 controls telomere function and gene expression through binding to telomeric and extratelomeric sites. *Nat Cell Biol* **12**(8)**:** 768-780

Martinez P, Thanasoula M, Munoz P, Liao C, Tejera A, McNees C, Flores JM, Fernandez-Capetillo O, Tarsounas M, Blasco MA (2009) Increased telomere fragility and fusions resulting from TRF1 deficiency lead to degenerative pathologies and increased cancer in mice. *Genes Dev* **23**(17)**:** 2060-2075

Masutomi K, Yu EY, Khurts S, Ben-Porath I, Currier JL, Metz GB, Brooks MW, Kaneko S, Murakami S, DeCaprio JA, Weinberg RA, Stewart SA, Hahn WC (2003) Telomerase maintains telomere structure in normal human cells. *Cell* **114**(2)**:** 241-253

McClintock B (1941) The Stability of Broken Ends of Chromosomes in Zea Mays. *Genetics* **26**(2)**:** 234-282

Meshorer E, Yellajoshula D, George E, Scambler PJ, Brown DT, Misteli T (2006) Hyperdynamic plasticity of chromatin proteins in pluripotent embryonic stem cells. *Dev Cell* **10**(1)**:** 105-116

Mikkelsen TS, Hanna J, Zhang X, Ku M, Wernig M, Schorderet P, Bernstein BE, Jaenisch R, Lander ES, Meissner A (2008) Dissecting direct reprogramming through integrative genomic analysis. *Nature* **454**(7200)**:** 49-55

Mitchell JR, Wood E, Collins K (1999) A telomerase component is defective in the human disease dyskeratosis congenita. *Nature* **402**(6761)**:** 551-555

Montgomery RK, Carlone DL, Richmond CA, Farilla L, Kranendonk ME, Henderson DE, Baffour-Awuah NY, Ambruzs DM, Fogli LK, Algra S, Breault DT (2011) Mouse telomerase reverse transcriptase (mTert) expression marks slowly cycling intestinal stem cells. *Proc Natl Acad Sci U S A* **108**(1)**:** 179-184

Müller H (1938) The remaking of chromosomes. *Collecting NET*(13)**:** 181-198

Munoz P, Blanco R, de Carcer G, Schoeftner S, Benetti R, Flores JM, Malumbres M, Blasco MA (2009) TRF1 controls telomere length and mitotic fidelity in epithelial homeostasis. *Mol Cell Biol* **29**(6)**:** 1608-1625

Munoz P, Blanco R, Flores JM, Blasco MA (2005) XPF nuclease-dependent telomere loss and increased DNA damage in mice overexpressing TRF2 result in premature aging and cancer. *Nat Genet* **37**(10)**:** 1063-1071

Muntoni A, Reddel RR (2005) The first molecular details of ALT in human tumor cells. *Hum Mol Genet* **14 Spec No. 2:** R191-196

Nakagawa M, Koyanagi M, Tanabe K, Takahashi K, Ichisaka T, Aoi T, Okita K, Mochiduki Y, Takizawa N, Yamanaka S (2008) Generation of induced pluripotent stem cells without Myc from mouse and human fibroblasts. *Nat Biotechnol* **26**(1)**:** 101-106

Nichols J, Evans EP, Smith AG (1990) Establishment of germ-line-competent embryonic stem (ES) cells using differentiation inhibiting activity. *Development* **110**(4)**:** 1341-1348

Niwa H (2007) How is pluripotency determined and maintained? *Development* **134**(4)**:** 635-646

Ohki R, Tsurimoto T, Ishikawa F (2001) In vitro reconstitution of the end replication problem. *Mol Cell Biol* **21**(17)**:** 5753-5766

Ohmura H, Tahara H, Suzuki M, Ide T, Shimizu M, Yoshida MA, Tahara E, Shay JW, Barrett JC, Oshimura M (1995) Restoration of the cellular senescence program and repression of telomerase by human chromosome 3. *Jpn J Cancer Res* **86**(10)**:** 899-904

Okazaki R, Okazaki T, Sakabe K, Sugimoto K (1967) Mechanism of DNA replication possible discontinuity of DNA chain growth. *Jpn J Med Sci Biol* **20**(3)**:** 255-260

Okita K, Ichisaka T, Yamanaka S (2007) Generation of germline-competent induced pluripotent stem cells. *Nature* **448**(7151)**:** 313-317

Olovnikov AM (1971) [Principle of marginotomy in template synthesis of polynucleotides]. *Dokl Akad Nauk SSSR* **201**(6)**:** 1496-1499

Opresko PL, von Kobbe C, Laine JP, Harrigan J, Hickson ID, Bohr VA (2002) Telomere-binding protein TRF2 binds to and stimulates the Werner and Bloom syndrome helicases. *J Biol Chem* **277**(43)**:** 41110-41119

Pinto D, Robine S, Jaisser F, El Marjou FE, Louvard D (1999) Regulatory sequences of the mouse villin gene that efficiently drive transgenic expression in immature and differentiated epithelial cells of small and large intestines. *J Biol Chem* **274**(10)**:** 6476-6482

Poulet A, Buisson R, Faivre-Moskalenko C, Koelblen M, Amiard S, Montel F, Cuesta-Lopez S, Bornet O, Guerlesquin F, Godet T, Moukhtar J, Argoul F, Declais AC, Lilley DM, Ip SC, West SC, Gilson E, Giraud-Panis MJ (2009) TRF2 promotes, remodels and protects telomeric Holliday junctions. *EMBO J* **28**(6)**:** 641-651

Poulet A, Pisano S, Faivre-Moskalenko C, Pei B, Tauran Y, Haftek-Terreau Z, Brunet F, Le Bihan YV, Ledu MH, Montel F, Hugo N, Amiard S, Argoul F, Chaboud A, Gilson E, Giraud-Panis MJ (2011) The N-terminal domains of TRF1 and TRF2 regulate their ability to condense telomeric DNA. *Nucleic Acids Res* **40**(6)**:** 2566-2576

Raya A, Rodriguez-Piza I, Guenechea G, Vassena R, Navarro S, Barrero MJ, Consiglio A, Castella M, Rio P, Sleep E, Gonzalez F, Tiscornia G, Garreta E, Aasen T, Veiga A, Verma IM, Surralles J, Bueren J, Izpisua Belmonte JC (2009) Disease-corrected haematopoietic progenitors from Fanconi anaemia induced pluripotent stem cells. *Nature* **460**(7251)**:** 53-59

Raz V, Vermolen BJ, Garini Y, Onderwater JJ, Mommaas-Kienhuis MA, Koster AJ, Young IT, Tanke H, Dirks RW (2008) The nuclear lamina promotes telomere aggregation and centromere peripheral localization during senescence of human mesenchymal stem cells. *J Cell Sci* **121**(Pt 24)**:** 4018-4028

Redmer T, Diecke S, Grigoryan T, Quiroga-Negreira A, Birchmeier W, Besser D (2011) E-cadherin is crucial for embryonic stem cell pluripotency and can replace OCT4 during somatic cell reprogramming. *EMBO Rep* **12**(7)**:** 720-726

Robine S, Jaisser F, Louvard D (1997) Epithelial cell growth and differentiation. IV. Controlled spatiotemporal expression of transgenes: new tools to study normal and pathological states. *Am J Physiol* **273**(4 Pt 1)**:** G759-762

Rudolph KL, Chang S, Lee HW, Blasco M, Gottlieb GJ, Greider C, DePinho RA (1999) Longevity, stress response, and cancer in aging telomerase-deficient mice. *Cell* **96**(5)**:** 701-712

Samper E, Fernandez P, Eguia R, Martin-Rivera L, Bernad A, Blasco MA, Aracil M (2002) Long-term repopulating ability of telomerase-deficient murine hematopoietic stem cells. *Blood* **99**(8)**:** 2767-2775

Samper E, Flores JM, Blasco MA (2001) Restoration of telomerase activity rescues chromosomal instability and premature aging in Terc-/- mice with short telomeres. *EMBO Rep* **2**(9)**:** 800-807

Sangiorgi E, Capecchi MR (2008) Bmi1 is expressed in vivo in intestinal stem cells. *Nat Genet* **40**(7)**:** 915-920

Sato T, van Es JH, Snippert HJ, Stange DE, Vries RG, van den Born M, Barker N, Shroyer NF, van de Wetering M, Clevers H (2010) Paneth cells constitute the niche for Lgr5 stem cells in intestinal crypts. *Nature* **469**(7330)**:** 415-418

Savage SA, Calado RT, Xin ZT, Ly H, Young NS, Chanock SJ (2006) Genetic variation in telomeric repeat binding factors 1 and 2 in aplastic anemia. *Exp Hematol* **34**(5)**:** 664-671

Savage SA, Giri N, Baerlocher GM, Orr N, Lansdorp PM, Alter BP (2008) TINF2, a component of the shelterin telomere protection complex, is mutated in dyskeratosis congenita. *Am J Hum Genet* **82**(2)**:** 501-509

Savage SA, Giri N, Jessop L, Pike K, Plona T, Burdett L, Alter BP (2011) Sequence analysis of the shelterin telomere protection complex genes in dyskeratosis congenita. *J Med Genet* **48**(4)**:** 285-288

Schepers AG, Vries R, van den Born M, van de Wetering M, Clevers H (2011) Lgr5 intestinal stem cells have high telomerase activity and randomly segregate their chromosomes. *EMBO J* **30**(6)**:** 1104-1109

Scherthan H, Jerratsch M, Li B, Smith S, Hulten M, Lock T, de Lange T (2000) Mammalian meiotic telomeres: protein composition and redistribution in relation to nuclear pores. *Mol Biol Cell* **11**(12)**:** 4189-4203

Schoeftner S, Blasco MA (2008) Chromatin regulation and non-coding RNAs at mammalian telomeres. *Semin Cell Dev Biol* **21**(2)**:** 186-193

Schofield R (1978) The relationship between the spleen colony-forming cell and the haemopoietic stem cell. *Blood Cells* **4**(1-2)**:** 7-25

Sfeir A, Kosiyatrakul ST, Hockemeyer D, MacRae SL, Karlseder J, Schildkraut CL, de Lange T (2009) Mammalian telomeres resemble fragile sites and require TRF1 for efficient replication. *Cell* **138**(1)**:** 90-103

Shay JW, Wright WE (2006) Telomerase therapeutics for cancer: challenges and new directions. *Nat Rev Drug Discov* **5**(7)**:** 577-584

Shay JW, Wright WE (2011) Role of telomeres and telomerase in cancer. *Semin Cancer Biol* **21**(6)**:** 349-353

Siderakis M, Tarsounas M (2007) Telomere regulation and function during meiosis. *Chromosome Res* **15**(5)**:** 667-679

Siegl-Cachedenier I, Munoz P, Flores JM, Klatt P, Blasco MA (2007) Deficient mismatch repair improves organismal fitness and survival of mice with dysfunctional telomeres. *Genes Dev* **21**(17)**:** 2234-2247

Smith S, de Lange T (1997) TRF1, a mammalian telomeric protein. *Trends Genet* **13**(1)**:** 21-26

Smith S, Giriat I, Schmitt A, de Lange T (1998) Tankyrase, a poly(ADP-ribose) polymerase at human telomeres. *Science* **282**(5393)**:** 1484-1487

Smogorzewska A, de Lange T (2002) Different telomere damage signaling pathways in human and mouse cells. *EMBO J* **21**(16)**:** 4338-4348

Smogorzewska A, van Steensel B, Bianchi A, Oelmann S, Schaefer MR, Schnapp G, de Lange T (2000) Control of human telomere length by TRF1 and TRF2. *Mol Cell Biol* **20**(5)**:** 1659-1668

Snippert HJ, Haegebarth A, Kasper M, Jaks V, van Es JH, Barker N, van de Wetering M, van den Born M, Begthel H, Vries RG, Stange DE, Toftgard R, Clevers H (2010) Lgr6 marks stem cells in the hair follicle that generate all cell lineages of the skin. *Science* **327**(5971)**:** 1385-1389

Stadtfeld M, Maherali N, Breault DT, Hochedlinger K (2008a) Defining molecular cornerstones during fibroblast to iPS cell reprogramming in mouse. *Cell Stem Cell* **2**(3)**:** 230-240

Stadtfeld M, Nagaya M, Utikal J, Weir G, Hochedlinger K (2008b) Induced pluripotent stem cells generated without viral integration. *Science* **322**(5903)**:** 945-949

Stout GJ, Blasco MA (2009) Genetic dissection of the mechanisms underlying telomere-associated diseases: impact of the TRF2 telomeric protein on mouse epidermal stem cells. *Dis Model Mech* **2**(3-4)**:** 139-156

Subramanyam D, Lamouille S, Judson RL, Liu JY, Bucay N, Derynck R, Blelloch R (2011) Multiple targets of miR-302 and miR-372 promote reprogramming of human fibroblasts to induced pluripotent stem cells. *Nat Biotechnol* **29**(5)**:** 443-448

Takahashi K, Tanabe K, Ohnuki M, Narita M, Ichisaka T, Tomoda K, Yamanaka S (2007) Induction of pluripotent stem cells from adult human fibroblasts by defined factors. *Cell* **131**(5)**:** 861-872

Takahashi K, Yamanaka S (2006) Induction of pluripotent stem cells from mouse embryonic and adult fibroblast cultures by defined factors. *Cell* **126**(4)**:** 663-676

Takeda N, Jain R, LeBoeuf MR, Wang Q, Lu MM, Epstein JA (2011) Interconversion between intestinal stem cell populations in distinct niches. *Science* **334**(6061)**:** 1420-1424

Tejera AM, Stagno d'Alcontres M, Thanasoula M, Marion RM, Martinez P, Liao C, Flores JM, Tarsounas M, Blasco MA (2010) TPP1 is required for TERT recruitment, telomere elongation during nuclear reprogramming, and normal skin development in mice. *Dev Cell* **18**(5)**:** 775-789

Tian H, Biehs B, Warming S, Leong KG, Rangell L, Klein OD, de Sauvage FJ (2011) A reserve stem cell population in small intestine renders Lgr5-positive cells dispensable. *Nature* **478**(7368)**:** 255-259

Tichy ED (2011) Mechanisms maintaining genomic integrity in embryonic stem cells and induced pluripotent stem cells. *Exp Biol Med (Maywood)* **236**(9)**:** 987-996

Tomas-Loba A, Flores I, Fernandez-Marcos PJ, Cayuela ML, Maraver A, Tejera A, Borras C, Matheu A, Klatt P, Flores JM, Vina J, Serrano M, Blasco MA (2008) Telomerase reverse transcriptase delays aging in cancer-resistant mice. *Cell* **135**(4)**:** 609-622

Tsakiri KD, Cronkhite JT, Kuan PJ, Xing C, Raghu G, Weissler JC, Rosenblatt RL, Shay JW, Garcia CK (2007) Adult-onset pulmonary fibrosis caused by mutations in telomerase. *Proc Natl Acad Sci U S A* **104**(18)**:** 7552-7557

van Steensel B, de Lange T (1997) Control of telomere length by the human telomeric protein TRF1. *Nature* **385**(6618)**:** 740-743

Varela E, Schneider RP, Ortega S, Blasco MA (2011) Different telomere-length dynamics at the inner cell mass versus established embryonic stem (ES) cells. *Proc Natl Acad Sci U S A* **108**(37)**:** 15207-15212

Vaziri H (1997) Critical telomere shortening regulated by the ataxia-telangiectasia gene acts as a DNA damage signal leading to activation of p53 protein and limited life-span of human diploid fibroblasts. A review. *Biochemistry (Mosc)* **62**(11)**:** 1306-1310

Vaziri H, Benchimol S (1998) Reconstitution of telomerase activity in normal human cells leads to elongation of telomeres and extended replicative life span. *Curr Biol* **8**(5)**:** 279-282

Villasante A, Piazzolla D, Li H, Gomez-Lopez G, Djabali M, Serrano M (2011) Epigenetic regulation of Nanog expression by Ezh2 in pluripotent stem cells. *Cell Cycle* **10**(9)**:** 1488-1498

von Zglinicki T, Pilger R, Sitte N (2000) Accumulation of single-strand breaks is the major cause of telomere shortening in human fibroblasts. *Free Radic Biol Med* **28**(1)**:** 64-74

Wang Y, Jiang Y, Liu S, Sun X, Gao S (2009) Generation of induced pluripotent stem cells from human beta-thalassemia fibroblast cells. *Cell Res* **19**(9)**:** 1120-1123

Watson JD (1972) Origin of concatemeric T7 DNA. *Nat New Biol* **239**(94)**:** 197-201

Watson JD, Crick FH (1953) Molecular structure of nucleic acids; a structure for deoxyribose nucleic acid. *Nature* **171**(4356)**:** 737-738

Wernig M, Meissner A, Cassady JP, Jaenisch R (2008) c-Myc is dispensable for direct reprogramming of mouse fibroblasts. *Cell Stem Cell* **2**(1)**:** 10-12

Wisniewski JR, Zougman A, Nagaraj N, Mann M (2009) Universal sample preparation method for proteome analysis. *Nat Methods* **6**(5)**:** 359-362

Wong VW, Stange DE, Page ME, Buczacki S, Wabik A, Itami S, van de Wetering M, Poulsom R, Wright NA, Trotter MW, Watt FM, Winton DJ, Clevers H, Jensen KB (2012) Lrig1 controls intestinal stem-cell homeostasis by negative regulation of ErbB signalling. *Nat Cell Biol* **14**(4)**:** 401-408

Woo WM, Oro AE (2011) SnapShot: hair follicle stem cells. *Cell* **146**(2)**:** 334-334 e332

Wright WE, Tesmer VM, Huffman KE, Levene SD, Shay JW (1997) Normal human chromosomes have long G-rich telomeric overhangs at one end. *Genes Dev* **11**(21)**:** 2801-2809

Wu P, Takai H, de Lange T (2012) Telomeric 3' Overhangs Derive from Resection by Exo1 and Apollo and Fill-In by POT1b-Associated CST. *Cell* **150**(1)**:** 39-52

Yamaguchi H, Calado RT, Ly H, Kajigaya S, Baerlocher GM, Chanock SJ, Lansdorp PM, Young NS (2005) Mutations in TERT, the gene for telomerase reverse transcriptase, in aplastic anemia. *N Engl J Med* **352**(14)**:** 1413-1424

Yang J, Chang E, Cherry AM, Bangs CD, Oei Y, Bodnar A, Bronstein A, Chiu CP, Herron GS (1999) Human endothelial cell life extension by telomerase expression. *J Biol Chem* **274**(37)**:** 26141-26148

Ye JZ, de Lange T (2004) TIN2 is a tankyrase 1 PARP modulator in the TRF1 telomere length control complex. *Nat Genet* **36**(6)**:** 618-623

Ye JZ, Donigian JR, van Overbeek M, Loayza D, Luo Y, Krutchinsky AN, Chait BT, de Lange T (2004a) TIN2 binds TRF1 and TRF2 simultaneously and stabilizes the TRF2 complex on telomeres. *J Biol Chem* **279**(45)**:** 47264-47271

Ye JZ, Hockemeyer D, Krutchinsky AN, Loayza D, Hooper SM, Chait BT, de Lange T (2004b) POT1-interacting protein PIP1: a telomere length regulator that recruits POT1 to the TIN2/TRF1 complex. *Genes Dev* **18**(14)**:** 1649-1654

Yuan JS, Reed A, Chen F, Stewart CN, Jr. (2006) Statistical analysis of real-time PCR data. *BMC Bioinformatics* **7:** 85

Zhong Z, Shiue L, Kaplan S, de Lange T (1992) A mammalian factor that binds telomeric TTAGGG repeats in vitro. *Mol Cell Biol* **12**(11)**:** 4834-4843

Zhou XZ, Lu KP (2001) The Pin2/TRF1-interacting protein PinX1 is a potent telomerase inhibitor. *Cell* **107**(3)**:** 347-359

Zhu XD, Kuster B, Mann M, Petrini JH, de Lange T (2000) Cell-cycle-regulated association of RAD50/MRE11/NBS1 with TRF2 and human telomeres. *Nat Genet* **25**(3)**:** 347-352

Zhu XD, Niedernhofer L, Kuster B, Mann M, Hoeijmakers JH, de Lange T (2003) ERCC1/XPF removes the 3' overhang from uncapped telomeres and represses formation of telomeric DNA-containing double minute chromosomes. *Mol Cell* **12**(6)**:** 1489-1498

Zijlmans JM, Martens UM, Poon SS, Raap AK, Tanke HJ, Ward RK, Lansdorp PM (1997) Telomeres in the mouse have large inter-chromosomal variations in the number of T2AG3 repeats. *Proc Natl Acad Sci U S A* **94**(14)**:** 7423-7428

10. ACKNOWLEDGMENTS

To...

María, thank you a lot for giving me the possibility to do my Ph.D. thesis in your lab and for your guidance. It has been a pleasure to work in such a competitive group and with all the resources that have been provided from your part and the CNIO. In addition, I was given the possibility to participate in the spin-off company Life-Length. I know that I will appreciate this possibility and experience for the rest of my life. I wish you all the best as director of the CNIO and a lot of strength in these turbulent times in Spain.

Diego, thank you a lot for all your time spent with me in front of the microscope and during the analysis of the images and the programming with Definiens. It was nice to have a guy with so much knowledge and even more patience. Thanks also to your team, **Ximo** and **Manu** that are doing a great job.

Sagrario, many thanks to you and your team for the precious input and help with the iPS cells and everything around that topic. It was nice to know somebody around for all the kind of problems with these beasts.

Markus: Thank you for being ready to take the responsibility for my thesis at the University of Basel and for all the times I came to you with a problem that was solved very fast and efficiently!

Rosa, many thanks for your precious help, knowledge and work with all the possible problems that can occur with mice. C'était très drôle avec toi.

Angie: Vielen Dank für deine Hilfe!! Es war toll Dich kennen zu lernen und zu erfahren wieso alle Ph.D's in Basel Deine Arbeit so schätzen.

Martina, thank you a lot for your support, your English tongue and your Italian being. It was a pleasure to work with you and to eat your bad day cakes ;)

Nacho, Elsa, Andres: Thank you for the introduction in the telomere measurement analysis with all the different techniques.

Agueda, Nani, and **Paula**: You are the people that accompanied me during all the time of my thesis. Thank you a lot for your support and input.

Benjamin, Christian, Elisa, Gina, Ianire, Maria G., Bruno, Fabian B., Miguel, Nora: Somewhere along the track of my thesis you started your work in our group. I hope that you are having a good time in the lab and that you will enjoy the rest of your time at CNIO and on days the results do not fit, in the Montoya.

Adelaida, Ana, Christina, Daniela, Elena, Han, Lluc, Lucia, Maria, Sandrina, Susanna, Antonio, Cyan, Daniel, Manolo, Manuel, Pablo, Tim. Many thanks also to the group of **Manolo**. It was really nice to have you around in the lab, giving us a look over the rim of the teacup of telomere spots.

Luis, thank you for bringing order to the chaos and your corrections of my inexperienced Spanish writing.

Mercedes, Maria D., Alessandra, Marisol and Steve: Thank you a lot for your collaboration with Life Length, I hope the company provides you a good place to work and that it also profits from your enthusiasm**.**

Fjordi, it was fun to have you around in Madrid and now every time we see us in Lausanne. I hope that you will find your house at the lake ;)

Mahmut, ich hätte nicht gedacht, dass du dich nach Spanien traust. Am Ende war ich aber froh, dass ich jemanden hatte mit dem ich mich des Öfteren auf den Sattel schwingen konnte um über die Sierra zu pedalieren.

Mama und Papa, vielen, vielen Dank für eure Hilfe und Unterstützung während meiner Thesis. Es war immer wieder schön zu euch nach Hause zu kommen und ein paar Tage auszuspannen oder wenn ihr hier wart mit euch durch Spanien zu reisen.

Angelika, Beatrice und Charlotte, einen grossen Dank auch an euch, für all die Zeit die ihr mit mir verbracht habt vor, während und nach dieser Thesis. Ich habe es genossen meine Schwestern zu sehen wann immer ich auf Besuch war!

Paulina: Kochanie, I love you more than anything else and I am so thankful that you have been there when I needed any kind of support. Soon we will live together again and we can spend as much time with each another as we want. I am looking forward to it!!
From my side I wish you a lot of strength and luck with your research and, that something nice and satisfactory results from it.

11. CURRICULUM VITAE

Personal details

Name and Surname	**Ralph P. Schneider**
Date of Birth	5. August 1980
Nationality	Swiss

Education

2007- pending	**Ph.D Thesis in Molecular Oncology** (Spanish National Cancer Research institute (CNIO), Madrid, Spain in the lab of Prof. Maria A. Blasco under the responsibility of Markus Affolter.
2006	**Master of Science in Molecular Biology** (CBM/Biocenter, Basel)
2005	**Bachelor of Science in Biology; Major in Molecular Biology** (Biocenter, Basel)
2001 - 2006	Studies in molecular biology at the University of Basel (Biocenter)
2000	Matura type E (economics)
1996 – 2000	Commercial high school in Schwyz, Switzerland

Languages

German	Mother Tongue
English	Very well spoken and written / 3 month language course in Cairns, Australia and 1 month in Bath, England
Spanish	Very well Spoken and well written / 1 month language course in Malaga, Spain; living in Spain for 4,5 years; certified till level: B2
French	Well Spoken and written / 2 x 1 month language course in St.Malo, France

Working experience

Aug. 2012	**Publication submitted: The TRF1 telomere protein is essential for the generation of iPS cells and marks both pluripotent and adult stem cells.** **Ralph P. Schneider**, Ianire Garrobo, Alejandro Palácios, Rosa M. Marión , IgnacioFlores, Sagrario Ortega, and Maria A. Blasco Nat Communications
Apr. 2012	**Publication: Genetic inactivation of Cdk7 leads to cell cycle arrest and induces premature aging due to adult stem cell exhaustion.** Ganuza M, Sáiz-Ladera C, Cañamero M, Gómez G, **Schneider R**, Blasco MA, Pisano D, Paramio JM, Santamaría D, Barbacid M. EMBO J. 2012 Apr 13
Feb. 2012	**Publication: Identification of novel pathways involved in the pathogenesis of human adamantinomatous craniopharyngioma.** Andoniadou CL, Gaston-Massuet C, Reddy R, **Schneider RP**, Blasco MA, Le Tissier P, Jacques TS, Pevny LH, Dattani MT, Martinez-Barbera JP. Acta Neuropathol. 2012 Feb 18.

Aug. 2011	**Publication: Different telomere-length dynamics at the inner cell mass versus established embryonic stem (ES) cells.** Varela E, **Schneider RP**, Ortega S, Blasco MA Proc Natl Acad Sci U S A. 2011 Sep 13
Sept. 2010 - now	**Founding of the spin-off company LIFE LENGTH** as part of the founder team (www.lifelength.com) and since then working as research scientist and scientific adviser at phone conferences with costumers establishing procedures and protocol for the clients research.
Feb. – Mar. 2010	**Poster Presentation at the AACR meeting "The Role of Telomere and Telomerase in Cancer Research".** The poster was entitled Generation and characterization of an eGFP-TRF1 knock-in reporter mouse as a new tool for telomere analysis in living cells and mice Fort Worth, Texas, US.
Oct. 2009	**Talk at the Telomarker Partners midterm Meeting 2009**. My talk was entitled "Shelterins and Ageing". Gerrards Cross, UK.
Mar. 2008	**Talk at the Workshop "New battlefield in Cancer: Attacking on many fronts".** My talk was entitled "Telomere lengths: a road map to cancer stem cell niches". CNIO, Madrid, Spain
Sept. 2007 – Mar. 2008	**Member of the CNIO-Oncotrain Workshop-Committee** of the workshop: "New battlefield in Cancer: Attacking on many fronts" that took place the 10th and 11th of March 2008. The goal was to introduce Marie Curie grant-receiver into the organization of scientific meetings. CNIO, Madrid, Spain
Oct. 2006 – Apr. 2007	**Oro Clean Chemistry**, Zurich (Fehraltdorf), Switzerland Scientific writing on pathogens, susceptible for disinfectants of Oro Clean Chemistry, Zurich, Switzerland
Mar. 2005 – Sept. 2006	**Center for Biomedicine (CBM)**, University of Basel, Switzerland **Master thesis** with the title: "Modulating tumor progression by angiogenic growth factor traps", with the main emphasis on tumor angiogenesis including the techniques: Cloning, Cell culture, adenoviral-vector creation, immunohistochemistry and immunofluorescence staining. Under the direction of Prof. G. Christofori

IT / Computer skills

- Definiens DeveloperXD1.2-2.0
- MetaMorph
- ImageJ / Fiji
- GraphPad Prism
- LAS AF Leica
- MS Office (Word incl. EndNote, PowerPoint, Excel, Outlook)
- Adobe Illustrator, Adobe Photoshop

12. PUBLICATIONS

Different telomere-length dynamics at the inner cell mass versus established embryonic stem (ES) cells

Elisa Varela[a], Ralph P. Schneider[a], Sagrario Ortega[b], and Maria A. Blasco[a,1]

[a]Telomeres and Telomerase Group, Molecular Oncology Program, and [b]Transgenics Unit, Biotechnology Program, Spanish National Cancer Research Centre, Madrid E-28029, Spain

Edited by Inder M. Verma, The Salk Institute, La Jolla, CA, and approved July 15, 2011 (received for review April 6, 2011)

Murine embryonic stem (ES) cells have unusually long telomeres, much longer than those in embryonic tissues. Here we address whether hyper-long telomeres are a natural property of pluripotent stem cells, such as those present at the blastocyst inner cell mass (ICM), or whether it is a characteristic acquired by the in vitro expansion of ES cells. We find that ICM cells undergo telomere elongation during the in vitro derivation of ES-cell lines. In vivo analysis shows that the hyper-long telomeres of morula-injected ES cells remain hyper-long at the blastocyst stage and longer than telomeres of the blastocyst ICM. Telomere lengthening during derivation of ES-cell lines is concomitant with a decrease in heterochromatic marks at telomeres. We also found increased levels of the telomere repeat binding factor 1 (TRF1) telomere-capping protein in cultured ICM cells before telomere elongation occurs, coinciding with expression of pluripotency markers. These results suggest that high TRF1 levels are present in pluripotent cells, most likely to ensure proficient capping of the newly synthesized telomeres. These results highlight a previously unnoticed difference between ICM cells at the blastocyst and ES cells, and suggest that abnormally long telomeres in ES cells are likely to result from continuous telomere lengthening of proliferating ICM cells locked at an epigenetic state associated to pluripotency.

Nanog | Sox2 | Oct4 | embryo

Mouse embryonic stem (ES) cells are pluripotent, proliferate indefinitely, and bear very long telomeres (1–3). ES cells emerge from preimplantation blastocyst-stage embryos (4), but how this process takes place is largely unknown. In previous studies, we observed that telomeres of mouse ES cells were much longer than those of mouse embryonic fibroblasts (MEFs) of the same genetic background (5), which are typically obtained at embryonic day 13.5 (E13.5). This observation raised the issue of whether blastocyst inner cell mass (ICM) cells, which are the natural equivalents of ES cells, also have hyper-long telomeres. If this is the case, then telomeres must shorten during fetal development, despite high telomerase activity (6–8). An alternative explanation emerges, however, that hyper-long telomeres in ES cell are aberrant and may result from the in vitro establishment and expansion of ES cells.

ES-like pluripotent stem cells can be generated from differentiated cells (i.e., MEFs) by using defined factors, giving rise the so-called induced pluripotent stem (iPS) cells, which are considered functional equivalents of ES cells (9–16). We recently showed that iPS telomeres increase in length during and after nuclear reprogramming until reaching ES cell hyper-long telomeres. This elongation process occurs concomitantly to lower density of trimethylated histones H3K9 and H4K20 at the telomeric chromatin (5). Furthermore, hyper-long telomeres were not observed in iPS cells derived from first-generation telomerase-deficient MEFs, indicating that they do not originate from a selective reprogramming of a subset of parental cells with very long telomeres; instead, they result from an active telomere elongation by telomerase during and after nuclear reprogramming (5). Notably, early passage iPS cells had shorter telomeres than those of ES cells from the same genetic background and only acquired ES cell-like hyper-long telomeres after several passages in vitro (5). These findings suggest that hyper-long telomeres in iPS cells are the consequence of in vitro expansion of these cells, lending support to the possibility that a similar scenario may be true also for established mouse ES cell lines.

Results

To directly address these possibilities, we first analyzed telomere length at different stages of mouse embryonic and fetal development, including morula, blastocyst, E7.5, E10.5, and E13.5 (*Materials and Methods*). Embryo sections were hybridized with a telomeric probe and telomere length was measured at a single-cell level by using the telomapping technique (6) (*Materials and Methods*). We observed that average telomere length significantly increased from morula to the blastocyst stage (Fig. 1*A*) and that, although average telomere length was shorter at E7.5 compared with the blastocyst stage, it was maintained constant from E7.5 until E13.5, in agreement with the presence of high telomerase activity throughout embryo development (8, 17–21). Strikingly, ES cells processed in parallel showed much longer telomeres than those of blastocyst cells (Fig. 1*A*). To discard that differences in telomere length are caused by changes in probe accessibility, chromatin status associated to developmental stage, or ploidy, we performed quantitative-FISH (Q-FISH) with a centromeric major satellite probe and found no significant differences in centromeric fluorescence (*Materials and Methods* and Fig. S1). In this regard, centromeres and telomeres have been reported to share the same heterochromatic marks (22). We next performed a separate analysis of telomere length in trophectoderm (TE) cells versus ICM cells within the same blastocysts by using telomapping. Blastocysts cells were grouped into three categories according to their average telomere fluorescence intensity and a color was associated to each group (Fig. 1*B*, *Top*). Most of the cells with the longest telomeres (red color) localize to the ICM, and only a few to the trophectoderm (Fig. 1*B*), and the mean telomere length for the ICM was significantly higher compared with the TE (Fig. 1*B*, *Bottom*). Notably, telomeres of ICM cells were shorter than those of established ES-cell lines, suggesting that ES-cell telomeres undergo a significant lengthening during ES-cell in vitro expansion, in analogy to that previously reported for iPS cells (5). To test this finding, we analyzed in-parallel telomere length in blastocysts and two independent ES-cell lines at both early and late passages by telomapping. Mean telomere length of the ICM was significantly higher than that of the MEFs and trophectoderm cells and of a similar length to early passage ES cells (passage 5) (89 and 83 Kb, respectively) (Fig. 1*C*). Telomere length further increased from passage 5 (83 kb) to passage 12 (around 125 kb) (Fig. 1*C*). In addition, the increased recombination rates of ES cells compared with MEFs (23) could account for the increased heterogeneity in telomere length found in increasing passages of ES cells. By performing Q-FISH with a centromeric major satellite probe, we ruled out that these differences in telomere length were because of

Author contributions: E.V. and M.A.B. designed research; E.V., R.P.S., and S.O. performed research; E.V. and M.A.B. analyzed data; and E.V. and M.A.B. wrote the paper.

The authors declare no conflict of interest.

This article is a PNAS Direct Submission.

Freely available online through the PNAS open access option.

[1]To whom correspondence should be addressed. E-mail: mblasco@cnio.es.

This article contains supporting information online at www.pnas.org/lookup/suppl/doi:10.1073/pnas.1105414108/-/DCSupplemental.

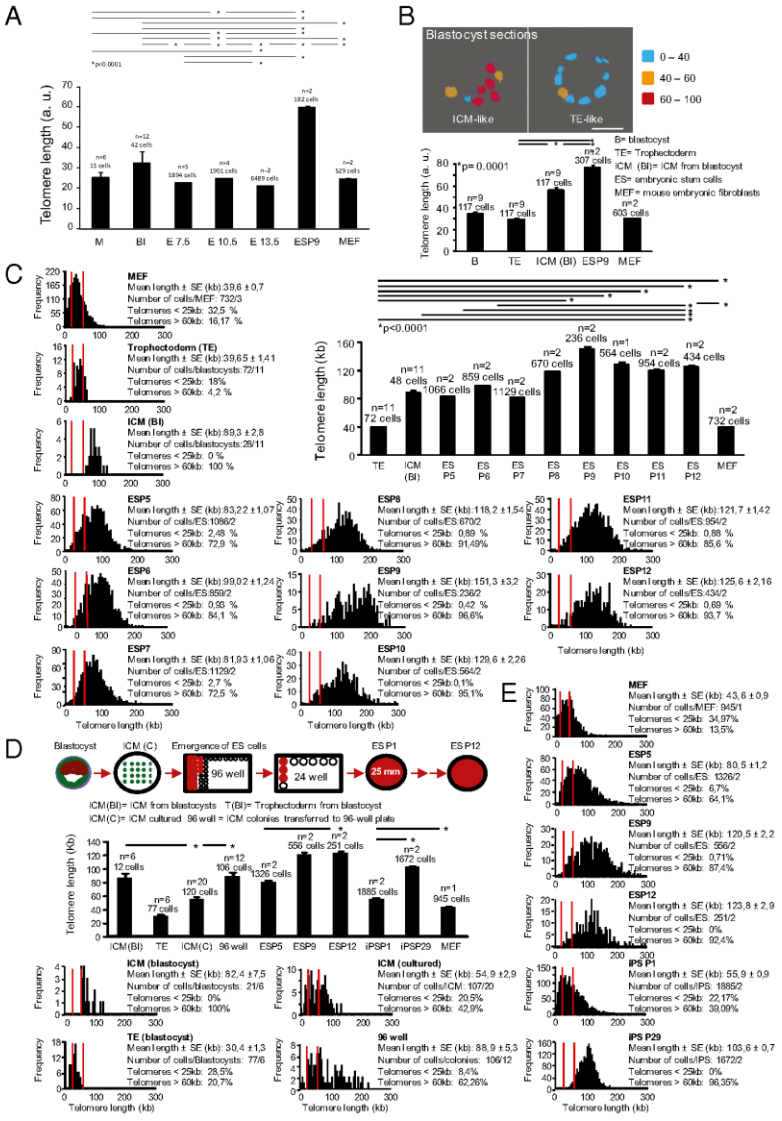

Fig. 1. Blastocyst ICM bears the longest telomeres which further lengthen upon expansion of ICM-derived ES cells. (*A*) Quantification of telomere length by telomapping analysis of embryo sections at the indicated stages of development, ES cells (passage 9) and primary MEFs (passage 2). Telomere-length quantification is given in arbitrary units of fluorescence (a.u.). *n* = number of embryos or independent cell cultures. (*B*) (*Top*) Representative image of a telomapping of a blastocyst section. Nuclei are colored according to their telomere length and normalized by the telomere length of ES cells. Because ES cells are derived from the ICM we reasoned that they should have equivalent telomere length. The division of the CY3 intensity value of each blastocyst cell by the mean CY3 intensity value of ES cells should render the blastocyst cells with the longest telomeres (values around or equal to 1). For the blastocyst map we grouped intensity values in three fractions to simplify the identification of the cells with the longest telomeres. Note that the longest telomeres localize to the ICM of the blastocyst. (Scale bar, 10 μm.) (*Lower*) Quantification of telomere length of blastocyst, ES cells and MEFs, as indicated. *n* = number of embryos or independent ES and primary MEF cultures. (*C*) Telomere-length frequency histograms of blastocysts, ES cells at the specified passages, and primary MEFs and mean telomere length for the same samples. Note that the telomere length of ES at early passages is similar to that found in the ICM. *n* = number of embryos or independent ES or primary MEFs cultures. (*D*) Scheme of the process of isolation of ES cells from blastocysts. In brief, *zona pellucida* is removed from blastocysts and they are transferred to a 60-mm dish. After 4 to 6 d the ICM has divided to ∼1,000 cells. Individual ICM colonies are transferred to a 96-well plate. At this step, ES colonies emerge and are transferred to a 24-well plate for expansion. From the 24-well plate, cells are transferred to 25-mm plates and are considered passage 1. Further passages are plate colonies or ES and primary MEF cultures. (*E*) Mean telomere length and telomere-length frequency histograms in ICM from the blastocyst, in vitro cultured ICM, emerging ES from the 96-well plate, established ES cells (passages 5, 9, and 12), iPS cells (passage 1 and 29), and primary MEFs determined by telomapping. Note that telomeres of the ICM at the blastocyst are longer than those of the cultured ICM.

changes in probe accessibility, chromatin status, or ploidy (*Materials and Methods* and Fig. S2). Of relevance, this continuous increment of telomere length over passages in pluripotent cells is not observed in established immortal human (Fig. S3) or mouse cell lines (24), which show stable telomeres over passages. To test whether telomere length was further increased after passage 12, we expanded the cells until passage 31 and performed telomapping analysis. We found that telomeres continued to increase their length at these late passages, although the difference between passage 24 and 31 was not statistically significant (Fig. S4). In conclusion, the reset of telomere length during development happens at the blastocyst stage, in accordance with a previous report showing telomere elongation at the transition from morula to blastocyst (25). Importantly, we first demonstrate here that the longest telomeres within blastocysts localize to the ICM, suggesting that telomere elongation specifically occurs in this subset of pluripotent embryonic cells. In addition, ES cells undergo a further increase in telomere length compared with ICM cells of the blastocyst.

The telomere length of the blastocyst ICM was comparable to that of ES cells at passage 5, raising the possibility that telomere length of established ES cells was inherited from the blastocyst ICM, and telomere lengthening restricted to in vitro expansion of established ES cell lines. To test this hypothesis, we sought to analyze in-depth telomere dynamics at the earliest steps during establishment of ES cells. The very first step is the in vitro ICM, obtained from 3.5-d blastocysts upon removal of the *zona pellucida*. After a few days, colonies of about 1,000 cells are formed (scheme in Fig. 1*D*; images of ICM colonies in Fig. S5; see also *Materials and Methods*). In vitro ICM colonies are individually trypsinized and transferred to 96-well plates, where ES cells start to emerge. Further expansion leads to the establishment of ES cells (Fig. 1*D*). We measured telomere length by telomapping in the ICM and troph-

oblasts in blastocysts, in cultured ICM, in the ICM-derived cells grown in 96-well plates, and in established ES-cell lines at passages 5, 9, and 12 (see scheme in Fig. 1*D*). We also included iPS cells at both early and late passages. We confirmed that telomeres lengthen during in vitro expansion of ES cells (80 kb at passage 5 compared with 123 kb at passage 12) (Fig. 1*E*). Similarly, iPS-cell telomeres increased with passages (Fig. 1*E*) (5). Interestingly, telomeres from the in vitro ICM (55 kb) were shorter than those of the blastocyst ICM (86 kb) but seemed to recover their length at the 96-well plate (89 kb) (Fig. 1*E*), which showed similar telomeres to early passage (passage 5) ES cells (80 kb). We confirmed these findings by using an independent technique based on Southern blotting (telomere restriction fragment analysis, TRF) (Fig. S6). These results may suggest that the cells from the ICM are susceptible culture-stress–induced telomere-length changes. Indeed, during the establishment of ES-cell lines, the transient ICM of the early blastocyst is forced to artificially exist and divide for several days in vitro. Under culture conditions, most ICM cells differentiate (only 17% and 38.5% of cells express the pluripotency factors Sox2 and Oct3/4, respectively), which in turn may lead to telomere shortening compared with pluripotent stem cells (5, 6).

To better understand the dynamics of telomere lengthening in the cultured ICM, and to avoid contamination with feeder cells (irradiated MEFs), we analyzed telomere length after 4 and 7 d of culture, in the absence of feeders, by using telomapping (Fig. S7). We did not find any statistically significant difference in the telomere length at 4 or 7 d of culture. We also ruled out that mean telomere length of the in vitro cultured ICM was lower than that of the blastocyst ICM because of the contribution of irradiated MEFs.

Next, we set to confirm telomere shortening in the in vitro ICM, as well as telomere lengthening of ES cell over in vitro expansion, by using Q-FISH on metaphase spreads. Metaphase spreads allow analysis of every single telomere at chromosomes of a given metaphase. We confirmed shorter telomeres in the cultivated ICM (50 kb), which increased in length with subsequent passages from a mean telomere length of 112 kb in passage 5 to a mean telomere length of 144 kb in passage 12 (Fig. 2*A* and Fig. S8*A*; note that absolute telomere-length values were higher than in the telomapping experiment, most likely because of differences in acquisition and the software used to measure intensity).

To in vivo test whether established ES cells have longer telomeres than those of the ICM of the blastocyst, we aggregated ES cells with hyper-long telomeres expressing GFP with eight-cell morulae (Fig. 2*B* and *Materials and Methods*). At the blastocyst stage, development was stopped and combined telomere FISH/GFP immunofluorescence was performed (*Materials and Methods*). We found that average telomere length in GFP-expressing ICM cells (derived from aggregated ES cells) was higher than that of non-GFP–expressing ICM cells (derived from the recipient morulae) (Fig. 2 *C* and *D* and Fig. S8*B*). These results demonstrate that established ES cells have longer telomeres than the cells of the blastocyst ICM. In addition, these results rule out possible effects of different developmental stages on telomere-length measurements, as we are comparing the same cell type within the blastocyst ICM. In summary, these findings strongly support the unique finding of active mechanisms, leading to very long telomeres in the process of ES-cell line establishment, which are likely to involve telomere elongation by telomerase (5).

We reasoned that the increase in telomere length observed in established and during the establishment of ES cells could be linked to the structure of chromatin and ultimately to the epigenetic status of telomeres, which is different to that observed in MEFs (5, 22). To test this idea, we first measured the global- and subtelomeric-DNA methylation (*SI Materials and Methods*). Because pericentric and subtelomeric repeats remain unaltered between ES and differentiated cells (5, 16), we analyzed the interspersed repeats (SINE repeats) and found no substantial difference in DNA-methylation between the passages of ES cells and MEFs (Fig. S9*A*). We found subtelomeric DNA mostly methylated with small variations between the passages, which were not statistically significant (Fig. S9 *B–D*). We next analyzed heterochromatic marks at telomeres by performing FISH with a telomere probe combined with immunofluorescence for both trimethylation at lysine 20 of histone H4 (H4k20me3) and at lysine 9 of histone H3 (H3k9me3) (5, 22, 26–29). H4k20me3 average fluorescence was similar in primary MEFs, ICM, and 96-well cells, but very significantly decreased in established ES cells. However, histograms of the frequency of cells with a given H4K20me3 fluorescence already show a population of cells with low H4k20me3 abundance in the cultured ICM and the cells in the 96-well plates. Indeed, the percentage of cells with H4k20me3

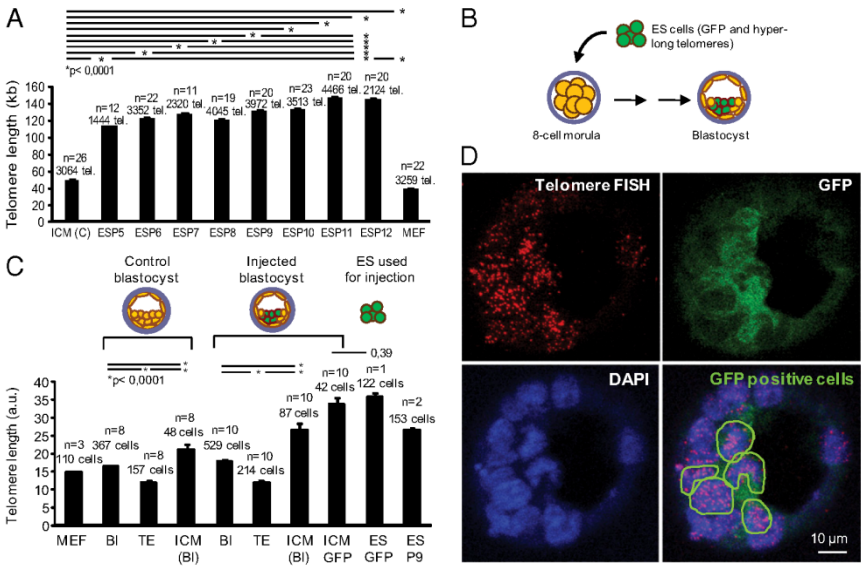

Fig. 2. Telomere-length dynamics during establishment and expansion of ES cell lines as well as in vivo aggregation of ES cells in morulae. (*A*) Mean telomere length for ICM cultivated from the 60-mm tissue-culture plate, and successive passages of ES cells. Telomere length was analyzed by metaphase Q-FISH. *n* = number of ICM colonies or independent ES and primary MEF cultures. (*B*) Scheme of the aggregation experiments. Established ES cells at passage 16 expressing GFP were microinjected in eight-cell morulae. Blastocyst from injected and noninjected morulae were fixed for the analysis of telomere length by telomapping. (*C*) Mean telomere length for primary MEFs (passage 2), noninjected and injected blastocysts, as well as GFP-ES cells before injection (passage 16) and ES cells at passage 9. *n* = number of blastocysts or independent clones of ES cells or primary MEFs. (*D*) Representative images of an injected blastocyst.

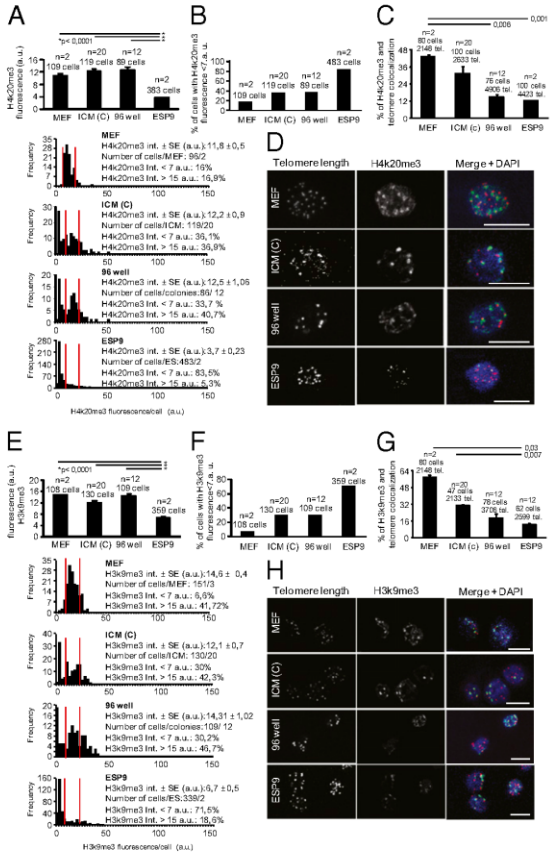

Fig. 3. The loss of heterochromatic marks accompanies telomere lengthening. (*A*) Mean H4k20me3 intensity for primary MEFs (passage 2), in vitro cultured ICM, cells from the 96-well plate, and established ES cells at passage 9. (*Lower* graphs) The H4k20me3 histograms for the same samples. Note that in the ICM as well as in the 96-well plate there are cells with low H4k20me3 signals. (*B*) Percentage of cells with less than 7 arbitrary units of H4k20me3 fluorescence. Note the portion of cells with low methylation signal in both the cultured ICM and the 96-well plate. (*C*) Colocalization of the H4k20me3 heterochromatic mark with telomeres in percentage for the samples described in *A*. (*D*) Representative images of telomeres and H4k20me3 signals for the samples described in *A*. (*E*) Mean H3k9me3 intensity and histograms for the samples described in *A*. (*F*) Percentage of cells with less than 7 arbitrary units of H3k9me3 fluorescence. Note the portion of cells with low methylation signal in the cultured ICM and the 96-well plate. (*G*) Percentage of colocalization of the H3k9me3 heterochromatic mark with telomeres for the samples described in *A*. (*H*) Representative images of telomeres and H3k9me3 signals for the samples described in *A*. *n* = number of ICM or 96-well plate colonies or independent ES, and primary MEF cultures. Arbitrary units of H4k20me3 fluorescence is plotted. (Scale bars, 10 μm.)

fluorescence below 7 arbitrary units increased from MEFs (16%) to the ICM (33.7%) and 96-well plate (36.9%), to reach 83.5% in established ES-cell lines (Fig. 3 *A–D*). Very similar results were observed for H3k9me3 (Fig. 3 *E–H*). A lower colocalization of heterochromatic marks with telomeres was also observed during the process of ES cell generation (Fig. 3 *C* and *G*) (5). Together, these results indicate a decrease in both H3K9me3 and H4K20me3 heterochromatic marks during the generation of ES cells compared with MEFs, starting in the in vitro ICM. These unprecedented findings suggest that telomere lengthening is concomitant with lower density of heterochromatic marks during the process of ES-cell establishment. Alternatively, only cells with a more open/less-compacted chromatin structure are selected from the blastocyst stage to obtain stable ES-cell cultures.

Next, we reasoned that the mechanisms leading to telomere elongation during the establishment of ES-cell lines might be linked to pluripotency (30–35). Indeed, adult stem-cell compartments bear the cells with the longest telomeres in mice (6). As a marker for pluripotency, we first tested Nanog, which is required to maintain pluripotency in the mouse epiblast and ES cells (32, 36). To this end we combined immunofluorescence using a Nanog antibody with FISH for telomeres (*Materials and Methods*). Again, ICM-cultured cells had shorter telomeres than those from the 96-well plate or established ES cells (Figs. S10 *A–C* and S11*A*). Interestingly, Nanog showed very low expression in the cultivated ICM (3% Nanog-positive cells) (Fig. S10*B*, *Lower* graph), which was dramatically increased at late-passage ES cells (Fig. S10*B*). Accordingly, the best positive slope between telomere length and Nanog was found only in established ES cells (Fig. S11*B*). These results suggest that Nanog expression and telomere length do not correlate during early stages of establishment of ES-cell lines, and this only occurs at later passages.

Several lines of evidence suggest a link between pluripotency and the telomere-binding proteins, known as shelterins (37–39). The shelterin protein TPP1 is essential for telomere elongation by telomerase during reprogramming of MEFs into iPS cells (40). In addition, deletion of TRF1 causes lethality at the blastocyst stage (41), and adult tissues conditionally deleted TRF1, show severe stem-cell defects (40, 42). Thus, we next explored the regulation of TRF1 during establishment of ES cell lines. TRF1 binds and protects telomeres (18, 37, 38) and is proposed to have a role in telomere length regulation (43–46). We observed high TRF1 levels already in the cultured ICM compared with primary MEFs (Figs. S10 *D–F* and S11*D*). TRF1 levels were also high in emerging (96-well) and established ES cells, and Nanog showed similar expression to the previous experiment (Fig. S10*B*). Thus, high levels of TRF1 were associated with high levels of Nanog expression in emerging or established ES cells, but not in the in vitro ICM. We therefore tested whether TRF1 levels in the in vitro ICM associated to other pluripotency markers. Oct3/4 or Sox2 function in the maintenance of pluripotency in early embryos and established ES cells (47–49) and are essential for the reprogramming of differentiated cells into iPS (14–16). To test this possibility, we performed immunofluorescence with TRF1 and Sox2 (Figs. S10 *G–I* and S12*A*). Interestingly, the mean intensity value for Sox2 in the cultured ICM was twice higher than in MEFs, and further increased in emerging and established ES cell lines (Figs. S10*H* and S12*A*). Similar results were found when TRF1 and Oct3/4 antibodies were used (Fig. 4 *A–C* and Fig. S12*D*). Of note, the percentage of positive cells for Sox2 and Oct3/4 in the in vitro ICM (17% and 38.5%, respectively) was higher than that of Nanog (3%). Despite the high levels of TRF1 associated to different pluripotency markers at every stage of establishment of ES cells, correlations were poor (Figs. S11 *B* and *C* and S12 *B* and *C*). To further study a possible correlation between pluripotency factors and TRF1, we used a mouse antibody against Oct3/4 in combination with our best TRF1 antibody. The mouse cell line L5178Y-R, which bears long telomeres but is not pluripotent, was included in our analysis to discard that association of high levels of TRF1 and pluripotency factors are coincidental. Our results show that the cells from the L5178Y-R line had a higher mean TRF1 intensity than MEFs, bur lower than the cultured ICM (Fig. 4 *D*, *F*, and *H*). Oct3/4 levels were basal in primary MEFs and L5178Y-R (Fig. 4 *E*, *G*, and *H*). Furthermore, we observed a clear correlation between TRF1 and Oct3/4 in established ES cells (Fig. 4*I*) and in the in vitro ICM in those cells expressing high levels of Oct3/4. Together, these results indicate that high levels of TRF1 occur in the presence of some pluripotency factors (i.e., Oct3/4) from the earliest step of derivation of ES cells. The unprecedented finding of elevated TRF1 levels before telomere elongation (cultured ICM) could represent a previously unnoticed mechanism to enable

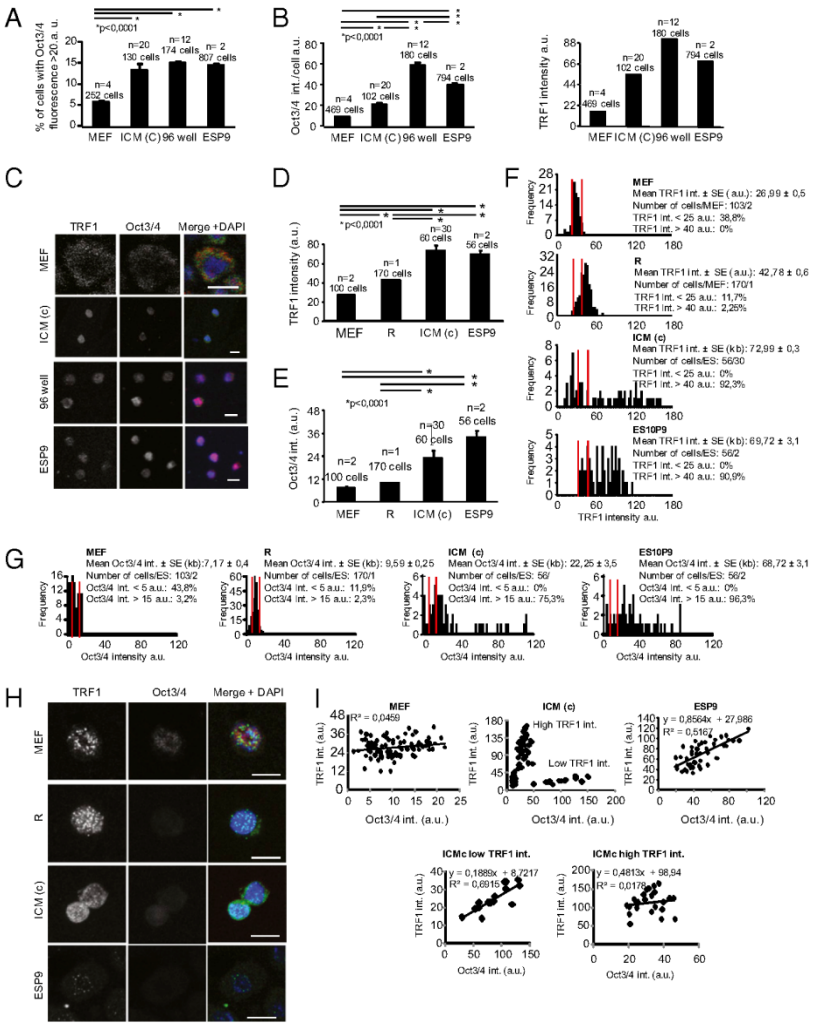

Fig. 4. Analysis of TRF1 and Oct4 expression during isolation of ES cells. (*A*) Mean TRF1 intensity for primary MEFs (passage 2), in vitro cultivated ICM, 96-well plate emerging ES cells, and established ES-cell lines at passage 9 analyzed by telomapping. (*B*) (*Left*) Mean Oct3/4 intensity for the same samples described in *A*. (*Right*) Percentage of cells with Oct3/4 intensity bigger than 20 a.u. Note that at the cultured ICM stage, a 38% of cells are Oc3/4 positive. (*C*) Representative images of TRF1 and Oct3/4 expression for the same samples described in *A*. (Scale bars, 10 μm.) *n* = number of ICM or 96-well plate colonies or ES and primary MEF cultures. (*D*) Mean TRF1 intensity values for primary MEFs, the cell line L5178Y-R or R cells, cultured ICM, and ES passage 9. (*E*) Mean Oct3/4 intensity for the samples described in *D*. (*F*) TRF1 expression frequency histograms corresponding for the samples described in *D*. (*G*) Oct3/4 expression frequency histograms corresponding to the samples described in *D*. (*H*) Representative images of TRF1 and Oct3/4 expression for the samples described in *D*. (Scale bars, 10 μm.) (*I*) TRF1 intensity values plotted against Oct3/4 intensity values to analyze correlation. Primary MEFs, cultured ICM, and established ES cells at passage 9 are shown in the *Upper* panels. (*Lower*) Cells from the cultivated ICM were divided in high or low TRF1 intensity for the analysis. *n* = number of ICM colonies or L5178Y-R, ES, primary MEF cultures.

cells to protect telomeres as they are elongated. In this manner, limiting TRF1 amounts could also limit further telomere elongation by telomerase.

Discussion

Here, we provide unprecedented evidence that telomeres are specifically elongated in the ICM at the blastocyst stage, and that in vitro cultured ICM cell telomeres undergo a further elongation during the establishment of ES cell lines, which is coordinated with decreased levels of histone trimethylation marks. Thus, in contrast to the intuitive idea of ES cells inheriting long telomeres from the cells of the blastocyst ICM, we show here that there are active mechanisms operating in the process of ES establishment, which act in an orderly manner.

We first describe changes in chromatin structure, specifically the loss of heterochromatic marks at early stages of ES cell establishment. In this context, a limited action of the histone metyltranferases Suv39 and Suv420 at telomeres may facilitate the generation of hyper-long telomeres in established ES cell lines, similar to that previously shown by us for iPS cells (26, 27). Second, our results provide evidence for high expression of TRF1 associated to early stages of ES-cell generation (cultivated ICM cells) coincidental with high Sox2 and Oct3/4 levels, and before telomere elongation and presence of high Nanog levels. High TRF1 expression at early stages of ES cell establishment, even before telomere elongation occurs, may be a mechanism to ensure proficient telomere capping, suggesting that the safeguard of chromosome stability could be coupled to pluripotency. Finally, the events described here associated to ES cell establishment, including the loss of heterochromatic marks, high levels of TRF1, and the elongation of telomeres, could also operate in the context of tumorigenesis to maintain cellular immortality.

Materials and Methods

Cell Culture Conditions and Embryo Collection. Cells and embryos used in this work were from the C57BL6 genetic background, unless specified otherwise. ES cells were derived at the Transgenic Mice Unit of the Spanish National Cancer Research Center (CNIO). IPS cells were reprogrammed from primary MEF (5), which were obtained from 13.5-d embryos (50). Culture conditions are described in *SI Materials and Methods*.

Isolation of ICM from Blastocysts. Embryos were harvested from E3.5-pregnant females. The *zona pellucida* was removed by treatment with Tirode's solution and then transferred to a 60-mm plate containing feeder cells (MEFs treated with Mytomicin-C). Blastocysts were cultured in ES-cell medium for 48 h. The outgrowth of the ICM were picked, usually 4 to 6 d after the initial plating, and transferred to a microdrop of trypsin for disaggregation.

Agregation Experiments. For ES cell microinjection, Hsd:ICR(CD-1) morulae were harvested from superovulated females at E2.5 d of gestation. Sixty-three morulae at the eight-cell stage were microinjected with 6 to 10 EGFP-expressing R1 ES cells (of 129 × 1/SvJ × 129S1/Sv genetic background as in ref. 5). Microinjected embryos were incubated overnight at 37 °C under oil. At the blastocyst stage embryos were fixed for analysis.

Quantitative FISH. ES cells and cultured ICM cells were blocked in metaphase with colcemid for 3 h, swollen in hypotonic buffer for 10 min at 37 °C, and fixed as described in ref. 51. Metaphases were dropped on slides and Q-FISH with a telomere or centromere probe was performed as in ref. 28. TFL-Telo software (52) was used to quantify the fluorescence intensity of telomeres from 5 to 10 metaphases for each datapoint. Microscope settings are described in *SI Materials and Methods*.

Telomapping of Blastocyst Sections. Quantitative image analysis was performed on confocal RGB images using the Definiens platform (version XD) as in ref. 6. For details, see *SI Materials and Methods*.

Immunfluorescence combined with FISH. Immunofluorescence was performed as in ref. 43 (*SI Materials and Methods*). Samples were fixed in 4% formaldehyde, dehydrated and incubated with a telomere probe labeled with CY3 (Panagene) as described in ref. (28).

Statistical Analysis. Statistical analyses were performed using the GraphPad Prism software version 5. Mean values reflect the arithmetic mean. Student *t* test with "two tails" was used to obtain the *P* value.

ACKNOWLEDGMENTS. Work in the laboratory of M.A.B. is funded by grants from the Minisetrio de Ciencia e Innovación (CONSOLIDER), the European Union, the European Research Council, The Lilly Foundation, and the Korber European Research Award.

1. Albert M, Peters AH (2009) Genetic and epigenetic control of early mouse development. *Curr Opin Genet Dev* 19(2):113–121.
2. Mattout A, Meshorer E (2010) Chromatin plasticity and genome organization in pluripotent embryonic stem cells. *Curr Opin Cell Biol* 22:334–341.
3. Shay JW, Wright WE (2010) Telomeres and telomerase in normal and cancer stem cells. *FEBS Lett* 584:3819–3825.
4. Evans MJ, Kaufman MH (1981) Establishment in culture of pluripotential cells from mouse embryos. *Nature* 292(5819):154–156.
5. Marion RM, et al. (2009) Telomeres acquire embryonic stem cell characteristics in induced pluripotent stem cells. *Cell Stem Cell* 4(2):141–154.
6. Flores I, et al. (2008) The longest telomeres: A general signature of adult stem cell compartments. *Genes Dev* 22:654–667.
7. Flores I, Blasco MA (2009) A p53-dependent response limits epidermal stem cell functionality and organismal size in mice with short telomeres. *PLoS ONE* 4:e4934.
8. Wright DL, et al. (2001) Characterization of telomerase activity in the human oocyte and preimplantation embryo. *Mol Hum Reprod* 7:947–955.
9. Aoi T, et al. (2008) Generation of pluripotent stem cells from adult mouse liver and stomach cells. *Science* 321:699–702.
10. Maherali N, et al. (2007) Directly reprogrammed fibroblasts show global epigenetic remodeling and widespread tissue contribution. *Cell Stem Cell* 1(1):55–70.
11. Nakagawa M, et al. (2008) Generation of induced pluripotent stem cells without Myc from mouse and human fibroblasts. *Nat Biotechnol* 26(1):101–106.
12. Okita K, Ichisaka T, Yamanaka S (2007) Generation of germline-competent induced pluripotent stem cells. *Nature* 448:313–317.
13. Stadtfeld M, Maherali N, Breault DT, Hochedlinger K (2008) Defining molecular cornerstones during fibroblast to iPS cell reprogramming in mouse. *Cell Stem Cell* 2:230–240.
14. Takahashi K, et al. (2007) Induction of pluripotent stem cells from adult human fibroblasts by defined factors. *Cell* 131:861–872.
15. Takahashi K, Yamanaka S (2006) Induction of pluripotent stem cells from mouse embryonic and adult fibroblast cultures by defined factors. *Cell* 126:663–676.
16. Wernig M, et al. (2007) In vitro reprogramming of fibroblasts into a pluripotent ES-cell-like state. *Nature* 448:318–324.
17. Betts DH, King WA (1999) Telomerase activity and telomere detection during early bovine development. *Dev Genet* 25:397–403.
18. Blasco MA, Funk W, Villeponteau B, Greider CW (1995) Functional characterization and developmental regulation of mouse telomerase RNA. *Science* 269:1267–1270.
19. Liu L, et al. (2007) Telomere lengthening early in development. *Nat Cell Biol* 9: 1436–1441.
20. Mantell LL, Greider CW (1994) Telomerase activity in germline and embryonic cells of Xenopus. *EMBO J* 13:3211–3217.
21. Xu J, Yang X (2001) Telomerase activity in early bovine embryos derived from parthenogenetic activation and nuclear transfer. *Biol Reprod* 64:770–774.
22. Blasco MA (2007) The epigenetic regulation of mammalian telomeres. *Nat Rev Genet* 8:299–309.
23. Jaco I, Canela A, Vera E, Blasco MA (2008) Centromere mitotic recombination in mammalian cells. *J Cell Biol* 181:885–892.
24. McIlrath J, et al. (2001) Telomere length abnormalities in mammalian radiosensitive cells. *Cancer Res* 61:912–915.
25. Schaetzlein S, et al. (2004) Telomere length is reset during early mammalian embryogenesis. *Proc Natl Acad Sci USA* 101:8034–8038.
26. Benetti R, et al. (2008) A mammalian microRNA cluster controls DNA methylation and telomere recombination via Rbl2-dependent regulation of DNA methyltransferases. *Nat Struct Mol Biol* 15(3):268–279.
27. García-Cao M, O'Sullivan R, Peters AH, Jenuwein T, Blasco MA (2004) Epigenetic regulation of telomere length in mammalian cells by the Suv39h1 and Suv39h2 histone methyltransferases. *Nat Genet* 36(1):94–99.
28. Gonzalo S, et al. (2006) DNA methyltransferases control telomere length and telomere recombination in mammalian cells. *Nat Cell Biol* 8:416–424.
29. Vera E, Canela A, Fraga MF, Esteller M, Blasco MA (2008) Epigenetic regulation of telomeres in human cancer. *Oncogene* 27:6817–6833.
30. Smith KP, Luong MX, Stein GS (2009) Pluripotency: Toward a gold standard for human ES and iPS cells. *J Cell Physiol* 220(1):21–29.
31. Orkin SH, et al. (2008) The transcriptional network controlling pluripotency in ES cells. *Cold Spring Harb Symp Quant Biol* 73:195–202.
32. Mitsui K, et al. (2003) The homeoprotein Nanog is required for maintenance of pluripotency in mouse epiblast and ES cells. *Cell* 113:631–642.
33. Liu N, et al. (2008) Identification of genes regulated by nanog which is involved in ES cells pluripotency and early differentiation. *J Cell Biochem* 104:2348–2362.
34. Kuroda T, Tada M (2006) Molecular network of transcriptional factors controlling pluripotency of ES cells. (Translated from Japanese) *Seikagaku* 78(2):137–141.
35. Dong WZ, Shen WZ, Hua JL, Dou ZY (2007) Study on pluripotency and cultivation of ES-like cells derived from male germ stem cells of bovine fetuses. (Translated from Chinese) *Sheng Wu Gong Cheng Xue Bao* 23:751–755.
36. Chambers I, et al. (2003) Functional expression cloning of Nanog, a pluripotency sustaining factor in embryonic stem cells. *Cell* 113:643–655.
37. de Lange T (2005) Shelterin: The protein complex that shapes and safeguards human telomeres. *Genes Dev* 19:2100–2110.
38. Blasco MA (2007) Telomere length, stem cells and aging. *Nat Chem Biol* 3:640–649.
39. Blasco MA (2005) Telomeres and human disease: Ageing, cancer and beyond. *Nat Rev Genet* 6:611–622.
40. Tejera AM, et al. (2010) TPP1 is required for TERT recruitment, telomere elongation during nuclear reprogramming, and normal skin development in mice. *Dev Cell* 18: 775–789.
41. Karlseder J, et al. (2003) Targeted deletion reveals an essential function for the telomere length regulator Trf1. *Mol Cell Biol* 23:6533–6541.
42. Martínez P, et al. (2009) Increased telomere fragility and fusions resulting from TRF1 deficiency lead to degenerative pathologies and increased cancer in mice. *Genes Dev* 23:2060–2075.
43. Ancelin K, et al. (2002) Targeting assay to study the *cis* functions of human telomeric proteins: Evidence for inhibition of telomerase by TRF1 and for activation of telomere degradation by TRF2. *Mol Cell Biol* 22:3474–3487.
44. Smogorzewska A, et al. (2000) Control of human telomere length by TRF1 and TRF2. *Mol Cell Biol* 20:1659–1668.
45. van Steensel B, de Lange T (1997) Control of telomere length by the human telomeric protein TRF1. *Nature* 385:740–743.
46. Muñoz P, et al. (2009) TRF1 controls telomere length and mitotic fidelity in epithelial homeostasis. *Mol Cell Biol* 29:1608–1625.
47. Avilion AA, et al. (2003) Multipotent cell lineages in early mouse development depend on SOX2 function. *Genes Dev* 17(6):126–140.
48. Nichols J, et al. (1998) Formation of pluripotent stem cells in the mammalian embryo depends on the POU transcription factor Oct4. *Cell* 95:379–391.
49. Niwa H, Miyazaki J, Smith AG (2000) Quantitative expression of Oct-3/4 defines differentiation, dedifferentiation or self-renewal of ES cells. *Nat Genet* 24:372–376.
50. Muñoz P, Blanco R, Flores JM, Blasco MA (2005) XPF nuclease-dependent telomere loss and increased DNA damage in mice overexpressing TRF2 result in premature aging and cancer. *Nat Genet* 37:1063–1071.
51. Samper E, Flores JM, Blasco MA (2001) Restoration of telomerase activity rescues chromosomal instability and premature aging in Terc-/- mice with short telomeres. *EMBO Rep* 2:800–807.
52. Zijlmans JM, et al. (1997) Telomeres in the mouse have large inter-chromosomal variations in the number of T2AG3 repeats. *Proc Natl Acad Sci USA* 94:7423–7428.

Acta Neuropathol
DOI 10.1007/s00401-012-0957-9

ORIGINAL PAPER

Identification of novel pathways involved in the pathogenesis of human adamantinomatous craniopharyngioma

Cynthia L. Andoniadou · Carles Gaston-Massuet · Rukmini Reddy · Ralph P. Schneider · Maria A. Blasco · Paul Le Tissier · Thomas S. Jacques · Larysa H. Pevny · Mehul T. Dattani · Juan Pedro Martinez-Barbera

Received: 6 January 2012 / Revised: 2 February 2012 / Accepted: 4 February 2012

Abstract Activating mutations in the gene encoding β-catenin have been identified in the paediatric form of human craniopharyngioma (adamantinomatous craniopharyngioma, ACP), a histologically benign but aggressive pituitary tumour accounting for up to 10% of paediatric intracranial tumours. Recently, we generated an ACP mouse model and revealed that, as in human ACP, nucleocytoplasmic accumulation of β-catenin (β-cat^{nc}) and overactivation of the Wnt/β-catenin pathway occurs only in a very small proportion of cells, which form clusters. Here, combining mouse genetics, fluorescence labelling and flow-sorting techniques, we have isolated these cells from tumorigenic mouse pituitaries and shown that the β-cat^{nc} cells are enriched for colony-forming cells when cultured in stem cell-promoting media, and have longer telomeres, indicating shared properties with normal pituitary progenitors/stem cells (PSCs). Global gene profiling analysis has revealed that these β-cat^{nc} cells express high levels of secreted mitogenic signals, such as members of the SHH, BMP and FGF family, in addition to several chemokines and their receptors, suggesting an important autocrine/paracrine role of these cells in the pathogenesis of ACP and a reciprocal communication with their environment. Finally, we highlight the clinical relevance of these findings by showing that these pathways are also up-regulated in the β-cat^{nc} cell clusters identified in human ACP. As well as providing further support to the concept that pituitary stem cells may play an important role in the oncogenesis of human ACP, our data reveal novel disease biomarkers and potential pharmacological targets for the treatment of these devastating childhood tumours.

Keywords Adamantinomatous · Craniopharyngioma · β-Catenin · Mouse · Pituitary tumour · Stem cells

Electronic supplementary material The online version of this article (doi:10.1007/s00401-012-0957-9) contains supplementary material, which is available to authorized users.

C. L. Andoniadou · C. Gaston-Massuet · R. Reddy · P. Le Tissier · T. S. Jacques · J. P. Martinez-Barbera (✉)
Neural Development Unit, UCL Institute of Child Health, 30 Guilford Street, London WC1N 1EH, UK
e-mail: j.martinez-barbera@ucl.acuk

R. P. Schneider · M. A. Blasco
Telomeres and Telomerase Group, Molecular Oncology Program, Spanish National Cancer Research Centre, 28029 Madrid, Spain

T. S. Jacques
Department of Histopathology, Great Ormond Street Hospital for Children, London WC1N 3JH, UK

L. H. Pevny
Department of Cell and Developmental Biology, Neuroscience Center, University of North Carolina, Chapel Hill, NC, USA

M. T. Dattani
Developmental Endocrinology Research Group, UCL Institute of Child Health, London WC1N 1EH, UK

Introduction

Adamantinomatous craniopharyngioma (ACP) is the most common non-neuro-epithelial brain tumour in children [31, 43, 47]. Although not metastatic and histologically benign, ACP is invasive and prone to recurrence after surgery, the conventional mode of treatment. Adamantinomatous craniopharyngioma often behaves aggressively with invasion of the hypothalamus and visual pathways. Therefore, total resection of the tumour without damage to vital surrounding structures such as the hypothalamus and

Published online: 18 February 2012

optic chiasm is not always possible. In these children, radical excision is associated with unacceptable morbidity and mortality whilst subtotal resection without adjuvant radiotherapy predisposes to a high (>60%) 3-year recurrence risk and further hypothalamic and visual compromise [34, 38, 44]. Although a conservative surgical approach with adjuvant radiotherapy for residual tumour has been recently adopted, both tumour recurrence and treatment-associated morbidity are still high. Consequences of the tumour and its treatment include obesity with associated Type 2 diabetes mellitus, learning difficulties, visual impairment and panhypopituitarism, which can be life-threatening. This poses a heavy burden to parents and carers as well as a heavy cost for health services.

A crucial role for Wnt/β-catenin signalling in the aetiology of ACP has been firmly established. Activating mutations in the gene encoding β-catenin (*CTNNB1*) have been identified in the majority of samples of human ACP [9, 51]. Recently, phenotypic analysis of a mouse model ($Hesx1^{Cre/+}$;$Ctnnb1^{lox(ex3)/+}$) expressing a mutant form of β-catenin that cannot be degraded, leading to over-activation of the pathway, has confirmed that these mutations, rather than a second hit, are causative of the tumours [18]. A characteristic histological finding in both human and mouse ACP is the restricted nucleocytoplasmic accumulation of β-catenin and over-activation of the Wnt/β-catenin pathway in very few cells that form clusters (β-cat^{nc} clusters). Despite harbouring the tumorigenic mutation in the β-catenin gene, all other cells only show the normal β-catenin staining in the cytoplasmic membrane without any nucleocytoplasmic accumulation (non-cluster β-cat^{m} cellular component of ACP) [18, 25, 26, 32]. Beyond the relevant diagnostic value of this unique histological feature to distinguish ACP from other pituitary tumours, little is known about the reason for this specificity or the relevance of the cluster cells in the disease. Recent evidence points towards a role in tumour progression and invasiveness into the brain [8, 27–29]. A deeper analysis of these cellular structures may provide novel insights into the pathogenesis of ACP resulting in the identification of new disease biomarkers and pharmacological targets.

An open question is the contribution of pituitary progenitors/stem cells (PSCs) in the aetiology and pathogenesis of ACP. Previously, we have demonstrated that one of the initial effects of mutated β-catenin is the increase of PSCs in the ACP murine model compared with control pituitaries. At late gestation and early postnatal stages, a proportion of β-catenin-accumulating cells within the clusters express the stemness marker SOX2 in the murine pre-tumoral pituitary [14, 18]. However, SOX2 is not expressed in the β-catenin accumulating clusters in human ACP, but rather in sporadic cells within the tumour [17]. This raises the question of what the connection is between the human and mouse β-catenin-accumulating clusters.

In this study, we have used the ACP mouse model to investigate the pathogenesis and the possible involvement of PSCs in the aetiology of human ACP. We demonstrate that β-catenin-accumulating cluster cells have functional and molecular characteristics of pituitary progenitors/stem cells. We present their global gene expression profile and reveal novel genes and signalling pathways expressed in both mouse and human ACP. This molecular analysis highlights interplay between clusters and surrounding cells through the secretion of signals involved in proliferation, survival, stem cell maintenance, cell migration and tumorigenesis.

Materials and methods

Mice

The $Ctnnb1^{lox(ex3)/+}$, *Hesx1-Cre* and *BAT-gal* mice have been previously described [2, 24, 41].

X-gal staining, in situ hybridisation and immunostaining

Wholemount X-gal staining, immunostaining and in situ hybridisation on 8 μm paraffin sections were performed as previously described [2, 18]. Samples of human ACP were obtained from the Department of Histopathology at Great Ormond Street Hospital for Children. At least three pituitaries or tumours and between two and six slides were analysed. As negative controls, sections were hybridized with sense riboprobes for in situ hybridisation or secondary antibody alone for immunohistochemistry/immunofluorescence.

Immuno-FISH

Paraffin tissue slides were deparaffinised and underwent citrate antigen retrieval, before a fluorescent is situ hybridisation was performed as previously described [49], After washing, the slides were incubated overnight with an anti β-catenin antibody (Sigma, dilution 1:100). The primary antibody was detected with an Alexa 488-conjugated secondary antibody before DNA counterstaining with DAPI in a 4 μg/ml solution in PBS. The slides were mounted using Vectashield (Vector Laboratories).

The β-catenin/telomere immuno-FISH 8-bit pictures were acquired with a Leica TCS-SP5 (AOBS) high-resolution confocal microscope. A 63×-Leica immersion objective was used with an additional magnification of 2.5×. Stacks of seven pictures were taken with a step size of 0.8 μm. Those were further maximum projected by the

LAS AF software (Leica) for analysis. Fluorescence analysis of intensities was performed with Definiens Developer XD1.8 software (Definiens). The β-cat^{nc} cluster and the β-cat^{m} surrounding cells used for the telomere analysis were selected by hand according to the β-catenin immunofluorescence staining.

Flow sorting

The β-catenin-accumulating cellular fraction (β-cat^{nc} cluster cells) was purified from surrounding (β-cat^{m}) cells of *Hesx1*$^{Cre/+}$;*Ctnnb1*$^{lox(ex3)/+}$;*BAT-gal* pituitaries by flow sorting taking advantage of their activation of the *BAT-gal* reporter. The *BAT-gal* transgene expresses *lacZ* (encoding β-galactosidase) under the regulation of TCF/LEF binding sites in cells with activated Wnt/β-catenin signalling [41]. For the assessment of the colony-forming potential of β-cat^{nc} cluster cells, three independent flow-sorting experiments were performed using a total of 17 *Hesx1*$^{Cre/+}$;*Ctnnb1*$^{lox(ex3)/+}$;*BAT-gal* pituitaries at 18.5 dpc. In brief, cells were dissociated by incubation for 4 h at 37°C in an enzyme mix containing collagenase type II (Sigma), trypsin (Gibco) and DNase I (Worthington) in HBSS (Gibco). After washing in HBSS, the cells were manually dissociated and then treated using the CMFDG kit (Invitrogen) according to manufacturer's recommendations, to yield a fluorescent product when the CMFDG substrate is cleaved by β-galactosidase. The cells were flow-sorted immediately in PBS containing 1% fetal calf serum and 25 mM HEPES using a MoFlo XDP (Beckman Coulter, Fullerton, California, USA). GFP fluorescence was detected using a 530/40 filter, and dead and auto-fluorescent cells were excluded using propidium iodide (Invitrogen) using a 613/20 filter. The analysis for cell sorting was carried out on Summit software (Dako). Flow sorting of cells from *Sox2*$^{eGFP/+}$ pituitaries was carried out as above, without CMFDG treatment or addition of propidium iodide. The data presented were obtained from three independent experiments using a total of 19 *Sox2*$^{eGFP/+}$ mice of 6–8 weeks of age. For subsequent culture, the cells were collected in culture medium and for RNA isolation, in RLT lysis buffer (Qiagen), flash frozen and stored at −80°C until processed.

Cell culture

Single cells were cultured as adherent colonies using methods described by Gleiberman et al. [20] and plated at a clonal density of 20 cells per well of a 96-well plate (roughly 60 cells per cm^2), or graded densities (1,000–4,000 cells per well) in six-well plates. The colonies were fixed after 1 week and stained with haematoxylin as previously described [18].

RNA extraction, microarray methods and quantitative real-time PCR

Total RNA isolation from pituitaries and flow-sorted cells was performed as described using the RNeasy Micro Kit (Qiagen) [3]. Approximately 3,000 β-cat^{nc} cluster cells were obtained from seven independent flow-sorting experiments of dissociated and CMFDG treated *Hesx1*$^{Cre/+}$;*Ctnnb1*$^{lox(ex3)/+}$;*BAT-gal* pituitaries ($n = 15$ mice). Linear amplification of purified RNA was carried out using the Ovation Pico WTA System (NuGEN), following manufacturer's recommendations, yielding approximately 5.5 μg of polyadenylated RNA. From this, 3.0 μg were used for microarray analysis, using standard Affymetrix labelling and hybridization protocols for hybridization on GeneChip Mouse 430_2 arrays. The remaining 2.5 μg were reverse transcribed to cRNA with Omniscript RT (Qiagen) and random hexamers (Promega) and used for qRT-PCR. RNA from *Sox2*$^{eGFP/+}$ flow-sorted pituitaries was isolated and processed as described and used only for qRT-PCR analyses. Reactions were run in triplicate on an ABI 7500 Fast cycler using MESA Blue reagent (Eurogentec) and repeated for a minimum of four independent samples for each cell type. Primer sequences are available on request. Results were analysed using the ΔΔCt method.

Results

β-Catenin-accumulating cells from tumorigenic murine pituitaries share properties with normal pituitary progenitors/stem cells

We have previously shown that tumorigenic pituitaries from *Hesx1*$^{Cre/+}$;*Ctnnb1*$^{lox(ex3)/+}$ mice contain higher numbers of cells with clonogenic potential, this being the ability to form colonies comprised of undifferentiated progenitors when cultured in stem-cell-promoting media [18]. However, it is not known whether these clonogenic cells correspond to the population accumulating β-catenin in the nucleus and cytoplasm (β-cat^{nc} clusters) or those showing only the normal membranous or sub-membranous β-catenin localization (β-cat^{m}) without any nucleocytoplasmic accumulation. This is clinically relevant since these two cell populations exist in human ACP and indeed, the presence of β-cat^{nc} clusters is used as a diagnostic histopathological feature that differentiates human ACP from other brain tumours of the sellar and suprasellar areas of the brain [26]. To provide insights into the cellular

nature of β-cat^{nc} clusters, we carried out detailed molecular and cell culture analyses in the mouse model.

As activation of the Wnt/β-catenin pathway, as assessed by the expression of Wnt/β-catenin target genes, is restricted to the β-cat^{nc} clusters in both mouse and human ACP [29, 52], we used a genetic tool in mouse to enable their purification. Specifically, we employed the *BAT-gal* mouse strain, a reporter line of active Wnt/β-catenin signalling, which expresses *lacZ*, encoding β-galactosidase, under the control of TCF/LEF binding sites [41]. In *Hesx1*$^{Cre/+}$;*Ctnnb1*$^{lox(ex3)/+}$;*BAT-gal* triple heterozygous pituitaries, β-galactosidase activity is present in clusters of cells (Fig. 1a), which corresponds to the cells that accumulate nucleocytoplasmic β-catenin and, a proportion of which, also express SOX2 (Fig. 1b) [18]. This enzymatic activity was used to generate a luminous product after treatment and fluorescent cells from dissociated pituitaries were sorted by flow cytometry resulting in the purification of two cell fractions: (1) BAT-gal^{+ve} that correspond to β-cat^{nc} cluster cells and (2) BAT-gal^{-ve} containing all the remaining cells from the intermediate and anterior pituitary lobes (β-cat^{m} cells) (Fig. 1c). The efficiency of the purification was demonstrated by the higher expression of Wnt/β-catenin targets (*Axin2*, *Lef1* and *CyclinD1*) as well as *lacZ* from the *BAT-gal* reporter specifically in the β-cat^{nc} fraction relative to surrounding β-cat^{m} cells (Fig. 1d) [18]. In addition, expression of genes associated with embryonic and adult pituitary progenitors/stem cells, such as *Sox2* and *Nestin*, were also elevated in the β-cat^{nc} fraction [14, 20]. In contrast, expression of specific pituitary cell lineage commitment and terminal differentiation markers (*Pit1*, *Pomc* and *Gh*) was significantly lower in the β-cat^{nc} fraction. These data confirm our previous findings suggesting that the β-catenin-accumulating cells may correspond to undifferentiated pituitary progenitors/stem cells (PSC).

Next, we sought to explore this possibility more definitively using an in vitro approach. When cultured in stem-cell-promoting media, normal PSC form adherent colonies arising from single cells, and fitting an undifferentiated profile [20]. To explore if β-cat^{nc} clusters contain colony-forming progenitor/stem cells, flow-sorted β-cat^{nc} (BAT-gal^{+ve} fraction) and β-cat^{m} cells (BAT-gal^{-ve} fraction) were cultured for 1 week and assessed for colony formation. It was clear that total numbers of colony-forming cells were significantly increased in the fraction containing the β-cat^{nc} clusters (8.48-fold increase; Fig. 1e, f). However, only around 5% of the β-catenin-accumulating cells were capable of expanding to give rise to a colony under these conditions, suggesting that stemness is likely associated with a different factor, such as *Sox2* expression, rather than nucleocytoplasmic β-catenin accumulation.

To test this idea, we used a *Sox2-eGFP* mouse model, in which *Sox2*-expressing cells are marked by eGFP expression [12]. Flow-sorting purification of eGFP-expressing cells followed by culture in stem-cell-promoting media showed that only cells within the *Sox2*-expressing fraction were capable of generating colonies (Fig. 2a–d). Cells not expressing eGFP did not form colonies, strongly suggesting that PSCs are contained within the *Sox2*-expressing population (Fig. 2e).

We have previously shown that in vivo β-cat^{nc} clusters in mouse and human ACP contain slow-dividing/quiescent cells, a feature often associated with stem cells [18]. Another feature linked to stemness is increased telomere length, as this gradually decreases with each cell cycle due to incomplete replication of telomeric DNA, but remains long in slow-dividing stem cells [15, 16]. Quantification of telomere length on histological sections of *Hesx1*$^{Cre/+}$;*Ctnnb1*$^{lox(ex3)/+}$ pituitaries at 18.5 dpc, showed that β-cat^{nc} cluster cells have significantly longer telomeres than the surrounding β-cat^{m} cells (Fig. 3a, c). However, a similar analysis on human ACP samples revealed longer telomeres in surrounding β-cat^{m} cells rather than β-cat^{nc} clusters (Fig. 3b, d). Together these data suggest that: (1) β-catenin-accumulating clusters in the murine ACP model exhibit a molecular profile and cellular behaviour characteristic of undifferentiated pituitary progenitors/stem cells; (2) β-catenin-accumulating clusters in human ACP, although slow-dividing and undifferentiated (i.e. lacking expression of terminal differentiation pituitary markers), do not express SOX2 or have longer telomeres and (3) mouse and human β-catenin-accumulating clusters may correspond to cells that are ontogenetically related but temporally distant; mouse cluster cells at 18.5 dpc relate to an early stage of tumour formation (pre-tumoral stage) whilst human cluster cells are present in clinically relevant and advanced tumours.

Global gene expression analysis of β-cat^{nc} cluster cells from murine tumorigenic pituitaries reveals novel pathways involved in ACP

Having purified the β-cat^{nc} cluster cells from tumorigenic mouse pituitaries, we decided to carry out a global gene profiling study to reveal new genes/signalling pathways involved in human ACP.

Microarray analysis of flow-purified β-cat^{nc} cells in comparison with β-cat^{m} cells confirmed previously characterised gene expression changes [18]. As mentioned above, activation of the Wnt/β-catenin pathway targets *Axin2* and *Lef1* is restricted to cells within the β-cat^{nc} clusters in the *Hesx1*$^{Cre/+}$;*Ctnnb1*$^{lox(ex3)/+)}$ mouse model as well as in human ACP, assessed by in situ hybridisation. In the array data, levels were 16.77-fold higher for *Axin2*, 9.51-fold higher for *Lef1*, and *Sp5*, another universal Wnt/β-catenin target [56, 61] was found to be 12.69-fold higher

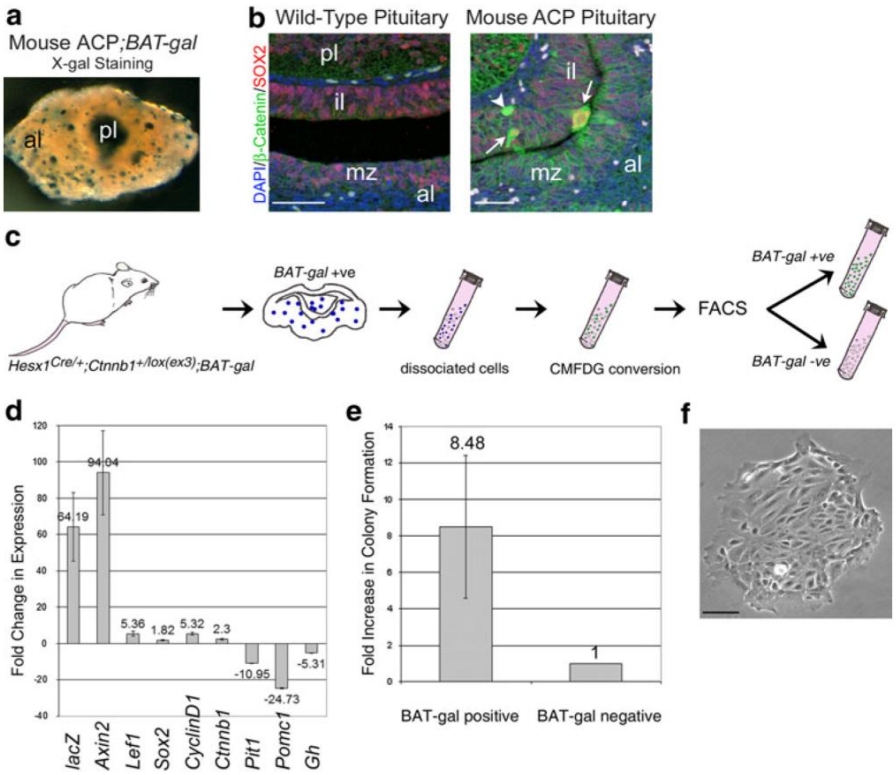

Fig. 1 Purification of β-catenin-accumulating cells from *Hesx1*$^{Cre/+}$;*Ctnnb1*$^{lox(ex3)/+}$;*BAT-gal* pituitaries. **a** X-gal staining of a *Hesx1*$^{Cre/+}$;*Ctnnb1*$^{lox(ex3)/+}$;*BAT-gal* mutant pituitary showing the activation of the *BAT-gal* reporter and expression of β-galactosidase in clusters within the anterior lobe. The posterior lobe is highly stained and was surgically removed prior to the purification procedure. **b** Double immunofluorescence staining against β-catenin (*green*) and SOX2 (*red*) in wild-type and *Hesx1*$^{Cre/+}$;*Ctnnb1*$^{lox(ex3)/+}$ (mouse ACP) pituitaries. Note the nucleocytoplasmic accumulation of β-catenin in very few cells that form clusters in the *Hesx1*$^{Cre/+}$;*Ctnnb1*$^{lox(ex3)/+}$ pituitary (*arrows*), whilst the majority of the cells show normal cytoplasmic staining as in the control pituitary. SOX2 is expressed in cells of the marginal zone around the lumen in the control but in *Hesx1*$^{Cre/+}$;*Ctnnb1*$^{lox(ex3)/+}$ pituitaries, some cells within the clusters also express SOX2 (*arrows*). Note a cluster that is negative for SOX2 expression (*arrowhead*). **c** Scheme of the strategy to purify the β-catenin-accumulating cell clusters. Triple heterozygous pituitaries (only anterior and intermediate lobes) are dissociated into single cell suspension, treated with CMFDG (a fluorogenic substrate for β-galactosidase) and subjected to flow-sorting. The two fractions are used for qRT-PCR analysis, gene profiling and stem cell culture. **d** qRT-PCR comparing BAT-gal^{+ve} (clusters) versus BAT-gal^{-ve} (non-clusters) cell fractions confirming the efficiency of the purification. Fold-changes in expression indicated on the *y*-axis, where >0 means higher expression in BAT-gal^{+ve} and <0 higher in BAT-gal^{-ve}. Cluster cells fit an undifferentiated profile (high *Sox2* and low *Pit1*, *Pomc1* and *Gh*) and show activation of the Wnt/β-catenin pathway (high *lacZ*, *Axin2*, *Lef1* and *CyclinD1*). **e**, **f** The BAT-gal^{+ve} fraction contains 8.48 times more cells with clonogenic potential (progenitors/stem cells, PSCs) (**e**) able to form single cell-derived colonies when cultured in stem cell-promoting media (**f**). *pl* posterior lobe, *il* intermediate lobe, *al* anterior lobe, *mz* marginal zone. *Scale bars* **b** 50 μm, **f** 100 μm

in β-cat^{nc} clusters relative to the β-cat^{m} fraction (Supplementary Table 1). Likewise, expression of SOX2 is up-regulated in a proportion of β-cat^{nc} cells within the clusters, and in the array, *Sox2* levels were 1.62-fold higher in the cluster fraction. Conversely, the expression of terminal differentiation markers, such as *Pomc* (pro-opiomelanocortin-alpha) and *Gh* (growth hormone), both undetectable within β-cat^{nc} clusters by immunohistochemistry and with higher expression in surrounding β-cat^{m} cells by qRT-PCR, was specifically lower in the β-cat^{nc} cluster fraction by microarray comparison (9.01-fold lower for *Pomc* and 3.4-fold lower for *Gh*) (Supplementary Table 2). Changes in gene expression were further validated by quantitative real-time PCR (Supplementary Figure 1), demonstrating the efficiency of the cell purification and the robustness of the microarray data.

We interrogated the array data aiming to identify differentially expressed genes in the β-cat^{nc} cluster cells. This analysis revealed increased expression of signalling molecules involved in multiple cellular processes and physiological functions including normal development or stem cell maintenance and pathogenic conditions in

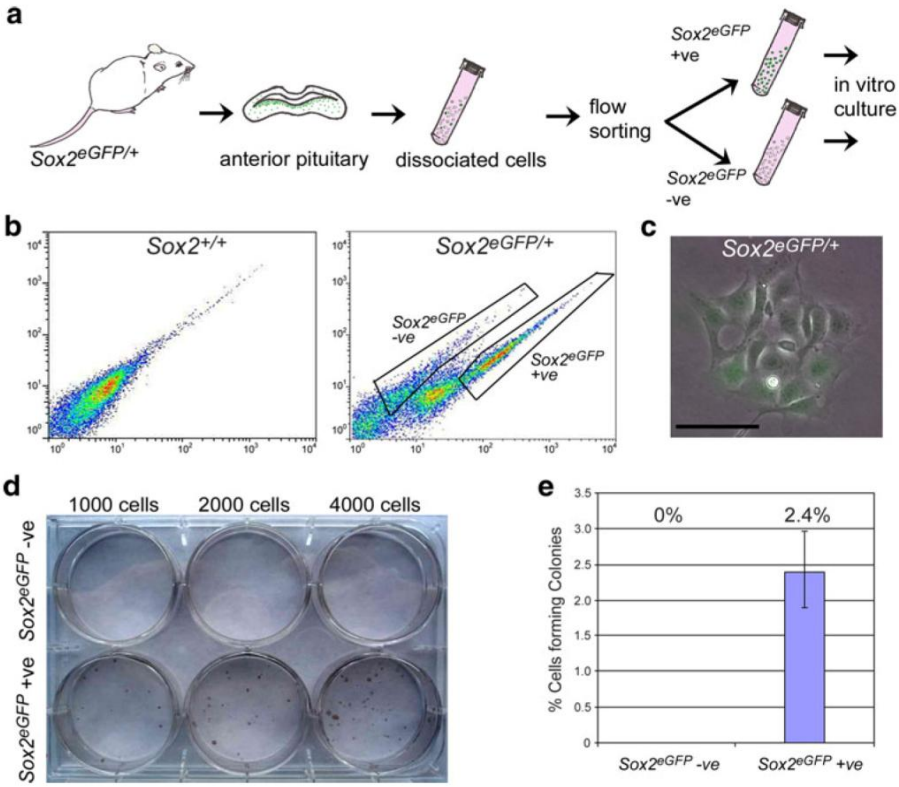

Fig. 2 Pituitary progenitors/stem cells (PSCs) are contained in the SOX2-expressing population. **a** Scheme of cell purification strategy: *Sox2*$^{eGFP/+}$ postnatal pituitaries (P14) are dissociated into single cell suspensions and flow sorted to separate the eGFP^{+ve} and eGFP^{-ve} fractions. **b** Scatter plots showing the isolation of the two fractions. The gates used are indicated on the plot. **c** Clonal culture of cell preparations from unpurified *Sox2*$^{eGFP/+}$ pituitaries in stem cell-promoting media gives rise to eGFP^{+ve} colonies demonstrating the activation of the SOX2 promoter in PSCs. **d** Photograph of a tissue culture plate containing fixed and hematoxylin-stained colonies demonstrate the presence of colonies only in the flow sorted purified eGFP^{+ve} fraction. **e** Approximately 2.4% of the eGFP (*Sox2*)-expressing cells are able to form colonies. *Scale bar* 50 μm

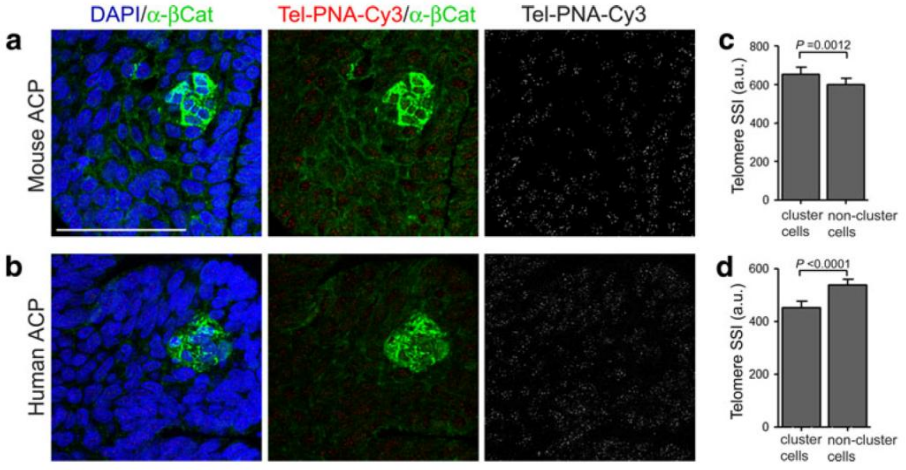

Fig. 3 Analysis of telomere length in β-catenin accumulating clusters and surrounding cells in mouse and human ACP. (**a**, **b**) Telomere PNA FISH (Cy3 conjugate) and β-catenin immunofluorescence on mouse pre-tumoral lesions at 18.5 dpc (**a**) and human ACP samples (**b**) allows visualisation of telomeres specifically in β-catenin accumulating cluster cells or non-cluster surrounding cells. **c**, **d** Quantification of telomere length as sum spot intensity reveals significantly longer telomeres in β-catenin accumulating cluster cells in the mouse (**c**) whereas these are significantly shorter in the advanced human ACP sample (**d**). The pictures shown (**a**, **b**) are representative examples corresponding to single optical confocal sections of 0.001 μm thickness. Indicated statistics prepared using a Students *t*-test, $n = 50$ clusters for mouse, $n = 25$ clusters for human. *Scale bar* 50 μm

humans such as tumorigenesis and cancer. These datasets have been deposited in ArrayExpress (Accession E-MEXP-3492) and are accessible to the scientific community. Here, we focus on a handful of genes and signalling pathways important for normal pituitary development or stem cell function, revealing an involvement of these in ACP.

The Hedgehog (HH) pathway participates in multiple developmental events and has been implicated in the maintenance of adult stem cell niches [7, 23, 39]. In addition, over-activation of the pathway has been identified in several human cancers as an important factor leading to tumour growth and metastasis [33, 40, 54]. When this pathway is down-regulated in the embryonic pituitary gland, progenitors of the Rathke's pouch, the anterior pituitary primordium, fail to proliferate, resulting in a hypoplastic anterior pituitary but normal terminal differentiation of hormone-producing cells [59, 60]. *Shh* (sonic hedgehog) expression was found to be expressed 10.07-fold higher in β-cat^{nc} cluster cells (Supplementary Table 3).

The fibroblast growth factor (FGF) family and transforming growth factor (TGF) superfamily of secreted signalling molecules, including bone morphogenetic proteins (BMPs), are key regulators of several biological processes and together with their receptors, they affect the development of many human cancers [11, 21, 22, 62, 63]. In the pituitary gland, secreted FGFs and BMPs are required for normal specification and cell proliferation of pituitary progenitors during early pituitary development [10, 13, 36]. By microarray, members of the FGF family, such as *Fgf3*, *Fgf4* and *Fgf20* among others were expressed at higher levels in the β-cat^{nc} clusters relative to the surrounding β-cat^{m} cells (6.99-, 20.73- and 15.77-fold higher, respectively) (Supplementary Table 4). Likewise, expression of *Bmp2*, *Bmp4* and *Bmp7*, was also enhanced (3.72, 9.47, and 5.67-fold in the β-cat^{nc} clusters, respectively) (Suppl. Table 5). Other members of the TGFβ family were also expressed at much higher levels in these cluster cells: *Tgfa*, 5.25; *Tgfb1*, 5.75; *Tgfb2*, 3.54. Genes encoding subunits of activin dimers were also found to be up-regulated in β-cat^{nc} cells: *Inhba*, 7.27; *Inhbb*, 9.74 (Supplementary Table 6). Collectively, these molecular data strongly suggest that the β-cat^{nc} cells within the clusters play a non-cell autonomous role (i.e. autocrine and paracrine signalling), which may be relevant in the pathogenesis of ACP.

In addition, the pattern of expression of several chemokines not only confirmed a non-cell autonomous function, but also revealed a reciprocal signalling interaction between the β-cat^{nc} clusters and surrounding β-cat^{m} cells. Several members of the CXC and CC families of chemokines and their receptors were highly expressed in β-cat^{nc} cluster relative to the β-cat^{m} cells (Supplementary Table 7). Of relevance to this study, CXCR4, a seven-transmembrane span G-protein-coupled receptor expressed in multiple normal and cancer stem cells was expressed 2.63-fold higher in the cluster cells [42, 46]. Conversely, CXCL12 (also known as stromal-derived factor 1, SDF-1), which primarily binds to CXCR4 was expressed 4.92-fold higher in β-cat^{m} cells surrounding the β-cat^{nc} clusters. Likewise, some of the CC chemokine and CSF (colony-stimulating factor) receptors showed higher expression in the β-cat^{nc} cluster cells. In summary, the gene profiling analysis of β-cat^{nc} has revealed a specific molecular signature characterised by a great increase in the expression of multiple signalling molecules and, in addition, illustrates a complex reciprocal interaction between β-catenin-accumulating cluster cells and their surrounding cells in ACP tumorigenesis.

Immunohistochemistry and in situ hybridisation studies demonstrate conserved novel pathways between mouse and human ACP

Several of the genes identified through array gene profiling of mouse ACP have not been previously implicated in the pathogenesis of human ACP. Therefore, we sought to validate the mouse array data described here with expression analysis for selected relevant genes on histological sections from both mouse and human ACP.

Hedgehog-secreted signals (e.g. SHH) bind to the receptor Patched 1 (*Ptch1*), leading to the de-repression of the transducer Smoothened (*Smo*). Activated SMO initiates the intracellular signalling cascade and the nuclear translocation of GLI, ultimately causing the transcriptional activation of target genes, including *Gli1* and *Ptch1* [30]. In *Hesx1*$^{Cre/+}$;*Ctnnb1*$^{lox(ex3)/+}$ tumorigenic pituitaries, the *Shh* expression pattern was very similar to that observed for β-catenin, i.e. in distinct foci within the anterior and intermediate lobes, suggesting the likely co-expression of these genes in the β-cat^{nc} cell clusters (Fig. 4c). Immunohistochemistry with SHH antibodies revealed specific staining in the cytoplasmic membrane of the vast majority of pituitary cells, as expected for a secreted molecule of lipophilic nature. Within the clusters, SHH protein was detected only on the basal surface of the cells, i.e. the surface limiting the clusters and surrounding cells, indicating polarized secretion outside the clusters (Fig. 4a). To identify the responding cells where the HH pathway was activated, we analysed expression of *Ptch1*, the SHH receptor and a target of the pathway. In *Hesx1*$^{Cre/+}$;*Ctnnb1*$^{lox(ex3)/+}$ pituitaries, strong signal was broadly detected throughout the anterior lobe with some regions of stronger expression (Fig. 4e). Together, these data indicate autocrine as well as paracrine SHH signalling activation in the β-cat^{nc} cluster and β-cat^{m} cells, respectively.

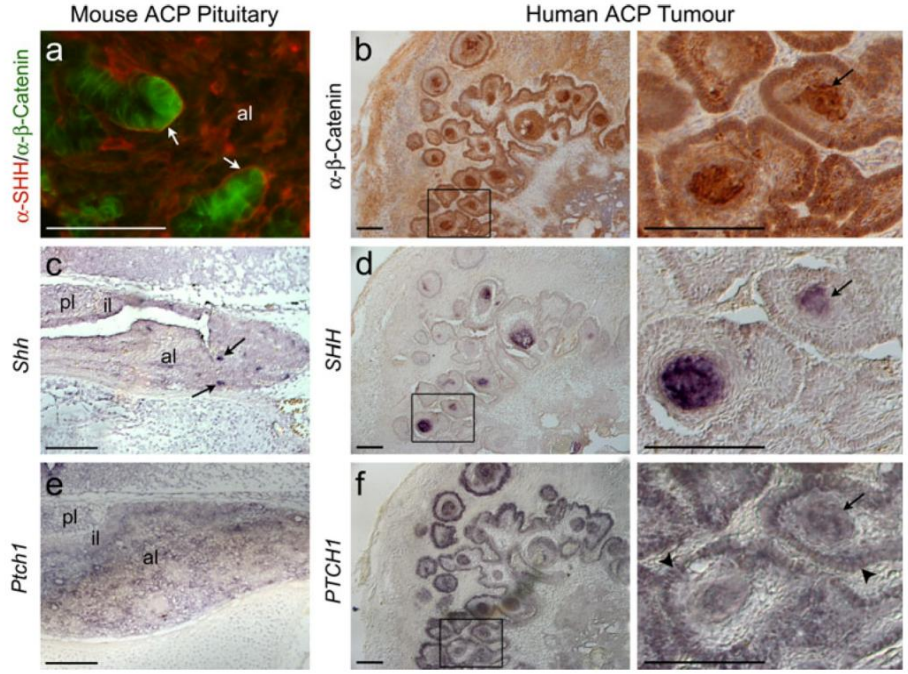

Fig. 4 SHH signalling is active in mouse and human ACP. **a** Double immunofluorescence using antibodies against β-catenin (*green*) and SHH (*red*) showing the localisation of SHH in cells within the clusters of pituitaries from the ACP murine model at 18.5 dpc. Note the SHH protein on the cell membrane facing the stromal cells (*arrows*). **b** Immunohistochemistry reveals the presence of several β-catenin-accumulating cell clusters on a human ACP sample (*arrows*). **c**, **d** In situ hybridisation on the ACP mouse model (**c**) and human ACP (**d**) with *Shh* antisense riboprobes showing the up-regulation of *Shh/SHH* in some of the β-catenin-accumulating cell clusters (*arrows*). **e**, **f** In situ hybridisation on the ACP mouse model (**e**) and human ACP (**f**) with *Ptch1* antisense riboprobes. *Ptch1*, a target of SHH signalling, is expressed throughout the pituitary of the mouse model and in both the palisading cells (*arrowheads*) and the β-catenin-accumulating cell clusters (*arrows*) in the human ACP sample. *Scale bars* **a**, **b**, **d**, **f**, 50 μm; **c**, **e** 150 μm

Next, we investigated whether the expression pattern of relevant HH signalling pathway components may be conserved in human ACP. A tentative role for this pathway in human ACP was proposed in a familial case of Gorlin syndrome showing the typical phenotype (basal cell carcinoma and craniofacial and bone malformations) in association with ACP and harbouring a mutation in *PTCH1*, but neither *SHH* nor *PTCH1* expression could be identified in this study [45]. In situ hybridisation on human ACP sections ($n = 5$) showed a pattern of *SHH* expression characterised by the presence of cell clusters analogous to the typical β-cat^{nc} cell clusters observed in these human tumours (Fig. 4d). Analysis on consecutive sections with SHH riboprobes and α-β-Catenin antibody revealed the co-expression of these two genes, as observed in the mouse model (Fig. 4b, d). Finally, expression of *PTCH1* was identified in cluster cells as well as in the palisading cells surrounding these typical lesions (Fig. 4f). These findings not only further validate our mouse model for the study of human ACP, but also demonstrate that the HH pathway is also active in human ACP in both the β-catenin-accumulating cell clusters, which secrete the SHH ligand, as well as in some surrounding β-cat^{m} cells.

Data from the array study showed elevated expression of *Bmp2*, *Bmp4* and *Bmp7* in the β-cat^{nc} clusters compared with non-cluster β-cat^{m} cells. This was confirmed by in situ hybridization analysis on *Hesx1*$^{Cre/+}$;*Ctnnb1*$^{lox(ex3)/+}$ tumorigenic pituitaries, which revealed a pattern of expression of these genes in restricted focal points reminiscent of the β-catenin accumulating clusters (Fig. 5a, c, e). In human ACP, *BMP4* has previously been shown to have increased expression within the β-cat^{nc} clusters [29]. We confirmed this finding and revealed a comparable expression pattern for *BMP2* and *BMP7* in human ACP samples (Fig. 5b, d, f). Expression of *Fgf3* and *Fgf4* was observed in the mouse β-cat^{nc} clusters, and we were able to confirm *FGF3* expression also in the human clusters (Fig. 5g–j).

Finally, we analysed the expression pattern of *Cxcr4* because of its known expression in numerous normal as well as cancer stem cell populations and its proposed role in cell migration and metastatic infiltration [6, 42, 46]. An activated CXCL12/CXCR4 axis has also been associated

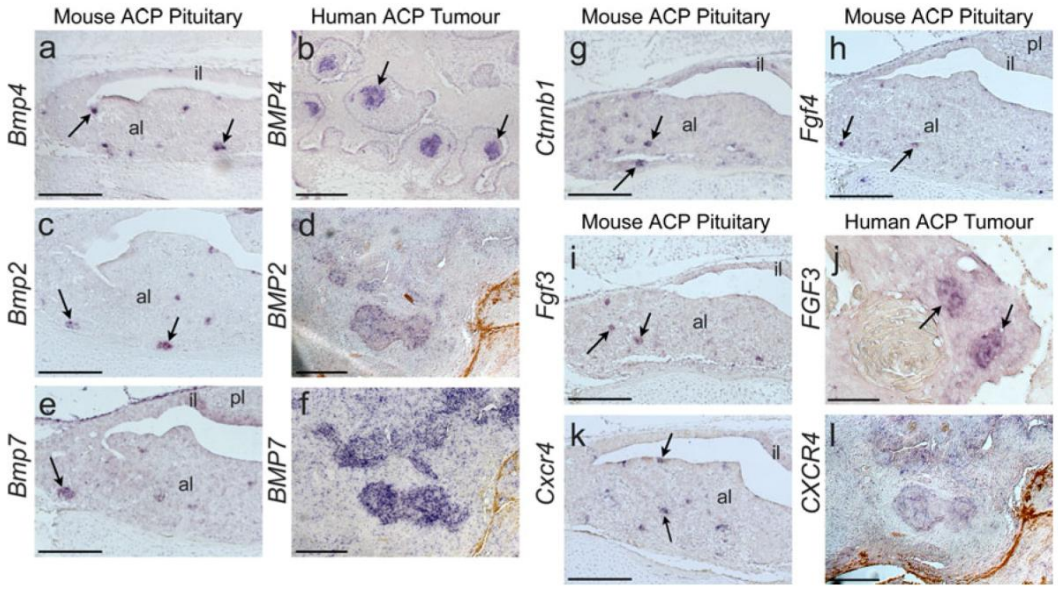

Fig. 5 Expression analysis by in situ hybridisation of mouse and human ACP. Mouse pituitaries at 18.5 dpc. **a–f** Expression of *Bmp/BMP* members 4, 2 and 7 is up-regulated in pre-tumoral mouse pituitaries at 18.5 dpc and human ACP (*arrows*). In the ACP mouse model pituitary, expression is mainly restricted to cell clusters. In human ACP, expression is up-regulated in cell clusters, but other tumour cells express *BMP2* and *BMP7*. **g**, **h** *Ctnnb1* and *Fgf4* expression in the ACP mouse model pre-tumoral pituitary is up-regulated in cluster cells (*arrows*). **i**, **j** *Fgf3/FGF3* expression is also up-regulated in cluster cells in both mouse and human ACP (*arrows*). **k**, **l** *Cxcr4* expression is detected in clusters in the ACP mouse model pituitary (*arrows*), but it is more widely expressed in human ACP. *Scale bars* **a**, **c**, **e**, **g**, **h**, **i**, **k**, 150 μm; **b**, **d**, **f**, **j**, **l** 50 μm

with proliferation of pituitary adenomas [4, 5]. In situ hybridization showed strong *Cxcr4* expression in restricted foci resembling the β-cat^{nc} cell clusters in mouse tumorigenic pituitaries (Fig. 5k). In human ACP samples, CXCR4 expression was not very abundant and broadly expressed throughout the tumour with weak up-regulation in some clusters (Fig. 5l). Overall, this expression analysis confirmed the array data and supports the concept that β-catenin-accumulating cells in mouse and human ACP function as signalling centres from where multiple secreted signals emanate to act on themselves and neighbouring cells.

Discussion

In this paper, we have utilised a recently generated mouse model for ACP and carried out an unbiased molecular screen demonstrating the de-regulation of numerous genes and signalling pathways with tumorigenic potential in both mouse and human ACP. We provide molecular and expression data indicating that β-cat^{nc} cluster cells act as a source of mitogenic and pro-survival signals for themselves and surrounding β-cat^{m} tumour cells. Our global gene profiling analysis has revealed that members of the SHH, FGF and BMP family of morphogens, which are critical during normal pituitary development [23, 30, 39], show higher expression levels in the β-cat^{nc} cluster cells in both mouse and human ACP. As well as providing novel insights into the pathogenesis of human ACP, this research has identified potential therapeutic targets for these tumours.

SHH is required during the normal development of several organs and in adulthood this pathway plays an important role in the maintenance of stem-cell niches [1, 30, 53]. Over-active HH signalling occurs in numerous human cancers and can be caused by either a mutation-driven (ligand-independent) mechanism or ligand-dependent signalling (i.e. autocrine/paracrine signalling). Inactivating mutations in PTCH1 or more rarely, activating mutations in SMO have been identified in most sporadic medulloblastomas [19, 48, 64]. Loss-of-function mutations in PTCH1 underlie the molecular cause of Gorlin syndrome (also known as nevoid basal cell carcinoma syndrome), a rare condition characterised by an increased risk of developing various tumours, commonly medulloblastoma, rhabdomyosarcoma and basal cell carcinoma [58]. In contrast, many epithelial cancers, including small-cell lung cancer, pancreatic, prostate and gastrointestinal malignancies, also exhibit over-active HH pathway, but this is caused by increased expression of SHH ligand without known mutations in pathway components. In these tumours, SHH is released to the stroma (paracrine action)

where it promotes tumour growth, infiltration and angiogenesis. In addition, activation of the SHH pathway in stromal cells is proposed to feedback signals to induce a more suitable environment for the SHH-expressing cells [58]. SHH autocrine signalling within the epithelial cells also appears to be important for cell renewal of cancer stem cells in breast cancer, multiple myeloma and chronic myelogenous leukaemia stem cells [64]. Our expression data strongly support a key role for HH signalling in the pathogenesis of mouse and human ACP, whereby SHH expression in the β-cat^{nc} cell clusters activates the pathway in both β-cat^{nc} (autocrine action) and β-cat^{m} cells (paracrine signalling). Whether over-activating mutations in the HH pathway components may underlie ACP tumorigenesis requires further research.

Over-activating mutations in FGF receptors have been identified in several human cancers, including breast, bladder, prostate, endometrial and lung cancers as well as haematological malignancies [62]. Expression levels of the FGF receptors 1–4 remained essentially unchanged between β-cat^{nc} clusters and surrounding β-cat^{m} cells. We noticed, however, that expression of *Fgfrl1* (FGF receptor like-1), a recently identified receptor lacking the critical intracellular domain responsible for signal transduction and thought to act as a decoy receptor able to inhibit FGF signalling in the expressing cells [55], was expressed 8.99-fold higher in the cluster cells. Although bestowed with several functional activities, FGFs are potent mitogenic signals in a variety of cell contexts, including the pituitary gland. It is tempting to speculate that β-cat^{nc} cell clusters may act as a source of FGFs inducing surrounding β-cat^{m} cells to actively divide, while protecting themselves by expressing higher levels of *Fgfrl1*. This could explain the paradoxical observation that cluster cells in both mouse and human ACP remain quiescent (e.g. Ki67 negative), but cells in the immediate vicinity are mitotically active [18]. Related to this notion, β-cat^{nc} cells express high levels of anti-apoptotic proteins of the Bcl2/Bcl-xL family.

An interesting concept that can be inferred from our data relates to the origin of the β-catenin accumulating (β-cat^{nc}) cluster cells. In mouse, these cells have an embryonic origin in Rathke's pouch undifferentiated precursors (i.e. HESX1 and SOX2 expressing cells) [18]. However, SOX2 is not uniformly expressed in all clusters or every cell within the clusters in the mouse pre-tumoral pituitary at late gestation or early postnatal life (Fig. 1b) [18]. Subsequently, in advanced mouse tumours, SOX2 expression is rarely observed, although at this stage, β-cat^{nc} clusters are not identifiable and most of the tumour cells exhibit accumulation of β-catenin in the nucleus, cytoplasm or both [18]. Similarly, although SOX2 positive cells have been identified in human ACP [17] (our unpublished observations), they are not present in the β-cat^{nc} cluster cells. This suggests that β-cat^{nc} cluster cells in human ACP and β-catenin-accumulating cells in advanced mouse ACP may derive from undifferentiated precursors/stem cells present in the embryonic or postnatal pituitary, but have lost cell stemness and down-regulated SOX2 expression.

Our data on telomere length on mouse and human β-cat^{nc} cluster cells are compatible with the idea that this similar cellular component of the tumours may correspond to different temporal stages of ACP development. Mouse β-cat^{nc} cluster cells in the pre-tumoral pituitaries exhibit longer telomeres than surrounding β-cat^{m} cells, suggesting the presence of stem cells in these structures. In contrast, β-cat^{nc} cluster cells in fully established human ACP have shorter telomeres than the rest of the non-cluster β-cat^{m} cells, suggesting that they do not contain stem cells. This could indicate the cellular ontogenesis of the β-cat^{nc} clusters in ACP, whereby SOX2^{+ve} stem cells with long telomeres are initially present but differentiate at later stages of tumour development losing SOX2 expression and shortening their telomeres. Unfortunately, species differences in ACP prevents us from testing this idea experimentally as fully established tumours in our mouse model do not contain β-cat^{nc} clusters and early stages of human ACP are not available.

Regardless, it is tempting to speculate that human ACP may be a tumour of stem cell origin, in which pituitary progenitors/stem cells played a role solely at an early stage of tumorigenesis. Advanced and clinically relevant human ACP would be devoid of such cells. This is different from the general dogma for cancer stem cells, where they self-renew and give rise to progeny that populate the tumour bulk. Instead, the contribution of the stem cell could be to initiate a cascade of signalling events leading to the perpetuation of a pathogenic unit (β-cat^{nc} cluster cells and microenvironment), without further need for the original stem cells. Therefore, the tumour-initiating mutation may occur in a progenitor/stem cell but the propagation of the tumour may require a different cell type. This is in agreement with findings in other tumours such as glioma and medulloblastoma [37, 50]. The data presented here strongly suggest an important autocrine/paracrine function of the cluster cells as signalling centres within the tumour and the interplay with the stromal cells, which is maintained after loss of SOX2 expression.

Current treatments for human ACP are far from ideal and associated with high morbidity and significant mortality [31, 43]. Our data highlight several genes and pathways likely to play essential roles in the pathogenesis of human ACP, as they do in several other human cancers. For some of these pathways, specific small-molecule inhibitors have been designed and their efficacy is currently being tested in a variety of clinical trials [35, 57]. The research presented here is expected to promote the

development of chemical-based therapies leading to more efficient and safer treatments for these childhood tumours.

Acknowledgements This work was carried out with the support of the UCL Institute of Child Health and Great Ormond Street Hospital Flow Cytometry Core facility, UCL Genomics, the ICH Embryonic Stem Cell/Chimera Production facility and UCL Biological Services Unit. The authors thank S. Neda Mousavy Gharavy, Lee Langer, Nicoletta Charolidi and Massimo Signore for help with genotyping mice and embryos and Alison John for help with histopathology. C.G.-M. is a recipient of a NIHR GOSH/UCL-ICH BRC fellowship. The authors thank the DSHB (University of Iowa) and the NHPP (Harbor-UCLA Medical Centre) for providing some of the antibodies used in this study. This work was funded by the Wellcome Trust (Grants 084361, 078432, 086545).

References

1. Alvarez-Medina R, Le Dreau G, Ros M, Marti E (2009) Hedgehog activation is required upstream of Wnt signalling to control neural progenitor proliferation. Development 136(19): 3301–3309. doi:10.1242/dev.041772
2. Andoniadou CL, Signore M, Sajedi E, Gaston-Massuet C, Kelberman D, Burns AJ, Itasaki N, Dattani M, Martinez-Barbera JP (2007) Lack of the murine homeobox gene Hesx1 leads to a posterior transformation of the anterior forebrain. Development 134(8):1499–1508. doi:10.1242/dev.02829
3. Andoniadou CL, Signore M, Young RM, Gaston-Massuet C, Wilson SW, Fuchs E, Martinez-Barbera JP (2011) HESX1- and TCF3-mediated repression of Wnt/beta-catenin targets is required for normal development of the anterior forebrain. Development 138(22):4931–4942. doi:10.1242/dev.066597
4. Barbieri F, Bajetto A, Porcile C, Pattarozzi A, Schettini G, Florio T (2007) Role of stromal cell-derived factor 1 (SDF1/CXCL12) in regulating anterior pituitary function. J Mol Endocrinol 38(3):383–389. doi:10.1677/jme-06-0014
5. Barbieri F, Bajetto A, Stumm R, Pattarozzi A, Porcile C, Zona G, Dorcaratto A, Ravetti JL, Minuto F, Spaziante R, Schettini G, Ferone D, Florio T (2008) Overexpression of stromal cell-derived factor 1 and its receptor CXCR4 induces autocrine/paracrine cell proliferation in human pituitary adenomas. Clin Cancer Res 14(16):5022–5032. doi:10.1158/1078-0432.ccr-07-4717
6. Ben-Baruch A (2006) The multifaceted roles of chemokines in malignancy. Cancer Metastasis Rev 25(3):357–371. doi:10.1007/s10555-006-9003-5
7. Brownell I, Guevara E, Bai CB, Loomis CA, Joyner AL (2011) Nerve-derived sonic hedgehog defines a niche for hair follicle stem cells capable of becoming epidermal stem cells. Cell Stem Cell 8(5):552–565. doi:10.1016/j.stem.2011.02.021
8. Burghaus S, Holsken A, Buchfelder M, Fahlbusch R, Riederer BM, Hans V, Blumcke I, Buslei R (2010) A tumor-specific cellular environment at the brain invasion border of adamantinomatous craniopharyngiomas. Virchows Arch 456(3):287–300. doi:10.1007/s00428-009-0873-0
9. Buslei R, Nolde M, Hofmann B, Meissner S, Eyupoglu IY, Siebzehnrubl F, Hahnen E, Kreutzer J, Fahlbusch R (2005) Common mutations of beta-catenin in adamantinomatous craniopharyngiomas but not in other tumours originating from the sellar region. Acta Neuropathol 109(6):589–597. doi:10.1007/s00401-005-1004-x
10. Davis SW, Castinetti F, Carvalho LR, Ellsworth BS, Potok MA, Lyons RH, Brinkmeier ML, Raetzman LT, Carninci P, Mortensen AH, Hayashizaki Y, Arnhold IJ, Mendonca BB, Brue T, Camper SA (2010) Molecular mechanisms of pituitary organogenesis: in search of novel regulatory genes. Mol Cell Endocrinol 323(1):4–19. doi:10.1016/j.mce.2009.12.012
11. Dorey K, Amaya E (2010) FGF signalling: diverse roles during early vertebrate embryogenesis. Development 137(22):3731–3742. doi:10.1242/dev.037689
12. Ellis P, Fagan BM, Magness ST, Hutton S, Taranova O, Hayashi S, McMahon A, Rao M, Pevny L (2004) SOX2, a persistent marker for multipotential neural stem cells derived from embryonic stem cells, the embryo or the adult. Dev Neurosci 26(2–4):148–165. doi:10.1159/000082134
13. Ericson J, Norlin S, Jessell TM, Edlund T (1998) Integrated FGF and BMP signaling controls the progression of progenitor cell differentiation and the emergence of pattern in the embryonic anterior pituitary. Development 125(6):1005–1015
14. Fauquier T, Rizzoti K, Dattani M, Lovell-Badge R, Robinson IC (2008) SOX2-expressing progenitor cells generate all of the major cell types in the adult mouse pituitary gland. Proc Natl Acad Sci USA 105(8):2907–2912. doi:10.1073/pnas.0707886105
15. Flores I, Benetti R, Blasco MA (2006) Telomerase regulation and stem cell behaviour. Curr Opin Cell Biol 18(3):254–260. doi:10.1016/j.ceb.2006.03.003
16. Flores I, Canela A, Vera E, Tejera A, Cotsarelis G, Blasco MA (2008) The longest telomeres: a general signature of adult stem cell compartments. Genes Dev 22(5):654–667. doi:10.1101/gad.451008
17. Garcia-Lavandeira M, Saez C, Diaz-Rodriguez E, Perez-Romero S, Senra A, Dieguez C, Japon MA, Alvarez CV (2011) Craniopharyngiomas express embryonic stem cell markers (SOX2, OCT4, KLF4, and SOX9) as pituitary stem cells but do not coexpress RET/GFRA3 receptors. J Clin Endocrinol Metab. doi:10.1210/jc.2011-2187
18. Gaston-Massuet C, Andoniadou CL, Signore M, Jayakody SA, Charolidi N, Kyeyune R, Vernay B, Jacques TS, Taketo MM, Le Tissier P, Dattani MT, Martinez-Barbera JP (2011) Increased Wingless (Wnt) signaling in pituitary progenitor/stem cells gives rise to pituitary tumors in mice and humans. Proc Natl Acad Sci USA 108(28):11482–11487. doi:10.1073/pnas.1101553108
19. Gibson P, Tong Y, Robinson G, Thompson MC, Currle DS, Eden C, Kranenburg TA, Hogg T, Poppleton H, Martin J, Finkelstein D, Pounds S, Weiss A, Patay Z, Scoggins M, Ogg R, Pei Y, Yang ZJ, Brun S, Lee Y, Zindy F, Lindsey JC, Taketo MM, Boop FA, Sanford RA, Gajjar A, Clifford SC, Roussel MF, McKinnon PJ, Gutmann DH, Ellison DW, Wechsler-Reya R, Gilbertson RJ (2010) Subtypes of medulloblastoma have distinct developmental origins. Nature 468(7327):1095–1099. doi:10.1038/nature09587
20. Gleiberman AS, Michurina T, Encinas JM, Roig JL, Krasnov P, Balordi F, Fishell G, Rosenfeld MG, Enikolopov G (2008) Genetic approaches identify adult pituitary stem cells. Proc Natl Acad Sci USA 105(17):6332–6337. doi:10.1073/pnas.0801644105
21. Gordon KJ, Blobe GC (2008) Role of transforming growth factor-beta superfamily signaling pathways in human disease. Biochim Biophys Acta 1782(4):197–228. doi:10.1016/j.bbadis.2008.01.006
22. Gotoh N (2009) Control of stemness by fibroblast growth factor signaling in stem cells and cancer stem cells. Curr Stem Cell Res Ther 4(1):9–15
23. Han YG, Spassky N, Romaguera-Ros M, Garcia-Verdugo JM, Aguilar A, Schneider-Maunoury S, Alvarez-Buylla A (2008)

Hedgehog signaling and primary cilia are required for the formation of adult neural stem cells. Nat Neurosci 11(3):277–284. doi:10.1038/nn2059
24. Harada N, Tamai Y, Ishikawa T, Sauer B, Takaku K, Oshima M, Taketo MM (1999) Intestinal polyposis in mice with a dominant stable mutation of the beta-catenin gene. EMBO J 18(21): 5931–5942. doi:10.1093/emboj/18.21.5931
25. Hassanein AM, Glanz SM, Kessler HP, Eskin TA, Liu C (2003) beta-Catenin is expressed aberrantly in tumors expressing shadow cells. Pilomatricoma, craniopharyngioma, and calcifying odontogenic cyst. Am J Clin Pathol 120(5):732–736. doi:10.1309/EALE-G7LD-6W71-67PX
26. Hofmann BM, Kreutzer J, Saeger W, Buchfelder M, Blumcke I, Fahlbusch R, Buslei R (2006) Nuclear beta-catenin accumulation as reliable marker for the differentiation between cystic craniopharyngiomas and rathke cleft cysts: a clinico-pathologic approach. Am J Surg Pathol 30(12):1595–1603. doi:10.1097/01.pas.0000213328.64121.12
27. Holsken A, Buchfelder M, Fahlbusch R, Blumcke I, Buslei R (2010) Tumour cell migration in adamantinomatous craniopharyngiomas is promoted by activated Wnt-signalling. Acta Neuropathol 119(5):631–639. doi:10.1007/s00401-010-0642-9
28. Holsken A, Gebhardt M, Buchfelder M, Fahlbusch R, Blumcke I, Buslei R (2011) EGFR signaling regulates tumor cell migration in craniopharyngiomas. Clin Cancer Res 17(13):4367–4377. doi:10.1158/1078-0432.ccr-10-2811
29. Holsken A, Kreutzer J, Hofmann BM, Hans V, Oppel F, Buchfelder M, Fahlbusch R, Blumcke I, Buslei R (2009) Target gene activation of the Wnt signaling pathway in nuclear beta-catenin accumulating cells of adamantinomatous craniopharyngiomas. Brain Pathol 19(3):357–364. doi:10.1111/j.1750-3639.2008.00180.x
30. Ingham PW, Placzek M (2006) Orchestrating ontogenesis: variations on a theme by sonic hedgehog. Nat Rev Genet 7(11):841–850. doi:10.1038/nrg1969
31. Karavitaki N, Brufani C, Warner JT, Adams CB, Richards P, Ansorge O, Shine B, Turner HE, Wass JA (2005) Craniopharyngiomas in children and adults: systematic analysis of 121 cases with long-term follow-up. Clin Endocrinol (Oxf) 62(4):397–409. doi:10.1111/j.1365-2265.2005.02231.x
32. Kato K, Nakatani Y, Kanno H, Inayama Y, Ijiri R, Nagahara N, Miyake T, Tanaka M, Ito Y, Aida N, Tachibana K, Sekido K, Tanaka Y (2004) Possible linkage between specific histological structures and aberrant reactivation of the Wnt pathway in adamantinomatous craniopharyngioma. J Pathol 203(3):814–821. doi:10.1002/path.1562
33. Katoh Y, Katoh M (2009) Hedgehog target genes: mechanisms of carcinogenesis induced by aberrant hedgehog signaling activation. Curr Mol Med 9(7):873–886
34. Kiehna EN, Merchant TE (2010) Radiation therapy for pediatric craniopharyngioma. Neurosurg Focus 28(4):E10. doi:10.3171/2010.1.focus09297
35. Kim JM, Lee YH, Ku CR, Lee EJ (2011) The cyclic pentapeptide d-Arg3FC131, a CXCR4 antagonist, induces apoptosis of somatotrope tumor and inhibits tumor growth in nude mice. Endocrinology 152(2):536–544. doi:10.1210/en.2010-0642
36. Labeur M, Paez-Pereda M, Haedo M, Arzt E, Stalla GK (2010) Pituitary tumors: cell type-specific roles for BMP-4. Mol Cell Endocrinol 326(1–2):85–88. doi:10.1016/j.mce.2010.04.006
37. Liu C, Sage JC, Miller MR, Verhaak RG, Hippenmeyer S, Vogel H, Foreman O, Bronson RT, Nishiyama A, Luo L, Zong H (2011) Mosaic analysis with double markers reveals tumor cell of origin in glioma. Cell 146(2):209–221. doi:10.1016/j.cell.2011.06.014
38. Liubinas SV, Munshey AS, Kaye AH (2011) Management of recurrent craniopharyngioma. J Clin Neurosci 18(4):451–457. doi:10.1016/j.jocn.2010.10.004
39. Madison BB, Braunstein K, Kuizon E, Portman K, Qiao XT, Gumucio DL (2005) Epithelial hedgehog signals pattern the intestinal crypt-villus axis. Development 132(2):279–289. doi:10.1242/dev.01576
40. Mao L, Xia YP, Zhou YN, Dai RL, Yang X, Duan SJ, Qiao X, Mei YW, Hu B, Cui H (2009) A critical role of Sonic Hedgehog signaling in maintaining the tumorigenicity of neuroblastoma cells. Cancer Sci 100(10):1848–1855. doi:10.1111/j.1349-7006.2009.01262.x
41. Maretto S, Cordenonsi M, Dupont S, Braghetta P, Broccoli V, Hassan AB, Volpin D, Bressan GM, Piccolo S (2003) Mapping Wnt/beta-catenin signaling during mouse development and in colorectal tumors. Proc Natl Acad Sci USA 100(6):3299–3304
42. Miller RJ, Banisadr G, Bhattacharyya BJ (2008) CXCR4 signaling in the regulation of stem cell migration and development. J Neuroimmunol 198(1–2):31–38. doi:10.1016/j.jneuroim.2008.04.008
43. Muller HL (2010) Childhood craniopharyngioma: current concepts in diagnosis, therapy and follow-up. Nat Rev Endocrinol 6(11):609–618. doi:10.1038/nrendo.2010.168
44. Muller HL (2011) Consequences of craniopharyngioma surgery in children. J Clin Endocrinol Metab 96(7):1981–1991. doi:10.1210/jc.2011-0174
45. Musani V, Gorry P, Basta-Juzbasic A, Stipic T, Miklic P, Levanat S (2006) Mutation in exon 7 of PTCH deregulates SHH/PTCH/SMO signaling: possible linkage to WNT. Int J Mol Med 17(5):755–759
46. Ratajczak MZ, Zuba-Surma E, Kucia M, Reca R, Wojakowski W, Ratajczak J (2006) The pleiotropic effects of the SDF-1-CXCR4 axis in organogenesis, regeneration and tumorigenesis. Leukemia 20(11):1915–1924. doi:10.1038/sj.leu.2404357
47. Roderick E, Karavitaki N, Wass JA (2008) Craniopharyngiomas. Historical aspects of their management Hormones (Athens) 7(3):271–274
48. Romer JT, Kimura H, Magdaleno S, Sasai K, Fuller C, Baines H, Connelly M, Stewart CF, Gould S, Rubin LL, Curran T (2004) Suppression of the Shh pathway using a small molecule inhibitor eliminates medulloblastoma in Ptc1(±)p53(−/−) mice. Cancer Cell 6(3):229–240. doi:10.1016/j.ccr.2004.08.019
49. Samper E, Flores JM, Blasco MA (2001) Restoration of telomerase activity rescues chromosomal instability and premature aging in Terc−/− mice with short telomeres. EMBO Rep 2(9):800–807. doi:10.1093/embo-reports/kve174
50. Schuller U, Heine VM, Mao J, Kho AT, Dillon AK, Han YG, Huillard E, Sun T, Ligon AH, Qian Y, Ma Q, Alvarez-Buylla A, McMahon AP, Rowitch DH, Ligon KL (2008) Acquisition of granule neuron precursor identity is a critical determinant of progenitor cell competence to form Shh-induced medulloblastoma. Cancer Cell 14(2):123–134. doi:10.1016/j.ccr.2008.07.005
51. Sekine S, Shibata T, Kokubu A, Morishita Y, Noguchi M, Nakanishi Y, Sakamoto M, Hirohashi S (2002) Craniopharyngiomas of adamantinomatous type harbor beta-catenin gene mutations. Am J Pathol 161(6):1997–2001
52. Sekine S, Takata T, Shibata T, Mori M, Morishita Y, Noguchi M, Uchida T, Kanai Y, Hirohashi S (2004) Expression of enamel proteins and LEF1 in adamantinomatous craniopharyngioma: evidence for its odontogenic epithelial differentiation. Histopathology 45(6):573–579. doi:10.1111/j.1365-2559.2004.02029.x
53. Shin K, Lee J, Guo N, Kim J, Lim A, Qu L, Mysorekar IU, Beachy PA (2011) Hedgehog/Wnt feedback supports regenerative proliferation of epithelial stem cells in bladder. Nature 472(7341):110–114. doi:10.1038/nature09851
54. Song Z, Yue W, Wei B, Wang N, Li T, Guan L, Shi S, Zeng Q, Pei X, Chen L (2011) Sonic hedgehog pathway is essential for maintenance of cancer stem-like cells in human gastric cancer. PLoS One 6(3):e17687. doi:10.1371/journal.pone.0017687

55. Steinberg F, Zhuang L, Beyeler M, Kalin RE, Mullis PE, Brandli AW, Trueb B (2010) The FGFRL1 receptor is shed from cell membranes, binds fibroblast growth factors (FGFs), and antagonizes FGF signaling in Xenopus embryos. J Biol Chem 285(3): 2193–2202. doi:10.1074/jbc.M109.058248
56. Takahashi M, Nakamura Y, Obama K, Furukawa Y (2005) Identification of SP5 as a downstream gene of the beta-catenin/Tcf pathway and its enhanced expression in human colon cancer. Int J Oncol 27(6):1483–1487
57. Takebe N, Harris PJ, Warren RQ, Ivy SP (2011) Targeting cancer stem cells by inhibiting Wnt, Notch, and Hedgehog pathways. Nat Rev Clin Oncol 8(2):97–106. doi:10.1038/nrclinonc.2010.196
58. Theunissen JW, de Sauvage FJ (2009) Paracrine Hedgehog signaling in cancer. Cancer Res 69(15):6007–6010. doi:10.1158/0008-5472.can-09-0756
59. Treier M, O'Connell S, Gleiberman A, Price J, Szeto DP, Burgess R, Chuang PT, McMahon AP, Rosenfeld MG (2001) Hedgehog signaling is required for pituitary gland development. Development 128(3):377–386
60. Wang Y, Martin JF, Bai CB (2010) Direct and indirect requirements of Shh/Gli signaling in early pituitary development. Dev Biol 348(2):199–209. doi:10.1016/j.ydbio.2010.09.024
61. Weidinger G, Thorpe CJ, Wuennenberg-Stapleton K, Ngai J, Moon RT (2005) The Sp1-related transcription factors sp5 and sp5-like act downstream of Wnt/beta-catenin signaling in mesoderm and neuroectoderm patterning. Curr Biol 15(6):489–500. doi:10.1016/j.cub.2005.01.041
62. Wesche J, Haglund K, Haugsten EM (2011) Fibroblast growth factors and their receptors in cancer. Biochem J 437(2):199–213. doi:10.1042/bj20101603
63. Wu MY, Hill CS (2009) Tgf-beta superfamily signaling in embryonic development and homeostasis. Dev Cell 16(3): 329–343. doi:10.1016/j.devcel.2009.02.012
64. Yauch RL, Gould SE, Scales SJ, Tang T, Tian H, Ahn CP, Marshall D, Fu L, Januario T, Kallop D, Nannini-Pepe M, Kotkow K, Marsters JC, Rubin LL, de Sauvage FJ (2008) A paracrine requirement for hedgehog signalling in cancer. Nature 455(7211):406–410. doi:10.1038/nature07275

The EMBO Journal (2012) 00, 1–13 | © 2012 European Molecular Biology Organization | All Rights Reserved 0261-4189/12
www.embojournal.org

THE EMBO JOURNAL

Genetic inactivation of Cdk7 leads to cell cycle arrest and induces premature aging due to adult stem cell exhaustion

Miguel Ganuza[1], Cristina Sáiz-Ladera[2], Marta Cañamero[3], Gonzalo Gómez[4], Ralph Schneider[5], María A Blasco[5], David Pisano[4], Jesús M Paramio[2], David Santamaría[1,*] and Mariano Barbacid[1,*]

[1]Experimental Oncology, Molecular Oncology Programme, Centro Nacional de Investigaciones Oncológicas (CNIO), Madrid, Spain, [2]Department of Basic Research, Molecular Oncology Unit, CIEMAT, Madrid, Spain, [3]Comparative Pathology Unit, Biotechnology Programme, Centro Nacional de Investigaciones Oncológicas (CNIO), Madrid, Spain, [4]Bioinformatics Unit, Structural Biology and Biocomputing Programme, Centro Nacional de Investigaciones Oncológicas (CNIO), Madrid, Spain and [5]Telomeres and Telomerase Group, Molecular Oncology Programme, Centro Nacional de Investigaciones Oncológicas (CNIO), Madrid, Spain

Cyclin-dependent kinase (Cdk)7, the catalytic subunit of the Cdk-activating kinase (CAK) complex has been implicated in the control of cell cycle progression and of RNA polymerase II (RNA pol II)-mediated transcription. Genetic inactivation of the *Cdk7* locus revealed that whereas Cdk7 is completely dispensable for global transcription, is essential for the cell cycle via phosphorylation of Cdk1 and Cdk2. *In vivo*, *Cdk7* is also indispensable for cell proliferation except during the initial stages of embryonic development. Interestingly, widespread elimination of Cdk7 in adult tissues with low proliferative indexes had no phenotypic consequences. However, ablation of conditional *Cdk7* alleles in tissues with elevated cellular turnover led to the efficient repopulation of these tissues with Cdk7-expressing cells most likely derived from adult stem cells that may have escaped the inactivation of their targeted *Cdk7* alleles. This process, a physiological attempt to maintain tissue homeostasis, led to the attrition of adult stem cell pools and to the appearance of age-related phenotypes, including telomere shortening and early death.

The EMBO Journal advance online publication, 13 April 2012; doi:10.1038/emboj.2012.94
Subject Categories: signal transduction; cell cycle
Keywords: CAK; Cdk7; *in vivo* elimination; mouse model; stem cell exhaustion

*Corresponding author. D Santamaria or M Barbacid, Experimental Oncology, Molecular Oncology Programme, Madrid, 28029, Spain. Tel.: +34 917328015; Fax: +34 912246980;
E-mail: dsantamaria@cnio.es or mbarbacid@cnio.es.

Received: 22 November 2011; accepted: 20 March 2012

Introduction

Cell cycle regulation in eukaryotic cells is controlled by a family of conserved heterodimeric serine/threonine kinases made of a regulatory subunit, generically known as Cyclin, and a catalytic component designated as Cyclin-dependent kinase (Cdk) (Malumbres and Barbacid, 2005). Cyclins are essential to activate the catalytic activity of their cognate Cdks and to provide substrate specificity. However, optimal kinase activity requires additional steps, one of which involves phosphorylation of a key threonine residue located within the activating segment, also known as T-loop, of the Cdk subunit (Harper and Elledge, 1998). This activating step is carried out by the Cdk-activating kinase (CAK), a trimeric kinase whose catalytic activity is also provided by a Cdk, known as Cdk7. Cdk7 becomes activated by binding to Cyclin H (CycH) and to a third regulatory subunit known as Mat1 (Harper and Elledge, 1998).

Interestingly, CAK is also a component of the general transcription factor TFIIH, a large protein complex involved in the phosphorylation of serine residues (mainly Ser5) located at the carboxy terminal domain (CTD) of the large subunit of RNA polymerase II (RNA pol II). Thus, CAK has also been implicated in the regulation of promoter clearance and progression of the basic transcriptional machinery (Palancade and Bensaude, 2003). Yet, recent evidence suggests that RNA pol II-mediated transcription may not be overtly affected by the absence of CAK activity. For instance, a temperature-sensitive allele of Mcs6, the corresponding orthologue in *S. pombe*, only affects transcription of a selective cell-division gene cluster, representing <5% of all transcripts (Lee *et al*, 2005). Similarly, Cdk7 deficiency results in severe mitotic defects in *C. elegans* and *D. melanogaster* without concomitant loss of CTD phosphorylation or transcriptional integrity, respectively (Larochelle *et al*, 1998; Wallenfang and Seydoux, 2002). Finally, mouse cells defective in the regulatory subunit Mat1 present functional *de novo* transcription (Rossi *et al*, 2001). Regardless of its potential role in regulating the cell cycle and/or transcription, genetic studies have shown that *Cdk7* is an essential gene in *D. melanogaster* (Larochelle *et al*, 1998). Likewise, Mat1 or CycH deficiency results in an early embryonic lethality in mice (Rossi *et al*, 2001; Patel and Simon, 2010).

We undertook the present study to analyse the physiological role of Cdk7 in mice by genetic targeting. We report that loss of Cdk7 causes impaired T-loop phosphorylation of cell cycle Cdks, leading to cessation of cell division *in vitro* and early embryonic lethality *in vivo*. In contrast, RNA pol II-mediated transcription is unaffected with the exception of E2F-controlled genes, an indirect consequence of deficient Cdk function. Loss of Cdk7 expression in adult mice has a little effect on non-proliferating tissues. However, elimination of Cdk7 in proliferating tissues leads to the premature onset of age-related phenotypes most likely due

to depletion of progenitor cells and exhaustion of their renewal capacity.

Results

Cdk7 is required for cell proliferation but not for global transcription

Cdk7$^{lox/lox}$ mouse embryonic fibroblasts (MEF) were generated from *Cdk7*$^{lox/lox}$ embryos (see Materials and methods). These MEFs were subsequently infected with adenoviral vectors expressing the Cre recombinase (Ad-Cre) to generate *Cdk7*$^{mut/mut}$ MEFs that lack detectable levels of Cdk7 expression (Supplementary Figure 1). These mutant MEFs failed to proliferate and to enter S phase upon serum stimulation (Supplementary Figure 2A and B). As expected, loss of Cdk7 expression caused degradation of the other CAK subunits, CycH and Mat1 (Supplementary Figure 2C; Rossi *et al*, 2001). Likewise, Cdk7 was also degraded upon shRNA-mediated knockdown of either Mat1 or CycH (data not shown).

Cdk7 is thought to activate transcription by phosphorylating serine residues, mainly Ser5, located within the CTD of RNA pol II (Palancade and Bensaude, 2003). Interestingly, the phosphorylation levels of this residue were unaffected in *Cdk7*$^{mut/mut}$ MEFs (Figure 1A), indicating that either Cdk7 is not involved in the phosphorylation of this critical residue or that this activity can be carried out by another kinase with similar efficiency. This result prompted us to assess whether RNA pol II-mediated transcription was affected in the absence of Cdk7. To this end, 7 days after exposure to Ad-Cre, *Cdk7*$^{mut/mut}$ MEFs were infected with a lentiviral vector expressing a green fluorescent protein (GFP) from a constitutive promoter. After 72 h, the intensity of the GFP reporter in *Cdk7*$^{mut/mut}$ MEFs was comparable to that of *Cdk7*$^{lox/lox}$ controls (Supplementary Figure 2D). Likewise, *Cdk7*$^{mut/mut}$ and *Cdk7*$^{lox/lox}$ MEFs were serum starved in order to match their proliferation rates. Under these conditions the rate of *de novo* protein synthesis, as measured by [^{35}S]methionine incorporation, was not affected in the absence of Cdk7 (Supplementary Figure 2E). All together, these results suggest that Cdk7 is dispensable for *de novo* transcription and translation.

To further characterize the transcriptional status of cells devoid of Cdk7, we compared the gene expression profile of *Cdk7*$^{lox/lox}$ with *Cdk7*$^{mut/mut}$ MEFs by standard microarray analysis. To rule out a possible bias due to their different proliferation rates, we decided to perform a gene set enrichment analysis (GSEA) on a predefined subset of 443 housekeeping genes, as expression of this cluster has been shown to be proliferation-rate independent (Eisenberg and Levanon, 2003). Our results indicated that transcription of this housekeeping gene-set was not statistically altered 10 days after the elimination of Cdk7 (false discovery rate (FDR) 0.339) (Supplementary Figure 2F–H) thus indicating that the inability of *Cdk7*$^{mut/mut}$ MEFs to proliferate was not due to a defect in global transcription. Indeed, when we analysed the entire microarray data set in *Cdk7*$^{mut/mut}$ MEFs (FDR$<$0.05), we detected the upregulation in 1250 genes along with the presence of 1218 additional genes that showed no variation in their levels of expression (data not shown) thus supporting the notion that Cdk7 is dispensable for RNA pol II-mediated global transcription.

Cdk7 is essential for activation of cell cycle Cdks

Cdk7$^{mut/mut}$ MEFs showed no detectable phosphorylation of Thr160, the activating residue in the T-loop of Cdk2 (Figure 1A). Similar results were observed in quiescent cells upon serum stimulation (Figure 1B). The rapid decline of Cdk1 levels following the elimination of Cdk7 prevented us from analysing the overall level of phosphorylation of the corresponding Thr161 residue of Cdk1. The CAK complex can also activate the other interphase Cdks, Cdk4 and Cdk6 (Lolli and Johnson, 2005). Unfortunately, no phospho-specific antibodies for their T-loop threonine residues are available. Thus, we examined whether their expression levels and overall *in vitro* kinase activity was affected in MEFs lacking Cdk7. As illustrated in Figure 1A, *Cdk7*$^{mut/mut}$ MEFs expressed normal levels of Cdk4 and Cdk6. Moreover, the kinase activity of Cdk4 and Cdk6 immunoprecipitates derived from *Cdk7*$^{mut/mut}$ cells were significantly decreased, suggesting that CAK activity is compromised in cells lacking Cdk7 (Figure 1C). Similar results were obtained using Cdk2 immunoprecipitaes (Figure 1C). The kinase activity of Cdk1 could not be examined due to its low levels of expression in *Cdk7*$^{mut/mut}$ MEFs (Figure 1A and B).

Next, we interrogated whether Cdk7^{T170A}, a Cdk7 mutant that retains normal CAK function but $<$5% of the kinase activity towards the CTD of RNA pol II (Larochelle *et al*, 2001), was capable of rescuing proliferation of Cdk7 *null* cells. As illustrated in Figure 2, *Cdk7*$^{mut/mut}$ MEFs ectopically expressing the Cdk7^{T170A} mutant proliferated and formed colonies with efficiencies similar to those of cells ectopically expressing the wild-type Cdk7 protein. As a negative control, Cdk7^{K41A}, a kinase dead mutant, failed to induce both proliferation and colony formation (Figure 2A and B). These results support the notion that Cdk7 plays an essential role in cell proliferation by providing CAK activity whereas its CTD kinase activity is dispensable.

Cdk7 is required for T-loop phosphorylation of cell cycle Cdks

Next, we expressed phosphomimetic mutants of each of the cell cycle Cdks to determine which CAK substrate was responsible for cell proliferation. Neither Cdk4^{T174E} nor Cdk6^{T177E} mutants were able to convey proliferative properties to cells lacking Cdk7 (data not shown), suggesting that constitutive activation of these kinases is not sufficient to drive cell proliferation. We then performed a rescue assay using Cdk2^{T160E} or Cdk1^{T161E} phosphomimetic mutants. We observed that expression of Cdk2^{T160E} or Cdk1^{T161E}, but not their wild-type counterparts, partially restored proliferation and colony formation in Cdk7-deficient cells (Figure 2C and D). Colonies expressing these mutant proteins were analysed by Southern blotting to verify the absence of *Cdk7*^{lox} alleles (Supplementary Figure 2G). Yet, the proliferation rate and the number of colonies obtained with these Cdk1 and Cdk2 phosphomimetic mutants was lower than those observed with vectors expressing the wild-type Cdk7 protein (Figure 2C and D). Whether these differences are due to limited activity of the Cdk2^{T160E} or Cdk1^{T161E} mutants or to the fact that Cdk7 has additional functions that contribute to cell proliferation, remains to be determined.

Previous studies have shown that Cdk2 is neither essential for cell proliferation nor compensates for the absence of Cdk1, even when expressed from the *Cdk1* locus

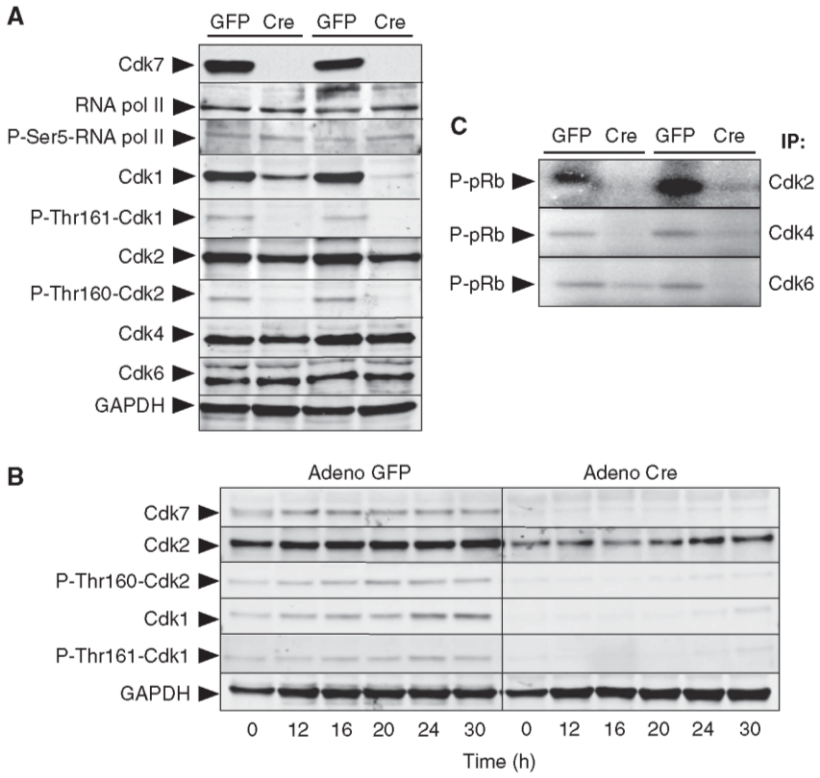

Figure 1 Deficient cell cycle Cdk activation in MEFs lacking Cdk7. (**A**) Immunoblot analysis of Cdk7, RNA pol II, P-Ser5-RNA pol II, Cdk1, P-Thr161-Cdk1, Cdk2, P-Thr160-Cdk2, Cdk4 and Cdk6 expression in extracts from $Cdk7^{lox/lox}$ MEFs infected with adenoviral particles expressing GFP or Cre recombinase. Results from two independent experiments are shown. GAPDH serves as a loading control. (**B**) Immunoblot analysis of Cdk7, Cdk2, P-Thr160-Cdk2, Cdk1 and P-Thr161-Cdk1 expression at the indicated time points after addition of serum to quiescent $Cdk7^{lox/lox}$ MEFs infected with adenoviral particles expressing GFP or Cre recombinase. GAPDH serves as a loading control. (**C**) *In vitro* kinase activity associated with Cdk2, Cdk4 and Cdk6 immunoprecipitates obtained from $Cdk7^{lox/lox}$ MEFs after infection with adenoviral particles expressing GFP or Cre recombinase. Recombinant pRb was used as substrate. Results from two independent experiments are shown. Figure source data can be found with the Supplementary data.

(Berthet *et al*, 2003; Ortega *et al*, 2003; Satyanarayana *et al*, 2008). Thus, we examined the mechanism by which the $Cdk2^{T160E}$ mutant conferred proliferative properties to Cdk7-deficient cells. As shown in Figure 2G, expression of $Cdk2^{T160E}$ in $Cdk7^{mut/mut}$ MEFs restored normal levels of Cdk1 protein that was properly phosphorylated in its Thr161 residue. These observations suggest that in the absence of Cdk7, $Cdk2^{T160E}$ induces the synthesis of Cdk1 through inhibition of pRb and subsequent activation of the E2F-dependent transcriptional programme. Moreover, they also raised the possibility that $Cdk2^{T160E}$ might activate Cdk1 by inducing phosphorylation in its critical Thr161 residue.

Restoration of E2F-dependent transcription rescues proliferation of Cdk7-defective cells

Microarray analysis revealed that, unlike housekeeping genes, the E2F-controlled programme (Bracken *et al*, 2004) was consistently downregulated (FDR 0.068) in $Cdk7^{mut/mut}$ MEFs (Supplementary Figure 2H). Downregulated genes included critical cell cycle regulators such as CycE1, CycA2, CycB1 and Cdk1. These observations were confirmed by western blotting (data not shown). These results suggest that reactivation of the E2F transcriptional programme by inactivation of the Rb family of proteins might alleviate the proliferative defects caused by elimination of Cdk7. To test this hypothesis, we expressed the T121 fragment of the SV40 large T antigen in $Cdk7^{mut/mut}$ MEFs. This polypeptide is known to inactivate the three members of the Rb family and improve the proliferation rate of cells lacking all interphase Cdks (Santamaría *et al*, 2007). As illustrated in Figure 2E and F, ectopic expression of T121 restored the proliferative properties of $Cdk7^{mut/mut}$ cells to the same level as the wild-type Cdk7 protein. Interestingly, these T121-expressing $Cdk7^{mut/mut}$ MEFs displayed normal levels of Cdk1 and Cdk2. Moreover, both kinases were properly phosphorylated in their activating T-loop Thr residues (Figure 2G). These observations indicate that cells have mechanisms other than Cdk7-mediated CAK activity to phosphorylate Cdk1 and Cdk2, providing that the Rb family of proteins has been inactivated.

Cdk7 deficiency causes early embryonic lethality

To characterize the impact of Cdk7 deficiency *in vivo*, we generated mice from ES cells carrying a $Cdk7^{loxfrt}$ allele (Supplementary Figure 1). Heterozygous animals had normal lifespan and did not display obvious phenotypes. However, crosses between heterozygous animals failed to produce live

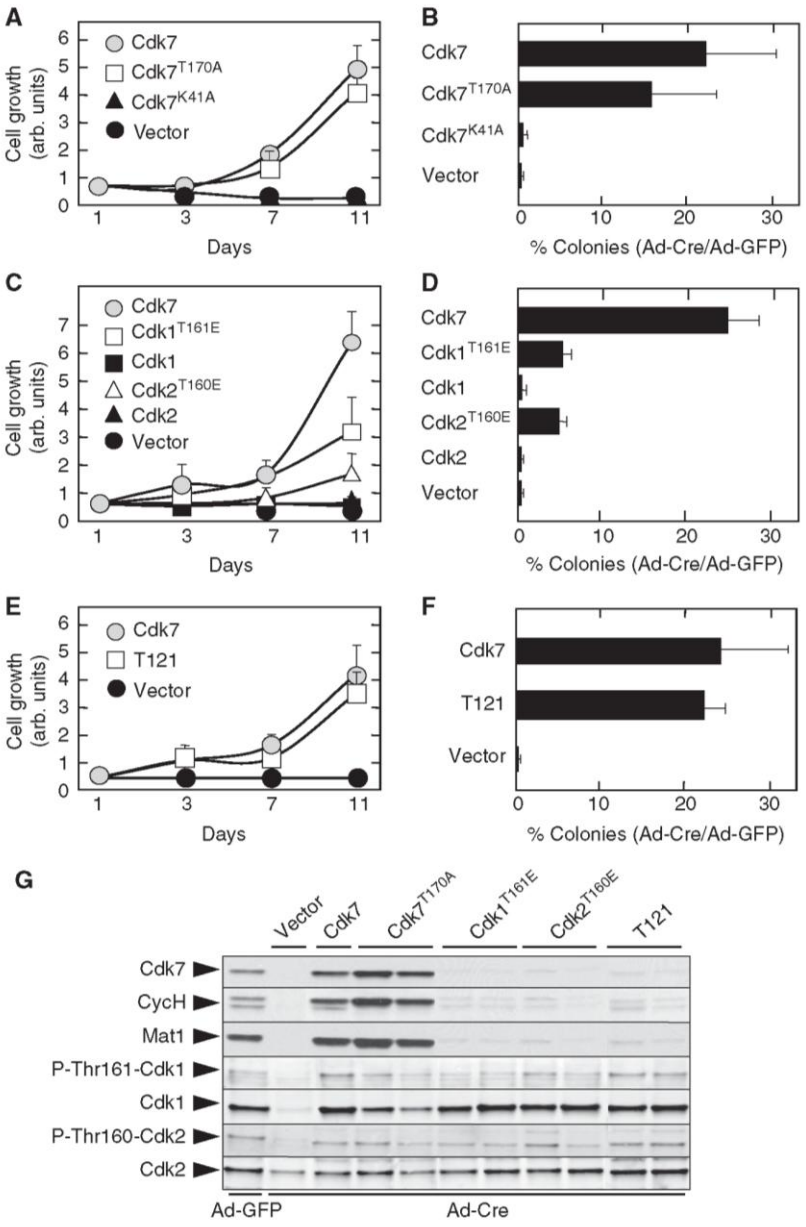

Figure 2 The CAK activity of Cdk7 is essential for cell proliferation. (**A**) Growth of immortalized *Cdk7*$^{lox/lox}$ MEFs infected with retroviral vectors expressing cDNAs encoding wild-type Cdk7 (grey circles), Cdk7^{T170A} (open squares), Cdk7^{K41A} (solid triangles) or control vector (solid circles) and subsequently infected with Ad-Cre to inactivate the *Cdk7*^{lox} alleles. (**B**) Percentage of colonies observed in *Cdk7*$^{lox/lox}$ MEFs infected with retroviral vectors expressing cDNAs encoding wild-type Cdk7, mutant Cdk7^{T170A}, mutant Cdk7^{K41A} or with control vector and subsequently infected with Ad-Cre, normalized to those observed in parallel cultures infected with control Ad-GFP. Data shown as mean ± s.d., $n=3$. (**C**) Growth of immortalized *Cdk7*$^{lox/lox}$ MEFs infected with retroviral vectors expressing cDNAs encoding wild-type Cdk7 (grey circles), phosphomimetic Cdk1^{T161E} mutant (open squares), wild-type Cdk1 (solid squares), phosphomimetic Cdk2^{T160E} mutant (open triangles), wild-type Cdk2 (solid triangles) or with control vector (solid circles) and subsequently infected with Ad-Cre to inactivate the *Cdk7*^{lox} alleles. (**D**) Percentage of colonies observed in *Cdk7*$^{lox/lox}$ MEFs infected with retroviral vectors expressing cDNAs encoding wild-type Cdk7, phosphomimetic Cdk1^{T161E} and Cdk2^{T160E} mutant proteins, wild-type Cdk1 or Cdk2 proteins or with control vector and subsequently infected with Ad-Cre, normalized to those observed in parallel cultures infected with Ad-GFP. Data shown as mean ± s.d., $n=3$. (**E**) Growth of immortalized *Cdk7*$^{lox/lox}$ MEFs infected with retroviral vectors expressing a cDNA encoding wild-type Cdk7 (grey circles), the T121 fragment of the SV40 large T antigen (open squares) or with control vector (solid circles) and subsequently infected with Ad-Cre to inactivate the *Cdk7*^{lox} alleles. (**F**) Percentage of colonies observed in *Cdk7*$^{lox/lox}$ MEFs infected with retroviral vectors expressing a cDNA encoding wild-type Cdk7, the T121 fragment of the SV40 large T antigen or with control vector and subsequently infected with Ad-Cre, normalized to those observed in parallel cultures infected with Ad-GFP. Data shown as mean ± s.d., $n=3$. (**G**) Immunoblot analysis of Cdk7, CycH, Mat1, Cdk1, P-Thr161-Cdk1, Cdk1, P-Thr160-Cdk2 and Cdk2 expression in representative colonies of immortalized *Cdk7*$^{lox/lox}$ MEFs infected with retroviral vectors expressing cDNAs encoding wild-type Cdk7, mutant Cdk7^{T170A}, phosphomimetic Cdk1^{T161E} and Cdk2^{T160E} mutants, the T121 fragment of the SV40 large T antigen or with control vector and subsequently infected with Ad-Cre to inactivate the *Cdk7*^{lox} alleles or with control Ad-GFP. Figure source data can be found with the Supplementary data.

Cdk7$^{loxfrt/loxfrt}$ offspring as well as E13.5 and E9.5 embryos, thus suggesting that *Cdk7*^{loxfrt} alleles failed to express normal levels of Cdk7 (see below). Analysis of E5.5 embryos derived from these crosses revealed deciduas with a high percentage of apoptotic cells within the embryonic body that were negative for Cdk7 immunostaining (Supplementary Figure 3A), thus suggesting that homozygous *Cdk7*$^{loxfrt/loxfrt}$ embryos died at peri-implantation stages. Interestingly, E2.5 as well as E3.5 *Cdk7*$^{loxfrt/loxfrt}$ embryos (blastocyst stage) were obtained with Mendelian ratios. As the E2.5 mutant embryos did not express detectable levels of Cdk7 (Figure 3A), the apparently normal development of *Cdk7*$^{loxfrt/loxfrt}$ blastocysts is unlikely to be due to contribution by the maternal Cdk7 protein.

To study the defects responsible for the death of *Cdk7*$^{loxfrt/loxfrt}$ embryos, we isolated E2.5 embryos and maintained them under *in vitro* culture conditions. One day later, the resulting E3.5 *Cdk7*$^{loxfrt/loxfrt}$ blastocysts were indistinguishable from the heterozygous and wild-type littermates, including normal levels of expression of Nanog, an inner cell mass (ICM) marker (Figure 3B), thus indicating that early embryo cells can differentiate into ICM lineages in the absence of Cdk7. However, at E4.5, *Cdk7*$^{loxfrt/loxfrt}$ embryos showed conspicuous staining of the apoptotic marker-activated Caspase 3A within the ICM (Figure 3C), leading to the disappearance of ICM cells 2 days later in hatching embryos (Figure 3D). At this time (E6.5–E7.5), visual inspection of *Cdk7*$^{loxfrt/loxfrt}$ embryos revealed the presence of trophoblasts. However, their nuclei appeared smaller (3–4-fold) than those of trophoblasts present in control embryos (Supplementary Figure 3B and C). These observations suggest that *Cdk7*$^{loxfrt/loxfrt}$ embryos die during peri-implantation stages due to apoptotic death of ICM cells. Furthermore, the smaller size of the nuclei of *Cdk7*$^{loxfrt/loxfrt}$ trophoblasts suggests additional defects in the trophoectodermal lineage, most likely due to limited endoreplicative cycles.

Cdk7 is required for skin development

Next, we analysed the role of Cdk7 during skin development. To this end, we generated a conditional *Cdk7*$^{lox/lox}$ mice by crossing *Cdk7*$^{loxfrt/loxfrt}$ animals to a Flpase-expressing strain, as described in Materials and methods. The resulting *Cdk7*$^{lox/lox}$ animals were subsequently crossed to K5-Cre, a transgenic strain that selectively expresses the Cre recombinase within the basal layer of the epidermis (Tarutani *et al*, 1997). *Cdk7*$^{lox/lox}$; K5-Cre$^{+/T}$ compound mice were born with Mendelian ratios. However, they displayed small size, widespread lack of hair, scaly skin and died soon thereafter, between postnatal days 1 and 4 (P1–P4) (Figure 4A). Immunohistochemical analysis of the skin of these mice revealed mosaic elimination of Cdk7, with patches of epidermis showing positive staining interspersed with regions lacking Cdk7 expression (Figure 4B). In agreement with *in vitro* studies, phosphorylation in the Ser5 residue of the CTD of RNA pol II was unaffected in these cells (Figure 4B). Likewise, cells lacking Cdk7 displayed pRb hypophosphorylation and were negative for P-Thr160-Cdk2, suggesting that Cdk7 is also required for the activation of Cdk2 *in vivo*.

Histopathological analysis of skin samples of *Cdk7*$^{lox/lox}$;K5-Cre$^{+/T}$ mice revealed a complex phenotype. The epidermis of these animals showed scattered hyperplastic and hypoplastic regions (Figure 4C). The latter were devoid of Cdk7 staining and contained non-proliferating cells as indicated by the absence of PCNA staining, a marker of cell proliferation (Figure 4D). On the

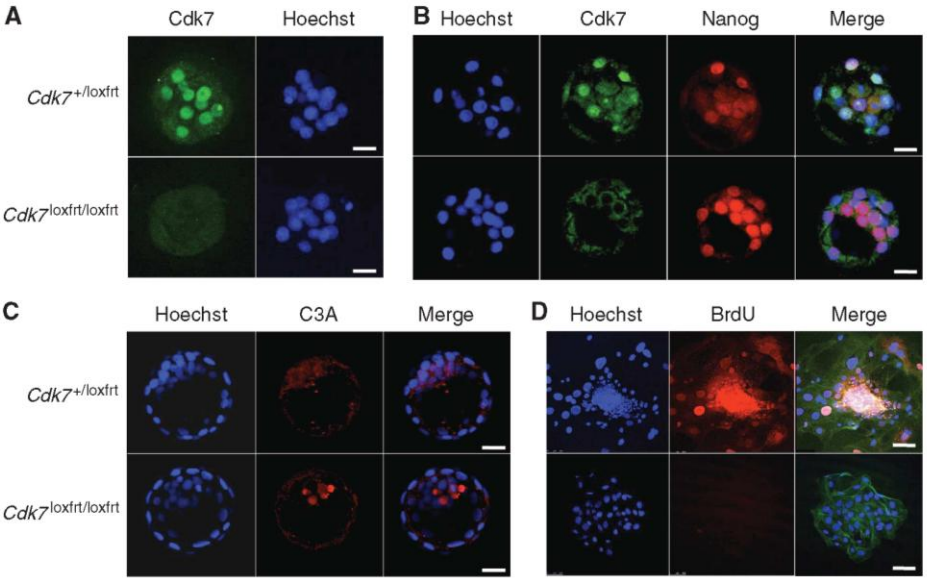

Figure 3 *Cdk7* germ line deficiency results in an early embryonic lethality. (**A**) Embryos of the indicated genotypes were isolated at E2.5 and analysed for Cdk7 expression by immunofluorescence (green). Nuclei were stained with Hoechst 33342 (blue). Bar, 25 μm. (**B**) Embryos of the indicated genotypes were isolated at E2.5, cultured *in vitro* and analysed by immunofluorescence at E3.5. Co-staining for Cdk7 (green) and Nanog (red) is shown. Nuclei were stained with Hoechst 33342 (blue). Bar, 25 μm. (**C**) Embryos of the indicated genotypes were isolated at E2.5 and cultured *in vitro* for 2 days (E4.5 stage). Active Caspase 3 was detected by immunofluorescence (red). Nuclei were stained with Hoechst 33342 (blue). Bar, 25 μm. (**D**) Embryos of the indicated genotypes were isolated at E2.5 and cultured *in vitro* for 5 days (E7.5 stage). BrdU incorporation was assessed by immunofluorescence (red). Nuclei were stained with Hoechst 33342 (blue). Actin filaments were stained with Phalloidin (green). Bar, 100 μm.

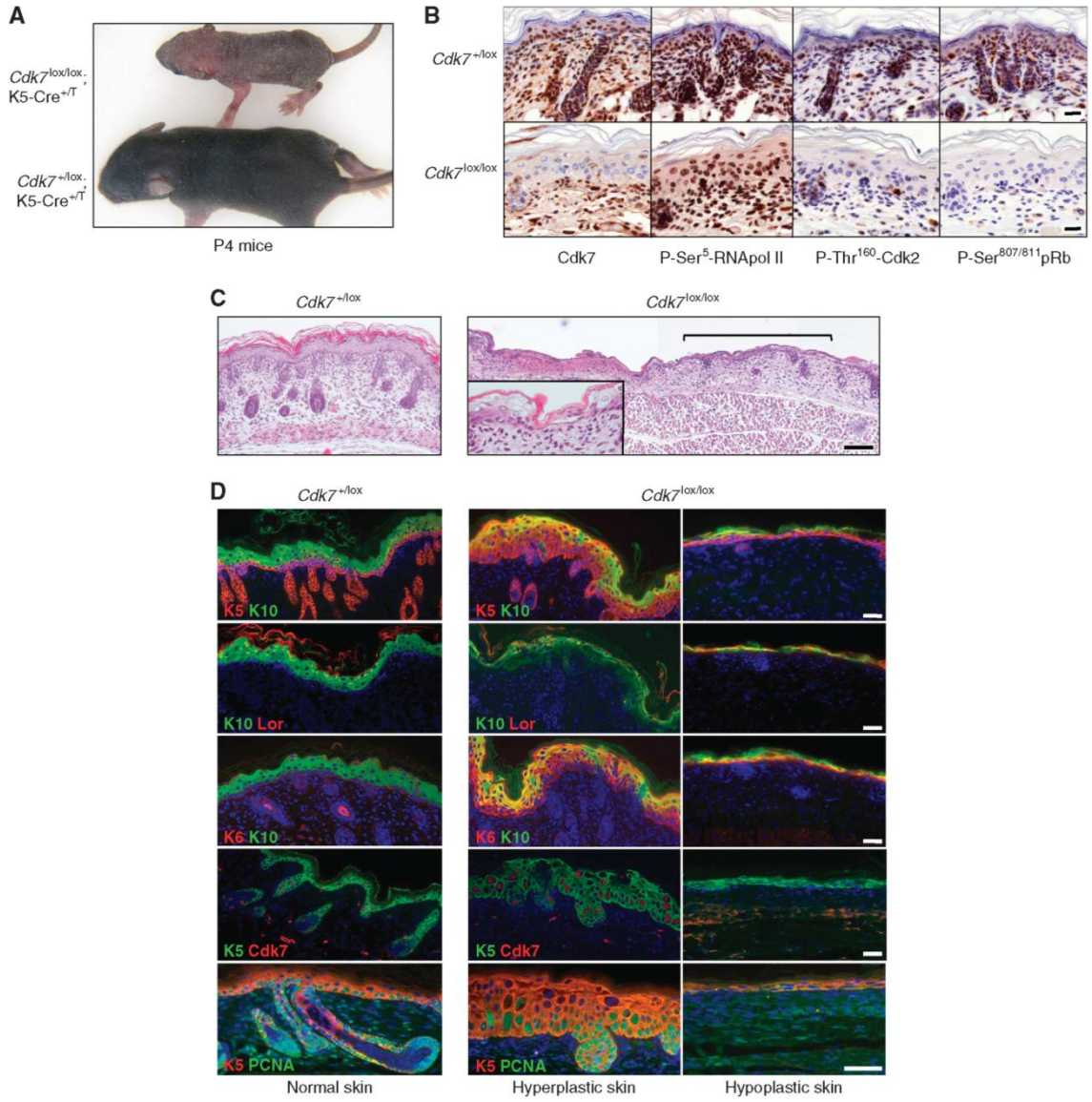

Figure 4 Cdk7 is required for skin development. (**A**) Overall appearance of $Cdk7^{+/lox}$;K5-$Cre^{+/T}$ and $Cdk7^{lox/lox}$;K5-$Cre^{+/T}$ P4 mice. (**B**) Immunohistochemical staining of representative skin areas obtained from $Cdk7^{+/lox}$;K5-$Cre^{+/T}$ and $Cdk7^{lox/lox}$;K5-$Cre^{+/T}$ P4 mice using antibodies against Cdk7, P-Ser5-RNA pol II, P-Thr160-Cdk2 and P- Ser807/811-pRb. Bar, 20 μm. (**C**) H&E staining of skin sections of $Cdk7^{+/lox}$;K5-$Cre^{+/T}$ and $Cdk7^{lox/lox}$;K5-$Cre^{+/T}$ P4 mice. Bracket indicates a hypoplastic area in the skin of a $Cdk7^{lox/lox}$;K5-$Cre^{+/T}$ P4 mouse flanked by hyperplastic regions. Inset shows a magnified image of hypoplastic skin flanked by hyperplastic areas of a $Cdk7^{lox/lox}$;K5-$Cre^{+/T}$ P4 mouse. Bar, 100 μm. (**D**) Immunofluorescence analysis of normal skin sections of $Cdk7^{+/lox}$;K5-$Cre^{+/T}$ P4 mice (left) and of hyperplastic (middle) and hypoplastic (right) skin areas of $Cdk7^{lox/lox}$;K5-$Cre^{+/T}$ P4 mice using antibodies raised against keratin K5, keratin K6, keratin K10, Cdk7, Loricrin (Lor) and PCNA. Antibodies are labelled in red or green colour according to the immunofluorescence they displayed in the corresponding sections. Bar, 50 μm.

contrary, cells within the hyperplastic regions were positive for Cdk7 expression, indicating that recombination of $Cdk7^{lox}$ alleles was not complete. Most of these Cdk7-expressing cells were also positive for PCNA, indicating that they were actively proliferating.

The hypoplastic regions displayed delayed development, thinning of the suprabasal layers as determined by keratin K10 staining and a severe reduction in the number of hair follicles (Figure 4D). Furthermore, they showed an altered differentiation pattern illustrated by the misexpression of keratin K6 in both the basal and suprabasal layers of the interfollicular epidermis (Figure 4C and D). Interestingly, keratin K6 was also misexpressed throughout the epidermis in hyperplastic areas, suggesting that these regions also experienced an altered homeostasis. Finally, hyperplastic regions were additionally characterized by an expansion of keratin K5-expressing cells to the suprabasal layers and by a concomitant disorganization of these layers as determined by

the expression pattern of keratin K10 and loricrin (Figure 4D). Altogether, these observations suggest that ablation of Cdk7 in the epidermis results in the cessation of cell proliferation leading to hypoplastic skin. As a consequence, neighbouring areas that retained Cdk7 expression due to mosaic recombination of the *Cdk7*^{lox} alleles underwent an aberrant hyperproliferative response, most likely a homeostatic attempt to compensate the lack of proliferation within the nearby hypoplastic patches.

Deletion of Cdk7 in adult mice

These results prompted us to investigate the consequences of widespread elimination of Cdk7 in adult tissues. To this end, *Cdk7*$^{+/lox}$ mice were crossed to Ub-CreERT2$^{+/T}$ animals, a transgenic strain that expresses the tamoxifen-inducible CreERT2 recombinase under the control of the human ubiquitin C promoter (Ruzankina *et al*, 2007). *Cdk7*$^{lox/lox}$;Ub-CreERT2$^{+/T}$ mice were exposed at weaning to a tamoxifen-containing diet to ablate the conditional *Cdk7* alleles. Four-month-old *Cdk7*$^{lox/lox}$;Ub-CreERT2$^{+/T}$ animals were phenotypically normal in spite of lacking Cdk7 expression in most (>90%) cells within low proliferating tissues such as liver, kidney or cerebellum (Figure 5A). These mice exhibited normal physiological levels of several key biochemical parameters in plasma including glucose, amylase, bilirubin, albumin and alanine aminotransferase (Supplementary Figure 4). Other parameters such as total protein, globulin, calcium, phosphate and ureic nitrogen also remained at normal levels in *Cdk7*$^{lox/lox}$;Ub-CreERT2$^{+/T}$ animals (Supplementary Figure 4). Similar results were obtained when we analysed the endocrine pancreas. *Cdk7*$^{lox/lox}$;Ub-CreERT2$^{+/T}$ mice had the same pattern of insulin and glucagon-expressing cells as control *Cdk7*$^{+/lox}$;Ub-CreERT2$^{+/T}$ animals, in spite of the fact that most of these cells lacked Cdk7 expression (Figure 5B). As illustrated above in newborn skin (Figure 4B), the levels of phosphorylated Ser5 residues in RNA pol II of *Cdk7*$^{lox/lox}$;Ub-CreERT2$^{+/T}$ mice were unaffected by the loss of Cdk7 expression in all tissues examined (Figure 5A). Phosphorylation levels of Cdk1^{T161} and Cdk2^{T160} could not be determined as these proteins are not expressed in the large majority of cells (>98%) in these non-proliferating tissues (data not shown).

Loss of Cdk7 expression in actively dividing tissues results in accelerated aging

Cdk7$^{lox/lox}$;Ub-CreERT2$^{+/T}$ animals retained Cdk7 expression in their proliferating tissues such as the intestine and skin, even when exposed to the tamoxifen diet for 7 months (Figure 6A). An observation that might explain the relatively long survival of these mice (Supplementary Figure 5B). Expression of Cdk7 in these highly proliferating tissues was not due to impaired recombination of their *Cdk7*^{lox} alleles as they were efficiently ablated in heterozygous *Cdk7*$^{+/lox}$;Ub-CreERT2$^{+/T}$ mice exposed to the same diet (Supplementary Figure 5A). To explain these observations, we hypothesized that the presence of Cdk7 in these proliferating tissues might be due to an active process of cell renewal sustained by a pool of adult stem cells that had retained Cdk7 expression. If so, such a continuous demand on adult stem cells should result in their premature exhaustion leading to the appearance of aging-like phenotypes (Krishnamurthy and Sharpless, 2007). Indeed, visual inspection of 8-month-old

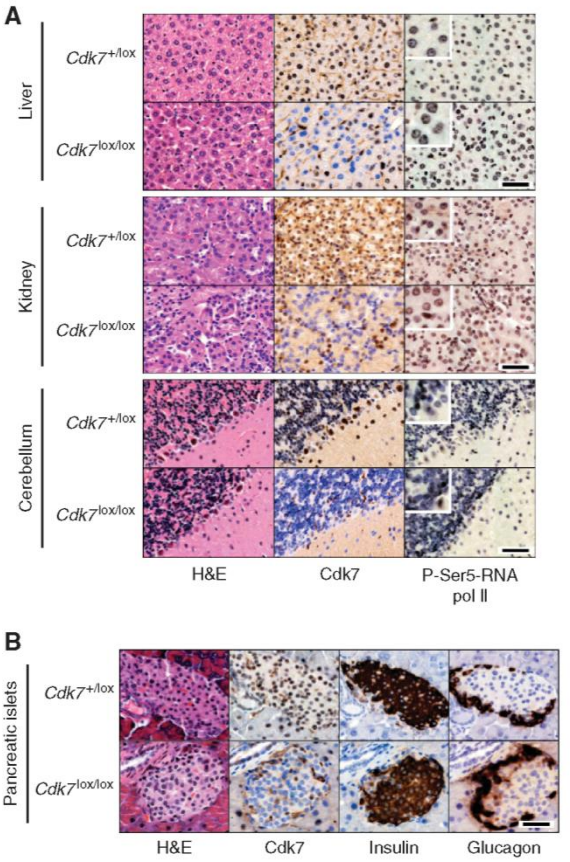

Figure 5 Lack of physiological defects upon Cdk7 elimination in young mice. (**A**) H&E and immunochemical staining of sections obtained from liver (top), kidney (middle) and cerebellum (bottom) of 4-month-old *Cdk7*$^{+/lox}$;Ub-CreERT2$^{+/T}$ and *Cdk7*$^{lox/lox}$;Ub-CreERT2$^{+/T}$ littermates exposed to a tamoxifen diet for 3 months. Immunostaining was carried out with antibodies elicited against Cdk7 and against P-Ser5-RNA pol II. Insets show magnified images of representative areas. Bar, 50 μm. (**B**) H&E and immunochemical staining of consecutive sections of pancreatic islets obtained from 4-month-old *Cdk7*$^{+/lox}$;Ub-CreERT2$^{+/T}$ and *Cdk7*$^{lox/lox}$;Ub-CreERT2$^{+/T}$ littermates exposed to a tamoxifen diet for 3 months. Immunostaining was carried out with antibodies elicited against Cdk7, insulin and glucagon. Bar, 50 μm.

Cdk7$^{lox/lox}$;Ub-CreERT2$^{+/T}$ mice exposed to a tamoxifen diet as weaning revealed a variety of age-related phenotypes not present in *Cdk7*$^{+/lox}$;Ub-CreERT2$^{+/T}$ control littermates (Figure 6B). These phenotypes included a significant body weight loss, with *Cdk7*$^{lox/lox}$;Ub-Cre$^{+/T}$ females weighing an average of 30% less than the control animals ($14.36 \pm 2.63\,g$ versus $20.27 \pm 1.28\,g$; $n=8$; $P<0.001$), diffuse alopecia, pervasive hair-greying and kyphosis (Figure 6B).

Further characterization of these mice revealed additional age-related phenotypes affecting bones, hematopoietic and intestinal tissues as well as skin. Densitometric analysis of the femurs of *Cdk7*$^{lox/lox}$;Ub-CreERT2$^{+/T}$ animals revealed that their mineral content was significantly reduced compared with that of control littermates ($0.33 \pm 0.003\,g$ versus $0.41 \pm 0.021\,g$; $n=4$; $P<0.001$). Furthermore, computed tomography (CT) scanning revealed that the cortical cross section (0.40 mm ± 0.009 versus 0.54 mm ± 0.03; $n=4$;

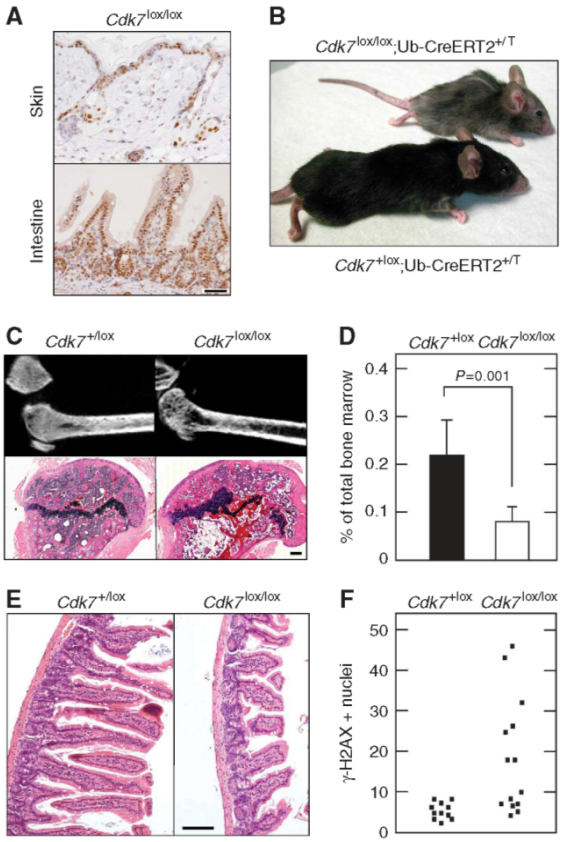

Figure 6 Widespread elimination of Cdk7 expression in adult mice results in premature aging. (**A**) Immunochemical staining of skin (top) and the small intestine (bottom) from 8-month-old *Cdk7*$^{lox/lox}$;Ub-CreERT2$^{+/T}$ animals exposed to a tamoxifen diet for 7 months. Bar, 50 μm. (**B**) Overall appearance of 8-month-old *Cdk7*$^{+/lox}$;Ub-CreERT2$^{+/T}$ mice and *Cdk7*$^{lox/lox}$;Ub-CreERT2$^{+/T}$ littermates exposed to a tamoxifen diet for 7 months. (**C**) Micro-CT analysis of femurs (top) and H&E staining of femur sections (bottom) obtained from 8-month-old *Cdk7*$^{+/lox}$;Ub-CreERT2$^{+/T}$ and *Cdk7*$^{lox/lox}$;Ub-CreERT2$^{+/T}$ littermates exposed to a tamoxifen diet for 7 months. Bar, 100 μm. (**D**) Quantification of hematopoietic Lin^{-}Sca-1^{+}c-Kit^{hi} progenitors in the bone marrow of *Cdk7*$^{+/lox}$;Ub-CreERT2$^{+/T}$ (solid bar, $n=5$) and *Cdk7*$^{lox/lox}$;Ub-CreERT2$^{+/T}$ (open bar, $n=7$) littermates exposed to a tamoxifen diet for 7 months. Data shown as mean ± s.d. A student's *t*-test was used to calculate statistical significance. (**E**) H&E staining of small intestine sections of *Cdk7*$^{+/lox}$;Ub-CreERT2$^{+/T}$ and *Cdk7*$^{lox/lox}$;Ub-CreERT2$^{+/T}$ littermates exposed to a tamoxifen diet for 7 months. Bar, 100 μm. (**F**) Number of cells showing positive nuclei for γ-H2AX phosphorylation in liver sections of *Cdk7*$^{+/lox}$;Ub-CreERT2$^{+/T}$ and *Cdk7*$^{lox/lox}$;Ub-CreERT2$^{+/T}$ littermates exposed to a tamoxifen diet for 7 months. Each dot represents the total number of nuclei with positive staining in 20 microscope fields. Positive cells were detected by immunohistochemistry.

$P<0.001$) and the trabecular bone content were also reduced in the *Cdk7*$^{lox/lox}$;Ub-CreERT2$^{+/T}$ cohort (Figure 6C). In addition, some of the bone marrow had been replaced by adipose tissues (Moerman *et al*, 2004).

Eight-month-old *Cdk7*$^{lox/lox}$;Ub-CreERT2$^{+/T}$ mice exposed to tamoxifen diet also had reduced levels of Lin^{-}Sca-1^{+}c-Kit^{hi} hematopoietic progenitors (Figure 6D), hypoplastic crypts and villi in the small intestine (Figure 6E) and increased the number of hepatocytes with positive staining for phosphorylated histone γ-H2AX (Figure 6F, Ruzankina *et al*, 2007; Matheu *et al*, 2007). All *Cdk7*$^{lox/lox}$;Ub-CreERT2$^{+/T}$ mice examined ($n=8$) a displayed progressive nephropathy and severe medullary calcification, two age-related defects that were only marginally present in some *Cdk7*$^{+/lox}$;Ub-CreERT2$^{+/T}$ control littermates (Supplementary Figure 5C, Chuttani and Gilchrest, 1995; Haines *et al*, 2001). Finally, skin tissue also showed phenotypic marks associated with premature aging, including reduced dermal thickness, loss of the subcutaneous adipose layer and transformation of follicular epithelium into sebaceous glands (Figure 7A and B). Interestingly, most of the physiological parameters of these 8-month-old *Cdk7*$^{lox/lox}$;Ub-CreERT2$^{+/T}$ mice, including key biochemical factors in plasma as well as levels of globulin, calcium, phosphate and ureic nitrogen, remained mostly unaffected (Supplementary Figure 4).

Stem cell exhaustion in Cdk7 depleted skin

As reasoned above, these ageing phenotypes are likely to result from the exhaustion of stem cell compartments that have retained Cdk7 expression. As illustrated in Figure 7A, the bulge region of the hair follicles of *Cdk7*$^{lox/lox}$;Ub-CreERT2$^{+/T}$ mice were almost deprived of epithelial stem cells characterized by coexpression of keratin K15 and CD34 (Lyle *et al*, 1998; Blanpain *et al*, 2004). Progressive shortening of telomeres is a hallmark associated with persistent cell division that parallels a decline in stem cell functionality (Flores *et al*, 2008; Flores and Blasco, 2010). Thus, telomere length may serve as a marker to determine whether the reduced number of stem cells in the skin of *Cdk7*$^{lox/lox}$;Ub-CreERT2$^{+/T}$ mice arose as a consequence of stem cell exhaustion. As shown in Figure 7C, quantitative telomere Q-FISH analysis revealed a significant reduction in the average telomere length in the skin cells of *Cdk7*$^{lox/lox}$;Ub-CreERT2$^{+/T}$ mice compared with those of *Cdk7*$^{+/lox}$;Ub-CreERT2$^{+/T}$ littermate controls. Furthermore, the overall distribution of telomere length in *Cdk7*$^{lox/lox}$;Ub-CreERT2$^{+/T}$ skin was shifted towards undersized values with a substantial increase in the percentage of short telomeres (Figure 7D and E). This difference is maximized when the skin telomere length is normalized to that of a non-proliferative tissue (Figure 7F), thus arguing that indeed telomere shortening occurred as a consequence of increased proliferative demand and not as a cell autonomous defect associated to Cdk7 elimination. Notably, the increased frequency of short telomeres, rather than the mean telomere length, is particularly determinant for telomere dysfunction and correlates with aging phenotypes (Hemann *et al*, 2001; Canela *et al*, 2009). Altogether, these observations indicate that skin cells of *Cdk7*$^{lox/lox}$;Ub-CreERT2$^{+/T}$ mice have endured an extended proliferative period, most likely to compensate for those cells that lost their proliferative capacity due to inactivation of their *Cdk7*^{lox} alleles.

Discussion

In this study, we have provided genetic evidence indicating that Cdk7, the catalytic subunit of the trimeric CAK complex, is essential for cell proliferation. Indeed, Cdk7 is essential for activation of the cell cycle through phosphorylation of key threonine residues in the T-loops of the Cdks. In contrast,

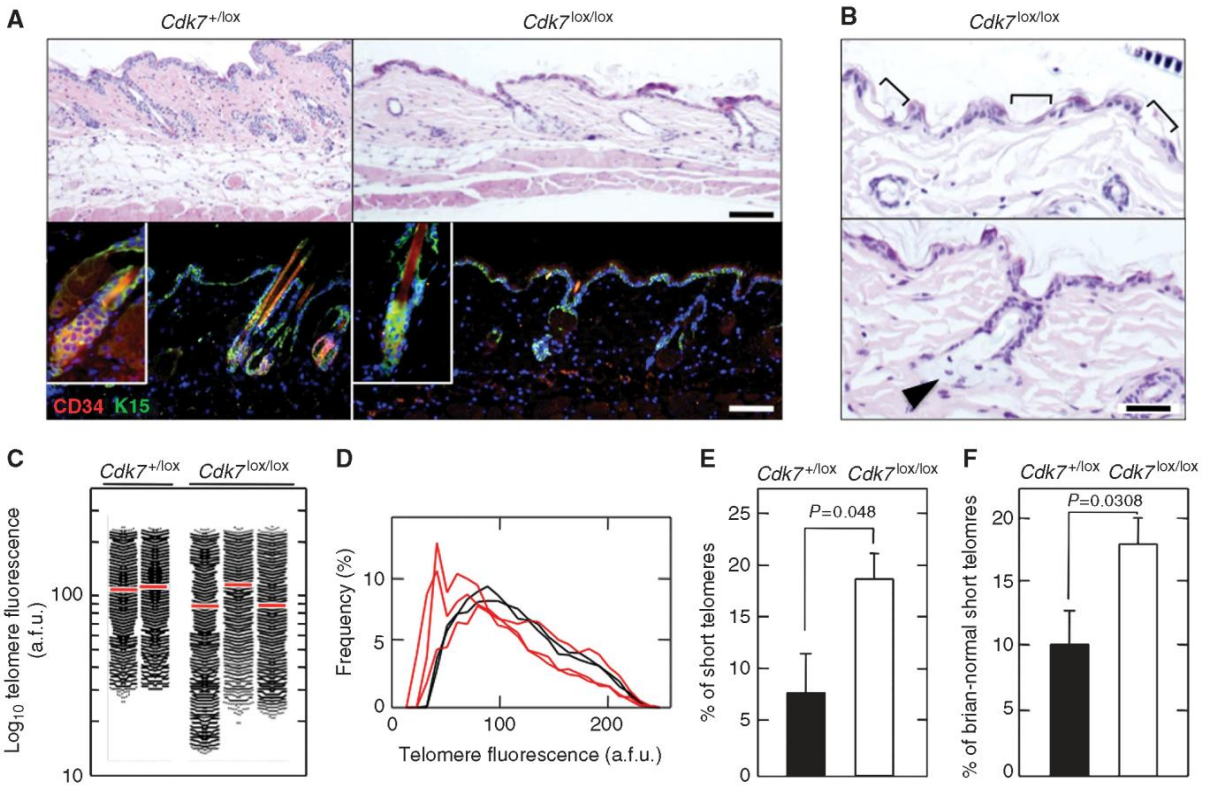

Figure 7 Loss of Cdk7 in the epidermis causes stem cell depletion and telomere shortening. (**A**) H&E (top) and immunuofluorescence (bottom) staining using antibodies against CD34 and keratin K15 of representative skin areas from 8-month-old $Cdk7^{+/lox}$;Ub-CreERT2$^{+/T}$ and $Cdk7^{lox/lox}$;Ub-CreERT2$^{+/T}$ mice exposed to a tamoxifen diet for 7 months. Antibodies are labelled in red or green colour according to the immunofluorescence they displayed in the corresponding sections. Insets show magnified images to illustrate that the stem cell pool of the hair bulge is mostly exhausted in $Cdk7^{lox/lox}$;Ub-CreERT2$^{+/T}$ mice. Bar, 100 μm. (**B**) Magnified images of skin areas of $Cdk7^{lox/lox}$;Ub-CreERT2$^{+/T}$ mice to illustrate extreme epidermal thinning (brackets) (top) and conversion of hair follicles into adipose tissue (arrowhead) (bottom). Bar, 50 μm. (**C**) Telomere Q-FISH analysis of skin sections of 8-month-old $Cdk7^{+/lox}$;Ub-CreERT2$^{+/T}$ and $Cdk7^{lox/lox}$;Ub-CreERT2$^{+/T}$ mice exposed to a tamoxifen diet for 7 months. Red bars indicate average telomere fluorescence intensity. a.f.u., arbitrary fluorescence units. (**D**) Q-FISH histograms showing telomere fluorescence frequencies of data shown in **C** for $Cdk7^{+/lox}$;Ub-CreERT2$^{+/T}$ (black) and $Cdk7^{lox/lox}$;Ub-CreERT2$^{+/T}$ (red) mice. (**E**) Percentage of short telomeres (intensity ⩽10th percentile) in the skin of $Cdk7^{+/lox}$;Ub-CreERT2$^{+/T}$ (solid bar; $n=5$) and $Cdk7^{lox/lox}$;Ub-CreERT2$^{+/T}$ (open bar; $n=6$) littermates. Data shown as mean ± s.d. A student's *t*-test was used to calculate statistical significance. (**F**) Percentage of short telomeres (intensity ⩽10th percentile) in skin upon normalization to their respective brain values from $Cdk7^{+/lox}$;Ub-CreERT2$^{+/T}$ (solid bar; $n=4$) and $Cdk7^{lox/lox}$;Ub-CreERT2$^{+/T}$ (open bar; $n=4$) littermates. Data shown as mean ± s.d. A student's *t*-test was used to calculate statistical significance.

Cdk7 is completely dispensable for phosphorylation of the critical Ser5 residue located in the CTD of RNA pol II and for regulating overall transcription. These results are reminiscent of those previously obtained for Mat1, one of the regulatory subunits of the CAK complex (Rossi *et al*, 2001; Korsisaari *et al*, 2002), and with previous findings in lower organisms in which RNA pol II-mediated transcription is only marginally affected upon elimination of Cdk7 activity (Larochelle *et al*, 1998; Lee *et al*, 2005; Wallenfang and Seydoux, 2002).

Genetic inactivation of $Cdk7^{lox}$ alleles led to a loss of T-loop phosphorylation, damped Cdk activity and cell cycle arrest. Indeed, the Cdk1 and Cdk2 T-loop phosphomimetic mutants, Cdk1^{T161E} and Cdk2^{T160E}, partially restored proliferation in cells deprived of Cdk7. These observations suggest that the inability of Cdk7-defficient cells to proliferate could be explained by the lack of Cdk1 activity. However, the mechanism by which Cdk2^{T160E} induces cell proliferation in the absence of Cdk7 is less clear as previous genetic studies have demonstrated that Cdk2 is completely dispensable for cell division (Berthet *et al*, 2003; Ortega *et al*, 2003). The presence of active P-Thr161-Cdk1 in Cdk2^{T160E}-expressing $Cdk7^{mut/mut}$ cells suggests that Cdk2^{T160E}, either directly or indirectly, induces phosphorylation of the T-loop of Cdk1. Whether Cdk2 plays a role in the activation of Cdk1 in normal cells expressing Cdk7 remains to be determined.

Loss of Cdk7 also contributes to cell cycle arrest by decreasing the E2F-controlled transcription levels, including genes essential for cell cycle progression such as CycA2 and Cdk1. In view of the lack of effect of Cdk7 on RNA pol II-driven global transcription, the decreased levels of expression of E2F-controlled genes is most likely a consequence of the decreased Cdk activity and subsequent hypophosphorylation of the pocket proteins. These observations are reminiscent of those observed in *S. pombe* where loss of Mcs6, the Cdk7 orthologue, showed a modest effect on global gene expression while selectively affected the expression of a cell-division cluster (Lee *et al*, 2005). Indeed, inactivation of the three Rb family members by ectopic expression of the SV40 T121 fragment

restored the proliferation of Cdk7-deficient MEFs. Interestingly, these T121-expressing *Cdk7*$^{mut/mut}$ cells displayed normal levels of P-Thr161-Cdk1 and P-Thr160-Cdk2.

Our results cannot rule out a requirement of Cdk7 for transcription of E2F-controlled genes. Yet, we favour the concept that E2F-mediated transcription is only affected indirectly upon Cdk7 ablation due to an overall decrease in Cdk activity and hypophosphorylation of pRb. The lack of effect on RNA pol II-mediated transcription might simply reflect the compensation of Cdk7 function by other kinases. Indeed, several proteins, including the closely related Cdk9, have been reported to phosphorylate Ser5 in the CTD of RNA pol II (Palancade and Bensaude, 2003). Furthermore, inhibition of Cdk7 and Cdk9 is concomitantly required to eliminate Ser5 phosphorylation of RNA pol II (Ni *et al*, 2004). In fact, activation of Cdk9 does not rely on Cdk7 and therefore would remain active following CAK inhibition (Kim and Sharp, 2001).

Embryos lacking Cdk7 developed to peri-implantation stages before undergoing massive apoptosis. These observations are reminiscent of those obtained upon ablation of the Mat1 regulatory subunit (Rossi *et al*, 2001). However, Cdk7 mutant embryos do not require expression of the maternal Cdk7 protein. *In vitro*, these embryos also progressed to the blastocyst stage, but at E6.5 their ICM cells underwent apoptotic death. As Cdk1 activity is essential during the first cell divisions (Santamaría *et al*, 2007), these observations suggest that early embryonic stem cells may have alternative mechanisms to activate Cdk1. Trophoblasts also developed in the absence of Cdk7 but the small size of their nuclei suggests that they have reduced endoreplication cycles, a phenomenon also observed in *Mat1* knockout embryos (Rossi *et al*, 2001).

Selective inactivation of *Cdk7*^{lox} alleles in skin during embryonic development resulted in defective Cdk phosphorylation, hypophosphorylation of the pocket proteins and proliferative arrest. However, phosphorylation of the Ser5 residue of RNA pol II was unaffected, thus extending the results obtained with cultured MEFs. Skin areas lacking Cdk7 displayed an altered differentiation pattern and a severe reduction in the number of hair follicles. Interestingly, adjacent regions in which the *Cdk7*^{lox} alleles had not undergone genetic recombination exhibited a hyperplastic phenotype, most likely a compensatory response to the defects present in the neighbouring hypoplastic areas.

Widespread loss of Cdk7 expression in young adult mice did not lead to an obvious phenotype. Interestingly, low proliferative organs such as liver, kidney or brain displayed normal histology and the animals maintained standard levels of physiological parameters in spite of extensive loss of Cdk7 expression in these tissues thus, suggesting that Cdk7 is not essential to maintain cellular homeostasis in low proliferating organs. In contrast, highly proliferative tissues such as intestine or skin retained Cdk7 expression in most of their cells. These observations were not due to inefficient recombination of the *Cdk7*^{lox} alleles as the heterozygous *Cdk7*$^{+/lox}$; Ub-CreERT2$^{+/T}$ mice displayed a widespread occurrence of recombined *Cdk7*^{mut} alleles. Instead, these findings must be a consequence of the efficient replacement of cells lacking Cdk7 by cells derived from a pool of stem cells that had retained expression of this kinase, thereby maintaining normal organ function. This hypothesis would predict that as mice age, these pools of Cdk7-expressing stem cells should become exhausted. Indeed, *Cdk7*$^{lox/lox}$;Ub-CreERT2$^{+/T}$ mice exposed to a continuous tamoxifen diet developed a variety of age-related phenotypes including diffuse alopecia, pervasive hair-greying and kyphosis. Moreover, these mice underwent premature death with $<20\%$ of the animals surviving more than a year.

Detailed examination of their tissues revealed defects characteristic of premature aging such as decreased bone mineral content, accumulation of fat cells in the bone marrow and presence of hepatocytes positive for phosphorylated histone γ-H2AX. In addition, *Cdk7*$^{lox/lox}$;Ub-CreERT2$^{+/T}$ mice presented hypoplastic crypts and villi in the small intestine, as well as progressive nephropathy and severe medullary calcification in their kidneys. Their skin also presented phenotypic marks associated with premature aging including reduced dermal thickness, loss of subcutaneous adipose layer and transformation of follicular epithelium into sebaceous glands. Moreover, the bulge region of the hair follicles had limited numbers of progenitor cells. Finally, the substantial increase in the percentage of short telomeres in the epidermis (Figure 7) reinforces the hypothesis that the stem cell pool in adult *Cdk7*$^{lox/lox}$;Ub-Cre$^{+/T}$ animals has endured an extended proliferative period.

Activation of tissue renewal in adult mice devoid of Cdk7 relies entirely on physiological signals. Therefore, the mobilization of progenitor pools required to maintain homeostasis in highly proliferative tissues upon Cdk7 elimination may provide a useful tool for the identification of adult stem cell niches by lineage tracing experiments. Finally, Cdk7 has been considered a putative therapeutic target to inhibit tumour development (Fisher, 2005). The maintenance of normal physiological parameters by critical tissues such as liver, kidney or the endocrine pancreas in the absence of Cdk7 suggests that Cdk7 inhibitors may not cause a significant toxicity, providing that they are not administered for long periods of time. Yet, the potential use of such inhibitors may depend on the relative ability of adult stem cells to replenish highly proliferating tissues versus cancer stem cells to replace Cdk7-deficient tumour cells. Conditional ablation of the *Cdk7*^{lox} alleles described here in well-defined mouse tumour models should help to evaluate the therapeutic potential of Cdk7 as a cancer target.

Materials and methods

Mouse strains

All animal experiments were approved by the CNIO Ethical Committee and performed in accordance with the guidelines stated in the International Guiding Principles for Biomedical Research Involving Animals, developed by the Council for International Organizations of Medical Sciences (CIOMS). *Cdk7*$^{+/loxfrt}$ mice were generated from an ES cell clone (Ref D032B11) purchased from the German Gene Trap Consortium (Schnütgen *et al*, 2005). The *Cdk7*^{loxfrt} allele carries the genetrap vector in the active orientation and prevents *Cdk7* gene expression (Supplementary Figure 1). To generate the *Cdk7*$^{+/lox}$ strain, *Cdk7*$^{+/loxfrt}$ mice were crossed to the ACTB-FLPe tool strain that expresses the FLPe recombinase in the germ line to invert the genetrap to allow reexpression of the targeted allele (Supplementary Figure 1; Rodríguez *et al*, 2000). *Cdk7*$^{+/lox}$ and *Cdk7*$^{lox/lox}$ mice were crossed to the K5-Cre and Ub-CreERT2 transgenic strains to eliminate the expression of *Cdk7* alleles via Cre-mediated recombination. This allele has been designated as *Cdk7*^{mut} to indicate that it retains all the *Cdk7* genomic sequences, yet it does not produce detectable *Cdk7* transcripts or Cdk7 protein

(Supplementary Figure 1C and Figure 1, respectively). To induce CreERT2-mediated recombination in *Cdk7*$^{lox/lox}$;Ub-CreERT2$^{+/T}$ mice, animals were fed *ad libitum* with tamoxifen-containing diet (Harland-Tekald CRD TAM^{400}) starting after weaning (P21-P30). The K5-Cre and Ub-CreERT2 strains have been described elsewhere (Tarutani *et al*, 1997; Ruzankina *et al*, 2007).

Genotyping

Primers used for genotyping these *Cdk7* alleles included primers ExN (5′-GTTCCTTACCCCATCATCTGTCAC-3′) and Ex12RC (5′-GTTG CCCAGGGGGAATAAAGG-3′) for amplification of the wild-type *Cdk7* allele (310 bp); primers IntL (5′-GGAGACTCTTGCAAAAA CTAACCCCACCTC-3′) and B40 (5′-GGGTCGATGGTGATGCTTGGCA ATTC-3′) for amplification of the *Cdk7*^{loxfrt} allele (650 bp); and primers ExN and B48 (5′-TCCCACTGTCCTTTCCTAATAA-3′) for amplification of the *Cdk7*^{lox} allele (852 bp). Primers CreF (5′-CCC GCAGAACCTGAAGATGT-3′) and CreR (5′-GTTCGAACGCTAGAGCC TGTTT-3′) were used to genotype the K5-Cre and Ub-CreERT2 transgenes (220 bp). All alleles were amplified as follows: 94°C for 2 min; 35 cycles at 94°C for 30 s; 60°C for 30 s; 72°C for 30 s and then followed by 72°C for 10 min.

Real-time PCR analysis

Cdk7 mRNA levels were assayed using Power SYBR® Green PCR Master Mix (Applied Biosystems). Primers detecting Cdk7 wild-type mRNA: Cdk7-FW1 (located in exon 2, 5′-CAGTTTGCGACGGTCTA-TAAGG-3′), Cdk7-RV4 (located in exon 3, 5′-GCTTTATCTCCCTT-AAGGCTGTTC-3′). β-Actin mRNA levels were used as internal controls. The following β-Actin mRNA primers were used: β-Actin-QRT5 (5′-GACGGCCAGGTCATCACTATTG-3′) and β-Actin-QRT3 (5′-AGGAAGGCTGGAAAAGAGCC-3′).

In vivo imaging

Bone mineral analysis from total body imaging was carried out with the help of dual-energy X-ray absorptiometry (DEXA) using a Lunar PIXImus Densitometer (GE Medical Systems). Acquisition time was 5 min with 2% isofluorane as inhalatory anaesthesia. The analysis of bone mineral density was performed using a manual region of interest (ROI) in the femur. For the analysis of the trabecular area, the femur was imaged using the eXplore Locus micro-CT scanner (GE Healthcare). The reconstructed images were viewed and analysed using MicroView 2.2 Advanced Bone Analysis software (ABA, GE Healthcare). The isotropic resolution was set to 45 μm. The micro-CT image acquisition consisted of 400 projections collected in one full rotation of the gantry in ~10 min. The X-ray tube settings were 80 kV and 450 μA. The resulting raw data were reconstructed to a final image volume of 875 × 875 × 465 slices at (93 μm^3) voxel dimensions. The reconstructed slices were output in the CT manufacturer's raw format and were corrected to Hounsfield units.

Immunofluorescence

Embryos were fixed with cold methanol during 15 min at −20°C, washed in PBS containing 4% BSA, blocked with PBS containing 4% BSA for 1 h and incubated with primary antibodies for 90 min at 37°C. Secondary antibodies carrying Alexa 488, 594 or 647 fluorochromes were obtained from Molecular Probes (Invitrogen). Embryos were transferred to Vectashield mounting medium (Vector) on μClear plates (Greiner) for image acquisition. Images were obtained using a confocal ultra-spectral microscope (Leica TCS-SP5-AOBS-UV). For trophoblast analysis, embryos were grown on μClear plates and were allowed to hatch. Nuclear volumes were calculated on confocal images using ImageJ software. Antibodies used included anti Cdk7 (sc-7344, Santa Cruz), Nanog (NB100-588, Novus) and BrdU (RPN202, GE Healthcare). Nuclei were stained with Hoechst 33342 (Invitrogen). Embryos were genotyped by nested PCR, following immunofluorescence staining and confocal analysis.

Cell culture assays

MEFs were isolated from E13.5 embryos of the corresponding genotype and propagated according to standard 3T3 protocols. For proliferation assays, 500 cells were plated in 96-well plates in DMEM supplemented with 10% fetal bovine serum and their growth rate determined by the MTT 'Cell proliferation kit' (Roche). To obtain *Cdk7*$^{mut/mut}$ MEFs, *Cdk7*$^{lox/lox}$ MEFs were infected with Ad-Cre (Supplementary Figure 1). All *Cdk7*$^{mut/mut}$ MEFs were positive upon X-Gal staining demonstrating that the genetrap is integrated in the active orientation. These MEFs failed to express detectable levels of Cdk7 protein. (Figure 1A and Supplementary Figure 2C). Adenoviral infections were performed using a MOI of 150. The Cdk7^{T170A}, Cdk7^{K41A}, Cdk4^{T174E}, Cdk6^{T177E}, Cdk2^{T160E} and Cdk1^{T161E} mutants were generated using the QuickChange site directed mutagenesis kit (Stratagene) and delivered by retroviral infection. For labelling of cellular proteins, 5×10^5 MEFs were seeded in triplicate in six-well plates 1 week after infection with Ad-GFP or Ad-Cre particles and serum starved for 72 h. MEFs were then incubated in the presence of 100 μ Ci ^{35}S-protein labelling mix (Amersham) for 2 and 4 h. Cells were washed twice with PBS and lysed with 1% Triton X-100 PBS buffer. Total protein was precipitated from lysates with 10% TCA. Pellets were subjected to liquid scintillation counting to measure incorporated radioactivity.

Gene expression analysis

MEFs were infected with Ad-Cre or Ad-GFP particles and harvested after 1 week in culture. Cells were tripsinized and re-plated as necessary to maintain sub-confluent cultures. RNA was extracted using RNeasy kit (Quiagen). RNA integrity was assayed by Lab-chip technology on an Agilent 2100 Bioanalyzer. One microgram per sample was labelled with 'Two-Color Microarray-Based Gene Expression Analysis (Agilent)' and purified with silica-based RNeasy spin columns (Qiagen). Samples were hybridized to Mouse WMG 4 × 44K (Agilent). Microarrays were scanned on a G2565C DNA microarray scanner (Agilent). Images were quantified using Agilent Feature Extraction Software (version 10.1.1). Microarray background subtraction was carried out using normexp method. To normalize the data set, we performed loess within arrays normalization and quantiles between arrays normalization. Differentially expressed genes were obtained by applying linear models with R limma package (Smyth *et al*, 2005) available at the Bioconductor Project (http://www.bioconductor.org). To account for multiple hypotheses testing, the estimated significance level (*P* value) was adjusted using Benjamini & Hochberg false discovery rate (FDR) correction. Those genes with FDR <0.05 were selected as differentially expressed between Ad-Cre- and Ad-GFP-infected cultures. GSEA was applied using annotations from a curated version of Biocarta, KEGG (Reactome, GenMapp). Custom gene sets were built from literature (Bracken *et al*, 2004; Eisenberg and Levanon, 2003). Genes were ranked based on limma-moderated *t* statistic. After Kolmogorov–Smirnoff testing, those gene sets showing FDR <0.25, a well-established cut-off for the identification of biologically relevant gene sets (Subramanian *et al*, 2005), were considered enriched between classes under comparison. Microarray experiments data have been deposited at the NCBI Gene Expression Omnibus (GEO) database and are freely accessible: GSE36050.

Histopathology and immunostaining

For routine histological analysis, tissues were fixed in 10%-buffered formalin (Sigma) and embedded in paraffin. Immunohistochemical staining was performed on 3–4 μm paraffin sections. Antibodies used included those elicited against Cdk7 (sc-7344, Santa Cruz), P-Thr160-Cdk2 (2561, Cell Signalling), P-Ser5-RNA pol II (H14, Covance), P- Ser807/811-pRb (9308, Cell Signalling), Insulin (A0564, Dako), Glucagon (G2654, Sigma) and phosphorylated γ-H2AX (05-636, Millipore). Immunofluorescence staining of skin sections was performed with the following antibodies: Cdk7 (sc-7344, Santa Cruz), keratin K5 (PRB-160, Covance), keratin K6 (PRB-169, Covance), keratin K10 (M7002, Dako), loricrin (PRB-145, Covance) and PCNA (PC10, Thermo Scientific).

Protein analysis

Cell pellets were processed for western blotting and kinase assays, as previously described (Santamaría *et al*, 2007). Primary antibodies used included those elicited against Cdk7 (sc-7344, Santa Cruz), Cdk2, Cdk4 and Cdk6 (our own rabbit polyclonals), P-Thr160-Cdk2 (2561, Cell Signalling), Cdk1 (sc-54, Santa Cruz), P-Thr161-Cdk1 (9114, Cell Signalling), Mat1 (sc-13142, Santa Cruz), CycH (2927, Cell Signalling), pRb (554136, BD Pharmingen), P-Ser807/811-pRb (9308, Cell Signalling), RNA pol II (8WG16, Covance), p-Ser5-RNA pol II (H14, Covance) and GAPDH (Sigma).

Supplementary data
Supplementary data are available at *The EMBO Journal* Online (http://www.embojournal.org).

Acknowledgements

We thank C Timón, MC González, M San Román and R Villar for their excellent technical assistance. We thank EJ Brown (Abramson Family Cancer Research Institute, University of Pennsylvania School of Medicine, Philadelphia) and J Takeda (Osaka University) for kindly providing the Ub-CreERT2 and K5-Cre transgenic mice, respectively. Work in the laboratory of MB was supported by grants from the EU-Framework Programme (LSHG-CT-2007-037665), European Research Council (ERC-AG/250297-RAS AHEAD), Spanish Ministry of Science and Innovation (MICINN) (SAF2006-11773 and CSD2007-00017), Autonomous Community of Madrid (GR/SAL/0587/2004 and S2006/BIO-0232) and *Fundación de la Mutua Madrileña del Automóvil*. MG was supported by an FPU fellowship (MICINN). Work in the laboratory of JMP was supported by grants from the MICINN (SAF2006-00121 and SAF2011-26122-C02-01), Autonomous Community of Madrid (S2006/BIO-0232) and Spanish Ministry of Health (ISCIII-RETIC RD06/0020/0029). MB is an AXA-CNIO Professor of Molecular Oncology.

Author contributions: DS and MB supervised the entire project and designed the experiments together with MG and JMP. DS and MB wrote the manuscript with comments from co-authors. MG generated and characterized all mouse strains and carried out most of the experiments. CS performed skin immunofluorescence studies. MC was responsible for histopathological analysis. DP and GG analysed microarray data. MAB and RS performed telomeric length analysis.

Conflict of interest

The authors declare no conflict of interest.

References

Berthet C, Aleem E, Coppola V, Tessarollo L, Kaldis P (2003) Cdk2 knockout mice are viable. *Curr Biol* **13:** 1775–1785

Blanpain C, Lowry WE, Geoghegan A, Polak L, Fuchs E (2004) Self-renewal, multipotency, and the existence of two cell populations within an epithelial stem cell niche. *Cell* **118:** 635–648

Bracken AP, Ciro M, Cocito A, Helin K (2004) E2F target genes: unraveling the biology. *Trends Biochem Sci* **29:** 409–417

Canela A, Vera E, Klatt P, Blasco MA (2009) High-throughput telomere length quantification by FISH and its application to human population studies. *Proc Natl Acad Sci USA* **104:** 5300–5305

Chuttani A, Gilchrest BA (1995) Aging. In *Handbook of Physiology*, Masoro EJ (ed) pp 309–324. Oxford Univ. Press, New York

Eisenberg E, Levanon EY (2003) Human housekeeping genes are compact. *Trends Genet* **19:** 362–365

Fisher RP (2005) Secrets of a double agent: CDK7 in cell-cycle control and transcription. *J Cell Sci* **118:** 5171–5180

Flores I, Blasco MA (2010) The role of telomeres and telomerase in stem cell aging. *FEBS Lett* **584:** 3826–3830

Flores I, Canela A, Vera E, Tejera A, Cotsarelis G, Blasco MA (2008) The longest telomeres: a general signature of adult stem cell compartments. *Genes Dev* **22:** 654–667

Haines DC, Chattopadhyay S, Ward JM (2001) Pathology of aging B6;129 mice. *Toxicol Pathol* **29:** 653–661

Harper JW, Elledge SJ (1998) The role of Cdk7 in CAK function, a retro-retrospective. *Genes Dev* **12:** 285–289

Hemann MT, Strong MA, Hao LY, Greider CV (2001) The shortest telomere, not average telomere length, is critical for cell viability and chromosome instability. *Cell* **107:** 67–77

Kim JB, Sharp PA (2001) Positive transcription elongation factor B phosphorylates hSPT5 and RNA polymerase II carboxyl-terminal domain independently of cyclin-dependent kinase-activating kinase. *J Biol Chem* **276:** 12317–12323

Korsisaari N, Rossi DJ, Paetau A, Charnay P, Henkemeyer M, Mäkelä TP (2002) Conditional ablation of the Mat1 subunit of TFIIH in Schwann cells provides evidence that Mat1 is not required for general transcription. *J Cell Sci* **115:** 4275–4284

Krishnamurthy J, Sharpless NE (2007) Stem cells and the rate of living. *Cell Stem Cell* **1:** 9–11

Larochelle S, Chen J, Knights R, Pandur J, Morcillo P, Erdjument-Bromage H, Tempst P, Suter B, Fisher RP (2001) T-loop phosphorylation stabilizes the CDK7-cyclin H-MAT1 complex *in vivo* and regulates its CTD kinase activity. *EMBO J* **20:** 3749–3759

Larochelle S, Pandur J, Fisher RP, Salz HK, Suter B (1998) Cdk7 is essential for mitosis and for *in vivo* cdk-activating kinase activity. *Genes Dev* **12:** 370–381

Lee KM, Miklos I, Du H, Watt S, Szilagyi Z, Saiz JE, Madabhushi R, Penkett CJ, Sipiczki M, Bähler J *et al* (2005) Impairment of the TFIIH-associated CDK-activating kinase selectively affects cell cycle-regulated gene expression in fission yeast. *Mol Biol Cell* **16:** 2734–2745

Lolli G, Johnson LN (2005) CAK-Cyclin-dependent activating kinase: a key kinase in cell cycle control and a target for drugs? *Cell Cycle* **4:** 572–577

Lyle S, Christofidou-Solomidou M, Liu Y, Elder DE, Albelda S, Cotsarelis G (1998) The C8/144B monoclonal antibody recognizes cytokeratin 15 and defines the location of human hair follicle stem cells. *J Cell Sci* **111:** 3179–3188

Malumbres M, Barbacid M (2005) Mammalian Cyclin-dependent kinases. *Trends Biochem Sci* **30:** 630–641

Matheu A, Maraver A, Klatt P, Flores I, Garcia-Cao I, Borras C, Flores JM, Viña J, Blasco MA, Serrano M (2007) Delayed ageing through damage protection by the Arf/p53 pathway. *Nature* **448:** 375–379

Moerman EJ, Teng K, Lipschitz DA, Lecka-Czernik B (2004) Aging activates adipogenic and suppresses osteogenic programs in mesenchymal marrow stroma/stem cells: the role of PPAR-gamma2 transcription factor and TGF-beta/BMP signaling pathways. *Aging Cell* **3:** 379–389

Ni Z, Schwartz BE, Werner J, Suarez JR, Lis JT (2004) Coordination of transcription, RNA processing, and surveillance by P-TEFb kinase on heat shock genes. *Mol Cell* **16:** 55–65

Ortega S, Prieto I, Odajima J, Martín A, Dubus P, Sotillo R, Barbero JL, Malumbres M, Barbacid M (2003) Cyclin-dependent kinase 2 is essential for meiosis but not for mitotic cell division in mice. *Nat Genet* **35:** 25–31

Palancade B, Bensaude O (2003) Investigating RNA polymerase II carboxyl-terminal domain (CTD) phosphorylation. *Eur J Biochem* **270:** 3859–3870

Patel SA, Simon MC (2010) Functional analysis of the Cdk7.cyclin H.Mat1 complex in mouse embryonic stem cells and embryos. *J Biol Chem* **285:** 15587–15598

Rodríguez CI, Buchholz F, Galloway J, Sequerra R, Kasper J, Ayala R, Stewart AF, Dymecki SM (2000) High-efficiency deleter mice show that FLPe is an alternative to Cre-loxP. *Nat Genet* **25:** 139–140

Rossi DJ, Londesborough A, Korsisaari N, Pihlak A, Lehtonen E, Henkemeyer M, Mäkelä TP (2001) Inability to enter S phase and defective RNA polymerase II CTD phosphorylation in mice lacking Mat1. *EMBO J* **20:** 2844–2856

Ruzankina Y, Pinzon-Guzman C, Asare A, Ong T, Pontano L, Cotsarelis G, Zediak VP, Velez M, Bhandoola A, Brown EJ (2007) Deletion of the developmentally essential gene ATR in adult mice leads to age-related phenotypes and stem cell loss. *Cell Stem Cell* **7:** 113–126

Santamaría D, Barrière C, Cerqueira A, Hunt S, Tardy C, Newton K, Cáceres JF, Dubus P, Malumbres M, Barbacid M (2007) Cdk1 is sufficient to drive the mammalian cell cycle. *Nature* **448:** 811–815

Satyanarayana A, Berthet C, Lopez-Molina J, Coppola V, Tessarollo L, Kaldis P (2008) Genetic substitution of Cdk1 by Cdk2 leads to embryonic lethality and loss of meiotic function of Cdk2. *Development* **135:** 3389–3400

Schnütgen F, De-Zolt S, Van Sloun P, Hollatz M, Floss T, Hansen J, Altschmied J, Seisenberger C, Ghyselinck NB, Ruiz P, Chambon P, Wurst W, von Melchner H (2005) Genomewide production of multipurpose alleles for the functional analysis of the mouse genome. *Proc Natl Acad Sci USA* **102:** 7221–7226

Smyth GK, Michaud J, Scott HS (2005) Use of within-array replicate spots for assessing differential expression in microarray experiments. *Bioinformatics* **21:** 2067–2075

Subramanian A, Tamayo P, Mootha VK, Mukherjee S, Ebert BL, Gillette MA, Paulovich A, Pomeroy SL, Golub TR, Lander ES, Mesirov JP (2005) Gene set enrichment analysis: a knowledge-based approach for interpreting genome-wide expression profiles. *Proc Natl Acad Sci USA* **102:** 15545–15550

Tarutani M, Itami S, Okabe M, Ikawa M, Tezuka T, Yoshikawa K, Kinoshita T, Takeda J (1997) Tissue-specific knockout of the mouse Pig-a gene reveals important roles for GPI-anchored proteins in skin development. *Proc Natl Acad Sci USA* **94:** 7400–7405

Wallenfang MR, Seydoux G (2002) cdk-7 is required for mRNA transcription and cell cycle progression in Caenorhabditis elegans embryos. *Proc Natl Acad Sci USA* **99:** 5527–5532